UNIVERSITY OF NAPLES FEDERICO II

School of Polytechnic and Basic Sciences

Department of Chemical, Materials and Production Engineering

PhD Thesis in

Industrial Product and Process Engineering

XXXI cycle

TITANIUM DIOXIDE BASED HYBRID MATERIALS FOR ADVANCED OXIDATION PROCESSES

Claudio Imparato

Supervisor:

Prof. Antonio Aronne

Coordinator:

Prof. Giuseppe Mensitieri

2015 – 2018

TABLE OF CONTENTS

LIST OF ABBREVIATIONS

2,4-D	2,4-dichlorophenoxyacetic acid
2,4-DCP	2,4-dichlorophenol
4-CPA	4-chlorophenoxyacetic acid
acac	acetylacetonate
ace	acetate
AFM	Atomic Force Microscopy
AOP	Advanced Oxidation Process
asc	ascorbate
cat	catecholate
cit	citrate
CB	conduction band
CV	Cyclic Voltammetry
dbm	dibenzoylmethane
dea	diethanolamine
dop	dopamine
DMPO	5,5-dimethyl-1-pyrroline N-oxide
DOS	density of states
DRUV-vis	Diffuse Reflectance UV-visible
DSSC	dye-sensitized solar cell
EPR	Electron Paramagnetic Resonance
FT-IR	Fourier Transform Infrared
HOMO	highest occupied molecular orbital
HSGT, HT	hybrid sol-gel titania (TiO_2-acac)
LMCT	ligand-to-metal charge transfer
LUMO	lowest unoccupied molecular orbital
MCPA	4-chloro-2-methylphenoxyacetic acid
MCPB	4-(4-chloro-2-methylphenoxy) butanoic acid
NHE	normal hydrogen electrode
PAH	polycyclic aromatic hydrocarbon
PHE	phenanthrene
ROS	reactive oxygen species
rpm	rounds per minute
SGT	sol-gel titania (reference TiO_2)
TA	terephthalic acid
TAOH	2-hydroxyterephthalic acid
TG-DTA	Thermogravimetric – Differential Thermal Analysis
VB	valence band
XPS	X-ray Photoelectron Spectroscopy
XRD	X-ray Diffraction

INTRODUCTION

Nowadays the rising concern for the environmental and energetic issues pushes research toward the development of innovative processes and materials for the control of pollution and the generation of energy from renewable sources. The release and dispersion of toxic or harmful chemicals in ground and surface water, soil and atmosphere causes serious risks for human health and for the entire ecosystem. In this context, advanced oxidation processes (AOP) offer a varied choice of chemical treatments to remove contaminants, in particular from water, by means of reactive oxygen species (ROS) generated *in situ*. They include heterogeneous photocatalysis, with the advantageous possibility of exploiting solar radiation energy for the purification and disinfection of water and air, as well as for the production of energy carriers. Despite the large interest, few AOP are established technologies; efficient, inexpensive and scalable methods for water treatment or remediation have still to be developed [1,2]. Generating hydrogen by water splitting or simple carbon-based fuels by CO_2 reduction using solar radiation would represent remarkably sustainable methods to deal with the issue of renewable energy storage. Unfortunately, these processes are still far from commercial viability, as a consequence of thermodynamic and kinetic limitations, so they need strong improvements.

Semiconducting transition metal oxides are central materials in catalysis, photocatalysis and related fields. Among them, titanium dioxide (TiO_2) is intensely studied and widely used because of its combination of chemical and photochemical stability, biocompatibility, availability at low cost, electronic properties and versatility. It presents interesting acid and redox properties, but its limited surface reactivity imposes its coupling with metals or other oxides to realise efficient catalysts. TiO_2, as the reference material in the research on photocatalysis, is the subject of an impressive number of works. Nonetheless, some drawbacks restrict its efficiency, namely the large band gap and the high recombination rate of charge carriers. Moreover, TiO_2 is used in second generation photovoltaic cells, like dye-sensitized and perovskite solar cells, where metal oxide thin films act as electron transport layer between the light absorbing phase and an electrode. The optimization of this layer and its interfaces is crucial in the development of more efficient and stable solar cells.

The modification of the chemical and electronic structure is the most efficient way to face the limitations and enhance specific functional properties of a semiconductor. Hence the motivation of the present PhD research project: the design, synthesis and characterization of materials based on TiO_2 exhibiting suitable properties for improved performances in catalysis (both dark and photoinduced) and linked applications. The pathway followed to achieve this aim is the synthesis of hybrid inorganic-organic materials, in which organic molecules complex titanium atoms in the oxide structure. The interplay between the inorganic and organic component leads to emerging characteristics with respect to those of the single components.

The method chosen for the synthesis is the sol-gel technique. The innovative procedure developed consists in a bottom-up approach, in which the metal precursor reacts with the complexing organic ligand before hydrolysis and condensation take place. This approach is alternative to the frequently employed top-down method, in which the organic compounds are adsorbed on the surface of oxide nanoparticles or films, and produces materials with different features. The proposed procedure ensures high control on the composition and a functionalization extended to the bulk. The macroscopic amorphous xerogels derived from homogeneous chemical gels have some other practical advantages, like the easier separation from solution and the possibility to use the material in a continuous flow reactor. Relatively few studies concern amorphous TiO_2, since it is considered less efficient than the crystalline polymorphs in photochemical applications. Anyway it presents some merits, such as the simple synthesis at low temperature, extended surface area and high hydroxylation, therefore it is interesting to explore its functional properties [3–5].

In the present work, selecting the appropriate synthesis parameters allowed to prepare TiO_2-based hybrid chemical gels, powders or stable sols. The sols were deposited by spin coating to produce hybrid thin films. Some of the amorphous dried gels (xerogels) were also thermally treated in various conditions, obtaining defective crystalline TiO_2. Different classes of organic components were explored: diketones (acetylacetone and dibenzoylmethane), carboxylic acids (citric and acetic acid), enediols (catechol, dopamine, ascorbic acid). The choice of these compounds was inspired by previous researches or by results obtained during this activity. The corresponding hybrid samples showed diverse properties, dependent on the structure of the organic molecules and their interaction with the oxide matrix.

The characterization of the samples was performed combining several complementary techniques, allowing to draw a complete picture of the studied materials. They included X-ray diffraction, scanning electron microscopy, thermogravimetric and differential thermal analysis, spectroscopic techniques (Fourier transform infrared, UV-visible diffuse reflectance, electron paramagnetic resonance and X-ray photoelectron spectroscopies), electrochemical methods (photocurrent, cyclic voltammetry and

spectroelectrochemical measurements). Additional techniques were involved in the characterization of thin films: optical microscopy, atomic force microscopy, profilometry, ellipsometry and electrical resistivity measurements.

The formation of ligand-to-metal charge transfer complexes was observed in the hybrid materials, with interesting effects on their electronic properties, optical absorption, photoresponsivity and reactivity. Some ligands were found to induce the generation and long-term stabilization of superoxide radical anions on the hybrid surface of the xerogels. This unique ability was previously detected only in analogous ZrO_2-based hybrid gels [6–8]. It provided the material excellent activity in the oxidative degradation of various organic pollutants through radical mechanisms activated without any light irradiation [9,10]. Another effect of charge transfer is the photosensitization of TiO_2, with the appearance of visible light absorption bands, associated to the generation of photocurrent and photocatalytic activity of some xerogels in the same range. Preliminary photocatalytic tests evidenced also an activity of the annealed gels prevalently in the UV range, despite their wide light absorption related to the structural defectivity.

Morphological, optical and electric properties of the amorphous and crystallised films were observed to vary depending on the nature of the organic ligand and on preparation conditions, like the spinning rate or the drying and annealing temperature. The response to the UV irradiation of the films, a treatment often performed to improve the surface reactivity and wettability, was also examined, finding different behaviours according to the organic ligand.

In summary, three principal aims of the present work can be distinguished, based on a series of TiO_2-based hybrid materials synthesized by sol-gel:

- a deep study on the process of generation and stabilization of superoxide radicals on the hybrid surfaces, as well as on the consequent oxidative activity in the dark;
- the achievement of enhanced photoresponsivity of the materials, possibly including visible light, through different mechanisms, namely direct photosensitization by ligand-to-metal charge transfer, and self-induced structural defects produced by simple heat treatments of the xerogels;
- a wide investigation on thin films, in particular the amorphous hybrid films prepared at low temperature, including the structural features, optical response and electrical conductivity.

The last point was developed in the framework of a collaboration between the Department of Chemical, Materials and Production Engineering of the University of Naples Federico II, where most of the PhD activity was conducted, with the ENEA Research Centre, on a project promoted by the

Ministry for Economic Development, regarding the production of TiO_2 thin films as electron transport layers for perovskite solar cells.

This PhD research activity has also benefited of collaborations with other Departments and Universities: the Departments of Chemical Sciences and of Agricultural Sciences of the University of Naples Federico II, the University of Cagliari (Department of Chemical and Geological Sciences), the University of Salerno (Department of Industrial Engineering). For a visiting period of three months the activity was carried out at the Jagiellonian University in Krakow (Poland), at the Faculty of Chemistry.

The present dissertation is structured in 6 chapters, whose content is briefly described as follows. Chapter 1 presents the current state of scientific knowledge about the main topics treated in the work: titanium dioxide and hybrid materials, advanced oxidation processes and reactive oxygen species, photocatalysis, related applications and issues, the sol-gel process. Chapter 2 describes the materials and methods used in all the stages of the experimental work. Chapter 3 describes the synthesis experiments and discusses the outcomes. Chapter 4 reports the entire characterization of the xerogels and annealed samples, divided in structural and surface, optical, electronic, and electrochemical properties. Chapter 5 presents the results of the functional tests, regarding the oxidative activity in the dark and some preliminary data of photocatalytic activity. Chapter 6 reports the characterization of the thin films. Finally, the Conclusions summarise the most important results attained and advancements brought by this PhD project and suggest some interesting future developments and further studies which can be opened by the presented findings.

- CHAPTER 1 -

BACKGROUND

1.1. Titanium oxide and its applications

Titanium dioxide (TiO_2) is the most common oxide of titanium, a transition metal found in group IV of the periodic table, with atomic number 22. Titanium is the ninth most abundant element and the fourth most abundant metal (and the second transition metal after iron) in the Earth's crust (about 0.6 %). The most relevant mineral sources are rutile, ilmenite and leucoxene, containing varying amounts of titanium dioxide. The world's production of TiO_2 is over 4 million tons per year. The majority is used as white pigment, because of its opacity and high refraction index (2.5 - 2.7, according to the crystalline structure). TiO_2 can be found as pigment in paints, plastic, ceramics, paper, toothpastes and other cosmetics, pharmaceuticals and food (as E171 colouring agent). It is commonly a component of sunscreen formulations for its ability of blocking ultraviolet radiation [11,12].

TiO_2 exists in several crystalline forms (11 have been identified), the most important at common temperatures and pressures being rutile, anatase and brookite. In these structures each Ti^{4+} cation is coordinated by six O^{2-} anions, and the phases differ by the distortion and assembly patterns of the $[TiO_6]$ octahedra. In rutile each $[TiO_6]$ octahedron is surrounded by ten octahedra, sharing an edge

with two of them and a corner with the other eight, in a tetragonal crystalline system; in anatase each [TiO_6] octahedron is surrounded by eight octahedra (four edge-sharing and four corner-sharing), in a distorted tetragonal system, with longer Ti-Ti and shorter Ti-O distances; in brookite the octahedra share three edges in an orthorhombic system. These differences in the crystal lattice cause differences in mass density (4.26, 4.11 and 3.84 g/cm^3 for anatase, brookite and rutile, respectively) and electronic structure, e.g. the band gap energy. Rutile is the most thermodynamically stable phase at most temperatures and pressures, due to its linearity which allows relaxation of Ti-Ti bonds, while metastable anatase and brookite are kinetic products. Anatase is the most commonly produced phase at low temperatures, while brookite can be obtained as byproduct or in specific synthesis conditions. The conversion of anatase to rutile occurs at T > 600 °C and depends on factors like particle size and the presence of surface or lattice defects [11–13].

Titanium dioxide is characterized by large availability, low cost, chemical and mechanical stability, biological inertness, good electrical properties. Besides the use as pigment, it finds applications in gas sensing, biomaterials (in bone implants), anti-reflective, anti-corrosion or anti-fogging coatings, photochromics and electrochromics, dielectrics, photovoltaic cells, catalysis and photocatalysis (including self-cleaning surfaces).

As catalyst, TiO_2 is employed in particular for its redox ability, in reactions like the selective reduction of NO_x to N_2, the decomposition of volatile organic compounds (VOC), hydrogen production by water gas shift, Fischer-Tropsch synthesis, CO oxidation by O_2, H_2S oxidation to S and SO_2 reduction to S by CO [11]. TiO_2 was also proposed as an acid heterogeneous catalyst, as anatase was shown to have a considerable density of Lewis acid sites that can work stably in water [14]. TiO_2 is often used as catalyst support; the possibility of tailoring its surface and morphological properties (crystalline phase, exposed facets, particle size and shape, surface area, porosity) favours the obtainment of catalytic materials with the desired features, by functionalization and deposition of active species, such as metals or other metal oxides.

As a wide band gap semiconductor, TiO_2 is the reference metal oxide in the research on photocatalysis. Heterogeneous photocatalysis refers to the process involving redox reactions on the surface of a semiconductor by means of electrons and holes separated by the absorption of light (more details are reported in Section 1.4). Several advantages, besides those mentioned above, justify the focus on TiO_2 in fundamental and applicative photocatalytic studies: chemical and electrochemical stability in a wide range of conditions, photostability, high photoreactivity (with photonic efficiency up to 10 %), high electron mobility, suitable redox potential of valence and conduction bands [15,16]. The first hints on the reactivity of TiO_2 under sunlight have been recognized in the first half of the XX century, for example observing the degradation of the organic components of paints containing titania [16].

Nonetheless, the interest on its photoresponsive properties started growing after the renowned paper published in 1972 by Honda and Fujishima, demonstrating water splitting to H_2 and O_2 on an illuminated rutile electrode [17].

TiO_2 has a band gap energy between the valence and conduction bands generally ranging from 3.0 eV (rutile) to 3.2 eV (anatase), with slightly higher values for amorphous samples and thin films, and values lower of about 0.2 eV reported for some nanosized samples (up to 5-10 nm) due to the quantum confinement effect. The valence band potential is positive enough to promote the O_2 evolution from water and the generation of the strongly oxidizing hydroxyl radical ($^{\bullet}OH$), while the conduction band potential is negative enough to allow water reduction to H_2 and O_2 reduction to superoxide radical ($O_2^{\bullet-}$), another important reactive oxygen species [16]. The properties of TiO_2 are strictly dependent on both the crystalline form and the structure and morphology of the material; different nanostructures, e.g. nanoparticles, nanorods, nanotubes, nanosheets, hollow spheres, can be obtained using different synthesis methods and show peculiar behaviour with respect to the bulk oxide. The anatase polymorph has been commonly recognized as the most active in photocatalysis, mainly because of its higher electron mobility, lower dielectric constant, better band positions and more efficient surface interaction with oxygen species [16]. Nevertheless, recent studies have provided contrasting data on the actual band potentials of anatase and rutile, and showed that rutile can be more efficient in reducing processes [18,19]. The most investigated commercial TiO_2 is known as "P25", a mixture of about 75% anatase and 25% rutile, usually taken as a standard reference for photocatalytic activity. Its outstanding activity is related to the charge transfer between the two phases, anyway a complete knowledge of the exact mechanism of their interplay is not yet achieved. Brookite and other TiO_2 polymorphs have received less attention, also because of the difficulty in obtaining them in pure form.

Amorphous titanium oxide is generally considered of very restricted photocatalytic activity, since the disordered structure hinders the transport of electron and holes, fostering their recombination [20]. On the other hand, amorphous materials can present some favourable characteristics for a catalytic process, for instance large surface area, high surface hydroxylation and hydration, therefore a better adsorption of substrate molecules, easiness of preparation. Few reports of amorphous TiO_2 with interesting photocatalytic performances are indeed found in literature, for instance hydrated, defective or H_2O_2-modified amorphous TiO_2 samples, prepared by sol-gel or precipitation method [3–5,21,22].

Different strategies have been proposed for the modification of the structural and electronic features of TiO_2, in order to enhance its efficiency in catalysis, photocatalysis or related fields. These methods are described in Section 1.5, as some of them are object of the present work.

1.2. Hybrid metal oxides

The core of the present PhD project is the synthesis of hybrid materials based on titanium oxide. Here the term "hybrid" indicates, as frequently occurs, the organic-inorganic composition, in this case an organic compound linked by chemical bonds to a metal oxide matrix. Hybrid organic-inorganic materials can be broadly defined as nanocomposites with organic and inorganic components which are intimately mixed [23]. As happens in other classes of composites, binding together components with completely different nature and features results in materials whose properties are not merely the sum of the properties of the single phases; indeed, new emerging properties appear, which cannot always be simply predicted and need careful investigation to be understood and applied. The nature of the inner interface between the organic and inorganic phases has a predominant role and leads to distinguish two classes of materials: in *class I*, there are only weak interactions between the components of the structure (hydrogen bonds, van der Waals or electrostatic forces), whereas in *class II* they are linked through strong chemical bonds (covalent or iono-covalent) [23,24].

Hybrid composites play an important role among advanced functional materials, as they offer virtually unlimited possibilities for tailoring shape and physicochemical properties, and facilitate miniaturization and integration, opening promising applications in many fields: optics, electronics, catalysis, sensors, membranes, functional and protective coatings, medicine, biotechnology, etc. [23]. Many kinds of inorganic-organic materials are currently commercially available.

Concerning transition metal oxides, examples of hybrid materials close to the ones studied in the present work are represented by titanium dioxide coupled with dyes or other complexing organic molecules acting as photosensitizers, i.e. widening the spectrum of absorbed light. Dye-sensitized solar cells are based on these systems, and they are also studied for photocatalytic applications (see Sections 1.4 and 1.5). Dyes and photoactive organic species incorporated into oxide matrices are important also for other optical devices: lasers, sensors, photochromics, luminescent solar concentrators, non-linear optics.

Another large field is represented by bioactive hybrids. Biomolecules, enzymes, antibodies and even microorganisms can be encapsulated or immobilized on solid substrates, in order to protect them from denaturation, make them stable and reusable. Ceramic hosts offer significant advantages over the biocompatible polymers used for the same scope, like better mechanical strength, chemical and thermal stability. Moreover they do not swell in most solvents, preventing the leaching of entrapped biomolecules. Such materials, in particular those containing enzymes, can be applied not only in medicine, but also in bio-sensing and catalysis, performing transformations with high specificity [23,25].

Biomimetics indicates the selection of ideas and principles from nature and their application in engineering products [26]. Many biomaterials and bio-inspired systems are hybrids, for instance some surface coatings with hydrophobic, protective, anti-fouling or adhesive characteristics.

A class of materials of rapidly rising interest are metal-organic frameworks (MOF), regular structures constituted by metal centres bound by organic linkers, with widely variable and tunable properties for catalytic, optical and sensing uses.

Various chemical methods are available to prepare hybrid materials: sol-gel, hydrothermal, solvothermal, assembling or dispersion of nanobuilding blocks, self-assembling procedures. The use of precursors with functionalized or bridging ligands, of templating or structure-directing agents, organic connectors or coordinating solvents influences the nanostructure, allowing to obtain periodically organized porosity, highly dispersed or hierarchical architectures. Nanomaterials with different dimensionality can be produced: nanoparticles, nanotubes, lamellae, core-shell structures, 3D-frameworks, etc. Processing and post-synthesis treatments can give the final shape of the material, as in the case of coatings, especially with polymer-based composites [24]. Sol-gel chemistry is a powerful and versatile tool for the solution synthesis of hybrid oxide-based materials, as its mild conditions allow inorganic and organic components to be mixed at the nanometric scale. This is the synthetic method used in the present work, and is described in Section 1.6.

1.3. Advanced oxidation processes

Advanced oxidation processes (AOP) have attracted an increasing number of researches for the last three decades. They refer to a variety of chemical processes which share the final aim of a complete mineralization of environmental organic pollutants, i.e. their oxidation to CO_2, H_2O and other inorganic species, by means of reactive oxygen species (ROS) and specifically the hydroxyl radical ($^{\bullet}OH$). Chemical oxidation results more convenient and environmentally friendly than other processes, like biological treatment, which is quite selective and is inhibited by the presence of toxic or recalcitrant compounds, or methods like precipitation and adsorption, which only transfer the pollutants from one phase to another, producing a hazardous sludge that must be disposed of properly. On the contrary, AOP rely on the low selectivity of oxygen radicals, which are able to decompose most organics completely or at least partially, converting them to less harmful species. Another advantage is that AOP usually operate at or near ambient temperature and pressure.

The most studied processes belonging to this category are: Fenton process, homogeneous and heterogeneous photocatalysis, plasma treatment and ozonation. In a broader definition of AOP, electrolysis, ultrasound-assisted oxidation and wet air oxidations are encompassed. More recently evolving processes also include microwaves, ionising radiation or specific oxidants, such as ferrates [2].

The Fenton reaction has been known for a long time as a simple way of producing $^{\bullet}OH$ radicals without specific equipment, by decomposition of hydrogen peroxide in the presence of a Fe^{2+} salt:

$$Fe^{2+} + H_2O_2 \longrightarrow Fe^{3+} + OH^- + {}^{\bullet}OH \qquad (1.1)$$

Furthermore, the produced ferric ions can react again, in the so-called Fenton-like reaction, releasing a hydroperoxide radical and regenerating ferrous ions:

$$Fe^{3+} + H_2O_2 \longrightarrow Fe^{2+} + H^+ + HO_2^{\bullet} \qquad (1.2)$$

This process is strictly depending on pH (the optimum value is around 3), so modifications have been introduced to extend the operating range of pH, for instance using organic chelators for Fe [1]. It was observed that the degradation of organic pollutants by Fenton oxidation was sensibly accelerated by UV-visible light. In these conditions the photolysis of Fe^{3+} complexes occurs:

$$Fe(OH)^{2+} + h\nu \longrightarrow Fe^{2+} + {}^{\bullet}OH \qquad (1.3)$$

The resulting photo-Fenton process is the classical example of homogeneous photocatalysis. Heterogeneous photocatalysis, the most extensively studied AOP, is presented in Section 1.4.

Plasma oxidation is regarded as a competitive technology for the removal of organic pollutants, also from soils. Low-temperature plasma, particularly the techniques based on pulsed corona discharge and dielectric barrier discharge, is under investigation. The process generates high energy electrons, which provide highly reactive radicals and molecules ($^{\bullet}OH$, $H^{\bullet}$, $O^{\bullet}$ O_3, H_2O_2, etc.), which can directly or indirectly start oxidation reactions. Ozone (O_3) can act as an oxidant, and shows a complex chemistry in basic water solution. Its decomposition, initiated by OH^-, brings about the formation of $^{\bullet}OH$ and other ROS. The presence of H_2O_2 or UV irradiation enhance the yield of oxidants, making O_3/H_2O_2 and O_3/UV common systems for cleaning or sterilization on a small scale.

Wet air oxidation consists in the use of oxygen or air to achieve pollutant oxidation at high temperature (130-300 °C) and pressure (0.5-20 MPa). It is an exothermic process, suitable for a relatively high organic load (COD > 20 g/L); with such loads it becomes autothermic, with savings on the cost of fuel [27].

Wastewater treatment remains the largest research area for AOP, covering effluents of different origin, such as industries, hospitals, municipal wastewater treatment plants, and the removal of micro-

pollutants like pesticides and heavy metals from water. The most efficient approach for wastewater treatment should be chosen according to the specific characteristics of the effluent, e.g. its organic load (expressed at TOC, total organic carbon, or COD, chemical oxygen demand), its biodegradability and toxicity. In complex cases, an AOP pre-treatment to convert more toxic and recalcitrant compounds into more biodegradable species can be combined with common wastewater treatment or with a biodegradation post-treatment [2].

AOP are generally presented as more environmentally friendly and more efficient treatments than the conventional ones, despite the higher costs due to the use of chemicals, such as H_2O_2 or catalysts, the higher energy consumption, for example for UV illumination, and in some cases the required installation of new systems. Probably, the actual sustainability of the process should be assessed in every specific case. The development of inexpensive, active, stable and recyclable catalytic materials would have a determining role in making the AOP more convenient and competitive with regard to existing technologies.

1.3.1. Reactive oxygen species

Reactive oxygen species (ROS) define a class of highly reactive oxygen-bearing molecules. They include the species formed upon incomplete reduction of molecular oxygen, namely superoxide radical anion ($O_2^{\bullet -}$), hydrogen peroxide (H_2O_2), hydroperoxyl radical ($HO_2^{\bullet}$) and hydroxyl radical ($OH^{\bullet}$), also known as reactive oxygen intermediates (ROI), ozone (O_3) and singlet oxygen ($^1O_2$). In addition to these fundamental species, peroxyl ($ROO^{\bullet}$), alkoxyl ($RO^{\bullet}$), carbonate ($CO_3^{\bullet -}$) radicals and organic hydroperoxides are encountered in the definition of ROS, and sometimes hypochlorous (HOCl), hypobromous (HOBr) and hypoiodous acids (HOI) are also mentioned [28].

Ground-state molecular oxygen is a paramagnetic biradical with two electrons occupying separate π^* orbitals with parallel spins (triplet configuration, Figure 1.1). This causes a spin restriction for the reaction of O_2 with most organic molecules, which are diamagnetic, with electrons pairs with opposite spins, due to the unfavourable interaction of these pairs with the π^* orbitals. Hence O_2 preferably accepts one electron at a time during redox reactions. It can react fast by single-electron transfer with radicals or other species bearing unpaired electrons, such as transition metals in some oxidation states. The one-electron reduction of O_2 results in the formation of the superoxide radical anion. Subsequent redox conversions produce other ROS, as illustrated in Scheme 1.1.

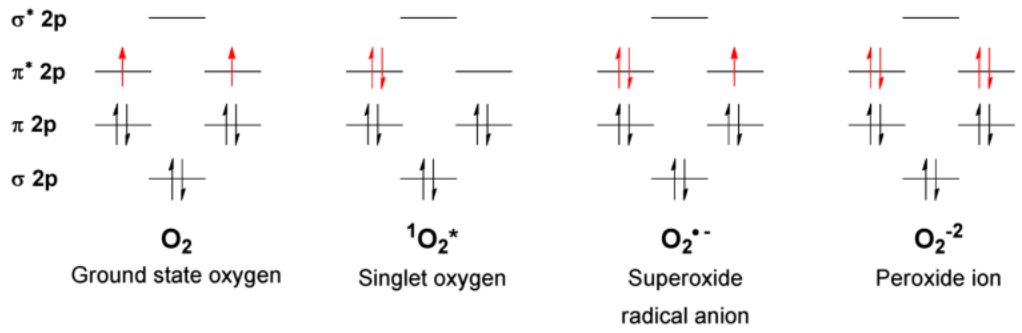

Figure 1.1. *Molecular orbital diagrams for ground-state molecular oxygen and some ROS: singlet oxygen, superoxide anion and peroxide ion (deprotonated form of hydrogen peroxide) [28].*

Molecular O_2 can be converted to a more reactive form by energy transfer: singlet oxygen has paired electrons with opposite spins, thus an increased oxidizing ability (about 1 V more positive reduction potential) compared to ground-state (triplet) O_2.

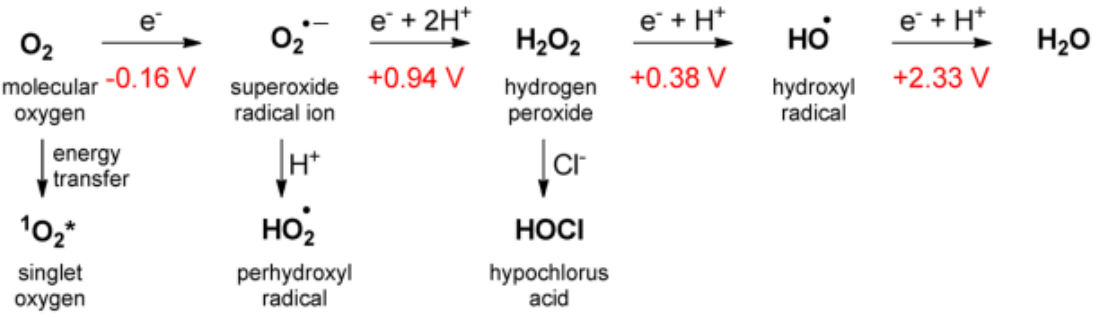

Scheme 1.1. *Formation of ROS through energy and electron transfer reactions. Standard redox potentials are reported (standard concentration of oxygen regarded as 1 M), adapted from reference* [28].

Reactive oxygen radicals are implicated in oxidative damage on fatty acids, DNA, proteins and other cellular components. An overproduction of ROS is associated with numerous disorders, such as cancer, cardiovascular, inflammatory and neurodegenerative diseases. According to the long-held free radical theory of aging, the noxious effects of ROS, generated during cellular respiration, are directly involved in aging processes, although this hypothesis is under revision. On the other hand, ROS may have a beneficial physiological role, acting as messengers in cellular signalling, by reaction with specific functional groups of target proteins which lead to covalent protein modification. Thus, ROS and reactive nitrogen species (RNS) are involved in redox regulation, relevant for the expression of transcription factors and other signal transduction molecules, cell adhesion, amplification of immune response and programmed cell death [28]. A complete understanding of the complex impact of ROS chemistry on living organisms is a current multidisciplinary challenge.

1.3.2. Superoxide radical and its generation on metal oxide surfaces

Among reactive oxygen species, the superoxide radical anion, $O_2^{\bullet-}$, is one of the most important and studied. Superoxide is capable of participating in various reactions, such as disproportionation, deprotonation, one-electron transfer and nucleophilic substitution. Its reactivity is determined by its nucleophilicity, basicity and redox potentials. Superoxide reacts with a proton donor to form the hydroperoxide radical, $HO_2^{\bullet}$, a relevant reaction in both chemical and biological systems. In protic solvents $O_2^{\bullet-}$ readily disproportionates to form O_2 and either H_2O_2 or hydroperoxide anion:

$$2O_2^{\bullet-} + 2H^+ \rightleftarrows O_2 + H_2O_2 \qquad (1.4)$$

$$2O_2^{\bullet-} + H_2O \rightleftarrows O_2 + HO_2^- + OH^- \qquad (1.5)$$

In the absence of protons, $O_2^{\bullet-}$ has the tendency to attack the positively charged moieties of any organic species, due to its exceptional nucleophilicity. $O_2^{\bullet-}$ can selectively act as an oxidant for susceptible substrates through a H atom transfer mechanism. However, it is not generally involved in direct one-electron oxidation because solvated $^{\bullet}O_2^{2-}$ has a relatively high energy. On the other hand, superoxide acts as a moderate one-electron reducing agent toward both organic and inorganic compounds (e.g. transition metal complexes). The oxidation of $O_2^{\bullet-}$ has been used in chemiluminescence methods for its detection [29].

Owing to its reactivity, superoxide radical can find various applications. The destruction of hazardous chemicals, such as chlorinated hydrocarbons or sulphur compounds, and the remediation of contaminated soil and water, by means of *in situ* chemical oxidation, using Fenton's reaction, have been successfully tested. $O_2^{\bullet-}$ has a primary role especially in the degradation of hydrophobic contaminants and non-aqueous phase liquids (NAPL), showing higher reactivity than hydroxyl radical [29]. Several studies have been devoted to the use of superoxide in organic synthesis. Due to its important biological functions, the reactivity of superoxide with enzymes, other proteins and metabolic intermediates attracts large interest. Together with other ROS, it is studied in photodynamic therapy for cancer treatment.

A number of methods are available for the generation of superoxide radicals [29]:

- physical methods, such as sonolysis or pulse radiolysis;
- biological methods;
- chemical and electrochemical methods;
- photochemical and photocatalytic reactions.

A typical way to produce $O_2^{\bullet-}$ is the dissolution of alkali metal superoxides (NaO_2, KO_2) or their reaction with O_2. Many examples of photochemical generation of superoxide ions are reported. Solar

radiation naturally induces the formation of $O_2^{\bullet-}$ in surface waters, by electron transfer from an excited state organic molecule to O_2, or in effluent organic matter (in particular on phenyl moieties of humic and fulvic acids) in the presence of photoactive metals. Anyway, from an engineering perspective superoxide radical has seldom been considered because of the difficulty of maintaining it in a stable state [29].

One of the most promising strategies for the generation of stable superoxide radicals is their adsorption on oxide surfaces, allowing the subsequent participation in processes occurring at the liquid-solid or gas-solid interface. Photo-induced or direct electron transfer from the oxide surface to O_2, surface intermolecular electron transfer and decomposition of H_2O_2 are potential mechanisms for the formation of adsorbed $O_2^{\bullet-}$.

When molecular oxygen is contacted with the surface of a metal oxide, the formation of $O_2^{\bullet-}$ will in principle occur if the LUMO energy of the adsorbed species lies below the Fermi level of the solid. The electrostatic contribution to the stabilisation of the anion on the surface metal cations plays a fundamental role. Pure and mixed oxides can thus be divided into two classes: the former groups the few systems capable of electron transfer towards O_2 without any preliminary reductive treatment, while the latter encompasses oxides which must be reduced prior to O_2 adsorption. An example of the first class is MgO, an insulator, doped with Co^{2+}, thanks to the ability of Co ions to form adducts with oxygen. Many reducible semiconducting oxides which present non-stoichiometric composition or cations stable in more oxidation states are capable of O_2 reduction. The electron transfer can originate from donor centres in the band gap, in n-type semiconductors, or localized defect centres acting as electron traps (e.g. oxygen vacancies) [30].

In the case of titanium oxide, after surface reduction or dehydration by heating in vacuum, the formation of superoxide radicals after contact with O_2 was revealed by electron paramagnetic resonance (EPR) spectroscopy. The reactivity of anatase and rutile surfaces was found to be different, and different adsorption sites, including vacancy sites, were individuated. Some of the generated radicals remained stable at ambient conditions for at least one day [30–32]. A similar behaviour was observed on zirconium dioxide, although it is a less reducible oxide than TiO_2. Photo-induced electron transfer is activated by irradiation of semiconductors to excite electrons in the conduction band, as described in the next Section.

Nanoparticles, metal complexes, enzymes, quinones or other sensitizers have been studied to increase the oxygen reduction efficiency. Visible light irradiation of TiO_2 in the presence of sensitizing compounds, like porphyrins or carotenoids was found effective in the formation of superoxide [33–35]. Another possible mechanism on oxides with basic properties, like MgO and ZrO_2, involves adsorbed hydrocarbons, inducing surface intermolecular electron transfer. Low-coordinate surface O^{2-}

ions are able to heterolitically split the hydrocarbon molecule forming a proton and a carbanion. The latter is unstable and readily reacts with O_2, transferring an electron to form $O_2^{\bullet-}$, which can be stabilized on a metal centre [30,36]. Finally, a further method to generate oxygen radicals on oxide surfaces is the treatment with a solution of hydrogen peroxide. H_2O_2 decomposes giving adsorbed superoxide and hydroxyl radicals, according to the above mentioned equilibria [30,36,37].

1.4. Heterogeneous photocatalysis

Photocatalysis describes the process of acceleration of a reaction occurring in the presence of a substance when it absorbs light quanta of sufficient energy [38,39]. A typical heterogeneous photocatalyst is a semiconductor, a material in which the electronic band structure has a valence band (VB), occupied by the electrons, and a conduction band (CB), theoretically empty, separated by a gap of forbidden energy (band gap) of limited width. The general mechanism of heterogeneous photocatalysis is shown in Figure 1.2.

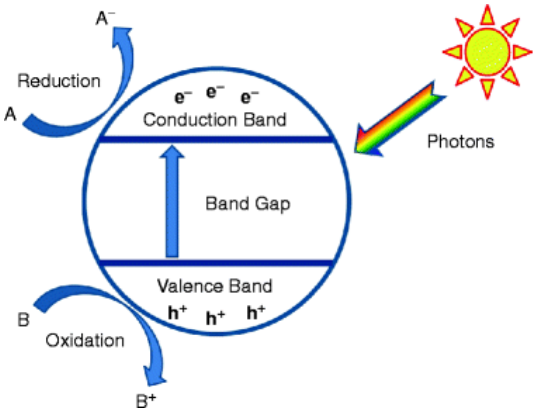

Figure 1.2. *Mechanism of heterogeneous photocatalysis through photoexcitation of a semiconductor particle.*

When light of higher energy than the band gap is absorbed by the semiconductor particle, electrons are excited from the valence to the conduction band, resulting in the formation of electron/hole pairs:

$$SC + h\nu \longrightarrow e^- + h^+ \qquad (1.6)$$

where SC is a generic semiconductor, e.g. TiO_2.

CB electrons and VB holes are strong reducing and oxidizing agents, respectively, which can reach the surface and initiate redox reactions of adsorbed acceptor or donor molecules. The photo-induced process involves different possible steps after excitation:

- charge carrier trapping;
- charge carrier recombination;
- interfacial charge transfer.

These steps and their different timescales have been observed by means of time-resolved spectroscopic techniques, such as photoluminescence, transient absorption, pump-probe diffuse reflectance, photoacoustic spectroscopy, laser flash photolysis, and by time-resolved microwave conductivity [15,16,39,40]. The following data refer to TiO_2, which is the object of most fundamental studies. Excitation is extremely fast, in the order of fs. The penetration depth of UV light in the material is limited (about 160 nm), so the e^-/h^+ pairs are generated in a relatively superficial region [15]. As the free e^- and h^+ "walk randomly" in the semiconductor bulk, they can be trapped, in the bulk or at the surface. A driving force for the migration towards the surface is due to the lower energy levels for trapped charge carriers at the surface than in the bulk, calculated by theoretical models [15]. Charge trapping takes place in timescales of 100 fs, then relaxation of e^- and h^+ to trap sites with energy deeper in the band gap can also occur, in the order of 100 ps [16]. Interfacial charge transfer, i.e. the transfer of e^- or h^+ to an adsorbed e^- acceptor or donor species, happens in variable time scales depending on the nature of the species: from about 300 ps for the oxidation of methanol by a hole to μs or ms. All these processes must compete with charge carrier recombination, that is, the deactivation of the electron by energy emission, by radiative or non-radiative (heat release) pathways. Actually, most of the photogenerated e^-/h^+ pairs (> 90 %) recombine, limiting the photonic efficiency, defined as the formation rate of reaction products divided by the incident photon flow, to relatively low values (< 10 %) [15]. The recombination process, though very relevant and frequently mentioned in the discussion on photocatalysis, is not known in details yet.

Charge carrier trapping is needed in a photocatalytic process to suppress recombination and increase the probability of interfacial charge transfer. Some data show that trapped carriers are also more efficient in charge transfer, for example the reduction of O_2 to superoxide $O_2^{\bullet-}$ ion is faster with a trapped rather than a free electron [16]. Theoretical and experimental studies predict bulk rather than surface trapping sites for electrons. A useful technique to trace trapped electrons and holes is electron paramagnetic resonance (EPR) spectroscopy, which identifies species with unpaired electrons. The primary traps for electrons in TiO_2 are Ti^{4+} ions, which can host an e^- giving Ti^{3+}; oxygen vacancies also have an important role as shallow electron traps. Hole trap sites are usually $O^{\bullet-}$ radicals, deriving from O^{2-} ions, either lattice or surface, or from surface hydroxyl groups. However, some charge traps may act as recombination centres: for example surface Ti^{4+}-OH groups can trap electrons, giving Ti^{3+}-OH species, which in turn can attract holes, causing recombination. The energy levels of shallow and deep charge trapping states have been evaluated by different methods. Electron trap states in TiO_2 materials

are generally found between 0.2 and 1 eV below the conduction band edge. Less data is available regarding hole traps: some works estimated states at 1.3 – 1.5 eV above the valence band edge for deeply trapped holes, while shallow trapped ones have short lifetimes and are easily excited thermally into the valence band, showing a comparable mobility and reactivity to free holes [16].

Photogenerated electrons and holes are able to reduce and oxidize a substrate either directly or indirectly, by means of reactive oxygen species (ROS) which are first produced. Holes, especially free or in shallow traps, can rapidly react with chemisorbed organic compounds, such as alcohols or carboxylic acids, producing an organic radical, which can then undergo further oxidation steps. The hydroxyl radical, $^{\bullet}OH$, is considered the most important ROS, generated by the reaction of adsorbed water or OH^- ion with a h^+:

$$H_2O_{(ads)} + h^+ \rightarrow {}^{\bullet}OH + H^+ \qquad (1.7)$$

Although the formation of $^{\bullet}OH$ has been confirmed by EPR spin trapping experiments, recent studies argued that its role in photocatalytic processes is overestimated. Alternative mechanisms have been proposed for $^{\bullet}OH$ generation as well as for photoxidation reactions, mediated by terminal oxygen radicals [15,16].

Photogenerated electrons are generally less available for direct reduction on the surface, also because they tend to relax from shallow to deeper traps with lower energy. In fact, TiO_2 is often modified to assist reduction reactions, for example by deposition of noble metal nanoparticles, as in the case of hydrogen production (see Section 1.4.2). Molecular oxygen is the primary e^- acceptor: the product is the superoxide radical anion, $O_2^{\bullet-}$, another important ROS:

$$O_2 + e^- \rightarrow O_2^{\bullet-} \qquad (1.8)$$

The function of superoxide was already discussed (Section 1.3.2). The other ROS that can play a role in photocatalytic processes include hydroperoxyl radical, $HO_2^{\bullet}$, hydrogen peroxide, H_2O_2, and singlet oxygen, $^1O_2$.

Besides TiO_2, a number of other semiconductors have been explored in terms of photocatalytic properties, including many other binary oxides, like ZnO, SnO_2, ZrO_2, Fe_2O_3, Cu_2O, Nb_2O_5, WO_3, sulfides like CdS and ZnS, ternary oxides like titanates ($CaTiO_3$, $BaTiO_3$, $SrTiO_3$), $AgPO_4$ or $BiVO_4$, and, recently, carbon-based materials, in particular graphitic carbon nitride (g-C_3N_4) [11,41].

Among the applications of photocatalysis, the two widest fields, environmental and energetic, will be addressed in the next sections.

1.4.1. Environmental applications

The growing concern about environmental pollution urges the research of new technologies for cleaning and removal of harmful substances and microorganisms from water and atmosphere. Some of the most investigated applications of photocatalysis head in this direction:

- degradation of water pollutants;
- purification of air and gas flows;
- elimination of bacteria and viruses;
- self-cleaning surfaces.

In the treatment of wastewaters, polluted surface or ground water, air and gas flows the chemical removal of undesired compounds occurs principally by oxidative degradation. Heterogeneous photocatalysis belongs to the advanced oxidations processes (AOP), presented in Section 1.3, and represent an efficient and attractive method, because it is able to degrade a variety of organic compounds, at ambient temperature and pressure, using generally only light and oxygen. A large number of organic compounds has been shown to decompose and often mineralize in aqueous environment in the presence of photocatalysts, in particular TiO_2: alkyl and aromatic hydrocarbons, including chlorinated ones, alcohols, carboxylic acids, phenols and derivatives, dyes, surfactants, pesticides, herbicides, polymers, pharmaceutical and cosmetic compounds and others. The list includes some endocrine disruptors, chemicals like polychlorobiphenyls, phthalates, bisphenol, which act on the hormonal system of mammalians, causing serious diseases. The activity is not restricted to organic pollutants: some toxic inorganic and metal ions can be reduced to less harmful species by photoexcited electrons, for instance nitrites, cyanides, Cr(VI), Hg(II), As(V) [12,38].

The commonly agreed mechanism for heterogeneous photocatalytic processes is of Langmuir-Hinshelwood type, involving the adsorption of reagents on the catalyst surface, the reaction on the surface and finally the desorption of the products, but alternative methods have been suggested as well. The degradation mechanisms are often complex and variable with the substrate and its interaction with the solid. Direct hole or electron transfer can occur, but generally reactive oxygen species mediate the initiation and propagation of the reactions.

Comparing the photocatalytic activities of materials studied by different research groups is not simple, since tests reported in literature are performed on different substrates, in various conditions, on TiO_2 materials with different crystallinity, morphology, chemical modifications etc. Photocatalytic reactions are sensible to several parameters, such as pH, which influences the surface charge of –OH groups, the adsorption equilibria and the stability of radicals; the intensity and wavelength of radiation; the concentration of catalyst; the presence of additional oxidants, like H_2O_2, ozone or

persulfates; the geometry and characteristics of the photoreactor [11,42,43]. Currently there is a tendency to use standard protocols to compare photocatalytic results, for example the degradation of phenol in given conditions. A parameter to quantify the photocatalytic activity of a material is quantum efficiency (or quantum yield), defined as the ratio between the reaction rate and the radiation absorption rate; however the absorption of radiation by the catalyst is difficult to determine, so the photonic efficiency (ratio between the reaction rate and the incident photon flow) is more often measured.

In the majority of laboratory experiments the material is used as suspension of powder or nanoparticles, thus a separation step through filtration or centrifugation is needed. In a practical application on industrial scale it is preferable to avoid this time and energy consuming step and opt for a continuous rather than a batch process, or at least an easier recovery of the catalyst for a subsequent reuse. A solution is the immobilization of the material on a support, for example glass, silica, alumina, zeolites, polymeric matrices or activated carbon, although this can cause a reduction of catalytic activity up to 60–70 %, related to the decrease of exposed surface area and mass transfer limitation [11,42]. Hence an important technological development is the production of stable surface coating on the desired support limiting the activity loss. Other issues to tackle in the scale-up for industrial applications are linked to the design of photoreactors, which must allow the maximum possible radiation intensity to reach uniformly the catalyst by means of appropriate lamps or, better, collectors to concentrate solar light.

In the last years TiO_2 has started to be employed on pilot and real scale for the depuration of wastewater, in particular industrial waste streams containing relevant amounts of some classes of chemicals. In a wastewater treatment plant photocatalytic oxidation can represent an alternative to established methods such as biological oxidation, which requests long times and controlled conditions for microorganisms, as they are might be sensitive to some toxic substances. It can be a convenient option especially for low-medium concentrations of toxic, persistent or recalcitrant compounds, difficult to decompose by other methods; moreover, photocatalysis can be combined with other physical, chemical and biological processes in order to enhance the overall efficiency of the treatment [16,42].

There is a potentiality also for the remediation of contaminated surface or groundwater, for instance by on-site techniques, involving pumping, treatment and reintroduction of water in the aquifer. However, the route towards a diffuse commercialization of efficient heterogeneous photocatalytic systems for water purification is still long and needs both chemical and engineering developments.

A relatively more mature technology is the purification and disinfection of air, especially indoor. Volatile organic compounds (VOC) are normally present in buildings, released by construction

materials and furniture, and are harmful for human health, as well as some bacteria that often contaminate public areas. In contrast to conventional filters, which simply catch the contaminants, photocatalytic filters can decompose organic substances and kill bacteria. This technology is applicable also for industrial effluent gases. Heterogeneous photocatalytic reaction in gas phase are similar in principle to those in liquid phase, but there are differences: the diffusion or reagents is favoured, oxygen is usually more abundant and seems to have a more relevant role, radiation absorption is increased, causing higher quantum yields [16]. On the other hand, the method is not appropriate for high flows and shows incomplete mineralization of some compounds, like aromatic and halogenated organics, with the risk of secondary pollution due to the products or catalyst deactivation. Deactivation is more pronounced than in liquid phase, since water contributes to the removal of species accumulated on the surface, but filters can be regenerated by a simple washing.

For the treatment of gas flows an adequate support for the photocatalyst is needed. Supports with high surface area or enhanced substrate adsorption have been shown to increase photocatalytic reaction rate and conversion. Other options are the use of layers of packed powder, porous 3D or honeycomb structures, or the choice of fluidized bed reactors.

Photocatalytic properties can be transferred to various surfaces producing thin coatings of active materials: self-cleaning surfaces have been obtained coating TiO_2 on glass, metal, plastic or concrete. Road pavements and building materials containing TiO_2 particles dispersed in their matrix have been tested for the abatement of NO_x and organic combustion products, in order to increase the quality of air in urban areas.

The ability of photocatalytic materials to eliminate bacteria is due to the generation of reactive oxygen species under irradiation. These attack and destroy the membranes and other components of the bacterial cells, leading to their death and decomposition [16,38]. The same effect was observed on viruses, algae and on cancer cells, with important potential in the phototherapy of tumours. The possibility to produce self-sterilizing surfaces, on which disinfection is induced by ambient light, is another promising perspective, especially for hospitals and clinics.

1.4.2. Energetic applications

The urgent need for renewable energy sources to power a sustainable development and cut the dependence on fossil fuels focuses huge research efforts on the exploitation of solar energy. Sunlight represents the largest continuous energy source available on Earth. Photocatalytic semiconductors are investigated for three main applications in the energetic field:

- hydrogen production by water splitting in photoelectrochemical cells or photoreactors;

- carbon-based fuels production by carbon dioxide reduction;
- electrical energy generation in photovoltaic solar cells.

Hydrogen obtained from water and simple carbon fuels (methane, methanol, ethanol) produced from CO_2 are often called "solar fuels". In water splitting and CO_2 reduction photon energy is converted into chemical energy, with largely positive changes in Gibbs free energy. These energetically uphill processes resemble photosynthesis performed by plants, where CO_2, H_2O and sunlight are used to produce organic matter carrying high loads of energy, therefore they can be regarded as examples of "artificial photosynthesis" [44].

In water splitting electrons and holes photogenerated in a semiconductor react with H_2O molecules, reducing hydrogen to H_2 and oxidizing oxygen to O_2, according to the following semireactions:

$$H^+ + e^- \longrightarrow \frac{1}{2}H_2 \qquad (E° = 0 \text{ V vs NHE}) \qquad (1.9)$$

$$H_2O \longrightarrow 2\,H^+ + \frac{1}{2}O_2 + 2e^- \qquad (E° = 1.23 \text{ V vs NHE}) \qquad (1.10)$$

A first requirement for a semiconductor to perform this reaction is an electronic structure with the bottom level of the CB more negative than $E°(H^+/H_2)$ and the upper edge of the VB more positive than $E°(O_2/H_2O)$. This thermodynamic prerequisite excludes numerous semiconductors from being considered for water splitting, unless their band edges are shifted by means of some chemical modifications. Other factors affecting the efficiency are the separation, mobility and lifetime of charge carriers, crystallinity, surface electronic states, surface area and active sites of the material. Several limitations can be individuated: the largely positive $\Delta G = +237$ kJ mol^{-1} for the overall reaction, the generation of O_2 involving 4 electrons, the easy surface back reaction between evolved H_2 and O_2, along with the rapid recombination of e^-/h^+ pairs and the lack of stability of the catalyst in the process conditions (e.g. due to the changes in the solution pH occurring during the reaction). All these issues cause relatively low quantum yields of water splitting systems and insufficient utilization of visible light, despite the large number of works devoted to find optimal water splitting photocatalysts [44].

To improve the efficiency sacrificial agents are often added to the solution, working as an external driving force for the surface redox reactions: electron donors, easily oxidizable, such as methanol, other alcohols or aldehydes, collect holes rapidly and irreversibly, leaving an excess of electrons on the photocatalyst and enhancing H_2 evolution; alternatively, electron acceptors, such as Ag^+ or Fe^{3+}, rapidly consume photogenerated electrons, enhancing O_2 evolution [12,44]. With organic substrates photocatalytic reforming (or photoreforming) can be achieved, with more favourable thermodynamics, using for instance biomass derived compounds (sugars, glycerol, ethanol). Since the reduction is usually the rate-limiting side of the process on TiO_2, metal nanoparticles, in particular Pt,

are frequently deposited on the surface as they collect conduction band electrons resulting as active sites for the reduction.

1.5. Chemical modifications of TiO_2 for enhanced photoactivity

Some shortcomings limit the efficiency and applicability of TiO_2 in photocatalytic and related processes. One of these is the limited harvesting of solar radiation, due to the electronic structure of the material. The band gap energies of anatase and rutile polymorphs, about 3.2 and 3.0 eV respectively, correspond to absorption onsets at 387 and 413 nm, meaning that light absorption is restricted to the UV region. UV radiation constitutes a small fraction (< 5 %) of the solar spectrum, while about 45 % of the spectrum is visible light and the remaining is infrared radiation. Therefore, great efforts have been made to extend the responsivity of TiO_2 to visible light, to achieve a more effective exploitation of solar radiation or artificial light.

Another drawback of TiO_2 is the fast recombination of photogenerated charge carriers, which reduces the quantum efficiency of a photocatalytic reaction or the photoconversion efficiency of a TiO_2-based solar cell. Recombination is normally facilitated by bulk or surface defects and impurities [39]. The surface and bulk modification of TiO_2 structure brings about changes in its electronic structure, with effects on the optical absorption and charge separation lifetime. Band gap engineering allows also some tuning of conduction and valence band edge potentials, making the material more suitable for certain redox reactions. Various methods for TiO_2 modification and functionalization have been explored [38,39,45–47]:

- doping with metals and/or non-metals;
- deposition of metal nanoparticles;
- formation of heterojunctions with other semiconductors;
- photosensitization by dyes or charge transfer complexes;
- introduction of non-stoichiometry and defects.

The last two methods, photosensitization and induced defectivity, are closely related to the present work and are discussed in the following.

Another aspect, particularly relevant in the degradation of organic pollutants, is the relatively low affinity of TiO_2 surface for organic compounds, especially hydrophobic ones. Their low adsorption causes mass transfer limitations which slow down the overall reaction kinetics. An increase of surface affinity and selectivity toward some substrates can be achieved by morphological modifications, for example different nanostructures, different crystal phase or exposed crystal facets, a higher surface area and pore distribution. Surface hydroxylation, i.e. the density of –OH groups, plays a role as well. Improvements have also been obtained by surface modification with organic compounds or carbon-based nanomaterials [48].

Besides, the use of nanoparticles for reactions in water carries some issues: their tendency to aggregate may hamper light incidence on the surface and active sites availability, and their difficult recovery from the reaction system imposes economic and safety concerns. To overcome these issues the immobilization of nanoparticles on suitable substrates, either inorganic or polymeric, has been tested, although it can cause a decrease in photocatalytic efficiency. Another attractive approach to facilitate the separation of nanoparticles from the reaction mixture is the synthesis of magnetic nanomaterials, often with a core-shell structure, coupling the photoactive semiconductor with iron oxides [48].

1.5.1. Photosensitization

The sensitization of a semiconductor allows the generation of photocurrent, namely the transfer of electrons in the conduction band, following the absorption of radiation with energy lower than the band gap. Various materials can act as photosensitizers: organic compounds, organometallic compounds, metals or semiconductors with narrower band gap. The most common overall mechanism comprises the transfer of an electron from the ground state (HOMO) of the sensitizer to the TiO_2 conduction band by visible light absorption. Such photoinduced charge injection can be realised in two different ways, as illustrated in Scheme 1.2 [46,47]:

- indirect photosensitization: a two-step process, involving the excitation of an electron from the HOMO to the LUMO (excited state) of the sensitizer, and consecutive transfer to the CB;
- direct (also known as *type II* or *ligand-to-metal charge transfer*) photosensitization: single step excitation of an electron from the ground state of the sensitizer to the CB (optical electron transfer).

The former mechanism has been long studied and is obtained with visible light absorbing dyes: these are organic compounds, often containing aromatic and heterocyclic rings, or transition metal complexes with porphyrin, polypyridine, phtalocyanin or similar ligands.

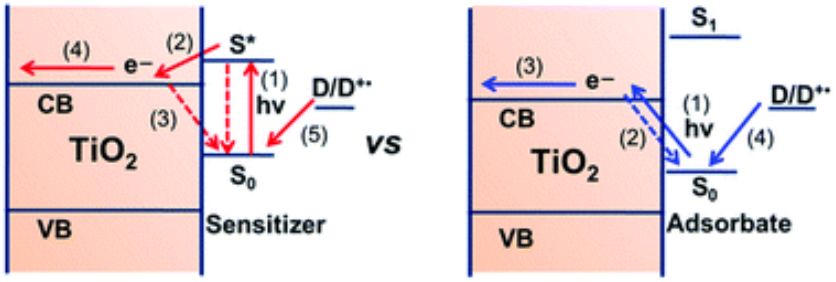

Scheme 1.2. *Illustration of two types of visible light activation of TiO_2: indirect dye sensitization (left) and direct ligand-to-metal charge transfer (LMCT) sensitization (right). The arrows indicate the possible involved electron paths: excitation of the dye, injection to the conduction band, recombination, electron transfer to an acceptor, regeneration of the sensitizer by an electron donor (D).*

Indirect sensitization is the working principle of dye-sensitized solar cells (DSSC). Electron injection occurs in the femtosecond scale, much faster than the recombination (back electron transfer). An electron donor in the reaction system can regenerate the initial state of the sensitizer. This role is covered by a I^-/I_3^- redox pair in a typical DSSC. Anyway, the stability of the dye, which can undergo self-degradation after electron transfer, is one of the major issues of dye sensitization [39]. Another disadvantage is the high cost and toxicity of some effective dye complexes, based on metals like Ru. Therefore novel metal-free dyes have been recently studied.

The direct photosensitization mechanism, elucidated only in the last years, makes use of compounds which do not absorb visible light on their own. When they are chemically adsorbed on the surface of TiO_2, giving a sufficient degree of electronic coupling between the molecular orbitals of the adsorbate and the energy levels of the semiconductor's bands, a direct electron injection can occur, without the involvement of the excited state of the molecule, as shown in Scheme 1.2. The process is called ligand-to-metal (or ligand-to-band) charge transfer (LMCT). In this case the electron transfer results more efficient than in dye sensitization, but also the back electron transfer can be facilitated [46,47].

Different classes of compounds, including small organic molecules, are able to form charge transfer complexes on TiO_2 surface, significantly extending its light absorption: catechol and derivatives are the most studied, but also carboxylic acids, diketones and inorganic metal complexes (e.g. hexacyanoferrate, $[Fe(CN)_6]^{4-}$) have been shown to have this property. The establishment of a strong electronic coupling is favoured in case of electron-rich ligands with suitable functional groups to form stable interactions, such as bidentate coordination, with surface Ti atoms [46]. Interesting results were obtained with polymerised ligands, for example phenolic resins, which are more stable due to the numerous bonds formed with the surface and their insolubility in water. Visible light induced charge transfer was also observed with compounds only physically adsorbed on TiO_2 surface, such as some polycyclic aromatic hydrocarbons and non-ionic surfactants with polyoxyethylene structure [47]. As

in the case of dyes, the oxidized ligand after charge transfer can be reduced again by an available electron donor, or undergo further reactions on the oxide surface leading to its degradation. Direct photosensitization offers some advantages, primarily the use of cheaper and more stable compounds than dyes. While its application in solar cells is not competitive with dye sensitization yet, the perspectives for pollutants degradation are promising.

1.5.2. Defectivity

Imperfections within the crystal structure significantly affect the electronic structure, light absorption, phase stability, charge transport and photochemical properties of TiO_2. Oxygen vacancies are the main lattice defects in many metal oxides. They are relevant adsorption and active sites, strongly influencing the reactivity of oxide surface in heterogeneous catalysis, especially in redox processes, and are believed to affect the electron–hole recombination rates in photocatalysts.

A missing oxygen atom from the bulk or surface of TiO_2 formally results in two electrons localized in a V_O state, taking the place occupied by the O^{2-} anion in the regular lattice. The formation of an oxygen vacancy (V_O) can be described by the following equilibrium [49]:

$$O^{2-}_{(\text{lattice})} \rightleftarrows V_O + \frac{1}{2}O_{2(g)} + 2e^- \qquad (1.11)$$

The reversibility of this process is shown by the slow disappearance of V_O observed in TiO_2 samples exposed to air. The electrons located in the V_O state form a partially occupied energy level located about 0.7–1.2 eV below the conduction band. Electrons can be excited to the V_O states from the VB with the energy of visible light, which gives rise to transitions in the visible region of the spectrum. For this reason, oxygen vacancies are called F centres, from *Farbe*, the German word for colour. Moreover, the excess electrons can be redistributed among the neighbouring Ti atoms around the V_O site, forming reduced Ti^{3+} centres. These are associated with shallow electron donor states below the conduction band, originating from Ti 3d orbitals. Ti^{3+} ions can therefore act as n-type dopants, and the shallow donor levels introduced are also responsible for wide visible light absorption bands [49–51].

After the report of a hydrogenated black TiO_2, with a strongly narrowed band gap and a remarkable visible light photocatalytic activity [52], wide interested has been aroused for the synthesis of self-doped or defective titanium oxide, featuring Ti^{3+}/V_O or H-doping. These materials are often referred to as “black titania” because of the resulting dark coloration (blue, grey or black).

Besides hydrogenation, different methods have been tested for the reduction of TiO_2 surface by thermal treatments [50,51,53]:

- reducing atmosphere (Ar, N_2);
- metal reductants (Al, Mg, Zn);
- organic (imidazole) or inorganic ($NaBH_4$) reductants;
- high energy treatments (plasma, electron beam).

Many other strategies were proposed for the synthesis of black titania nanomaterials: electrochemical reduction, ultrasonication, laser irradiation, synthesis by oxidation of TiH_2 or elemental Ti.

Each method developed for the synthesis of these materials have its own effect on their morphology, optical and functional properties, so that an appropriate method can be designed according to the desired properties. The introduction of defects modifies also the crystalline structure of TiO_2, as a disordered amorphous outer layer is often observed on crystalline nanoparticles and a rearrangement of the Ti-O bond length around the vacancy site occurs. The disordered surface structure is believed to be responsible for tails induced in the valence and conduction band states, related to the observed band gap narrowing. A suppressed electron-hole recombination is often reported and explained with the trapping of charge carriers in the mid-gap states, the increased concentration of electron donors and other factors [50,51,53].

Most of the works on black TiO_2 reports activity data in the typical photocatalytic reactions: degradation of dyes or other organics and water splitting. However, the remarkable solar light harvesting ability of these materials, extending to the visible and infrared range, and the modified electronic properties, have suggested other possible applications, such as solar cells, supercapacitors, batteries, microwave absorption and photothermal and photodynamic theranostics [50,51,53]. Some hydrogenated TiO_2 samples showed also interesting catalytic activity at room temperature, without light irradiation, for example in ethylene polymerization. This is probably related to the abundant surface defects [50].

A potential limitation of these materials is the stability of surface reduction, particularly in the presence of H-doping, since some samples were shown to be gradually reoxidized in contact with air, even in mild conditions. The ability to tune the type and density of defects in TiO_2 structure would allow to control their properties for specific applications. Despite the variety of experimental and theoretical work done, there are still open questions regarding the distribution and effects of different defects.

1.6. Sol-gel method in the synthesis of metal oxides

Many different techniques are available for the synthesis of metal oxides. Chemical synthesis methods from solution, such as sol-gel, hydrothermal, co-precipitation and microemulsion methods, are frequently preferred over other types of processes (e.g. solid state sintering, chemical or physical vapour deposition, spray pyrolysis, electrochemical methods), because they offer a high control over the properties of the product, simple procedures and mild operating conditions. In particular, the sol-gel technology allows to prepare various ceramic and glass materials with several advantages:

- control on the homogeneity, purity and composition up to the molecular scale,
- controlled particle size and morphology,
- possible addition of templates, structure-directing agents or dopants,
- low processing temperature.

The method involves the transition from a sol to a solid gel phase. A sol is a colloidal suspension of particles in the range of 1–1000 nm. It forms by hydrolysis and polycondensation reactions of metal precursors, usually metal alkoxide complexes or inorganic salts. Polycondensation reactions induce the growth of oligomers which begin to aggregate forming bonds randomly, finally resulting in a gel. A gel can therefore be generally defined as a continuous solid skeleton enclosing a continuous liquid phase [54] or as an interconnected, non-fluid three-dimensional network that extends through a fluid phase [55].

A classification of five different gel types was proposed by Kakihana in 1996 [55]:

- colloidal gel: particles connected by Van der Waals or hydrogen bonds;
- metal-oxane polymer: inorganic polymers interconnected via covalent or intermolecular bonding;
- metal complex gel: weakly interconnected metal complexes;
- polymer complex I, in situ polymerizable complex (Pechini method);
- polymer complex II, coordinating and crosslinking polymers.

During gel formation (gelation), the clusters present in the sol phase progressively become connected to the network and both the viscosity and stiffness of the system increase, until the elastic modulus becomes higher than the viscous modulus (a moment often considered as the gel point).

The sol-gel process is a versatile wet chemical route to produce ceramic and glass materials in a wide variety of forms:

- *xerogels (*dried gels*)*, obtained through evaporation of the liquid in a wet gel under normal conditions, accompanied by shrinking, with a several times smaller final volume;
- *aerogels,* with an extremely low density and high porosity, produced by removal of the solvent in a wet gel under supercritical condition, in autoclave;
- *ambigels*, similar to aerogels, but produced by ambient pressure drying in specific conditions;
- *monolithic materials*, by letting gelation occur in shaped containers and limiting the shrinking during drying;
- dense ceramic or glass materials, generated by successive thermal treatments;
- ceramic fibres, drawn adjusting the viscosity of the sol into a suitable viscosity range;
- ultra-fine and uniform ceramic powders, formed by precipitation, spray pyrolysis, or emulsion techniques.

Furthermore, thin films or porous membranes can be produced starting from sols, by means of techniques such as spin coating, dip coating or spray coating. Spin coating, used in the present work, is described in Section 1.6.2. An overview of the sol-gel process is illustrated in Scheme 1.3.

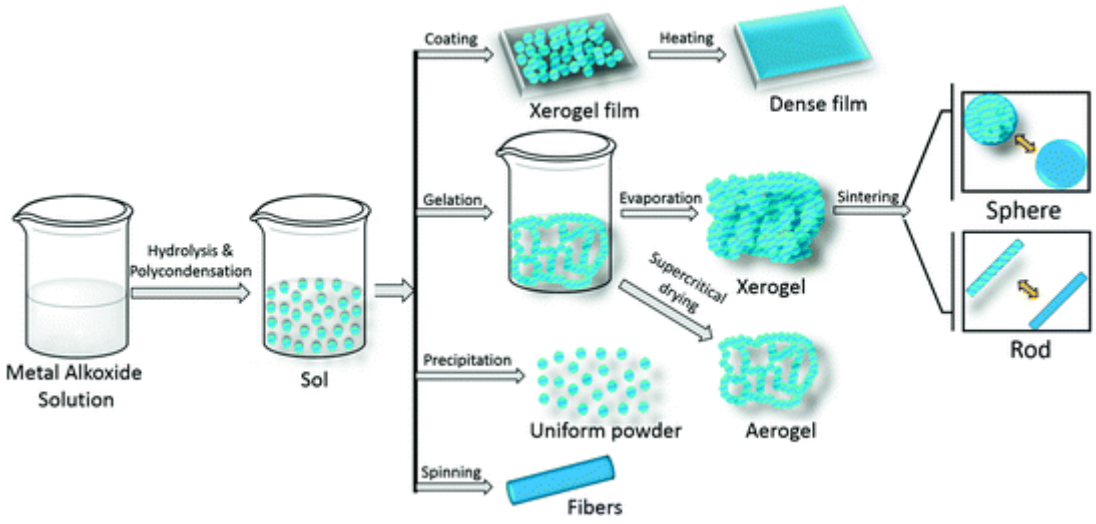

Scheme 1.3. *Schematic representation of the sol-gel process with the different obtainable products* [56].

Sol-gel synthesis process allows modulating the microstructure, morphological and textural properties of the final materials by means of the processing parameters (i.e. precursor concentration, water/metal molar ratio, temperature, pH of the reaction medium). For mixed oxides the products obtained are characterized by a high dispersion of the minor component in the matrix of the major phase on nanometric scale.

Metal alkoxides, with general formula $M(OR)_x$, are the most commonly used starting precursors. They exhibit useful properties to control the chemical synthesis of oxides, as the easy purification by distillation and the variety of available alkyl groups available, including mixed alkoxides, allowing a fine tuning of the reactivity in hydrolysis and condensation reactions. For multi-component systems, the choice of the molecular precursors plays a key role in the synthesis procedure. Actually, in order to obtain homogeneous sols, suitable molecular precursors with comparable hydrolysis rates should be used. In this way, cross-linking between clusters of different components with similar size will take place allowing gelation instead of precipitation or co-precipitation. In the former case, gels comprising permanent covalent bonds (chemical gels) are obtained, while in the latter, particulate gels, i.e. gels where temporary o reversible bonds connect the clusters, are formed (physical gels).

In the hydrolytic sol-gel method, the sol-gel transition involves two key steps: hydrolysis and polycondensation. Generally, hydrolysis is started by the addition of small amounts of water. When the precursors are insoluble in water, non-aqueous solvents such as alcohols are added to the reaction medium to form a homogeneous solution.

In the hydrolysis reaction, the alkoxide groups (OR) are replaced stepwise by hydroxyl groups by nucleophilic substitution (S_N, Scheme 1.4). The hydrolysis rate is determined by many factors. It is facilitated by the increase of the charge density on the metal and the number of metal ions bridged by an hydroxo- or oxo-ligand (M-OH, M=O). Hydrolysis is inhibited when the number of hydroxo-ligands coordinating the metal increases. The temperature, pH, amount of solvent, water/metal alkoxide molar ratio (hydrolysis ratio) can influence both the hydrolysis and condensation reactions. Fast hydrolysis rates are generally observed with metal alkoxides, more acidic and more susceptible to nucleophilic attack than non-metal (e.g., silicon) alkoxides [54,55,57].

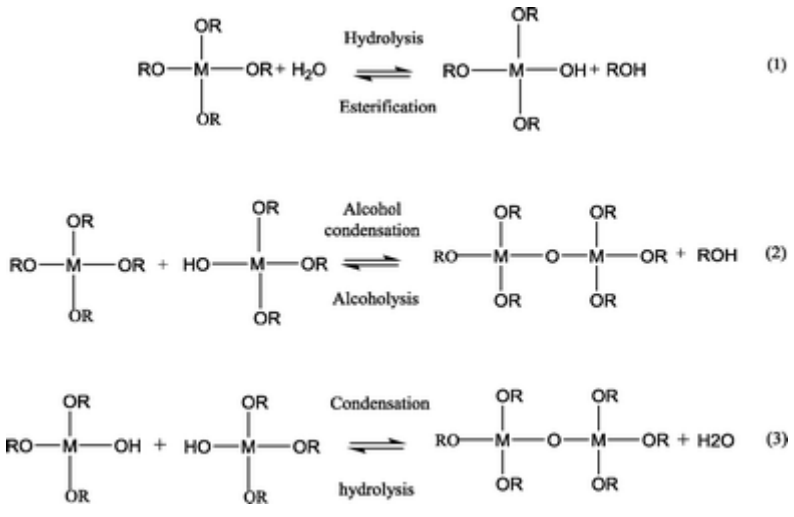

Scheme 1.4. *Key reactions of hydrolytic sol-gel process*

Condensation reactions can proceed by two mechanisms, depending on the coordination of the metal: when the preferred coordination is satisfied, condensation occurs by nucleophilic substitution (S_N, Scheme 1.4); if there are available coordination sites, condensation can occur by nucleophilic addition.

According to the partial charge model (two atoms combine giving a charge transfer so that each atom acquires a partial positive or negative charge), three different predominant species are formed depending on pH and the metal oxidation state: oxo-ions, $[MO_N]^{(2N-z)-}$, hydroxo-ions, $[M(OH)_N]^{(N-z)-}$, and aquo-ions, $[M(OH_2)_N]^{z+}$ (where *N* is the coordination number and *z* is the oxidation number). When the coordination number of the metal is greater than its charge (N-z > 0), condensation can occur by olation, during which the formation of a hydroxyl bridge (>OH) between two metal centres takes place. For coordinatively saturated hydroxo-aquo precursors, olation occurs by a S_N mechanism where the hydroxyl group is the nucleophile and H_2O is the leaving group. Therefore, the kinetics of olation is related to the ability to dissociate of the aquo ligand, which depends on size, electronegativity and the electronic configuration of metal.

The condensation reactions can also occur by oxolation, in which an oxo bridge (-O-) is formed between two metal centres. Oxolation occurs over a wider range of pH than olation, kinetics is usually slower. The thermodynamics of these reactions is governed by the strength of the entering nucleophile, the electrophilicity of the metal, and the partial charge and stability of the leaving group. Instead, the kinetics depends on the extent of coordinative insaturation of the metal (N-z) and the transfer ability of the proton.

Another factor that influences reaction kinetics is the extent of oligomerization (molecular complexity) of the metal alkoxides. The molecular complexity depends on both the nature of the metal atom and alkoxide ligand. The hydrolysis rate decreases with the alkyl chain length consistent with the steric effect expected for an associative S_N reaction mechanism. The alkyl chain also influences the morphology (particle size and surface area) and the crystallization behaviour of the resulting gel.

The hydrolysis and condensation rates are influenced by acid or basic catalysis. Acid catalysts can be used to protonate negatively charged alkoxide groups, producing good leaving groups. The resulting polymers are more extended and less branched. On the contrary, alkaline conditions produce strong nucleophiles via deprotonation of hydroxo ligands, leading to more compact and highly branched species [54,57].

The choice of the solvent also influences the kinetics and the resulting structure. Generally, the formation of alkoxy-bridging occurs in nonpolar and aprotic solvents, allowing the hydrolysis control and the formation of homogeneous gels; whereas, a rapid hydrolysis occurs in polar and protic solvent, giving highly condensed products and precipitates.

The gelation time depends on many factors: it decreases with an increase of the hydrolysis ratio, temperature, concentration and size of the alkoxide. After gelation, the chemical reactions carry on in the period called "aging" of the gel. During the aging process, therefore, many changes occur in the structure and properties of gels. These changes can be categorized as:

- *polymerization,* an increase in connectivity of the network produced by condensation reactions slowly occurring at room temperature;
- *syneresis,* a shrinkage of the gel network resulting in expulsion of liquid from the pores, caused by the same condensation reactions;
- *coarsening* or *ripening,* a process which consists in the growth of aggregates in aqueous conditions, starting from small primary particles restructured through dissolution-reprecipitation, resulting in the formation of larger and more stable particles.

Finally, to obtain a xerogel, the wet gel is subjected to specific heating treatments to avoid further modifications in the structure of the synthesized material. The removal of solvent occurs in several phases; initially, it is carried out with a constant evaporation rate during the which the volume reduction is evident. In this phase, same cracks can be formed. Then, the evaporation is carried on more slowly due to capillary pressure into the pores caused by several factors, such as temperature differences inside and outside the gel, the surface tension and the vapour pressure.

1.6.1. Role of organic ligands

Frequently, the reactivity of metal alkoxides towards water needs to be controlled, in order to achieve cross-linking between clusters and gelation instead of precipitation. This is the case of titanium alkoxides, $Ti(OR)_4$, which show a very high reactivity toward the hydrolysis and condensation reactions due to the high polarity of Ti-O bond, generating a positive partial charge on the Ti atom and making it very susceptible to nucleophilic attack. Chemical additives can be added during the synthesis procedure with the aim to moderate the reaction rate of the alkoxide. Complexing organic ligands (CL) are commonly used, in particular bidentate ligands able to form strong bridging or chelating coordination bonds with titanium. Widely studied examples are β-diketones, such as acetylacetone, and carboxylic acids, such as acetic or citric acid [54,55,57–59].

Metal alkoxides are Lewis acids, able to interact with compounds having a lone electron pair to increase their coordination. Bidentate ligands can react with them through nucleophilic substitution or addition, with the subsequent increase of coordination number. The reaction can be schematically written as follows, if CL-H is the complexing ligand and CL its deprotonated form:

$$M(OR)_n + x\,CL - H \rightleftarrows M(OR)_{n-x}(CL)_x + x\,ROH \qquad (1.12)$$

The heteroleptic compounds formed are new precursors having a different reactivity than the unmodified alkoxides. Their stability is determined by the equilibrium constant of the formation reaction. Multidentate ligands are more strongly bonded than monodentate ligands because of the chelate effect, therefore the stability constant of the corresponding complexes is higher. As a result, multidentate ligands are less readily hydrolysed than the remaining OR groups upon sol-gel processing. Although a partial cleavage of the M-CL bond normally cannot be avoided due to the coordination equilibrium, a substantial fraction of the CL can be retained in the obtained gels.

The replacement of one or more OR groups by CL has several consequences for the sol-gel processing:

- the degree of cross-linking of the gel network is decreased, because of the smaller fraction of hydrolysable OR groups;
- the substitution with multidentate ligands lowers the connectivity of the molecular building blocks, thus favouring the formation of gels instead of crystalline precipitates;
- the polarity variation by the organic groups has probably a similar effect on the network structure as changing the polarity of the solvent, affecting the formation of hydrogen bonds, important in the network structure;
- the complexing ligands may stereochemically direct the hydrolysis and condensation reactions because inductive effects give the site *trans* to an organic group a different reactivity than the *cis* sites.

A first mechanism proposed to explain the sol stabilization, is based on the hypothesis that a kinetic control is exerted by the modifying chelating ligand on hydrolysis and polycondensation reactions of metal alkoxides. According to this mechanism, chelating ligands block the coordination sites of ions such as Ti^{4+}, decreasing their rate of hydrolysis and condensation [60].

A quite different interpretation was suggested more recently by Kessler et al. [61,62]. They showed that the hydrolysis and polycondensation of titanium and zirconium alkoxides are actually facilitated by their chemical modification, that the reactions have thermodynamic rather than kinetic control, and their kinetics is not directly related with the sol-gel transition. The complexing ligands show high mobility and their exchange results favoured in protic solvents. Moreover, they increase the charge distribution in the complexes. As a consequence, chelating ligands increase the rate of hydrolysis and polycondensation, producing oxo-alkoxy oligomeric species. They apparently serve as nuclei for the growth of larger aggregates that, once reached a certain size (2-5 nm) become phase separated. These nanoparticles are formed by oxo-clusters (core) containing ligands on the surface (shell), exhibiting a structure typical of micelles, so they are called by the authors “micelles templated by self-assembly of ligands”. The stabilization of the sol is a consequence of the interfacial activity of these micelles. In

conclusion, if there are enough favourable interactions between the primary particles (including oxygen bridges and hydrogen bonding) and between the ligands and the solvent, and if hydrolysis is not too fast, the particles can aggregate, develop common surface and finally lead to the formation of a uniform gel [61,62].

The control of hydrolysis rate is very important when multi-component systems (mixed oxides) are prepared. In fact, the choice of molecular precursors with comparable hydrolysis rates plays a key role in obtaining homogeneous sols in which cross-linking is preferred to self-condensation.

Besides controlling the reactivity of the metal alkoxides and the network structure of the obtained gels, the bidentate ligands can also be used to introduce functional organic groups into gels by means of appropriately substituted derivatives.

1.6.2. Spin coating

Spin coating is a fast and practical method for the deposition of uniform films on flat substrates. The process can be divided into the following four stages, illustrated in Figure 1.3.

1. Deposition: an excess of liquid (for example a sol, a polymer solution or a suspension of nanoparticles) is dispensed on the substrate. The deposition mode can be static, on a still substrate, or dynamic, on the substrate already in rotation.
2. Spin-up: the spinning accelerates up to the set spin rate; the liquid flows radially outward, driven by centrifugal force.
3. Spin-off: the spinning proceeds at constant rate, excess liquid flows to the perimeter and leaves as droplets. Contemporarily the thickness of the layer gradually decreases. As the films thins, the rate of removal of excess liquid slows down, because the thinner the film, the greater the resistance to flow, and because the concentration of the non-volatile components increases due to evaporation of the solvent, raising the viscosity.
4. Evaporation: as the spinning proceeds, the evaporation of the volatile solvent takes over as the primary mechanism of thinning. Evaporation may accompany all the other stages; it controls the thinning until the final thickness is reached.

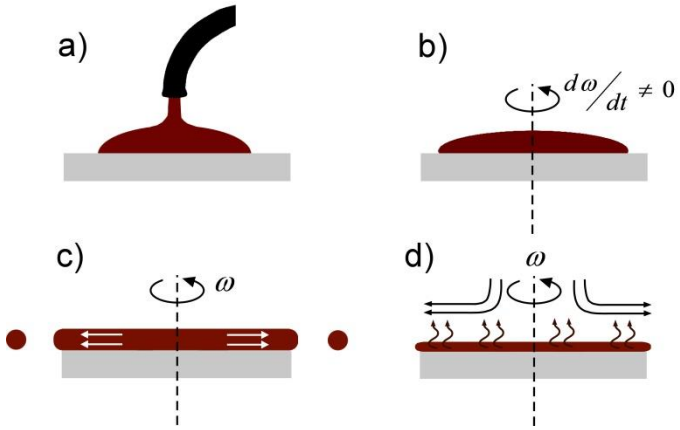

Figure 1.3. *The four main stages of spin coating: a) deposition of the solution; b) spin-up; c) spin-off; d) evaporation of the solvent.*

During spin-off, the layer tends to become uniform in thickness and to remain uniform, provided that the viscosity is not shear dependent and does not vary over the substrate. This tendency arises from the balance between the two main opposing forces: centrifugal force, which drives the flow radially outward, and viscous force (friction), which acts radially inward.

When spin coating is coupled with sol-gel, for example in the synthesis of metal oxide thin films, the evaporation of the solvent induces rapid gelation of the coated material, producing a gel film. It is usually amorphous and still contains a large amount of solvent, so a thermal treatment is performed to obtain a dense and possibly crystalline coating. Compared to dip coating, another common technique used in combination with sol-gel, spin coating has some advantages, such as a higher uniformity of the layer's thickness, the coverage of a single surface and a lower amount of stock solution needed.

Several chemical features of the sol influence the processing by spinning, similarly as in sol-gel processing. The precursor structure and concentration determines not only the reactivity, so the degree of polymerization obtained, but also the viscosity of the solution, and in turn the film thickness, and the interaction with the substrate material. The volatility of the solvent affects its evaporation rate, and therefore the structure of the film. The surface morphology and porosity can be tuned by the addition of templating agents. In general, many properties of the coatings can be tuned by a careful control of the operating parameters.

- CHAPTER 2 -

EXPERIMENTAL METHODS

2.1. Sol-gel synthesis

All the materials based on titanium dioxide studied in the present work were synthesized by sol-gel method in the laboratories of the Department of Chemical, Materials and Production Engineering of the University of Naples Federico II.

The reagents used in the syntheses are the following: Ti(IV) n-butoxide (97+%), 1-propanol (99.8+%), acetylacetone (acacH, 2,4-pentanedione, 99+%), dibenzoylmethane (dbm, 1,3-diphenyl-1,3-propanedione, 98%), citric acid monohydrate (99.0%), acetic acid (99%), catechol (1,2-dihydroxybenzene, 99%), dopamine hydrochloride (99%), L-ascorbic acid (99%), diethanolamine (dea, 98+%), cyclohexane (99.5%), ethanol (99.8+%), hydrochloric acid (37 wt%), ammonium hydroxide (28%). All the reagents were purchased by Sigma-Aldrich and used as received. Deionized (bidistilled) water was used in all the experimental stages.

The general procedure followed for the synthesis of the TiO_2 hybrid materials is illustrated in Scheme 2.1. In a typical synthesis, the desired amount of titanium(IV) n-butoxide, $Ti(OBu)_4$, is transferred to a conical Erlenmeyer flask, operating under a glove-box because of the high sensitivity of $Ti(OBu)_4$ to atmospheric moisture, which causes its rapid hydrolysis. The flask is closed and placed on a magnetic stirring plate under a fumehood, at room temperature. The organic ligand chosen is then added to $Ti(OBu)_4$ to obtain the desired complexation ratio (ligand/Ti molar ratio). It is added directly, if liquid

at room temperature, as in the case of acetylacetone, or after dissolution in a proper volume of organic solvent (usually 1-propanol), if it is in solid state. Complexation of Ti^{4+} ions by the organic ligands added is fast and often observable as a change of coloration of the solution from the pale yellow of $Ti(OBu)_4$ to a more intense yellow, orange or red colour, depending on the ligand and its concentration. Some of the organic ligands used (in particular citric acid and L-ascorbic acid) are poorly soluble in alcohol. When a higher amount of these ligands is used, to avoid the need for an excessive volume of solvent, the mixture containing the ligand is added to $Ti(OBu)_4$ even if dissolution is not completed. Then the advancement of the complexation with Ti^{4+} shifts the heterogeneous equilibrium of the ligand towards the liquid phase and the dissolution is completed in a few minutes.

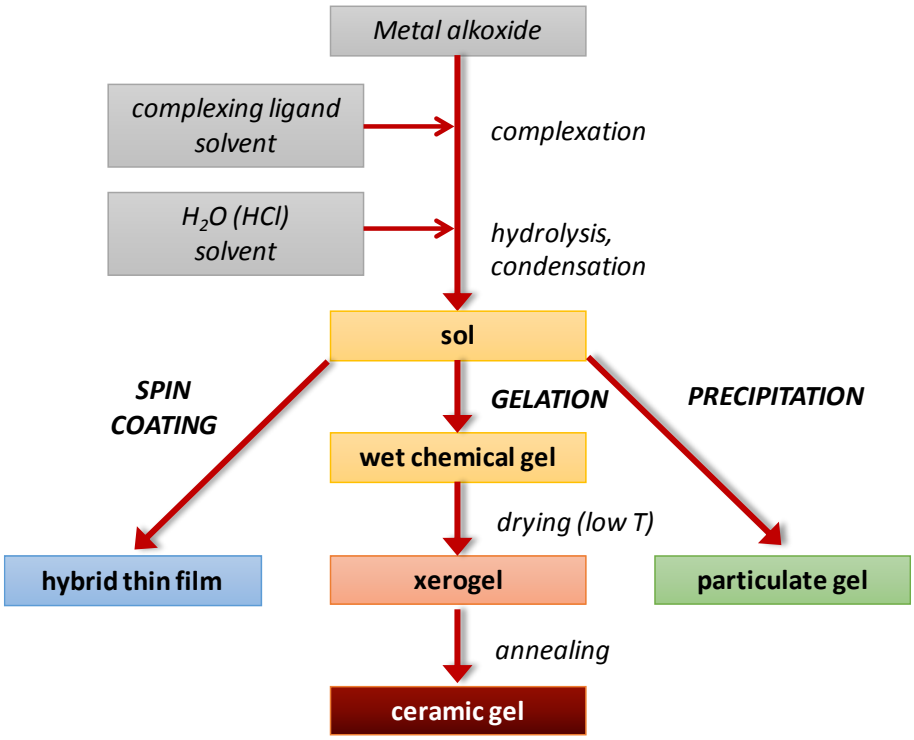

***Scheme 2.1**. General sol-gel procedure adopted in the present work, with the different possible outcomes.*

The homogeneous solution is continuously stirred for some time (about 15 min), while the hydrolytic solution is prepared, composed of deionized H_2O, a fraction of organic solvent, and a precise amount of HCl or NH_4OH when the effect of an acid or a base is tested. Water is diluted in the solvent to avoid local high concentrations of water during the addition, which could turn into non-uniform hydrolysis. The hydrolytic solution is slowly, or even dropwise, added to the reaction mixture, under intense stirring. Once the hydrolysis and condensation reactions start, a sol (colloidal dispersion of molecular aggregates) forms and the evolution of the system depends totally on the operating conditions, namely:

- nature and concentration of the complexing ligand,
- concentration of Ti precursor,
- concentration of water,
- type of solvent,
- temperature.

The effect of temperature was marginally assessed only on the TiO_2-acetylacetone system, but all the other syntheses were performed at room temperature to make the process simpler and less energy demanding. Depending to the other above mentioned parameters, different outcomes were obtained: precipitation is the usual result when no complexing ligand is added to the titanium precursor, but hybrid particulates were also obtained; gelation is the principal aim in this work, owing to the advantages of chemical gels over particulate materials, discussed in Chapter 3; sol stabilization is the aim for the production of thin films (coating is described in Section 2.2).

The wet gels and precipitates are left ageing for about 2 days, then the precipitates are usually washed in water for 2-4 times, stirring the suspension and then centrifuging to separate the supernatant. Finally, the samples are dried in a ventilated oven at low temperature (between 30 and 60 °C) until constant weight. Some of the xerogels were also washed in water in order to remove part of the excess ligand from the surface and check the stability of the hybrid structure for an application in solution. A typical sol-gel procedure leading to gelation is illustrated in Figure 2.1.

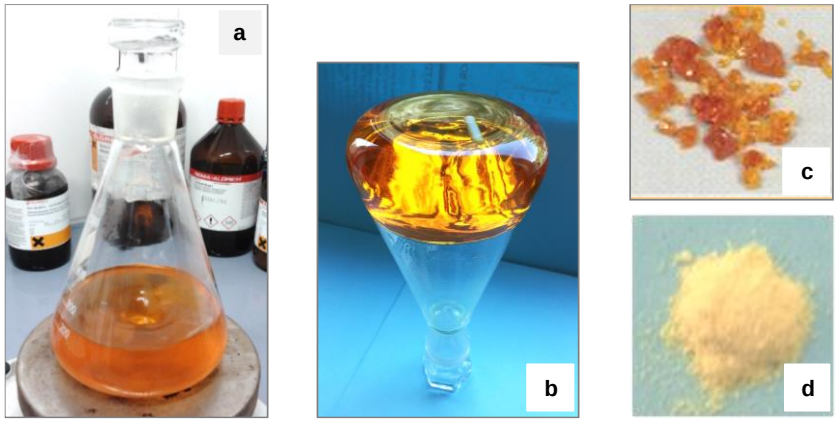

Figure 2.1*. Stages of the sol-gel synthesis of a TiO_2-acetylacetonate material: sol (a), wet gel (b), xerogel as dried (c) and after fine grinding (d).*

The conditions employed for the synthesis of the TiO_2-based materials are briefly summed up in Table 2.1, while the detailed information about the different samples of each hybrid system are reported in Sections 3.1 – 3.6, along with the description of the effect of the variables on the process.

The SGT (sol-gel titania) sample refers to a TiO_2 sample prepared with the same procedure as the hybrid T-acac, but without the addition of any organic ligand. It is taken as a reference sample

throughout the work. Every system containing a different ligand is peculiar and required a variation of the operating conditions with the aim of achieving gelation. In the syntheses with dibenzoylmethane and catechol a mixed solvent was introduced, including cyclohexane to decrease the polarity of the environment. In the study of the systems with catechol a second ligand (acetylacetone, citric acid or diethanolamine) was added to favour gelation and observe the features of a mixed hybrid material.

Some samples, in particular one of the T-acac series, were subjected to thermal treatments in order to analyse the properties of crystallized TiO_2 after the removal of the organic components. Calcination was performed in a tubular furnace in different conditions, usually at 400 °C, with a heating rate of 10 °C/min and a duration of 1 or 3 h, in air or in a more reducing atmosphere (nitrogen or hydrogen/nitrogen 3/97 v/v mixture). Cooling rate was approximately 3 °C/min.

Table 2.1*. Reaction conditions in the synthesis of different TiO_2 hybrid systems.*

Samples	**Ligand**	**Ligand / Ti** (mol/mol)	**[Ti]** (mol/L)	**H_2O / Ti** (mol/mol)	**Solvent**
SGT	-	-	1.1	10	1-propanol
T-acac	acetylacetone	0.1 - 0.5	0.8 - 1.0	4 - 10	1-propanol
T-dbm	dibenzoyl-methane	0.05 - 0.2	0.5 - 1.3	1 - 4	1-propanol, cyclohexane
T-cit	citric acid	0.3 - 0.5	1.2	0.3 - 2	1-propanol, ethanol
T-ace	acetic acid	1	0.9	4	1-propanol
T-cat	catechol	0.01 - 0.4	0.5 - 0.8	2 - 4	1-propanol, cyclohexane
T-dop	dopamine	0.05	0.5	4	1-propanol
T-asc	L-ascorbic acid	0.05 - 0.2	0.3	2 - 6	1-propanol, ethanol

The evolution of the materials structure after calcination at 600 and 800 °C for 1 h in air was also checked. The T-acac and reference SGT samples after calcination are named HT-x and SGT-x, where "HT" stands for hybrid TiO_2 and x is the temperature. The HT-400 samples prepared in different conditions are listed in Table 2.2 and the thermal treatment is discussed in Section 3.7.

***Table 2.2**. Thermal treatment conditions of TiO_2-acac samples.*

Sample	*Atmosphere*	*Time (h)*
HT-400 A1	air	1
HT-400 A3	air	3
HT-400 N1	N_2	1
HT-400 N3	N_2	3
HT-400 HN1	N_2/H_2 97/3 %	1
HT-400 HN3	N_2/H_2 97/3 %	3

2.2. Thin films deposition

Thin films of hybrid and bare TiO_2 were studied during the present activity in the framework of a collaboration between the Department of Chemical, Materials and Production Engineering of the University of Naples Federico II and the ENEA Research Centre in Portici (Naples). The films were produced by coupling the sol-gel method with the spin coating technique.

The preparation procedure of the sols used as stock solution for the deposition is analogous to that described in Section 2.1 for the TiO_2 gels. The conditions were adjusted in order to limit the extent of polycondensation and favour the stabilization of the sol, avoiding precipitation or gelation. This is generally attained in the following ways:

- reducing the concentration of Ti precursor,
- increasing the complexation ratio (ligand/Ti molar ratio),
- reducing the amount of water added,
- lowering the solution pH by adding an acid.

All these approaches were tested, in particular on the TiO_2-acetylacetonate system, on which an optimization of the preparation was carried out, studying the influence of different parameters on the features of the resulting films. Other ligands employed for the coatings are dibenzoylmethane, citric acid and diethanolamine, as reported in Table 2.3. Reference TiO_2 films (SGT) without organic components were also prepared.

Table 2.3. *Conditions applied in the preparation of different TiO_2 hybrid sols for the deposition of films.*

Samples	Ligand	Ligand / Ti (mol/mol)	[Ti] (mol/L)	H_2O / Ti (mol/mol)	Solvent
SGT	-	-	0.15	-	1-propanol
T-acac	acetylacetone	0.5 - 1	0.15 - 0.3	4 - 10	1-propanol
T-dbm	dibenzoyl-methane	0.2	0.15	4	1-propanol, cyclohexane
T-cit	citric acid	1	0.3	2	1-propanol
T-dea	diethanolamine	0.5 - 1	0.3	2	1-propanol

Two types of substrates were used for the deposition of thin films, depending on the scope:

- boron-aluminium silicate glass, with size 3x3 cm^2, for general characterization,
- silicon wafer (<100> orientation), with size 1x1 cm^2, for FT-IR characterization.

To ensure a uniform deposition of the films, careful cleaning of the substrates is necessary. The following procedure, with several cleaning steps aided by sonication, was applied for glass substrates:

1. diluted detergent in deionized water, with sonication (5 min);
2. 0.75 M NaOH solution, with sonication (15 min);
3. rinsing in acetone;
4. ethanol, with sonication (5 min);
5. cleaning solution $H_2O/H_2O_2/NH_4OH$ = 5:1:1 (v/v) (10 min at about 70 °C).

The last step in a warm oxidative solution of H_2O_2 and NH_4OH is an alternative to a UV/ozone or plasma treatment, useful to eliminate the last organic residuals from the surface. The glasses were rinsed with deionized water after each step, and finally dried by a gentle air flow.

Silicon substrates were also handled with care and rinsed with ethanol, a diluted HF solution and water before deposition.

Spin coating was performed with a Laurell WS-650 Series spin coater. Different spinning programs were tested to achieve the desired film thickness and uniformity. The conditions used are summarized as follows:

- spin rate: 1000 – 4000 rpm;
- acceleration: 1000 – 2000 rpm/s;

- spinning time: 30 s.

When a larger thickness was needed, two or more layers were deposited subsequently in the same conditions, with a drying step after each deposition. The films were dried in an oven, usually at 80 °C for 10 min. Some samples were finally annealed at different temperature (150 or 400 °C) for 1 h, with a 10 °C/min or lower heating rate. Selected samples were also subjected to UV irradiation, typically for 15 min, and then characterized in parallel to the analogous non-irradiated samples.

2.3. Characterization of the bulk materials

The hybrid TiO_2 dried gels and particulates, and the calcined TiO_2 gels were characterized by a series of analytical techniques to investigate their structural, physicochemical and functional properties. The xerogels were ground to obtain a powder prior to characterization. Here the instruments used, the measurement conditions and information about the elaboration of collected data are reported. The characterization procedures of thin films are described in the next section.

Scanning Electron Microscopy (SEM) analysis was performed at the Department of Chemical Sciences of the University of Naples Federico II by Prof. Oreste Tarallo. Nitrogen adsorption-desorption measurements were carried out at the National Research Council (CNR) or at the University of Salerno (Department of Industrial Engineering) by the research group of Prof. Vincenzo Vaiano.

2.3.1. X-Ray Diffraction (XRD)

The amorphous nature and crystallizing phases in the structure of the samples were ascertained by X-ray Diffraction (XRD) or Wide Angle X-Ray Scattering (WAXS), carried out in the laboratory of diffractometry of the Department of Chemical, Materials and Production Engineering (University of Naples Federico II) with a Philips X'PERT–PRO diffractometer. The system used monochromatized CuK_α radiation (40 mA, 40 kV, $K_{\alpha1}$: 1.54060 Å, $K_{\alpha2}$: 1.54443 Å, K_β: 1.39225 Å) over a 5-80° 2θ scan interval with a step width of 0.013° 2θ. Giuseppe Mocci is acknowledged for the measurements.

The diffractograms were interpreted by comparison with the PDF (powder diffraction files) data for titanium oxide. The crystal grain size, τ, was estimated by the Scherrer's equation:

$$\tau = \frac{K\,\lambda}{\beta\,\cos\theta}$$

where: K is the shape factor, assumed to be K = 0.9; λ is the X-ray radiation wavelength; β is the width at half maximum (FWHM) of the main diffraction peak (in radians); θ is the Bragg's angle.

2.3.2. Thermogravimetric – Differential Thermal Analysis (TG-DTA)

To study the thermal stability of the xerogels, and the physical and chemical processes occurring during their heating, simultaneous TG-DTA analyses were performed at the Department of Chemical, Materials and Production Engineering (University of Naples Federico II), using a TA Instruments SDT Q-600. The instrument is equipped with a horizontal microbalance (0.1 μg sensitivity) and has a 0.001 °C sensitivity on the temperature. The measurements were recorded using 15 – 20 mg of sample under nitrogen atmosphere, in the temperature range 30–800 °C, with a heating rate of 10 °C/min. An empty platinum pan was used as reference.

2.3.3. Fourier-Transform Infrared Spectroscopy (FT-IR)

FT-IR spectroscopy was used to perform a detailed analysis of the materials' structure, especially of the organic components and their binding with titanium, and to point out the modifications after heat treatments. The measurements were carried out at the Department of Chemical, Materials and Production Engineering (University of Naples Federico II), on a Nicolet system, Nexus model, equipped with a DTGS KBr (deuterated triglycine sulfate with potassium bromide windows) detector. The transmittance spectra were recorded at room temperature, in the 4000–400 cm^{-1} range, with a spectral resolution of 2 cm^{-1} on samples diluted in KBr pellets in 1 or 2 wt% concentration. The spectrum of each sample represents an average of 64 scans, corrected for the spectrum of the blank KBr.

2.3.4. X-Ray Photoelectron Spectroscopy (XPS)

XPS spectroscopy allowed the identification of the elements present on the surface of the materials, provided their speciation and their quantitative analysis. The measurements were performed on selected samples by the group of Prof. Antonella Rossi and Dr. Marzia Fantuzzi at the University of Cagliari, Department of Chemical and Geological Sciences. The instrument used is a PHI QuanteraSXM (ULVAC-PHI, Chanhassen, MN, U.S.A.) spectrometer equipped with a focused and scanned monochromatic Al K_α X-ray source with beam diameter of 100 μm at 25 W. The emitted electrons were collected and retarded with a gauze lens system at an emission angle, θ, of 45°. The system is also equipped with a high-performance, floating-column ion gun and an electron neutralizer

for charge compensation. The XPS spectra were acquired in fixed analyser transmission (FAT) mode, the pass energy being set to 69 eV and the step size to 0.125 eV. The fwhm of the Ag3d5/2 peak is 0.72 eV.

Survey spectra were acquired using a pass-energy of 280 eV and a step size of 1 eV. The residual pressure in the analysis performed using sputter-cleaned gold, silver, and copper as chamber was always below $7 \cdot 10^{-8}$ Pa. The calibration was reference materials according to ISO15472: 2014. The accuracy was found to be ±0.1 eV. High-resolution spectra were processed using CasaXPS software. The background subtraction was performed using the Shirley–Sherwood iterative method. The product of Gaussian and Lorentzian functions was used for curve fitting. The electron neutralizer was used during the analysis, in order to compensate for sample charging, and the spectra were further corrected with reference to adventitious aliphatic carbon taken at 285.0 eV. The quantitative evaluation of XPS data was performed using the first-principles method valid for homogeneous samples [10].

2.3.5. Diffuse Reflectance UV-visible spectroscopy (DRUV-vis)

Ultraviolet - visible spectroscopy in diffuse reflectance mode was used to examine the optical absorption of the solid samples. DRUV-vis spectra were recorded at the Department of Chemical Sciences of the University of Naples Federico II, on a double beam Jasco V-550 spectrophotometer equipped with an integrating sphere, in the range 190-800 nm. The powders were diluted in $BaSO_4$, used as a reflectance standard, in 5-10 wt% concentration. The reflectance spectra were collected at 200 nm/min scanning speed and 5.0 nm band width, and were corrected for the spectrum of the blank $BaSO_4$.

The measured intensity was expressed as the value of the Kubelka-Munk function, F(R):

$$F(R) = \frac{(1-R)^2}{2\,R}$$

where R is the measured reflectance.

The band gap energy of the samples (E_g) was evaluated on the basis of Tauc's equation:

$$[F(R)\,h\nu]^{1/n} = K\left(h\nu - E_g\right)$$

where n = 2 (for allowed indirect transitions), hν indicates the photon energy (eV) and K is a constant. The linearization of Tauc plot (or alpha plot) provided the estimated band gap value.

2.3.6. Electron Paramagnetic Resonance (EPR) spectroscopy

EPR spectroscopy allowed to detect and identify paramagnetic species, such as the superoxide radical anion, on the studied materials. The analyses were performed at the Department of Chemical Sciences of the University of Naples Federico II (research group of Prof. Gerardino D'Errico), using an X-band (9 GHz) Bruker Elexys E-500 spectrometer (Bruker, Rheinstetten, Germany).

The capillary containing the powered sample was placed in a standard 4 mm quartz sample tube. The temperature of the sample was regulated at 25 °C. The instrumental settings were as follows: sweep width, 140 G; resolution, 1024 points; modulation frequency, 100 kHz; modulation amplitude, 1.0 G; time constant, 20.5 ms. EPR spectra were measured with attenuation of 10 dB to avoid microwave saturation of resonance absorption curve. Usually 16 or 32 scans were accumulated to improve the signal-to-noise ratio. In the case of samples giving a very intense signal, the detector gain was lowered from 60 to 40 dB. The g values and the spin density of the samples were evaluated by means of an internal standard, Mn^{2+}-doped MgO, prepared by a modified synthesis protocol reported in literature [9,63]. The values were calibrated in reference to TEMPOL (4-hydroxy-2,2,6,6- tetramethyl-1-piperidinyl-1-oxyl) and DPPH (2,2-diphenyl-1-picrylhydrazyl) solutions.

The EPR investigation was extended to aqueous dispersions of the hybrid samples, in order to study the presence of radicals generated in water by means of spin trapping experiments, performed with the support of Dr. Giuseppe Vitiello. 5,5-dimethyl-1-pyrroline N-oxide (DMPO) was used as spin trap, in conditions similar to those adopted to perform catalytic tests (see Section 2.5). A suspension of sample powder was prepared (10 g/L) in water or in a 2 mM 4-CPA herbicide solution, and kept stirring in the dark. Then DMPO aqueous solution was added, so to obtain a DMPO concentration of 25 mM. After 1 min, the samples were centrifuged and the spectra of the supernatants were registered with an attenuation of 15 dB. Several scans were accumulated to improve the signal-to-noise ratio. The spectra were corrected, when needed, subtracting the contribution of the DMPO dimeric adduct.

2.3.7. Photocurrent measurements and cyclic voltammetry

The measurement of photocurrent generation by a material is a convenient method to receive clues on its photoactivity. Photocurrent analyses were carried out at the Jagiellonian University in Krakow (Poland), Faculty of Chemistry, in the research group of Prof. Wojciech Macyk. A three-electrode setup was used. The finely powdered sample was mixed with deionized water to produce a paste, which was carefully casted on an ITO-coated transparent PET foil of 60 Ω/sq resistance (Sigma-Aldrich) to build the working electrode. A platinum wire and Ag/AgCl were used as the counter and reference electrodes, respectively. The electrolyte (0.1 M KNO_3) was purged with argon for at least 15 min before

and during the measurements to displace dissolved O_2 from the solution. A 150 W xenon lamp (XBO-150), equipped with a water-cooled housing and an automatically controlled monochromator (Instytut Fotonowy), was used as the light source. The working electrodes were irradiated from the backside through the ITO layer in order to minimize the influence of the film thickness on the measured photocurrents. The measurements were controlled with a potentiostat (Instytut Fotonowy). The acquisition was performed generally under a potential scan between -0.2 and 1.0 V (vs. Ag/AgCl), in a wavelength range of 330-550 nm.

Additionally, some experiments in different conditions were designed to investigate specific characteristics of the samples. Some materials were tested under O_2 insufflation, instead of argon, observing the variation of cathodic photocurrent. Others were tested adding glycerol to the electrolyte solution to check the photocurrent multiplication behaviour. Glycerol was chosen in place of commonly used methanol because it is the sacrificial agent employed in the photoreforming tests (see Section 2.6).

Cyclic voltammetry (CV) is an electrochemical technique which gives information about oxidation and reduction processes occurring in a material or in solution. The same instruments and configuration of the three-electrode cell as for photocurrent measurements. A potential range between -0.3 and 1.0 V (vs. Ag/AgCl) was scanned, at a rate of 10 mV/s. At least two cycles were acquired for each sample.

2.3.8. Spectroelectrochemical measurements

A spectroelectrochemical method was recently developed by the research group of Prof. Wojciech Macyk, at the Jagiellonian University in Krakow (Faculty of Chemistry), on the basis of a previously reported method [64,65]. It correlates the variations of reflectance of a solid material as a function of the applied voltage with the potential and density of its electronic states in the band gap region close to the conduction band edge.

The measurements were carried out in a three-electrode system with Ag/Ag^+ electrode (10 mM $AgNO_3$ and 0.1 M $LiClO_4$ in acetonitrile) used as the reference electrode, a platinum wire as counter electrode and the powdered samples deposited onto a platinum foil as working electrode. The materials were finely ground and suspended in anhydrous acetonitrile prior to casting. The electrodes were placed in a cuvette with a quartz window filled with 0.1 M $LiClO_4$ solution in acetonitrile. Oxygen was thoroughly removed from the electrolyte by purging it with argon before (15 min) and during experiments. The cuvette was placed in front of the integrating sphere with the working electrode (platinum foil with deposited sample) facing the light source. The electrode potential was controlled by an electrochemical analyser (Bio-Logic, SP-150). The applied potential was swept from 0 to -2.7 V

(vs. Ag/Ag^+) with a stepwise ramp of 25 mV every 10 min. Changes in the reflectance at 600 nm were recorded using a PerkinElmer UV–vis Lambda 12 spectrometer equipped with a 5 cm diameter integrating sphere. The 600 nm wavelength is placed in the wide absorption band corresponding to Ti^{3+} species. The reflectance vs. time (potential) was recorded. The density of vacant states (DOS) was calculated as a difference in the Kubelka-Munk function values between two subsequent potential steps, by means of a code in R language.

2.4. Characterization of thin films

The TiO_2-based thin films produced by sol-gel and spin coating were characterized by a series of analytical techniques. The FT-IR spectroscopy measurements and part of the optical microscopy observations were done at the Department of Chemical, Materials and Production Engineering (University of Naples Federico II), while the rest of the characterization was carried out at the ENEA (Agenzia nazionale per le nuove tecnologie, l'energia e lo sviluppo economico sostenibile) Research Centre located in Portici (Naples), with the collaboration of Dr. Maria Luisa Addonizio.

The surface morphology of the films was examined by transmission optical microscopy by means of a Zeiss microscope, Axiopot model, and Atomic Force Microscopy (AFM), using a Veeco instrument, NSIV model.

The film thickness was usually measured with a profilometer (Profiler v. 8, KLA Tencor), after making a few scratches in the film surface with a scalpel. Thickness values were taken at different points, then the data were averaged. Some films were also analysed by ellipsometry. The resulting thickness values were in excellent agreement with those obtained by profilometry.

X-ray Diffraction was employed to examine the amorphous or crystalline nature of the films. A Philips X'Pert PRO MRD diffractometer with CuK_α radiation (λ = 0.154056 nm) was used, operating in grazing incidence mode (GIXRD) in order to obtain a higher sensitivity in the analysis of the thin coatings. The GIXRD diffraction pattern were collected with an incident angle of 0.5°.

Fourier-Transform Infrared (FT-IR) spectroscopy was used to analyse the structure or the samples, in particular the organic components bound to titanium, and to individuate the modifications after heat treatments and UV irradiation. The measurements were on the same instrument used for the bulk gel samples (see Section 2.3). The transmittance spectra were recorded at room temperature, in the 4000–400 cm^{-1} range, with a spectral resolution of 2 cm^{-1} on films deposited on silicon substrate with a polished <100> surface. The spectrum of each sample represents an average of 64 scans, corrected

for the spectrum of the blank (a clean silicon wafer). Despite the small thickness of some films, FT-IR spectra with an acceptable signal/noise ratio were collected.

The optical properties of the thin transparent films deposited on glass substrates were evaluated by UV-visible-NIR spectroscopy. A double beam Perkin Elmer (Lambda 900 model) spectrophotometer was used. It is equipped with an integrating sphere operating in the wavelength range 200-2500 nm. Spectra in transmittance and reflectance configuration were recorded for each film in the range 200-1500 nm. Absorbance was calculated by difference from the collected transmittance and reflectance data.

The electrical resistivity of the studied films was evaluated by two-point probe measurements in longitudinal geometry. Two parallel silver contacts were placed on the film's surface at a short distance (about 1 mm). Increasing voltages were applied by a potentiostat, in the range 1-80 V, measuring the current intensity. The measurement was conducted in the dark. The electrical resistivity, ρ (in Ω cm), was then calculated by the following equation:

$$\rho = \frac{V}{I}\frac{L\,S}{d}$$

where: V is the potential (V); I is the current intensity (A); L is length of the Ag contacts (cm), S is the film thickness (cm) and d is the distance between the Ag contacts (cm).

2.5. Catalytic and photocatalytic tests

2.5.1. Oxidative degradation of organic pollutants

The activity of some hybrid materials, related to their ability to generate and stably adsorb on their surface reactive oxygen species, was tested in the degradation of organic compounds in water solution. This part of the experimental work was performed at the Department of Agricultural Sciences of the University of Naples Federico II, located in Portici (Naples), in collaboration with Prof. Filomena Sannino. Different classes of organic pollutants were selected, to check the performance of the materials towards real water and soil contaminants. The experimental setup was similar for all the substrates, while the conditions of reaction and product analysis changed according to the substrate.

Phenanthrene (PHE), 2,4-dichlorophenol (2,4-DCP), and four chlorinated phenoxyalkanoic herbicides, namely 4-chlorophenoxyacetic acid (4-CPA), 2,4-dichlorophenoxyacetic acid (2,4-D), 4-chloro-2-methylphenoxyacetic acid (MCPA) and 4-(4-chloro-2-methylphenoxy)butanoic acid

(MCPB), were purchased from Sigma-Aldrich (UK; 99.0 % purity). All solvents were of HPLC grade (Carlo Erba, Italy) and were used without further purification. Milli-Q ultrapure water was used throughout all the experiments.

A stock aqueous solution of each pollutant were prepared, based on their water solubility: PHE (1.0 mg/L), 2,4-DCP (0.3 mmol/L), 4-CPA (2.7 mmol/L), 2,4-D (2.0 mmol/L), MCPA (0.9 mmol/L), MCPB (0.2 mmol/L). The stock solutions were kept refrigerated in the dark to avoid photodegradation reactions.

The removal tests were carried out in batch conditions, stirring the vials in a thermostatic rotary shaker, at room temperature or at 30 °C. All the reactions were performed in the dark, avoiding the exposure to light in every step, to exclude any contribution to the degradation due to the possible photocatalytic activity of the materials. The tests were carried out with different solid concentrations (ranging from 0.05 to 10 g/L; typically about 1 g/L) and with different reaction times. At the end of the run the samples were centrifuged to separate the solid and the supernatants were analysed by high pressure liquid chromatography (HPLC).

An Agilent 1200 HPLC apparatus (USA) equipped with a DAD and a ChemStation Agilent Software was used for the analytical determination of the concentration of the pollutants, along with a Macharey-Nagel Nucleosil 100–5 C18 column (stainless steel 250 × 4 mm). The HPLC analysis conditions varied depending on the substrate:

- PHE: 85 : 15 acetonitrile : water mobile phase, pumped at 1 mL/min flow in isocratic mode; detector set at 252 nm.
- 2,4-DCP: 65 : 35 acetonitrile : water (1 % acetic acid) mobile phase, pumped at 1 mL/min flow in isocratic mode; detector set at 280 nm.
- 4-CPA, 2,4-D: 40 : 60 acetonitrile : phosphate buffer (0.1 %, pH 2.5) pumped at 1 mL/min flow in isocratic mode; detector set at 283 nm.
- MCPA: 50 : 50 acetonitrile : phosphate buffer (0.1 %, pH 2.5) pumped at 1 mL/min flow in isocratic mode; detector set at 225 nm.
- MCPB: 60 : 40 acetonitrile : phosphate buffer (0.1 %, pH 2.5) pumped at 1 mL/min flow in isocratic mode; detector set at 225 nm.

The injection volume was 20 µL in all cases. The quantitative determination was performed using a calibration curve for each organic substrate investigated. All the experiments were carried out in triplicate and the relative standard deviation was lower than 4 %.

In order to establish whether the overall removal kinetics of 2,4-DCP is limited by intraparticle diffusion or by the adsorption/reaction steps, an approximate evaluation of the Thiele modulus (φ^2) was made, adopting the following definition:

$$\varphi^2 = \frac{R^2 \lambda_2}{D}$$

where: R is the average size of TiO_2 xerogel particles (R ≈ 100 μm), D is the diffusion coefficient of 2,4-DCP in water (D ≈ $7.8 \cdot 10^{-10}$ m^2 s^{-1}), λ_2 is the kinetic constant for the reaction (in s^{-1}), calculated modelling the data with a double exponential function. Further details are reported in related papers [8–10].

2.5.2. Photocatalytic conversion of terephthalic acid

A first screening of the photocatalytic performances of some TiO_2-based samples was carried out at the Jagiellonian University in Krakow, in the research group of Prof. Wojciech Macyk, studying the oxidation of terephthalic acid (TA). The conversion of TA to hydroxyterephthalic acid (TAOH) occurs specifically by the attack of a hydroxyl radical to one of the carbons adjacent to the carboxylic groups, so it allows to compare the efficiency in the generation of •OH, considered the dominant ROS in many photocatalytic oxidations

The powdered xerogels were suspended in a solution of terephthalic acid (98 %, Sigma Aldrich) (0.3 mM in an aqueous solution of 0.01 M NaOH, added to favour TA solubility, with pH about 12). The solid concentration was 1 g/L. The suspension was irradiated with an XBO-150 xenon lamp (Instytut Fotonowy). A water filter (10 cm) with a 0.1 M $CuSO_4$ solution was used to absorb NIR and IR radiation. The experiments were performed either under visible light (420 nm cutoff filter) or in a large UV/visible spectrum (320 nm cutoff). Samples of 2 mL were collected during 2 h of irradiation and filtered. In the reaction of non-fluorescent TA with hydroxyl radicals, the formation of TAOH can be monitored by recording emission spectra. TAOH shows a broad emission band at λ_{max} = 425 nm upon excitation at 315 nm. Fluorescence spectra were recorded using a FluoroLog-3 (Horiba JobinYvon) spectrofluorimeter and a 1 cm quartz cuvette.

2.5.3. Photoreforming tests

The photocatalytic production of H_2 is another typical process in which photocatalytic performances are evaluated. The annealed defective TiO_2 materials studied were tested in the photoreforming reaction under UV/visible light, using glycerol as a sacrificial agent (electron donor). The experiments were carried out at the University of Salerno (Department of Industrial Engineering), by the research group of Prof. Vincenzo Vaiano. The experiments were performed in a cylindrical batch photoreactor (total volume 200 mL), equipped with a nitrogen distributor device and four UV lamps (Philips, nominal power: 8 W each and main emission peak at 365 nm) around the external surface of the

photoreactor [66]. In a typical photocatalytic test, the treated solution volume was 80 ml at the spontaneous pH of the solution (pH = 7) with an initial glycerol concentration of 5 wt%, while the photocatalyst dosage was 1.5 g/L, determined as the optimal value through preliminary tests with different loads. The photocatalytic test under UV light lasted 4 h. The analysis of the gaseous phase coming from the photoreactor was performed by using continuous analysers (ABB Advance Optima) to measure the concentration of H_2 during the irradiation time.

RESULTS AND DISCUSSION

- CHAPTER 3 -

SOL-GEL SYNTHESIS OF HYBRID OXIDES

Hybrid materials composed by a metal oxide and organic compounds are subject of research in various fields: catalysis and photocatalysis, photovoltaics, sensing, drug delivery, etc. An overview on this kind of materials and their possible applications is given in Section 1.2. TiO_2, ZrO_2 and ZnO are among the most employed metal oxides in hybrid materials. The most common method for their preparation is the adsorption of the organic molecules on the surface of oxide nanoparticles or other nanostructures [45,67–69]. This can be regarded as a "top-down" approach, in which different modes of adsorption (chemical and physical) may be realised, similar to the wet impregnation of the active phase on a catalytic support. It is fast and easy, however it can present some drawbacks: the control on the amount of organic compound bound to the material is limited, as it depends on the relative concentration of inorganic particles and organic compound, and in turn on the available surface area

and the adsorption equilibrium. Consequently, only the accessible surface of the material can be functionalized. If the interactions are weak, especially in the case of large molecules with few functional groups able to coordinate metal ions, the hybrid structures may show insufficient stability in solution.

In the present work an alternative, "bottom-up" approach for the synthesis of metal oxide-organic hybrid materials is described: a simple and versatile hydrolytic sol-gel procedure. Focusing on titanium oxide, an alkoxide precursor (Ti(IV) n-butoxide) and a series of organic compounds (diketones, carboxylic acids, enediols) that are able to form coordination complexes with Ti were chosen for the experimental activity. These complexes are quickly formed when the above organic species are mixed with the Ti precursor, as this kind of bidentate ligands readily displace alkoxide ligands [57,58]. Then water addition triggers hydrolysis and condensation reactions, causing the growth of molecular clusters linked by Ti-O-Ti bonds (see Scheme 2.1, Section 2.1). Both the presence of the coordinating compounds and their features are crucial for the fate of the system, which can evolve in different directions depending on the interactions of the clusters between each other and with the solvent, hence on the composition of the reaction mixture [55,57,62]. The principal possibilities are:

- precipitation of sol aggregates, resulting in the formation of a particulate or physical gel or the deposition of fine particles;
- gelation of the whole mixture, resulting in a homogeneous chemical gel;
- stabilization of the sol, without precipitation or gelation for a long time.

In the resulting hybrid samples the organic component is chemically bound to Ti and can be uniformly distributed not only on the surface, but also in the bulk of the material.

Metal oxide nanoparticles possess many peculiar properties, related to their high surface/volume ratio, allowing quantum confinement effects, and the possibility to obtain many different nanostructures. On the other hand, their practical applications, for instance in heterogeneous catalysis, is hindered by their tendency to aggregate in solution, their difficult separation from liquid phase and generally tricky and risky handling. To realise catalysts easily separable after a batch process or compatible with a packed bed reactor for a continuous process, nanoparticles should be anchored on suitable supports. An alternative strategy is the production of bulk catalysts, such as xerogels, macroscopic granular materials, monoliths, porous blocks of material, ambigels and aerogels, characterized by very high pore volume and surface area. Coatings of active material on a support or on the walls of microreactors are another option to obtain a stable catalyst. Sol-gel technique allows to produce all these different structures and to control the composition and surface features of the product through the variation of the process parameters.

The present work describes a route to synthesize hybrid TiO_2 materials in the form of xerogels, small particles or thin films. For the above mentioned reasons, chemical gels are the desired products, although hybrid TiO_2 nanoparticles can also have interesting applicative properties, so some of the precipitate samples were characterized as well. The products are dried at low temperature in order to preserve the organic component in their structure and investigate the properties of the hybrid material. Thus the organic ligand plays a double role: as complexing agent it modulates the sol-gel process, as a reagent it is incorporated in the structure, becoming a constituent of the final product.

In Sections 3.1 – 3.6 the synthesis of chemical or particulate gels with different organic compounds is discussed. Each organic ligand requests specific synthetic conditions, therefore the procedure was optimized for each system through the variation of parameters such as the concentration of reagents, type of solvent and pH. Thermal annealing of some xerogels was also performed to study the resulting samples (Section 3.7). Section 3.8 is dedicated to the preparation of hybrid films by means of spin coating, starting from stable TiO_2 sols.

3.1. TiO_2 – acetylacetone

Acetylacetone (2,4-pentanedione or acacH) is the simplest β-diketone, an efficient chelating ligand for transition metals and probably the most commonly used stabilizing ligand in the sol-gel processing of TiO_2. The enol form of acacH, stabilized by resonance and by the formation of an intramolecular hydrogen bond, prevails in non-polar solvents, while the keto form is favoured in polar solvents (Figure 3.1). A proton in C3 position, adjacent to two carbonyl groups, is weakly acidic (pKa ~ 9). The conjugated base, acetylacetonate (acac) anion, has the negative charge stabilized by resonance.

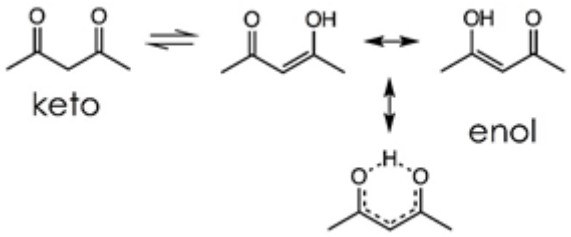

Figure 3.1*. Keto-enol tautomeric structures and resonance of acetylacetone (acacH).*

Acetylacetone forms stable coordination compounds with most transition metals in a bidentate chelating mode, whose stability is favoured by the formation of six member rings with partial charge delocalization. Acetylacetonate complexes, $M(acac)_n$, are known for most transition metals and some

of them are frequently used as metal precursors. Acac moieties have also been used as anchoring groups for dyes or biomolecules on metal oxides, owing to the strong chelation formed. The modification of titanium alkoxides with acacH and its effect on hydrolysis, condensation and gelation has been widely studied [57,58,61,70,71], as discussed in Section 1.6. Some authors evidenced the existence of charge transfer between acetylacetonate and Ti in TiO_2 sols or surface modified particles [58,72] and some characterization data on TiO_2 materials containing acacH are reported [73,74], however most studies concern the samples obtained after removal of the ligand by calcination. A comprehensive investigation on TiO_2-acac hybrid materials, including electronic, electrochemical and catalytic properties, does not seem to be available in literature. The choice of this organic molecule was also inspired by the interesting peculiar properties exhibited by ZrO_2-acac materials recently studied by the same research group where the present work was led [6,7,75].

The general protocol followed in the synthesis is illustrated in Scheme 2.1. In a typical experiment, acacH is added directly to $Ti(OBu)_4$, giving a yellow to orange coloured solution, depending on the acacH/Ti molar ratio (complexation ratio, *c*). Addition of the hydrolytic solution induces the formation of a sol which remains stable or gelates in a short time (a few seconds or a few minutes), in the conditions explored. The molar ratios are the following, Ti : acacH : H_2O : 1-propanol : HCl = 1 : *c* : *h* : 5 : 0.02. Table 3.1 reports the conditions applied in the tests that brought to gelation [9,76].

Table 3.1*. Reaction conditions in the synthesis of TiO_2–acac hybrid gels.*

Sample	***c*** **= acacH / Ti** (mol/mol)	**[Ti]** (mol/L)	***h*** **= H_2O / Ti** (mol/mol)
T-acac01	0.1	0.85	4
T-acac02	0.2	0.85	4
T-acac04	0.4	1.0	10
T-acac05	0.5	1.0	10

A quantity of water larger than the stoichiometric one was used to ensure the hydrolysis of Ti precursor, assuming that most of the acac is not hydrolysed even in that condition [58,70]. Acid catalysis is generally employed in sol-gel processing; here HCl was used. The synthesis of T-acac04 samples was also performed in neutral pH and in basic pH, by means of NH_3, obtaining gelation in a slightly longer time (about 5 min). The complexation ratio is found to be a key parameter in determining the result of the process. With *c* ranging from 0.1 to 0.4, chemical gels are obtained, in a time increasing with the acacH concentration and decreasing with water concentration (*h*). Actually,

when c = 0.25 or lower and *h* = 10, gelation occurs abruptly with water addition, giving an opaque and non-uniform gel. Lowering the hydrolysis ratio to 4 more homogeneous gelation is attained, as in the case of the gels with c = 0.4, which are limpid, transparent and homogeneous. The *c* = 0.5 appears to be a threshold value for the complexation ratio, since gelation results to be reversible with both time and temperature: a gel obtained at room temperature returned to a viscous sol state after 1 day; similarly, a gel obtained keeping the reaction mixture at 50 °C for 2 h apparently showed higher stability, but after 1 day part of the mixture turned again to a viscous liquid. At *c* > 0.5 sols stable for weeks or even months are obtained.

The observed behaviour can be explained according to amount of acacH molecules coordinated to Ti atoms. The substitution of a butoxide with an acac ligand causes the expansion of the coordination number of Ti from 4 to 5, leaving the charge balance unaltered. In the classical interpretation this lowers the rates of hydrolysis and condensation, allowing the growth of a polymeric network instead of the precipitation of oxo-hydroxide particles [60]. The interpretation by Kessler et al., mentioned in Section 1.6, argued that hydrolysis and condensation are actually facilitated by the chelating ligands, which have high mobility [61]. Here the effect is observed only on the sol-gel transition, so it does not allow to support one of the two hypotheses. Kessler et al. pointed at a thermodynamic control of the sol-gel process, with the formation of "micelles templated by self-assembly of ligands", stabilized in solution by surface ligands [61,62].

When the acac/Ti ratio is raised to 0.5, the connection of primary particles to form a gel is still possible, but the degree of cross-linking remains low, so the bonding is weak and the equilibrium can be easily reversed towards a viscous sol. Heating shifts the equilibrium towards the gel, but not definitively. Thermoreversible gelation was observed by Haridas et al., in a study of the "gellability zones" of titanium sols with *c* = 1, 2, 3 or 4, showing the range of temperature in which gelation is possible and how the gelation time decreases heating or cooling the reaction mixture [71]. When the complexation ratio is higher than 0.5, the chelating ligands hinder the formation of Ti-O-Ti bridges or further aggregation and the sol remains stable. The same effect was attained for *c* = 0.5 diluting the mixture, as seen during the preparation of sols for the deposition of films (Section 3.8).

The conditions chosen in the present work are close to those used by Ponton et al., who studied by rheological methods the gelation time of TiO_2-acacH systems with the variation of some parameters: *c* between 0.25 and 0.4, *h* between 8 and 12, [Ti] between 0.40 and 0.65 M and temperature between 10 and 35 °C. They find the expected trends for the gelation time, which increases as *h*, [Ti] and temperature decrease and as the acacH content increases, noting that the last parameter is the most influential [70,77]. The main difference in the present case is the higher [Ti], which causes faster gelation than reported by Ponton.

The characterization and testing was focused on the T-acac04 sample, since it was the stable gel with the highest acac content.

3.2. TiO_2 – dibenzoylmethane

To investigate the effects of the ligand structure on the characteristics of the hybrid TiO_2-based materials, a new series of samples was prepared using as organic component another β-diketone: dibenzoylmethane (dbm), or 1,3-diphenyl-1,3-propanedione. With respect to acetylacetone it has two phenyl rings instead of the methyl groups. The tautomeric keno-enol equilibrium is largely shifted towards the enol form, thanks to the formation of a strong intramolecular hydrogen bond, stronger than in acetylacetone [78]. In the enol form the structure of dbm is fully conjugated, giving a high charge delocalization. Like other β-diketones, dbm is an efficient chelating ligand for several metals and has been used for metal extraction from solutions. Metal (in particular rare earths) complexes of dbm are studied for applications related to their luminescent properties, as NMR shift agents or in laser technology. Dibenzoylmethane and its derivatives, such as avobenzone, are used in sunscreen formulations owing to their absorption of UV radiation and photostability. It is not harmful to humans (it is found as a minor constituent in the root extracts of licorice) and it has been even shown to have a variety of anti-cancer effects [79].

The only reports found in literature about materials containing dbm bound to TiO_2 are some works by the groups of Tohge and Segawa, who prepared photosensitive hybrid TiO_2 or ZrO_2 films by sol-gel adding acetylacetone, benzoylacetone or dbm to study the patterning induced by dissociation of the metal-chelate complex under UV irradiation [80–82]. Adding methacrylic acid to the gel films they obtained its polymerization aided by UV irradiation and by dbm radicals produced [82]. A couple of patents mention the possibility of using dbm among other diketones and chelating ligands for the preparation of metal oxide films and nanostructures [83,84].

The conditions employed for the synthesis of the TiO_2-dibenzoylmethane hybrid materials are summarized in Table 3.2. The dbm content was kept relatively low, due to its larger size and molar mass with respect to acacH and limited solubility in alcohol. The solubility of dbm in 1-propanol was experimentally found to be slightly higher than 30 mg mL^{-1}. The addition of a colourless dbm solution to $Ti(OBu)_4$ gives a bright yellow transparent solution, indicating that the complexation with Ti readily occurs. Working in 1-propanol the addition of the aqueous solution resulted in the formation of large flakes or particles that precipitated when stirring was interrupted. Raising the dbm content to c = 0.3,

reducing the hydrolysis ratio to 1 or diluting the mixture retarded, but did not prevent the precipitation.

Table 3.2*. Reaction conditions in the synthesis of TiO_2–dbm hybrid powders and gels; the "p" in the sample name indicates a precipitate.*

Sample	***c* = dbm / Ti** (mol/mol)	**[Ti]** (mol/L)	***h* = H_2O / Ti** (mol/mol)	**Solvent**
T-dbm01p	0.1	1.3	1	1-propanol
T-dbm02p	0.2	0.7	4	1-propanol
T-dbm005	0.05	1.1	4	1-propanol + cyclohexane
T-dbm01	0.1	0.7	4	1-propanol + cyclohexane
T-dbm02	0.2	0.5	4	1-propanol + cyclohexane

The addition of ammonia with the aim to favour condensation over hydrolysis had the effect of reducing the particles size, but did not lead to gelation. For T-dbm01p and T-dbm02p compositions the products obtained were separated by centrifugation, washed twice in water, then dried at 50 °C. The different behaviour of acac and dbm complexes is related to their molecular structure: the latter, when coordinating metal ions, exposes two phenyl rings, bulkier than acac methyl groups, making the complex and its aggregates more hydrophobic. The interaction between primary particles can occur via coalescence with formation of oxygen bridges; the interaction between the ligand shells and the solvent is essential in the process. In the presence of a suitable concentration of chelating ligands strongly interacting with the solvent, and if the hydrolysis ratio is not too high, the aggregates have a possibility to develop common surface [62]. This consideration suggested that the introduction of another solvent with lower polarity and better affinity towards phenyl groups should favour the interfacial activity of the growing micelles allowing the formation of a chemical gel. Cyclohexane was chosen, having relatively lower toxicity than other common non-polar solvents like benzene, tetrahydrofuran or n-hexane, and good miscibility with 1-propanol. The effect of solvent polarity was already pointed out in some reports about Zr n-propoxide originating precipitates when dissolved in propanol, ZrO_2 polymeric gel or monolith when dissolved in cyclohexane [85]. Here a mixed solvent cyclohexane/1-propanol in 3:4 and 6:4 molar ratio (corresponding to about 1:1 and 2:1 v/v) was used in both steps of the synthetic procedure (dbm solution and water solution). A higher ratio would make the polarity of the environment too low, causing phase separation with water addition, while these conditions allowed to remain in the miscibility zone of the ternary system. When more cyclohexane

was used (2:1 v/v) the approach was successful: with c = 0.1 and h = 1 a stable sol formed, then, carefully raising h up to 4, a transparent homogeneous chemical gel was produced. To prepare gels with different dbm content the dbm/solvent ratio was kept constant, thus varying the concentration of the species. This lead to increasing gelation times for the three samples: T-dbm005 (tens of seconds) < T-dbm01 (few minutes) < T-dbm02 (about 5 h), owing to both the increasing complexation ratio and dilution. After ageing a vacuum oven was used to dry the gels, avoiding the dispersion of solvent vapour, especially cyclohexane. The final products were intensely yellow coloured granular xerogels. Stable sols of TiO_2-dbm were also prepared for thin films deposition (see Section 3.8).

The implementation of a mixed solvent with decreased polarity with respect to the pure alcohol was demonstrated to be an effective way to promote the controlled polymerization and gelation of TiO_2 when Ti is complexed by ligands exposing non-polar groups, as in the Ti-dbm system.

3.3. TiO_2 – citric acid and TiO_2 – acetic acid

Citric acid (2-hydroxypropane-1,2,3-tricarboxylic acid) is a triprotic acid, with pK_{a1} = 3.13, pK_{a2} = 4.76 and pK_{a3} = 6.40, so it exists as four different species (from fully protonated H_3cit to fully deprotonated cit^{3-}) depending on solution pH. Actually an additional species produced by the deprotonation of the hydroxyl group should also be considered. It is abundant in nature and in human body, available and cheap. As an effective chelating and capping agent, it is useful in the synthesis of a wide range of nanomaterials, to control their size and morphology or to give surface functionality [55,86–89]. Citric acid has been used in different types of sol-gel procedures. Typically, aqueous metal salts are mixed with citric acid and the resulting solution heated to form a viscous solution or gel. Some reports describe the addition of bases such as ammonia or ethylene diamine to modify the pH and enhance cation binding to the citrate. Homogeneous solutions of different metal citrates can be obtained, and the aggregate size and stability can be controlled by varying the citric acid content or pH [86,89,90]. Metal oxide powders are produced by simple calcination in air of the gel precursor. Citrate ligands ensure a good dispersion of the metal centres and, despite their small size, can act as a template and also direct the crystal nucleation and growth, leading to crystallization at lower temperature or increasing the selectivity towards one crystalline phase [55,88,91]. For example, in the case of TiO_2 calcination or hydrothermal treatment of Ti-citrate precursors was shown to favour the formation of a stable anatase phase [87,89]. Citric acid is often used together with metal nitrates, in the combustion synthesis, where nitrate works as oxidant and citrate as fuel, giving a fast exothermic combustion, with

the production of large volume of gas that results in an open foam-like structure of the ceramic product [55]. Another classical modification of sol-gel method involving citric acid is the Pechini method, named after the author of the original patent [92]. It is based on the esterification reaction between citrate and ethylene glycol added to the solution, induced by heating and producing an extended covalent polyester network. The effect of the polymer prepared *in situ* is an excellent dispersion of the metals and a higher decomposition temperature, allowing more control on the growth of the ceramic oxide. Different variations of the Pechini method were proposed, changing conditions and organic precursors to yield different structures [55,91]. Citrate complexes of Ti are significant not only in materials chemistry, but also in medicinal chemistry, because citric acid is an abundant chelator in cellular fluids, so it can interact with Ti present in medical implants or introduced in the body through other exposure paths, and in environmental chemistry, because the occurrence of TiO_2 nanoparticles in soil and hydrosphere is growing and ubiquitous chelators such as citric acid affect their stability, mobility and bioavailability [86,93].

Despite the frequent use of citric acid in TiO_2 synthesis, a comprehensive investigation of TiO_2-citrate hybrid materials was not found in literature. This molecule was chosen with the idea of checking the influence of another class of organics, carboxylic acids, on the properties of TiO_2, in particular regarding the stabilization of radicals and photosensitization, also in relation with a few reports mentioning charge transfer complexes formation between organic acids and TiO_2 [46,47,94].

In the majority of the works citric acid is used to obtain stable TiO_2 sols, which are then dried by heating or separated for further processing, rather than chemical gels [55,87,89]. Citric acid/Ti molar ratios about 1 or higher are generally used. Here ratios not higher than 0.5 were preferred, to avoid a mainly organic composition of the products. The reaction conditions employed are reported in Table 3.3.

***Table 3.3**. Reaction conditions in the synthesis of TiO_2–cit hybrid gels.*

Sample	***c* = cit / Ti** (mol/mol)	**[Ti]** (mol/L)	***h* = H_2O / Ti** (mol/mol)	**Solvent**
T-cit03	0.3	1.2	0.3	1-propanol
T-cit04	0.4	1.2	0.4	1-propanol
T-cit05	0.5	1.2	0.5	1-propanol
T-cit05b	0.5	1.2	2	ethanol

The first observation was that citric acid, in spite of its polydentate nature and strong chelation to titanium, does not have the same efficiency as acetylacetone in slowing down hydrolysis and condensation reactions. Actually, in most of the synthesis tests, when citric acid was dissolved in alcohol with an alcohol/Ti molar ratio about 5, gelation occurred soon after the addition of this solution to $Ti(OBu)_4$, before the addition of the hydrolytic solution. The amount of water introduced with the monohydrate citric acid, although substoichiometric with respect to a complete hydrolysis and condensation (the theoretical stoichiometric ratio should be 2, considering a water molecule released during each condensation), is sufficient to induce gelation of the system in a few minutes. It cannot be excluded that the hygroscopic citric acid carries a slightly higher amount of water than the nominal 1:1 ratio, and some esterification reaction between the acid and the alcohol contributes to the water concentration in solution. The gels obtained were transparent, of a light yellow colour and apparently homogeneous, except for the T-cit03 sample, in which the gel matrix contained some white flakes that started precipitating during gelation. Therefore a complexation ratio lower than 0.3 was not tested, since it would not be expected to provide sufficient stabilization of the sol in the applied conditions. Attempts to dilute the mixture, increasing the propanol/Ti molar ratio to 20 or 40, and the hydrolysis ratio to 2-4, had the effect of an incomplete or inhomogeneous gelation.

The stronger reactivity of citrate-modified Ti alkoxide with respect to acac, which allows condensation with a higher water content, can be motivated by the extremely high polarity of the ligand. It has been reported that citric acid can chelate Ti through the central carboxylic and the hydroxyl group, forming a stable five-member ring [93], and leaving two free carboxylic groups. They can interact with other Ti clusters, accelerating condensation reactions. It was also shown that Ti coordination increases the acidity of citric acid and can induce its complete deprotonation (including the hydroxyl group) [86,93]. Studying the adsorption of citric acid on TiO_2 nanoparticles, Mudunkotuwa and Grassian showed that at low pH (2) citrate ions remain strongly coordinated and the particles tend to aggregate; on the other hand, at pH 6 the suspension appeared more stable against aggregation, despite a slightly lower degree of adsorption, contrarily to the common experience of TiO_2 suspensions stabilized at low pH [86]. Here the pH of the solution was not adjusted, so it is regulated by the citric acid concentration and the large H^+ availability could contribute to the advancement of hydrolysis despite the low water amount.

Considering the high polarity of the complexes, the substitution of 1-propanol with ethanol, a more polar solvent, was tried (sample T-cit05b). In this case gelation did not occur after citric acid solution addition, but required a limited addition of water. Also in this case it can be argued that more favourable ligand-solvent interactions enhance the stability of the primary particles and their ability to polymerize in a more controlled way.

TiO_2-citrate systems are characterized by complex acid-base equilibria, which could be exploited to direct the result of the synthesis tuning the pH, besides other conditions like the reagent concentration and the nature of the solvent. In the present work stable sols were prepared increasing the citric acid/Ti molar ratio to 1 (see Section 3.7).

In order to make a comparison between carboxylic acids with different structures, a hybrid material containing acetic acid was also synthesized. Acetic acid, a monoprotic acid (pKa = 4.76) is another common compound in sol-gel processing, added with the double purpose to decrease the solution pH, with an acid catalytic effect, and stabilize TiO_2 sols by coordination, in chelating or bridging mode [57,61,95–99]. Although its efficiency as a stabilizing agent is lower compared, for example, with acetylacetone [61], and it is sometimes used in combination with other additives [96,97], it can lead to slow gelation of TiO_2 if added in a suitable amount [57]. Acetic acid was also reported to contribute to the stabilization of the anatase phase up to high temperatures (1000 °C) in the derived oxide [96,100].

In the present work a hybrid TiO_2-acetate gel was prepared with the following molar ratios: Ti : acetic acid : 1-propanol : H_2O = 1 : 1 : 10 : 4. Gelation was very fast after pouring the hydrolytic solution into the acetic acid-Ti one, however the gel appeared quite transparent and uniform, with a pale yellow colour.

3.4. TiO_2 – catechol

Catechol (1,2-dihydroxybenzene or pyrocatechol) and its derivatives are found in nature taking part in a very broad range of biochemical processes and functions. This versatility arises principally from the unique properties and reactivity of the enediol (more precisely, o-dihydroxyaryl) chemical function: catecholic compounds (or "catechols") can act as weak acids (for catechol pK_{a1} = 9.2, pK_{a2} = 13) and as easily oxidizable reducing agents, while the vicinal hydroxyl groups make them ideal for bidentate coordination and hydrogen bonding. Some consequences are the ability to establish equilibria at moderate redox potential and pH, to irreversibly polymerize through oxidative mechanisms, to interact with all kinds of surfaces and strongly chelate many transition metals [26,46,67,101]. Hence the various possible functions of catechols: anchors, passive links to surfaces and/or covalent supports to other moieties; scaffolds, constituting the framework for two- or three dimensional structures, by polymerization or self-assembly; binding sites to metal ions or other molecules, also when incorporated into complex systems; sensors and switches, able to respond reversibly to external stimuli

in certain conditions [26]. The biomimetic approach, i.e. the attempt to reproduce structures and mechanisms observed in nature, leads to the design of catechol-based materials for biomedical, analytical and nanotechnology applications. Some examples related with dopamine and similar compounds are mentioned in Section 3.5.

The adsorption and coordination of catechol and derivatives on the surface of metal oxides, in particular TiO_2, has been extensively studied, both experimentally and theoretically [46,47,106–113,52,67,68,72,102–105]. Different binding modes have been proposed: bidentate chelating, bidentate bridging, monodentate, hydrogen bonding or mixed configurations. It is generally accepted that catechol interacts with surface Ti atoms similarly to Ti^{4+} ions in solution, complexing in deprotonated catecholate form, replacing a surface hydroxyl group, but the coordination mechanism can be complex and depending on the considered TiO_2 crystal polymorph and facet [46,67]. TiO_2-catechol hybrid materials have attracted interest for different reasons, including the existence of ligand-to-metal charge transfer (LMCT) transitions, causing radiation absorption in the visible range, with a potential in photocatalysis and photovoltaics, as discussed in Section 1.4.

In most reports about this kind of hybrid materials the samples are prepared by surface adsorption on commercial or synthesized TiO_2 nanoparticles or films. A scope of this work is the extension of the bottom-up synthetic approach used with diketones and carboxylic acids to catechol and other enediol ligands. The only known reports concerning the modification of Ti alkoxides with catechol in a similar sol-gel approach are two papers by the group of Suzaki and Sugahara [114,115]. They added catechol to Ti tert-butoxide or iso-propoxide in equimolar ratio and carefully studied the evolution of the system during hydrolysis and condensation, without a further investigation of the optical, electronic or functional features of the products, obtained by sol drying. Their synthesis protocol presented two separated steps of precursor preparation and hydrolysis and adopted large amounts of benzene or toluene and tetrahydrofuran [114,115]. Here the intention is to develop a simpler one-pot procedure, involving a lower catechol content, less abundant and less toxic solvents, and possibly allowing to attain hybrid chemical gels.

The main process parameters utilized in the synthesis experiments, whose products were subjected to characterization, are reported in Table 3.4. The first tests were carried out in conditions similar to those suitable for the TiO_2-acac system: Ti : catechol : 1-propanol : H_2O = 1 : *c* : 10 : 4. When the catechol solution is added to $Ti(OBu)_4$ the colour turns orange to dark red, depending on the concentration. In all cases with the addition of water the solution became turbid and the result was a precipitation, in shorter or longer times. A reduction of *h* to 2, a dilution of the mixture to [Ti] = 0.3 mol/L or a variation of the pH by adding HCl or NH_3 could delay precipitation but did not change the final result.

Catechol coordinated to Ti, similarly to dbm, exposes a benzene ring outwards. When the catechol content is relatively high (c ≥ 0.1) the hydrophobic coverage on the primary particles increases and, in a rather polar solvent like propanol, they become susceptible to gradually aggregate and precipitate, even if the separation from the solvent is not always marked and viscous sols can be formed.

***Table 3.4**. Reaction conditions in the synthesis of TiO_2–cat hybrid powders and gels; the "p" in the sample name indicates a precipitate.*

Sample	***c* = cat / Ti** (mol/mol)	**[Ti]** (mol/L)	***h* = H_2O / Ti** (mol/mol)	**Solvent (additive)**
T-cat001p	0.01	0.85	4	1-propanol
T-cat005p	0.05	0.85	4	1-propanol
T-cat01p	0.1	0.85	4	1-propanol
T-cat02p	0.2	0.85	4	1-propanol
T-cat04p	0.4	0.85	4	1-propanol
T-cat01A	0.1	0.85	4	1-propanol (acacH)
T-cat01C	0.1	0.52	2	1-propanol (citric acid)
T-cat01D	0.1	0.52	2	1-propanol (dea)
T-cat005	0.05	0.57	2	1-propanol + cyclohexane

With lower complexation ratio the hydrophobicity was reduced, but the ligand was unable to modulate the condensation and prevent the formation of small particles. Particulate gels with different catechol content were obtained after drying.

The challenge of achieving TiO_2-catechol chemical gels was faced through two different strategies: the addition of a second "auxiliary" ligand, known to favour gelation in similar conditions, and the use of a mixed solvent with lower polarity. In the first case the idea was also to explore the effect of a mixed hybrid system, including two ligands with different characteristics. Acetylacetone and citric acid, already studied in this work (see Section 3.1 and 3.2), were selected together with diethanolamine (dea). The latter is a secondary amine with two hydroxyl functions, so a potentially tridentate ligand, also frequently used in sol-gel processing, in particular for the stabilization of TiO_2 sols for coatings [61,96,97,116–118]. It was tested with the same purpose in the investigation on the hybrid films (see Section 3.7) and here, to complete the picture with a base along with an acid (citric acid) and a neutral

diketone (acacH). The molar ratios chosen were Ti : catechol : second ligand = 1 : 0.1 : 0.3. The complexation ratio 0.3 was the lowest possible at which all the three single systems without catechol showed gelation; the catechol content was set to 0.1 to facilitate the gel formation. The "auxiliary" ligand was added first, followed by catechol, which always caused the light coloured solution to turn intense red, showing that the other ligand does not prevent catechol complexation to Ti.

In all three cases the aim of gelation was accomplished. The TiO_2-cat-acac system (T-cat01A) appeared as the most sensitive to the reaction parameters and required their accurate optimization and the tuning of pH. According to the H_2O/propanol either a gel-like mass (physical gel) or a viscous sol were obtained. A homogeneous gel was finally obtained adding first a small amount of HCl (0.1 M) in the hydrolytic solution (h = 4, pH ~ 4), to assist hydrolysis and form a stable sol, and subsequently concentrated NH_3 solution, increasing pH to about 10, to catalyse polycondensation. The other two mixed systems with citric acid (T-cat01C) and diethanolamine (T-cat01D) required a higher dilution (propanol/Ti molar ratio = 20) and less water (h = 2) to yield apparently homogeneous, although not transparent gels; the former became a dark red gel in about 5 min, the latter a dark orange gel in about 10 min. It is interesting to note that citric acid and dea systems were less affected by the presence of catechol, which just prolonged the gelation time, even though in these systems the reaction mechanisms are probably different due to the acidic and basic pH established by the ligands. With acacH catechol completely inhibited gelation at acidic pH, as normally occurs for the T-acac materials (Section 3.1). Evidently even a limited content of coordinated catechol, with its bulkier non-polar group with respect to the methyls of an acac ligand, is sufficient to hinder extended cross-linking. This represents indeed a method to prepare a stable TiO_2 sol containing Ti-catechol complexes.

A more direct, yet successful approach was found to be the introduction of cyclohexane to reduce the environment's polarity, an expedient that allowed also TiO_2-dbm gelation. Here the molar composition of the reaction mixture was Ti : catechol : cyclohexane : 1-propanol : H_2O = 1 : 0.05 : 8.5 : 6 : 2, corresponding roughly to a cyclohexane/propanol 2:1 volume ratio. In a few minutes after water addition an opaque but uniform red gel was formed, clearly closer to a chemical gel than the precipitates formed in pure propanol. An analogous result was attained with c = 0.1; the sample T-cat005 was chosen for further characterization together with T-dop005 and T-asc005. The same considerations made for T-dbm about the importance of the ligand-solvent interactions hold in this case.

3.5. TiO_2 – dopamine

Dopamine (4-(2-aminoethyl)benzene-1,2-diol) belongs to catecholamines and phenylethylamines, is a neurotransmitter with many fundamental physiological functions and is synthesized biologically starting from the aminoacid L-tyrosine, generally through L-DOPA (L-dihydroxyphenylalanine). With respect to catechol the hydroxyl groups present slightly higher acidity (pKa1 = 8.9, pKa2 = 10.6) and the amino group provides wider reactivity. Dopamine represents an even better model for a variety of catecholic compounds. A common example of their natural occurrence is in the adhesive proteins produced by mussels, allowing them to adhere to practically every surface, even in wet conditions [26,67]. From the study of this mechanism in recent years polydopamine has emerged as a bio-inspired coating material, easy to produce by oxidative self-polymerization, characterized by versatility, affinity to a variety of substrates, organic and inorganic species. Polydopamine has great potential in adhesion of metals, nanostructures, electrodes, biomedical adhesion, specific immobilization of biomolecules or cells, functionalization of surface hydrophilicity, and so on [26,119]. It presents analogies with melanins, a family of biopolymers with interesting physicochemical properties, including anti-oxidant and free radical scavenging behaviour, wide visible light absorption, fast thermal relaxation, good electrical conductivity [26].

The interactions between TiO_2 and dopamine have been the object of theoretical [120–122] and experimental studies [68,72,117,123–126]. Many of them were aimed at unveiling the role of charge transfer in the increased photoresponse and ROS generation, but these hybrid materials attract interest also for sensing, drug delivery, surface enhanced Raman scattering (SERS), etc. The binding mode of dopamine on TiO_2 should be similar to that of catechol, but it can depend on the crystal surface and the amino group can contribute by coordination with another Ti atom [122]. Recently reports on the conjugation of TiO_2 with catecholic polymers appeared, concerning for example hybrids with polydopamine for photocatalysis [127] or with melanins, formed *in situ* by TiO_2-assisted polymerization of DOPA or DHICA (dihydroxyindole carboxylic acid), showing antimicrobial activity [128].

The present work intended to extend the sol-gel synthetic method to TiO_2-dopamine system. The conditions chosen, summed up in Table 3.5, in terms of molar ratios were: Ti : dopamine : 1-propanol : H_2O = 1 : 0.05 : 20 : 4.

The result was satisfying: in 10 min a dark red, limpid and homogeneous chemical gel formed (T-dop005). The remarkable difference with the behaviour of catechol (see Section 3.4) must be ascribed to the aminoethyl group which distinguish the two molecules and allows dopamine in bidentate

coordination through the diol moiety to interact with other Ti alkoxide, hydroxide or oxide clusters (or other dopamine molecules) through hydrogen bonds or acid/base reaction.

***Table 3.5**. Reaction conditions in the synthesis of TiO_2–dop hybrid gel and powder; the "p" in the sample name indicates a precipitate.*

Sample	***c* = dop / Ti** (mol/mol)	**[Ti]** (mol/L)	***h* = H_2O / Ti** (mol/mol)	**pH**
T-dop005	0.05	0.52	4	acidic
T-dop005p	0.05	0.52	4	basic

It should be noted that dopamine is introduced as hydrochloride adduct (dopamine·HCl), therefore the solution pH is moderately acidic and a catalytic effect on hydrolysis can be present. Since dopamine polymerization is reported to be initiated in basic environment, the effect of a basic pH was assessed, adding NH_3 in the hydrolytic solution while leaving unchanged the other conditions. The outcome was a fast precipitation of a dark orange powder, suggesting that slower and more branched condensation is obtained in acidic solution.

The preliminary result of this study, showing that a small amount of dopamine can readily promote gelation of a hybrid TiO_2, is promising and could be extended to other oxides, other catecholic compounds or to the sol-gel preparation of functionalized hybrid coatings without the need for other stabilizers.

3.6. TiO_2 – ascorbic acid

L-ascorbic acid, commonly known as vitamin C, is an essential bioactive compound. Most animals can produce it from glucose, but humans need a dietary intake from fruits and vegetables. Its acidity is related to its four hydroxyl groups, principally the ones on the ring (pK_{a1} = 4.17, pK_{a2} = 11.57). The moderate acidity of the C3 hydroxyl is due to the stabilization by resonance of the corresponding ascorbate anion. Ascorbic acid is a reducing agent and an antioxidant: it can undergo one electron oxidation to a relatively stable ascorbate radical (thanks to resonance) and a second oxidation to dehydroascorbic acid (another form with vitamin C activity), as illustrated in Figure 3.2. In fact, all known physiological and biochemical functions of ascorbate are due to its action as an electron donor.

The oxidation rate of ascorbate is pH-dependent and is generally accelerated by metal ions; in the absence of catalytic metals the autoxidation occurs *via* the dianion, Asc^{2-}, so it is quite slow at neutral pH and faster at basic pH.

Ascorbate can coordinate metals preferentially through the enediol group, in monodentate or bidentate mode. Complexes of ascorbic acid with Ti(IV) should be relatively strong and not prone to the metal-catalyzed ligand oxidation that renders many metal ascorbate complexes so reactive [129]. Complexes with many different structures can form as a function of pH.

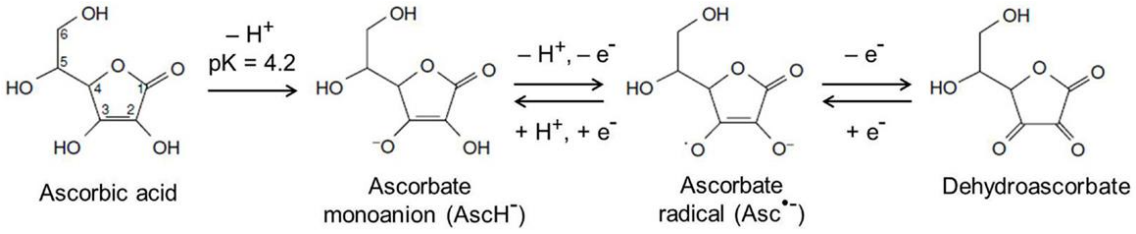

***Figure 3.2**. Chemical structures of ascorbate and its oxidation products* [130].

Ti ascorbate is object of studies as a biologically active form of titanium and was patented as a growth promoter for plants or animals, for applications in fertilizers or aquaculture [129]. Another source of interest is due to the ability of ascorbate to extend optical absorption and improve charge separation in TiO_2 though ligand-to-metal charge transfer, in a similar way to catecholic compounds [68,131–135]. Nevertheless, few works can be found in literature about this photosensitized hybrid system.

In the present work ascorbic acid has been chosen for various reasons: it is available, cheap and safe (contrarily from catechol, quite toxic); it forms chelate complexes with Ti and has many functional groups, but its role in sol-gel synthesis has not been examined; TiO_2-ascorbate hybrid materials have been rarely investigated; due to its reducing ability ascorbate could play a role in oxygen reduction to generate superoxide radicals [133] or in Ti^{4+} reduction to Ti^{3+} [136].

The addition of an ascorbic acid solution to $Ti(OBu)_4$ induces a dark red coloration, indicating the complex formation. Synthesis conditions similar to those used for acac, citrate or dopamine hybrids were not effective to produce homogeneous chemical gels in the TiO_2-ascorbate system. With complexation ratio 0.1 or 0.2 and [Ti] = 0.5 mol/L or higher, fast incomplete gelation occurred, leading to a non-uniform gel-like product. When the mixture was diluted to [Ti] = 0.3 mol/L and HCl was introduced with the hydrolytic solution in 0.1 mol/L concentration, a slower and "cleaner" gelation occurred. The condition of these tests are reported in Table 3.6.

A curious observation is the dramatic dependence of the gelation time on the complexation ratio: T-asc02 (few hours) < T-asc01 (about 3 days) < T-asc005 (about 5 days). It is an opposite behaviour

compared to the usual trend, i.e. an increase of the gelation time with the increase of the ligand concentration. In the synthesis of T-asc005 the viscosity of the mixture grew constantly but a small addition of water was required to finally obtain a stable and elastic wet gel. Supposing that complexation acts primarily through the enediol moiety, a possible explanation could be in the coordination of another Ti by the free hydroxyls of ascorbate, or a hydrogen bonding with another cluster, bringing the clusters closer and facilitating condensation reactions. As the pH was not modified, a slightly higher acidity with the increase of ascorbate concentration is also expected. These effects could contribute to a faster gelation, although more Ti coordination sites are occupied. Moreover, Buettner et al. stated that the binding of Ti^{4+} by ascorbate is strong enough to prevent hydrolytic precipitation, but weaker than binding by other common biological ligands such as citrate, and demonstrated that Ti ascorbate complexes introduced to a citrate solution undergo ligand exchange, according to the models [129]. Therefore, the possibility of a certain mobility of the ascorbate ligands could also be taken into account in the different equilibria established at different concentrations.

***Table 3.6**. Reaction conditions in the synthesis of TiO_2–asc hybrid powders and gels; the "p" in the sample name indicates a precipitate.*

Sample	***c* = asc / Ti** (mol/mol)	**[Ti]** (mol/L)	***h* = H_2O / Ti** (mol/mol)	**Solvent**
T-asc005	0.05	0.3	6	1-propanol
T-asc01	0.1	0.3	4	1-propanol
T-asc01p	0.1	0.3	2	ethanol
T-asc02	0.2	0.3	4	1-propanol

The effect of solvent was also checked: since ascorbic acid is an oxygen-rich molecule with slightly higher solubility in ethanol than in propanol [137], more favourable interactions of the Ti-ascorbate complexes with ethanol could be expected. Indeed, during water addition fast precipitation occurred (sample T-asc01p), while identical conditions in 1-propanol allowed a slow sol-gel transition.

In conclusion, the TiO_2-ascorbate system can be directed to different kinds of product, chemical, physical or particulate gels, and exhibits an interesting behaviour which is worth of deeper investigation.

3.7. Thermal treatment of xerogels

A thermal treatment at higher or lower temperature, often referred to as calcination or annealing, is typically the last step of the synthesis of metal oxides and other ceramic materials *via* solution methods, such as sol-gel. The principal scope is to obtain the pure, stoichiometric ceramic material, with a compact structure deprived of organic solvents, additives or templates, generally in a crystalline phase. The treatment temperature is often a compromise between a temperature sufficiently high to remove organic components and induce suitable formation and growth of a crystal phase, and on the other side low enough to keep satisfying surface properties. Specific surface area and pore volume normally decrease with the heating temperature, as a consequence of crystallization and sintering processes. A higher temperature can be preferred for instance to attain the transformation to another crystalline polymorph or favour the incorporation of a dopant in the lattice. The temperature ramp, namely the heating and cooling rate, can affect the results of the treatment. Another crucial factor is the atmosphere: a typical calcination is performed in air, allowing the organic compounds to be combusted and supporting the oxide structures to reach the stoichiometric composition. An inert atmosphere like nitrogen or argon can be chosen, for example to avoid dangerous explosive reactions, or a reducing atmosphere, often a hydrogen mixture with an inert gas, to promote the reduction of the material's surface, with the appearance of reduced metal centres, oxygen vacancies or other surface defects. In alternative the treatment can be performed in a vacuum furnace. More oxidative conditions, so an oxygen-enriched atmosphere, can also be used.

The synthesis of titanium dioxide by the sol-gel technique usually provides amorphous or poorly crystallized gels or particles. Treatments at temperature of at least 350-400 °C are then performed to trigger or advance crystallization. The most frequently resulting phase at these temperatures is anatase, even though specific synthetic procedures have been shown to produce other polymorphs, like rutile and brookite, at low temperature [138]. The anatase to rutile transition occurs in the range 600 – 1000 °C, strongly depending on the characteristics of the material. Annealing has been tested as a method to introduce defects in TiO_2 structure, in particular reduced Ti^{3+} and/or oxygen vacancies (V_O). Their presence and amount is supposed to cause a dark coloration of the materials, which are hence often called "black titania". In Section 1.5.2 the role of self-induced defects on the photocatalytic properties of TiO_2 is presented. Generally harsh annealing conditions are required, such as vacuum, a strongly reducing gas (hydrogenation), or external reducing agents [50,51].

The major part of the present work is devoted to the study of hybrid materials, which are dried at low temperature (30-60 °C) so that the organic ligands are retained in the material's structure without modifications. The thermal evolution of some samples was analysed, in order to assess their stability

and understand the possible effects of the organic components on the chemical and electronic structure of the oxide even after their removal. As a matter of fact, it was found that the thermal treatment of a hybrid gel can yield a completely different material than that derived from a pure TiO_2 sample.

This part of the study focused on TiO_2-acac hybrid gels, in particular the T-acac04 sample, the most widely characterized, taking as reference the SGT sample. By means of TG-DTA and XRD analysis it was seen that at 400 °C crystallization to anatase phase takes place, concomitant with the loss of most of the organic matter (Section 4.1). The first remarkable difference between the two samples treated at 400 °C for 1 h in air was the coloration: dark grey for T-acac, typically white for SGT. Further characterization evidenced the modified optical and electronic properties owing to the structural defects caused by the dissociation of the organic ligand, as discussed in the next Chapter. Then different calcination conditions were examined, i.e. the time (1 or 3 h) and atmosphere (air, nitrogen or nitrogen/hydrogen 97/3 v/v), to understand their influence in the defectivity generated in the samples. The transformation of the materials at higher temperature were followed by calcination at 600 and 800 °C for 1 h, observing again some differences between the samples, which confirm that the influence of the organic ligand on the structure of the gel-derived material persists after its removal, even at much higher temperature.

3.8. TiO_2-based thin films

Sol-gel technology offers a convenient route for the deposition of thin films by spin coating or dip coating techniques, as described in Section 1.5. An important advantage is given by the rapid gelation occurring during the rotation of the substrate or its withdrawal from the stock solution, induced by the evaporation of the solvent as the thickness of the layer decreases. Compared to a coating of nanoparticles, the sol-gel approach provides compact and uniform films, usually with good adhesion on the substrate. The adhesion is dependent on the surface chemistry of both substrate and coating materials, however generally a good contact at the interface is achieved, which is very important for applications requiring charge carrier transport between the layers, such as electrochemical and solar cells.

The first task in the sol-gel synthesis of films is the preparation of a stable stock solution. The simplest way to obtain a TiO_2 thin film by sol-gel is the spin coating of an alcoholic solution of Ti alkoxide precursor. The solution is usually diluted in alcohol and acidified by adding a concentrated acid (e.g.

HCl or HNO_3), in order to stabilize it, because of the protonation of oxygen in the Ti molecular clusters giving them positive charge and electrostatic repulsion. It was reported that during spinning and subsequent ageing and drying atmospheric moisture can cause a sufficient degree of hydrolysis to yield a compact titanium oxide film, although defective (TiO_{2-x}) [139,140]. On the other hand, in this approach the solution is sensitive to humidity, which can easily start precipitation, the gelation is strictly dependent on atmospheric humidity and the hydrolysis and therefore condensation of the precursor can be incomplete, leading to a certain variability in the results.

The addition of organic compounds able to coordinate Ti ions and stabilize sols in hydrolytic sol-gel process is widely used, since the presence of water ensures a high degree of hydrolysis, so that upon spinning or dipping condensation reactions are favoured to give a better cross-linking and uniformity to the gel film. In the present work, stable sols were prepared with some of the same organic ligands employed for the synthesis of hybrid xerogels, namely acacH, citrate and dibenzoylmethane, and with diethanolamine. AcacH is probably the most widespread stabilizing ligand for Ti in sol-gel chemistry, as already discussed [74,97,99,141,142], citric acid is common in the preparation of gels and powders, but less used for films, whilst dbm has been rarely studied [80–82]. Diethanolamine (dea) is a weak base, which can act as a tridentate ligand through the two hydroxyl groups and the nitrogen of the amino group [143]. It is also frequently used in sol-gel processing, in particular for the stabilization of TiO_2 sols for coatings [61,96,97,116–118] and has been tested here also to obtain a TiO_2-catechol-dea gel (see Section 3.4).

The conditions to achieve long-term stability of the precursor sol where optimized starting from those employed for hybrid gels preparation (Table 2.2, Section 2.1), and are summed up in Table 2.3 (Section 2.2). The influence of most of the process parameters were evaluated on the T-acac system. Stable sols with high Ti concentration (even at [Ti] > 1 mol/L) can be obtained with acac/Ti = 1 : 1 molar ratio. Alternatively, when the [Ti] was reduced to 0.3 mol/L, a more suitable value to produce uniform films which do not crack during drying, a lower complexation ratio of 0.5 could be used. HCl is always added as 0.1 mol/L solution in the hydrolytic solution, and the resulting sols are stable for more than one month even with excess water (h = 10). Varying h from 10 to 4 did not produce a significant effect on the principal properties of the T-acac films.

For the complexation with dea, c ratios 0.5 and 1 were tested, with [Ti] = 0.3 mol/L and h = 2. With c = 0.5 a sol was formed, but it did not show a long-lasting stability: after about two weeks it became opalescent and its viscosity increased until partial gelation. The sol with c = 1, a ratio often reported in literature [96,116,117], was stable for a longer time. Films were prepared starting from both the stock solutions.

Citrate was not able to effectively stabilize the sol with c = 0.5 in conditions analogous to those applied with dea, as gelation started in a few days, so only *c* = 1 was used, achieving good stability.

For the T-dbm system, the same cyclohexane/propanol ratio that led to gelation was kept, with *c* = 0.2 and *h* = 4, diluting the mixture to [Ti] = 0.15 mol/L (see Section 3.2). The sol resulted stable for at least 3 months, confirming a superior stabilizing ability of dbm over other ligands at relatively low complexation ratio.

As a reference, films of bare TiO_x were deposited from a solution of $Ti(OBu)_4$ in 1-propanol, with [Ti] = 0.15 mol/L, without the addition of an organic ligand nor water, which would have caused precipitation.

All the stock solutions were prepared at room temperature and stirred for 2 h, then left ageing at least one day prior to deposition and spin coated usually within one week from preparation. In table 2.3 (Section 2.2) the general data about the preparation of films are reported.

The most important variable in spin coating is the spinning rate, directly related to the film thickness. The most frequently used value was 2000 rpm, but other rates were tested when a thinner or thicker film was needed. At 1000 rpm some films resulted non-uniform because the rotation was too slow to spread the solution uniformly on the whole substrate surface. Acceleration was found to have a smaller influence on the film thickness and morphology. The films were generally dried at 80 °C for 10 min, a sufficient time for the evaporation of the solvent trapped in the thin gel films. When a higher thickness was desired and it could not be accomplished by a decrease in the spinning rate or an increase in the precursor concentration (TiO_2-acac films with [Ti] > 0.5 mol/L in the sol were observed to form cracks during drying or annealing), multilayer films were prepared, with a drying step after the deposition of each layer. A preliminary characterization was carried out also on a bilayer film made of a bottom layer of SGT and a top layer of T-acac (SGT+A), in order to reduce the organic content keeping the functionalization on the superficial part of the film. Many samples were not subjected to further thermal treatments after drying.

Two different annealing temperatures were explored: 150 and 400 °C. The former is a reference temperature, considered still feasible with limited manufacturing costs and compatible with flexible polymeric substrates and with multijunction solar cells structures [144]. At 150 °C the film can gain some density and compactness, losing most of the residual organic solvent, while the complexing ligands used seem to be stably retained, as shown in Section 6.1. 400 °C is usually the minimum temperature needed for crystallization of the amorphous sol-gel films into the anatase phase.

In conclusion, amorphous hybrid films with different organic ligands were prepared, investigating the role of the composition, deposition variables and heating temperature on their properties, which is discussed in Chapter 6.

- CHAPTER 4 -

CHARACTERIZATION OF HYBRID AND DEFECTIVE TiO_2 GELS

4.1. Structural and surface analysis

The synthesized materials were first characterized to determine their structural and morphological properties. The difference between the structures of a xerogel and a particulate sample can be visually recognized and is confirmed by the SEM images of two representative samples, the T-acac04 xerogel and the reference TiO_2 (SGT), displayed in Figure 4.1. After drying at low temperature, the gels are bulk granular materials, with size in the millimetre range. Grinding and sieving allow to select the particle size in the ranges of tens or hundreds μm. Conversely, precipitate samples such as SGT appear as aggregates of small particles of submicrometric size. Nearly spherical particles with a diameter of a few hundred nm and a limited dispersity can be observed in Figure 4.1d.

Xerogels typically possess large surface area and a developed porosity. The surface characterization of T-acac04 xerogel by N_2 adsorption-desorption isotherms estimated a BET specific surface area of 227 m^2/g and a pore volume of 18 mm^3/g, with a prevalently microporous distribution [9]. A significant decrease of surface area was observed after thermal treatment: the T-acac gels annealed at 400 °C for 1 or 3 h in air showed a BET specific surface area of about 40 and 30 m^2/g, respectively, while in those treated in N_2 or H_2/N_2 the values decreased to about 5 m^2/g.

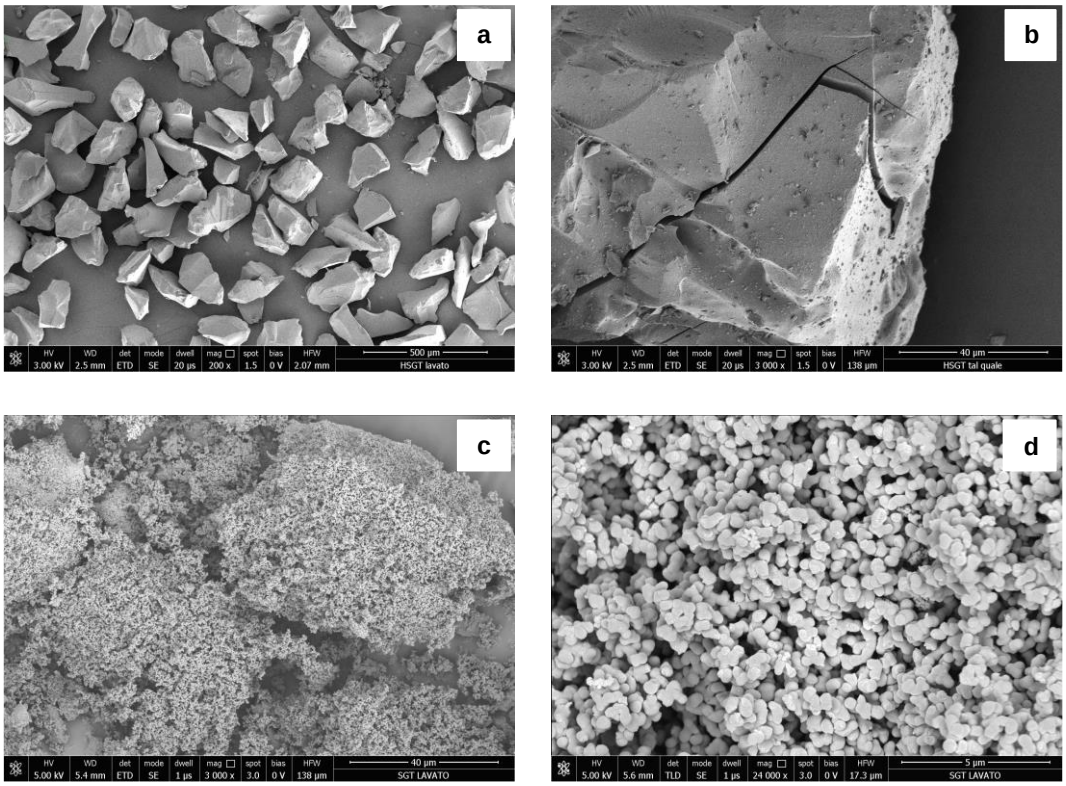

Figure 4.1. *Scanning electron microscopy (SEM) micrographs of T-acac04 xerogel, ground and sieved (90-125 µm fraction) (a, b), and SGT particulate (c, d) after washing in water (different magnifications).*

4.1.1. XRD characterization

The degree of structural order is one of the fundamental properties of a material, particularly important in semiconductors which need convenient charge carrier transport properties for many applications. The crystal phase and crystallinity degree of titanium oxide have a marked effect on the electronic structure, therefore the band gap and band potentials, on the electron and hole lifetime and conductivity, surface adsorption and other features. A first information on the structural organization of the materials is provided by X-ray diffraction. The profiles of a selection of dried gels and powders are shown in Figure 4.2.

The diffractograms of all the samples reported, except T-dbm01p, show an amorphous structure. They present very wide bands, commonly found in amorphous solids such as glasses, indicating a certain degree of short-range order on a sub-nanometric scale. It can be noted that the first of these bands is centred between 25° and 30° 2θ, in the range were the main peaks of crystalline TiO_2 polymorphs are found, except for T-dbm01, for which it is shifted around 20° 2θ, hinting at a somehow different organization.

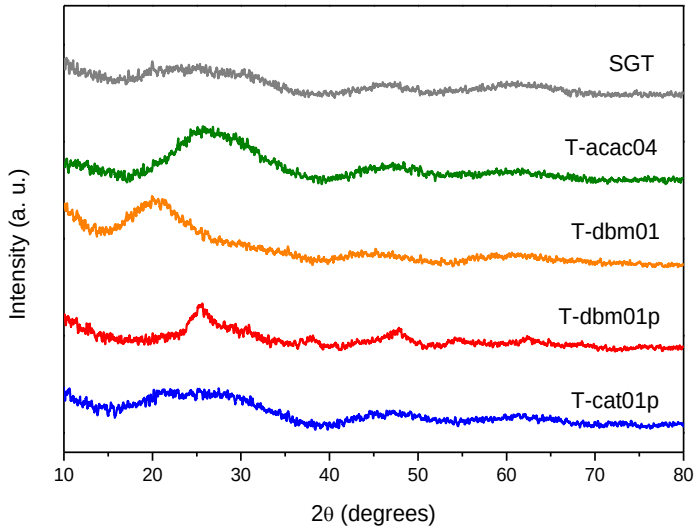

Figure 4.2. *Powder XRD profiles of some hybrid samples and the reference TiO_2 (SGT).*

A xerogel produced by the gelation of a sol is typically amorphous. A wet gel consists in a three-dimensional network of interconnected solid and liquid phase; during drying the solvent evaporates and the gel shrinks, reaching its final structure without the possibility to develop a long-range order, i.e. the growth of crystallites. Moreover, in the samples under investigation the organic ligands are expected to be distributed in the bulk of the materials, bound to Ti^{4+} ions, so they would be a hindrance to the growth of a crystalline lattice.

When the materials are formed *via* precipitation they may have more chance for nucleation and limited growth of a crystalline phase, although the separation from the liquid phase can be fast, so the outcome is variable, depending on the reaction conditions. T-dbm01p, which formed a coarse particulate, is the only analysed sample which exhibits a semicrystalline structure, with very small anatase nanocrystals dispersed in an amorphous matrix (not larger than a few nanometers, the width and low intensity of the peak make the use of Scherrer's equation for the grain size estimation unreliable). Anyway the possibility to synthesize crystalline hybrid materials by the bottom-up sol-gel method proposed here is interesting, since they could have different characteristics with regard to the amorphous counterparts.

The reference SGT sample, a TiO_2 particulate gel which was characterized in the present work, results to be amorphous. On the other hand, a sample previously synthesized in comparable conditions showed some nanocrystallinity [10], attesting the limited control exerted on the formation of oxides by precipitation without complexing ligands. It was reported that in sol-gel TiO_2 powders a prolonged ageing, even at low temperature, can enhance crystallinity; this could be another variable responsible for minor differences in the materials' structure.

Amorphous and poorly crystalline TiO_2 has received much lower attention for practical applications than anatase or rutile. Nonetheless, amorphous materials can present some advantages: they are easily prepared at low temperatures, with the possible incorporation of additives, usually possess large surface area, a significant porosity and high surface hydroxylation. They have been shown to have a potential also in the photochemical field, as photocatalysts or solar cell constituents [3–5,140,145,146].

The crystallization behaviour of some samples has been studied with the aid of thermogravimetric – differential thermal analysis (TG-DTA) data (see Section 4.1.2). Focusing on T-acac xerogels, the onset of crystallization is close to 400 °C. Heating the material up to 400 °C followed by cooling is not sufficient to start crystallization, while an isothermal treatment at the same temperature for 1 h allows the anatase phase to form. Figure 4.3 shows the diffractograms of the T-acac04 (HT) gel calcined at three different temperatures, and the analogous analysis on the reference SGT, while in Table 4.1 the crystal sizes estimated by Scherrer's equation are reported.

Both materials follow a similar evolution with calcination temperature: at 400 °C anatase crystals of about 10 nm are formed. The temperature requested to initiate the transformation of an amorphous TiO_2 structures to anatase is strongly dependent on the material's synthesis procedure, and is generally about 400 °C or higher [147]. Here it corresponds to the point at which the removal of most of the organic component from the xerogels is completing, leaving a free volume which probably favours the densification and reorganization of the structure. A longer isothermal step (3 h or 5 h) at 400 °C does not induce a remarkable growth of the crystallites, but rather an increase of the crystallization degree, visible by the reduction of the amorphous halo underlying the crystal peaks in the diffractograms (data not shown).

The effect of the atmosphere during annealing was also considered, treating T-acac04 in N_2 and H_2/N_2 3/97 v/v (see Section 3.7). The diffraction profiles, not reported, show only marginal differences, with slightly smaller crystallites in these samples than in the air-treated ones.

Upon heating at 600 °C a noticeable grain growth occurs, slightly faster in the HT sample than in SGT. During treatment up to 800 °C for 1 h the transformation of anatase to rutile takes place; HT-800 and SGT-800 show the diffraction pattern of the rutile polymorph. The phase transition is complete in HT, with larger crystallites (almost 70 nm), while in SGT a small fraction of anatase still remained (see Table 4.1). Also this transition temperature is widely variable with the material's synthesis and morphology [147].

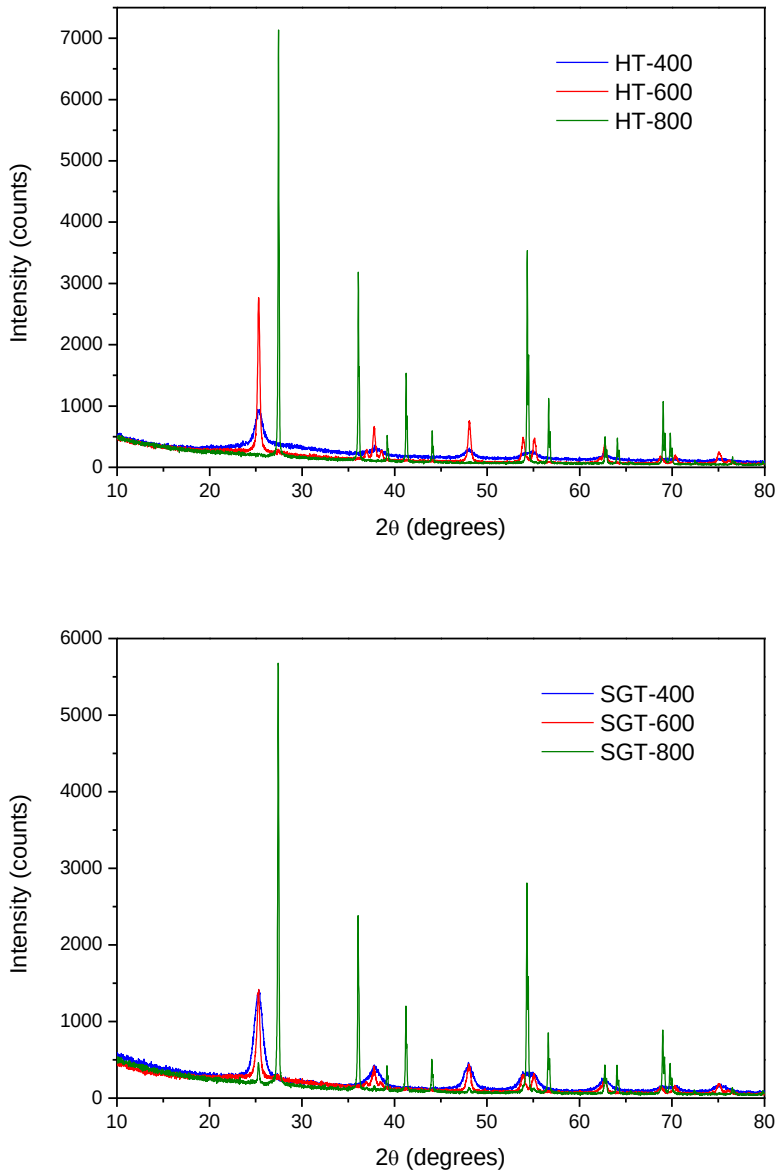

Figure 4.3. *Powder XRD profiles of hybrid TiO_2-acac (HT, top) and reference TiO_2 (SGT, bottom) samples after calcination at 400, 600 or 800 °C in air for 1 h.*

The two considered materials are different as a consequence of their synthesis: HT is a porous xerogel, SGT is composed of small particles. These results show that this intrinsic structural difference affects the characteristics of the samples even when they are treated at higher temperature than those needed for the removal of acac ligands. In the gel-derived material anatase crystallites grow faster with temperature increase, and the transformation to rutile starts, or at least is completed, at a lower temperature, which is possibly related to the microporosity initially present and later caused by the removal of the organic molecules from the bulk. An opposite effect has been reported with carboxylic acids used in the synthesis of TiO_2, which induce a delay of the anatase-to-rutile transformation. Nolan et al. stated that formic acid favoured a bridging mode of chelation depending on the reaction

conditions and that in particular the syn–anti binding hinders cross-linking of the gel network, resulting in a weakened structure and thus causing the rutile formation to occur at a lower temperature than with the syn–syn binding mode, where more ordered gel networks are formed [148].

Table 4.1*. Crystalline phase and grain size (estimated by Scherrer's equation) of some hybrid TiO_2-acac (HT) and reference TiO_2 (SGT) samples, after drying or calcination in air for 1 h at different temperatures.*

Sample	Crystal phase	Crystallite size (nm)
HT (T-acac)	amorphous	-
SGT	amorphous	-
HT-400-A1	anatase	9
SGT-400	anatase	8
HT-600	anatase	30
SGT-600	anatase	23
HT-800	rutile	68
SGT-800	rutile (95 %)	55
	anatase (5 %)	43

4.1.2. Thermal analysis

Coupling thermogravimetric and differential thermal analysis in a simultaneous measurement allows to obtain information about the thermal stability of the hybrid oxides, in particular regarding the organic component, to evaluate the organic content in the structure and the amount of adsorbed species and to individuate phase transformations. The TG-DTA curves for the reference TiO_2 sample (SGT) are displayed in Figure 4.4.

An overall mass loss of about 20 % is seen. Two main contributions can be distinguished, associated with two endothermic DTA peaks: the first one, up to about 150 °C, is due to the evaporation of water and organic solvent molecules adsorbed on the surface and inside the pores; the second one (~ 5 %), occurring between 200 and 300 °C, can be attributed to the evacuation of alkoxide ligands which were not hydrolysed and remained bound to Ti^{4+} ions. Given the low drying temperature (50 °C) of this and other samples, a part of the solvent is normally retained in the structure, as confirmed by some FT-IR spectra in which signals corresponding to the alcohol can be seen (see Section 4.1.3). A large amount

of water adsorbed by contact with air is expected in amorphous porous samples with extended surface and can provide an indication about the available surface area.

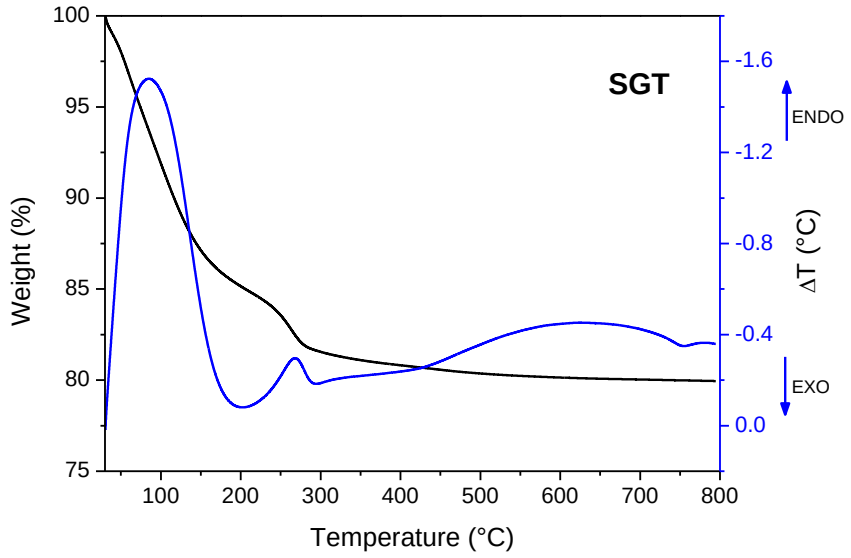

Figure 4.4. *TG (black) and DTA (blue) curves of dried SGT sample, recorded in nitrogen at 10 °C/min.*

As the temperature increases, n-propanol and n-butanol (produced by $Ti(OBu)_4$ hydrolysis) which were physically trapped gradually volatilize (their boiling points are 97 °C and 118 °C, respectively); then the alkoxide groups still linked to Ti (butoxide and propoxide, coming from a possible ligand exchange) are also removed, by simple volatilization or pyrolysis. At 300 °C the composition of the sample is essentially inorganic and the mass loss is almost completed. The exothermic DTA signal related to crystallization of the amorphous phase to anatase is not clearly visible, likely because the process occurs gradually with a low heat release, which is partly counterbalanced by the endothermic signals. Conversely, at about 750 °C there is a small exothermic DTA peak, due to the anatase to rutile transformation (see Section 4.1.1).

TiO_2 – acetylacetone.

The TG-DTA profiles of three TiO_2-acac gels synthesized with the addition of different amounts of ligand (0.25, 0.4 and 0.5 as acac/Ti molar ratio) are displayed in Figure 4.5.

The thermal behaviour of the three samples does not differ largely. The overall mass loss is between 32 and 37 %, with two main inflections associated with endothermic DTA peaks: the first one around 100 °C, related to adsorbed water and alcohol present in all samples, the second one between 250 and 410 °C, mostly due to the volatilization and pyrolysis of acac molecules [9,73,142]. This mass loss actually occurs in two steps in T-acac025 (inflection points at 275 and 360 °C), while a single inflection point is observed for the other two samples (350 °C). The exothermic DTA peak centred at 420 °C is

associated to the crystallization of the anatase phase, which starts as soon as the loss of organic species is completing.

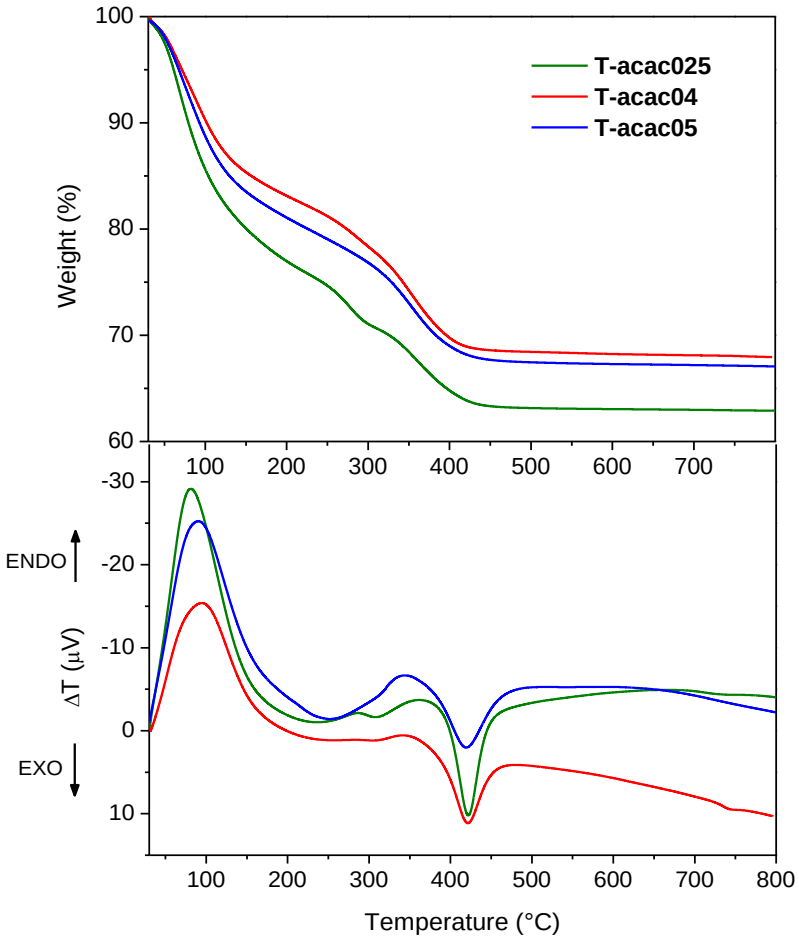

Figure 4.5. *TG (top) and DTA (bottom) curves of TiO_2-acac xerogels, recorded in nitrogen at 10 °C/min.*

Table 4.2 reports the extent of the mass losses, with the second one normalized to the mass of the sample at 150 °C. Assuming that at this temperature most of the water and alcohol has been removed and the complexing ligand is still entirely bound in the structure, the composition of the sample can be considered to be $TiO_2(ligand)_x$, so the second mass loss can be related to the ligand content and compared to the nominal value. This is a simplification which can provide only indicative values, for different reasons:

- the mass decrease is generally continuous, without well separated steps, so the choice for a temperature at which the ligand removal starts (in this case about 200 °C) is arbitrary;
- alkoxide groups remained bound to Ti^{4+} ions can resist up to temperatures higher than 200 °C, as shown by the TGA of SGT (Figure 4.4), and their contribution cannot be discerned from that of the ligand, potentially leading to an overestimation of the ligand content;

- small amounts of residual carbon produced by pyrolysis of the organics can be resistant to the heating in nitrogen, as suggested by a slightly larger mass loss recorded by the TG-DTA in air (data not shown); this could cause some underestimation of the ligand content.

***Table 4.2**. Mass loss events in two different temperature ranges for hybrid TiO_2-acac xerogels (the second value is weighted on the mass of the sample at 150 °C), with the corresponding estimated acac content.*

Sample	**Mass loss % (30 - 150 °C)**	**Norm. mass loss % (200 - 450 °C)**	**Estimated acac/Ti** (mol/mol)
T-acac025	20	17	0.14
T-acac04	15	18	0.14
T-acac05	17	16	0.13

The results regarding the T-acac system clearly show that the acac content is almost the same in the considered xerogels, independent on the initial amount added, and is lower than 0.2 as molar ratio. This suggests a maximum value allowed in the material's structure cannot be exceeded in the applied conditions, so the fraction of hydrolysed acac groups grows with their initial content, and the coordination, hydrolysis and condensation equilibria leave part of the ligand in the liquid phase. It is mainly volatilized together with the solvent during drying, but a certain amount can remain adsorbed on the surface and contribute to the first mass loss at low and intermediate temperatures during TG-DTA measurements. It can be argued that the ligand chemically bound to Ti and held responsible for the peculiar properties of the hybrid oxides is lost at higher temperatures (even if in a rather wide range) and can thus be approximately evaluated by this approach. The presence of nearly unmodified acac coordinated to Ti at 250 °C is attested by a FT-IR measurement on a T-acac04 sample heated up to that temperature [9].

Although the apparently very similar composition, some characterization was performed on the three T-acac samples, evidencing some differences in their onset of optical absorption, EPR spectra and activity in organic pollutants removal [76]. The excess ligand which is not incorporated into the final structure, plays however a relevant role in the synthesis, directing the sol to a homogeneous gel in a controlled way, even with high hydrolysis ratio (h = 10, see Section 3.1).

TiO_2 – dibenzoylmethane.

TG/DTA curves of the three TiO_2-dbm hybrid xerogels are displayed in Figure 4.6. Compared to the T-acac samples, the overall mass loss is higher (40 – 45 %), while the contribution related to the first step is lower (Table 4.3). This can be explained by the hydrophobic character of the T-dbm powders, whose surface exposes the phenyl groups of dbm, resulting less disposed to water adsorption.

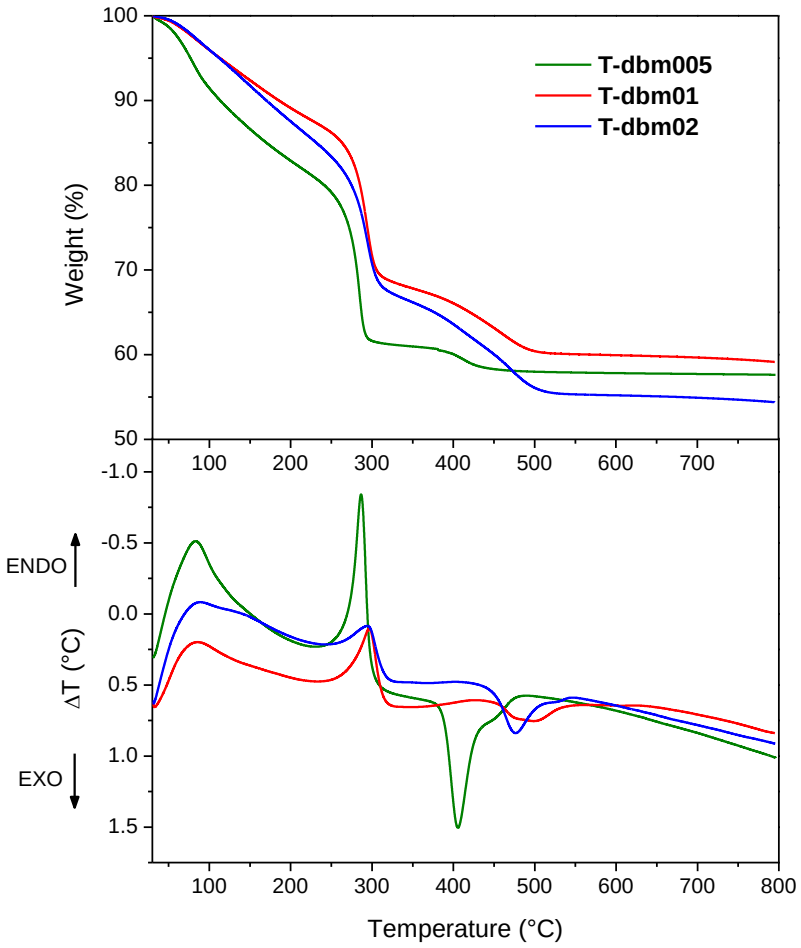

Figure 4.6. *TG (top) and DTA (bottom) curves of TiO_2-dbm xerogels, recorded in nitrogen at 10 °C/min.*

The strong hydrophobicity of the powders is evident when they are put in water, where they tend to aggregate and float on the surface rather than disperse in the liquid, even under intense stirring. In the 200-500 °C range the mass loss over 200 °C is neatly divided in two steps: the first one, more consistent and steep, has an inflection point at about 285 °C for T-dbm005 and 295 °C for T-dbm01 and T-dbm02; the second one, which increases with the nominal dbm content (3, 8 and 11 % respectively), takes place from about 350 °C to 450 °C (T-dbm005) or up to 520 °C (the other two samples). To clarify this behaviour, FT-IR spectra on the T-dbm01 sample heated at different temperatures in nitrogen were recorded (not shown). The FT-IR spectrum of the samples heated up to 240 °C reflects that of the as prepared gel, confirming the thermal stability of Ti-dbm complexes; conversely, the FT-IR spectrum of the sample heated up to 300 °C shows clear modifications, with the disappearance of some bands related to the complex, and the powders change colour, from yellow to red-brown. This means that below 300 °C pyrolysis of the ligand occurs, leaving organic products, probably containing aromatic rings and quite stable, which are volatilized or further decomposed at

higher temperatures. The same mechanism can be involved in the thermal decomposition under inert atmosphere of other hybrid materials.

***Table 4.3**. Mass loss events in two different temperature ranges for hybrid TiO_2-dbm xerogels (the second value is weighted on the mass of the sample at 150 °C), with the corresponding estimated dbm content.*

Sample	**Mass loss % (30 - 150 °C)**	**Norm. mass loss % (200 - 520 °C)**	**Estimated dbm/Ti** (mol/mol)
T-dbm005	13	28	0.10
T-dbm01	8	31	0.11
T-dbm02	8	35	0.12

The estimation of the mass fraction belonging to dbm ligands is not very reliable in this case, anyway from Table 4.3 a trend with the nominal composition of the samples can be observed, consistent with the entity of the last mass loss, indicating that in the samples with a higher dbm content more pyrolysis products, stable up to higher temperatures, are generated during the heating ramp.

Finally, a clear dependence of the crystallization temperature, indicated by the exothermic peak, can be noted as function of the temperature at which the loss of organic components is completed: it shifts from 405 °C (T-dbm005) to 480-500 °C. A careful inspection of the DTA curves shows that the exothermic peaks are actually composed of two partially overlapped contributions. Taking into account that a T-dbm005 sample heated up to 400 °C (above the onset of the exothermic peak) results still amorphous, it can be inferred that some structural rearrangement occurs before crystallization starts, giving an exothermic peak.

TiO_2 – citric acid.

The TG/DTA curves of a representative sample of the system containing citric acid (T-cit04) are displayed in Figure 4.7.

With respect to acac and dbm a higher overall mass loss is seen (almost 57 %), likely due to the relatively higher molar mass of citric acid than acetylacetone and the higher content in the gel of citric acid than dbm. The decrease is initially slow (11 % at 150 °C), then two consecutive losses are seen: a fast one with inflection point at 260 °C and a slower one between 300 and 460 °C. The behaviour is similar to that observed with T-dbm, and can be interpreted likewise, with the volatilization and pyrolysis of citrate ligands, followed by the elimination of the organic products.

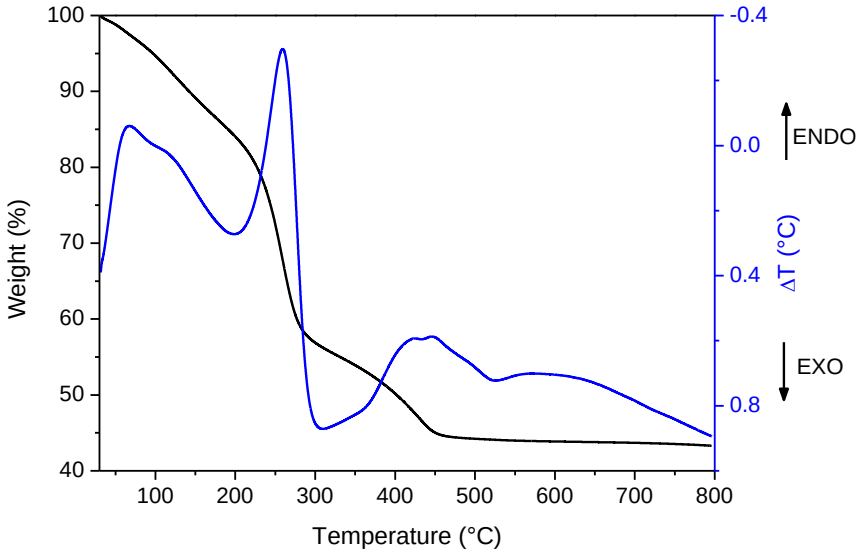

Figure 4.7. *TG (black) and DTA (blue) curves of T-cit04 xerogel, recorded in nitrogen at 10 °C/min.*

An estimation of the citrate content based on the mass loss starting from 200 °C indicates a citrate/Ti molar ratio about 0.18. Here an exothermic DTA peak associated with crystallization is not marked; an exothermic event centred at 520 °C could be related to the formation of the crystalline phase, at higher temperature than in previously discussed systems.

TiO_2 – catechol.

Three hybrid TiO_2 samples obtained by precipitation with the addition of different amounts of catechol were analysed (Figure 4.8).

The overall mass loss is again comparable among the samples, in the range 30-35 %. After the first loss at low temperature, the behaviour differs. T-cat001p shows a unique, concentrated mass decrease of 21 %, centred at 260 °C; T-cat01p and T-cat04p show two steps, a first one centred respectively around 250 and 270 °C and the second spread up to higher temperature (almost 600 °C in T-cat04p). The TG curve of T-cat001p, a sample in which the catechol content should be 1.5 wt%, highlights how alkoxide ligands must be responsible for a consistent fraction of the mass losses recorded around 250-280 °C.

Probably if the gelation or precipitation are very fast, less alkoxide groups are hydrolysed. Once the evacuation of the organic components occurs at relatively low temperature, like T-cat001p, it is free to crystallize as soon as the temperature is sufficient to meet the activation energy as attested by the intense and narrow exothermic DTA peak at 390 °C. In the other two samples wider exothermic peaks are found largely shifted, around 500 °C.

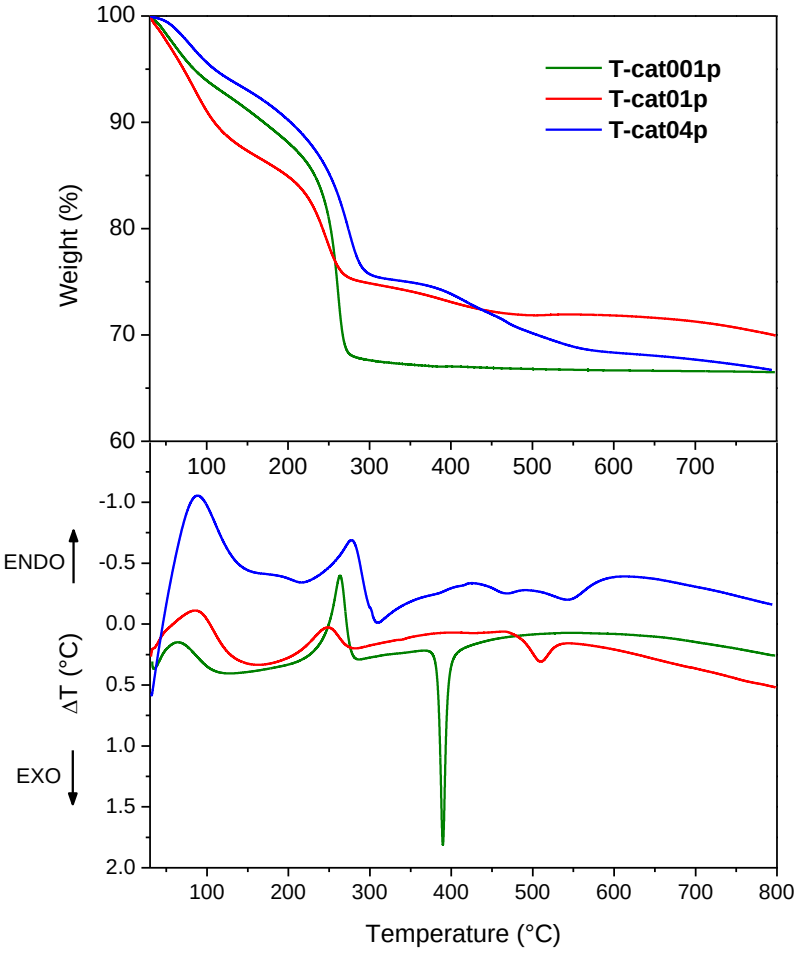

Figure 4.8. *TG (top) and DTA (bottom) curves of TiO_2-catechol dried particulate gels, recorded in nitrogen at 5 °C/min.*

4.1.3. Infrared spectroscopy

Infrared spectroscopy offers easy access to a variety of information about the chemical structure of a material, and an extremely rich picture when organic constituents are present. FT-IR characterization confirms the hybrid composition of the materials and often informs about the type of bonds existing in the organic phase and between the organic compounds and the inorganic matrix.

The FT-IR spectra of two SGT reference samples are displayed in Figure 4.9. SGT (a) has the typical aspect of TiO_2. Three principal features can be observed:

- $\nu < 800$ cm^{-1}: vibrations of Ti-O-Ti bonds;
- $\nu \sim 1620$ cm^{-1}: bending mode of adsorbed H_2O molecules (δ HOH);

- ν = 2800 – 3600 cm^{-1}: stretching modes of O-H bonds (ν OH) in hydroxyl groups, including surface titanol (Ti-OH) groups and H_2O molecules.

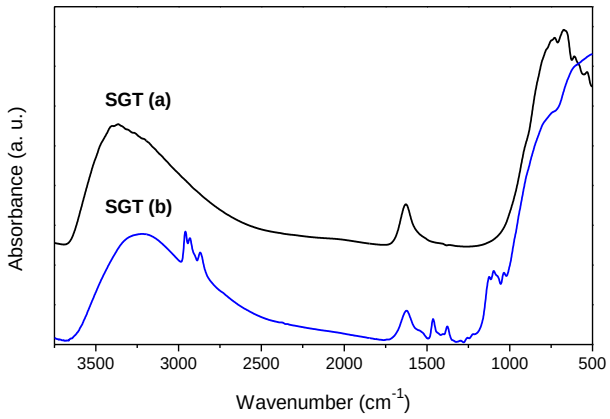

Figure 4.9. *FT-IR absorbance spectra of two SGT TiO_2 particulate samples: one completely hydrolysed and dried (a), the other containing residual alkoxide and/or alcohol (b).*

Surface hydroxyl groups are normally found in amorphous oxides prepared by solution methods. The adsorption of water as the material is exposed to air is also a natural phenomenon: the amount of adsorbed water increases with the specific surface area, pore volume and surface hydrophilicity and can be taken as an indicator for these parameters. The SGT (b) spectrum in Figure 4.9 refers to a sample which underwent incomplete hydrolysis or drying, retaining butoxide groups from the $Ti(OBu)_4$ precursor or alcohol molecules (n-propanol or n-butanol) of the solvent, a situation found also in other dried gels. The resulting additional bands are the following [149]:

- ν = 1035, 1097, 1123 cm^{-1}: CH_3 rocking, C-O stretching, also coupled with C-C;
- ν = 1377, 1462 cm^{-1}: symmetric and asymmetric bending of CH_3 and CH_2 groups;
- ν = 2870 – 2960 cm^{-1}: symmetric and asymmetric stretching of CH_3 and CH_2 groups.

TiO_2 – acetylacetone.

The TiO_2-acac hybrid gels have been analysed by FT-IR, as shown in Figure 4.10. The spectrum of free acetylacetone, liquid at room temperature, is reported in Figure 4.11. In polar solvents the keto form of acacH prevails, characterized by two bands related to the C=O stretching, one of which very strong and broad, found between 1600 and 1700 cm^{-1}. Coordination to a metal with Lewis acidity, like Ti^{4+}, occurs in the enol form, thanks to the formation of a stable delocalized chelating complex. The bands of the carbonyl groups shift to lower frequencies, depending on the strength of the coordinative bond with the metal ion [9,58,75,150,151]. The absence of an intense band close to 1700 cm^{-1} in the spectra of the hybrid materials confirms that there is no free acacH.

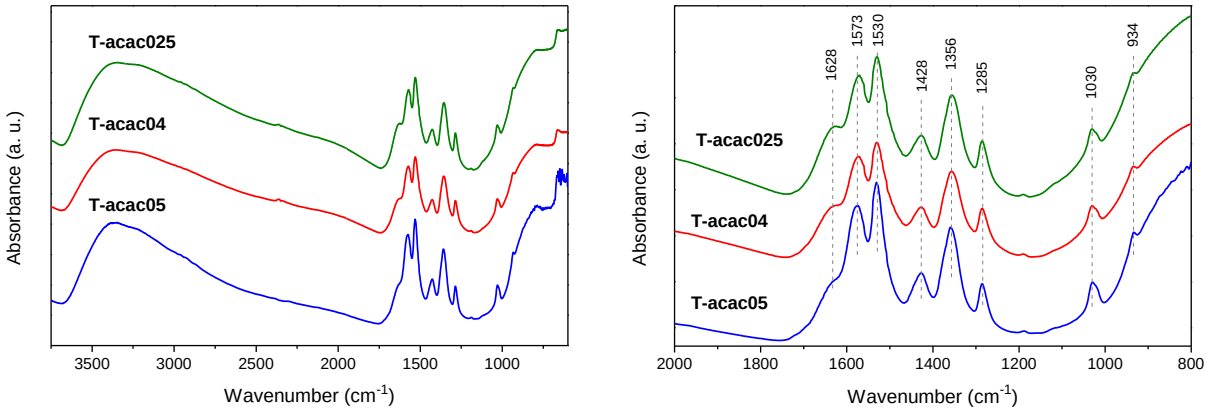

Figure 4.10. *FT-IR absorbance spectra of the TiO_2–acac xerogels, with magnification of the most relevant range.*

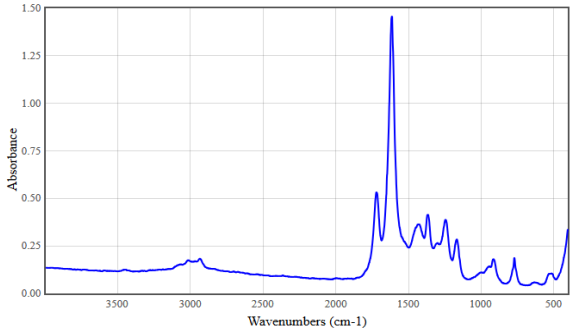

Figure 4.11. *Infrared absorbance spectrum of free acetylacetone [NIST Chemistry WebBook].*

All the samples present the same bands, whose assignment is summarized in Table 4.4. The assignment of the bands in infrared spectra, especially when complex molecules interact with an inorganic component, is not always straightforward and discrepancies in the interpretation of similar spectra can be found in literature, based on theoretical or experimental evidences. The two bands at 1576 and 1428 cm^{-1} can be attributed to the asymmetric and symmetric stretching of carbonyls in enol coordination [9,73,75,152], slightly shifted to higher frequencies compared to those predicted for the $Ti(acac)_3$ complex [153]. Although at 1428 cm^{-1} there could be different contributions [58,150], the assignment of this wavenumber to C=O stretching agrees with results on $Cu(acac)_2$ complexes [152] and ZrO_2-acac hybrid material [75]. The lower energy of this band with respect to the analogous in ZrO_2-acac can be explained with the stronger acid character of Ti^{4+} ions compared to Zr^{4+}, making the C-O bond weaker. The splitting between the two stretching bands, 145 cm^{-1}, is consistent with a bidentate coordination of acac. The band at 1530 cm^{-1}, also absent in free acacH, can be assigned to the enol C=C bonds [73,153–155], the one at 1356 cm^{-1} should be due to another C-O stretching, predicted at 1377 cm^{-1} in $Ti(acac)_3$ with a C=C contribution [153], and observed at 1373 cm^{-1} in ZrO_2-

acac [75], in fair agreement with the attribution of bands at 1379 and 1330 cm^{-1} in mixed Si-Ti-Zr sols with acac to C-O-M bonds stretching [156]. At 1285 cm^{-1} the assignment can be a coupling of C=C and C-CH_3 stretching [79,152,153] or a combination involving a C=O stretching [75,150]. It must be underlined that here C=C and C=O indicate not double bonds, but bonds with 1.5 order, in accordance to the resonance of the chelate ring. At lower wavenumbers typical bands of methyls and C-C single bonds are seen, related to residual alkoxide.

***Table 4.4**. Assignment of the principal FT-IR bands in T-acac spectra.*

Wavenumber (cm^{-1})	Assignment	Wavenumber (cm^{-1})	Assignment
1628	δ H-O-H	1356	ν C=O
1573	ν_s C=O	1285	ν C=C, ν C-CH_3/ν C=O
1530	ν C=C	1188	δ CH_3
1428	ν_a C=O	1030	ρ CH_3

The IR spectroscopic data confirm therefore the supposed bidentate chelating coordination of acac to Ti and the similarities between the studied T-acac xerogels.

TiO_2 – dibenzoylmethane.

Dibenzoylmethane, another β-diketone, is believed to behave in an analogous way as acacH in the coordination of metals. Pure dbm, in solid state, is prevalently in the enol form, stabilized by the formation of an intramolecular hydrogen bond. Accordingly, its FT-IR spectrum, reported in Figure 4.12, does not show any intense band of C=O bonds in the 1600-1800 cm^{-1} region. Such bands lack also in the spectra of the hybrid materials, excluding dbm in the keto form or in monodentate coordination through only one oxygen atom, which would yield a C=O signal [157].

The T-dbm spectra present a number of bands, often resulting from combinations involving vibration modes of the phenyl rings. The attribution of the most relevant bands is reported in Table 4.5. Many of them are not noticeably shifted compared to pure dbm, because it is already in the enol form, with a certain charge delocalization due to the intramolecular hydrogen bond. The major difference is the intense band appearing in the hybrid samples at 1360 cm^{-1}. It belongs to the Ti-dbm complex, since its intensity grows with the dbm/Ti nominal ratio and it does not correspond to the bands of alkoxide groups.

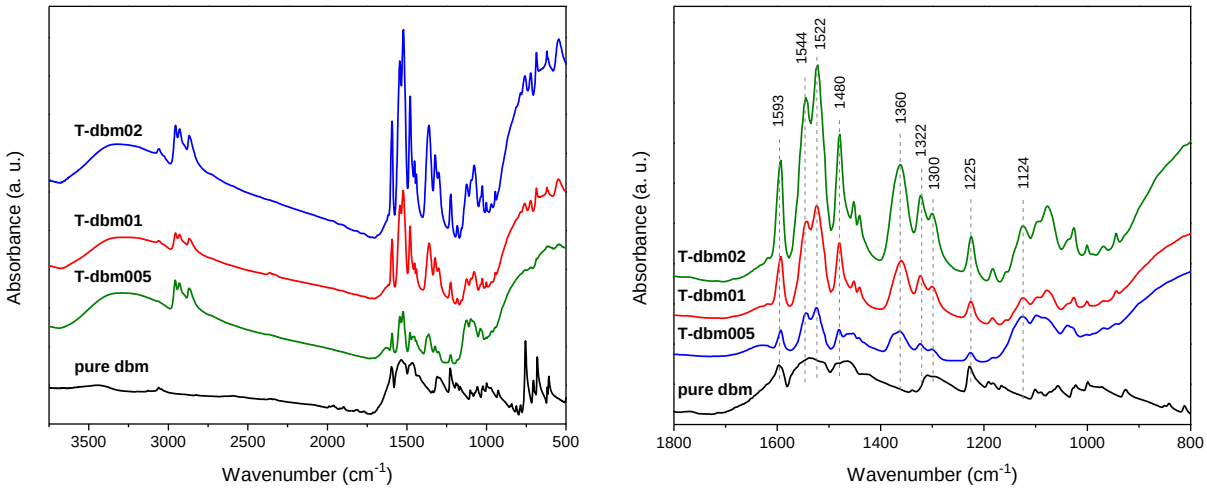

***Figure 4.12**. FT-IR absorbance spectra of the TiO_2–dbm xerogels and pure dibenzoylmethane, with magnification of the most relevant range.*

Although this frequency is not reported in other works, relatively close features were observed at 1401 or 1404 cm^{-1} in $Cu(dbm)_2$ complexes (about 15 cm^{-1} lower in frequency than in $Cu(acac)_2$) [79,152] or predicted at 1377 cm^{-1} for $Ti(acac)_3$ complexes and attributed to C=O stretching with some coupling [153]. Therefore this association can be proposed, in parallel to the 1356 cm^{-1} band in T-acac materials. A confirmation of the validity of this assignment as a distinctive feature of Ti-dbm complexation came from the UV irradiation of TiO_2-dbm hybrid films (see Section 6.1, Figure 6.4), which caused the disappearance of the bands at 1480 and 1360 cm^{-1}, replaced by another one at 1414 cm^{-1}. At the same time the visible light absorption band vanished, demonstrating the breakage of the Ti-dbm coordination bond, as reported in literature [82]. This observation suggests also that the band at 1480 cm^{-1}, assigned in literature to vibrations of the phenyl rings, may be related also to the C=O bonds involved in chelation. The band at 1124 cm^{-1}, not observed in pure dbm, is compatible with Ti-O-C bonds of alkoxide ligands [158].

The spectra of the samples obtained by precipitation (not reported) match perfectly those of the xerogels, showing that there are no differences in the chemical composition. The low capability of these hydrophobic samples to adsorb water is probed by the almost lacking bands around 1630 cm^{-1}. IR spectra support the bidentate chelating structure of both Ti-acac and Ti-dbm complexes in the studied materials.

***Table 4.5**. Assignment of the principal FT-IR bands in T-dbm spectra.*

Wavenumber (cm^{-1})	Assignment	Wavenumber (cm^{-1})	Assignment
1594	ν_s C=O, ν C-C (phenyl)	1360	ν_a C=O
1544	ν_s C=O	1322	ν_s C=C-C, phenyl
1522	ν_a C=C-C, phenyl	1300	ν_s C=C-C, ν_a C-phenyl
1480	phenyl, C=O vibration	1225	δ C-H$_\alpha$, ν_a C-phenyl

TiO_2 – acetic acid.

The FT-IR spectra of TiO_2-acetate hybrid xerogel and free acetic acid are shown in Figure 4.13 and 4.14.

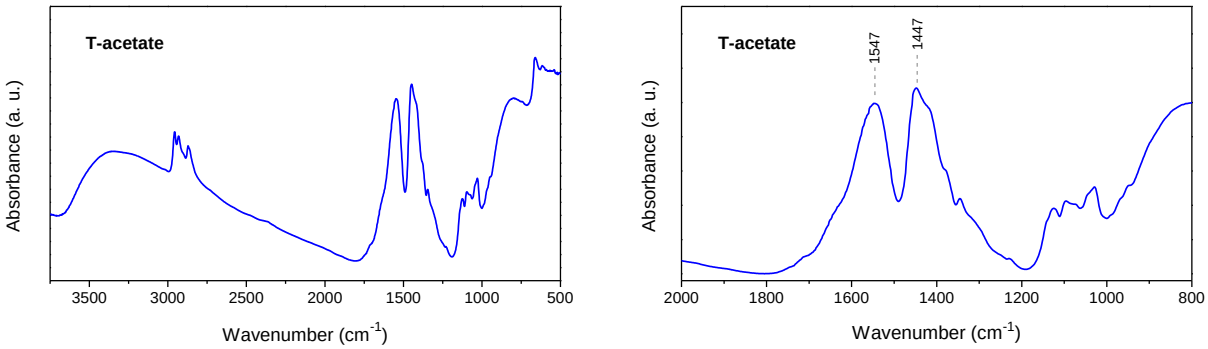

***Figure 4.13.** FT-IR absorbance spectrum of the TiO_2–acetate xerogel, with magnification of the most relevant range.*

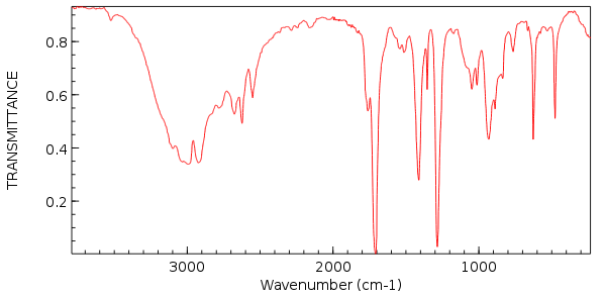

***Figure 4.14.** Infrared transmittance spectrum of free acetic acid in solution [NIST Chemistry WebBook].*

Carboxylic acids can form bidentate complexes with metals in chelating or bridging mode, distinguished by the splitting ($\Delta\nu$) between the two bands corresponding to the asymmetric and symmetric stretching of the carboxylate coordinated to the metal. In general the ranges are:

- $\Delta\nu$ = 50-150 cm^{-1}: chelating bidentate coordination;

- $\Delta\nu$ = 130-200 cm^{-1}: bridging bidentate coordination;
- $\Delta\nu$ > 200 cm^{-1}: monodentate coordination [159].

For Ti-acetate complexes, prepared by modification of Ti alkoxides, splitting values of 80-92 cm^{-1} for the chelating and 140-160 cm^{-1} for the bridging mode were reported [59,158]. In the TiO_2-acetate gel acetic acid is clearly coordinated to Ti, since the bands of free acetic acid around 1715 and 1280 cm^{-1}, due to the stretching of C=O and C-O bonds, have disappeared and two broad bands centred around 1547 and 1447 cm^{-1}, ascribed respectively to the asymmetric and symmetric stretching of the coordinated carboxylate (COO), in resonance form. The splitting, $\Delta\nu$ = 100 cm^{-1}, indicated a bidentate chelating mode, in good agreement with the works of Douff and Perrin [59,158]. They stated that chelating acetate is more resistant to hydrolysis than bridging acetate, so it remains in the gel structure. The shoulders at 1420 cm^{-1} and lower wavenumbers could indicate some other coordination mode, but are more likely related to CH_3 bending, considering also the symmetry of the peak centred at 1547 cm^{-1}, whose shoulder at about 1625 cm^{-1} is due to adsorbed water.

TiO_2 – citric acid.

In TiO_2-citrate hybrid materials the situation is more complex. The spectra of T-cit04 xerogel and pure citric acid are displayed on Figure 4.15. Citric acid in solid state shows two strong bands at 1750 and 1705 cm^{-1}, related to the stretching of free and dimerized carboxylic groups, and groups of bands around 1400 and 1200 cm^{-1}, associated to various stretching and bending modes of carboxylic and hydroxyl groups. In solution the spectra vary with pH, reflecting the varying speciation of the citric acid [86]. The hybrid sample exhibits the overlapping of several bands that can be assigned to coordinated carboxylate.

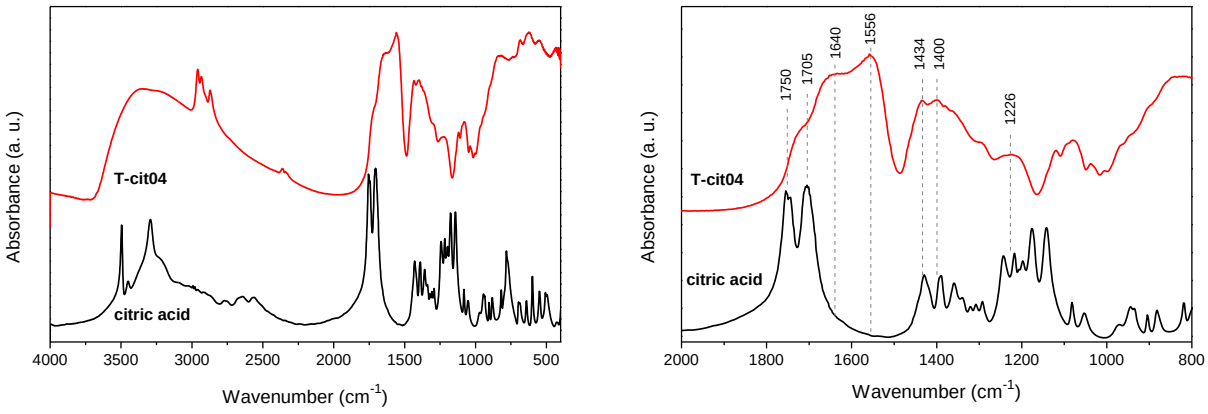

Figure 4.15. *FT-IR absorbance spectra of a TiO_2–citrate xerogel and pure citric acid, with magnification of the most relevant range.*

Mudunkotuwa and Grassian reported values about 1575 and 1400 cm^{-1}, the latter with an additional component at 1436 cm^{-1}, for the asymmetric and symmetric stretching of coordinated COO^- in citrate adsorbed on TiO_2 surface [86], while Guo et al. found these vibrations at 1550 and 1410 cm^{-1} for citrate added to a $TiCl_4$ solution [89]. Very similar wavenumbers are observed in the spectrum of T-cit xerogel: 1556, 1434 and 1400 cm^{-1}, with splitting of 122 and 156 cm^{-1}, suggesting a probably bidentate bridging coordination. The existence of contributions around 1640 and 1710 cm^{-1} and below 1400 cm^{-1} indicates a varied scenario, with a range of binding modes and some carboxylate groups which remained free or more weakly bound, for example through hydrogen bonds. The chelation by a carbonyl and the hydroxyl group of citrate can also be considered as a potential contribution [93], with the C-O coordinated to Ti possibly stretching in the region about 1100 cm^{-1}. Due to the substoichiometric hydrolysis ratios in the syntheses of T-cit gels, a consistent amount of residual alkoxide is still present, as testified by the CH_2 and CH_3 bending vibrations around 2900 cm^{-1}.

TiO_2 – catechol.

Catechol is able to firmly bind to metals in bidentate mode. Both its coordination with Ti^{4+} ions in solution and adsorption on TiO_2 nanoparticles or films have been subjected to several studies by spectroscopic techniques as well as theoretical calculations, due to the importance and ubiquity of catecholic compounds, and in general of metal-organic interactions through the enediol functional group. The FT-IR spectra of some of the TiO_2-catecholate materials are shown in Figure 4.16 and the assignments of most of the bands are listed in Table 4.6.

Two samples obtained by precipitation and a xerogel present the same bands, with an intensity increasing with the nominal catechol/Ti ratio. The vibrational spectrum of catechol includes several bands, mainly due to stretching modes of the aromatic ring and the phenol groups (C-O) and bending of O-H and C-H [105,108]. The modification with respect to the spectrum of pure catechol is in agreement with different literature reports: the two strongest bands at 1479 and 1256 cm^{-1} are ascribed to stretching vibrations of the C-C bonds in the aromatic ring and of C-O groups involved in the coordination [68,69,105–108]. The bidentate binding of catechol affects also the stretching of the aromatic ring, confirming a strong charge delocalization related to the complexation.

Although it is certain that the coordination of catechol to Ti occurs *via* both deprotonated phenol groups, from the IR data it is difficult to discriminate between a chelating or bridging configuration. Some authors claim that the former predominates [68,103,104,106,113], while others find the latter energetically more favoured [105,108,160]. Probably both geometries are possible and one can prevail according to surface coverage and adsorption sites, as terraces, edges and point defects of different crystalline surfaces favour different coordination modes [106,161,162].

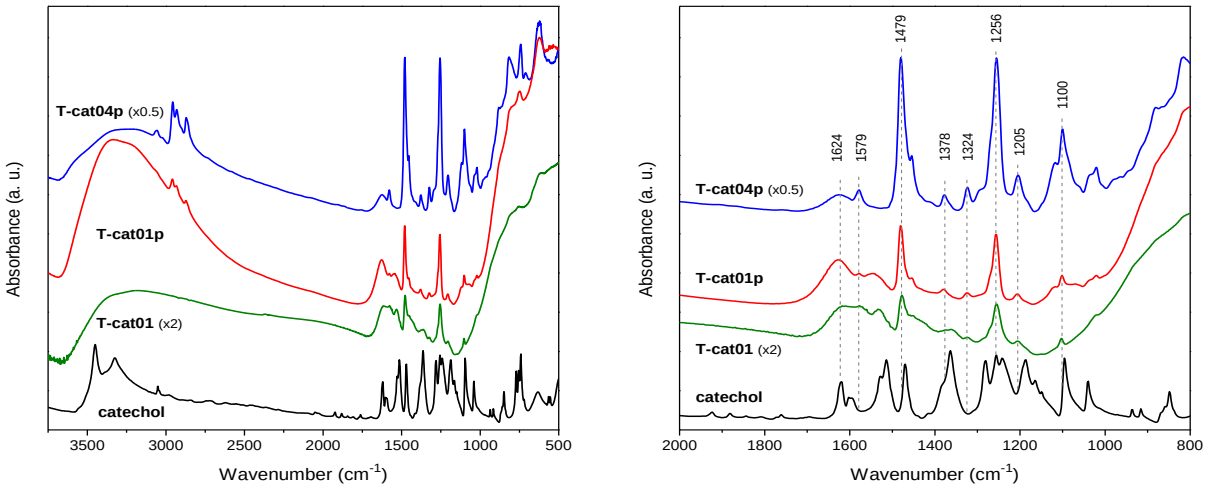

Figure 4.16. *FT-IR absorbance spectra of TiO_2–catechol particulate and xerogel and pure catechol, with magnification of the most relevant range.*

Table 4.6*. Assignment of the principal FT-IR bands in T-cat spectra.*

Wavenumber (cm^{-1})	Assignment	Wavenumber (cm^{-1})	Assignment
1624	δ H-O-H	1324	ν C-O + ν C=C/C-C
1579	ν C-O + ν C=C/C-C	1256	ν C-O
1479	ν C=C/C-C	1205	δ C-H, δ O-H
1378	δ O-H, ν C-O + ν C=C/C-C	1100	δ C-H

In the present case, since the complex is formed directly on the monomeric Ti alkoxide precursor in the first step of the synthesis procedure, assuming that it is highly stable and mostly not displaced during hydrolysis and condensation, the chelating bond seems the most likely geometry.

It is interesting to note that, when a second ligand (acetylacetone, citric acid or diethanolamine) was added during the TiO_2-catechol synthesis allowing gelation in a polar solvent (see Section 2.4), the features of both ligands appear in the FT-IR spectra, without remarkable modifications (Figure 4.17). The two stronger bands of bound catechol at 1479 and 1256 cm^{-1} result unchanged, while the others are covered by the bands of the second ligand because of its higher amount with respect to catechol (3:1 molar ratio) and the higher intensity of the bands of Ti-acac and Ti-citrate.

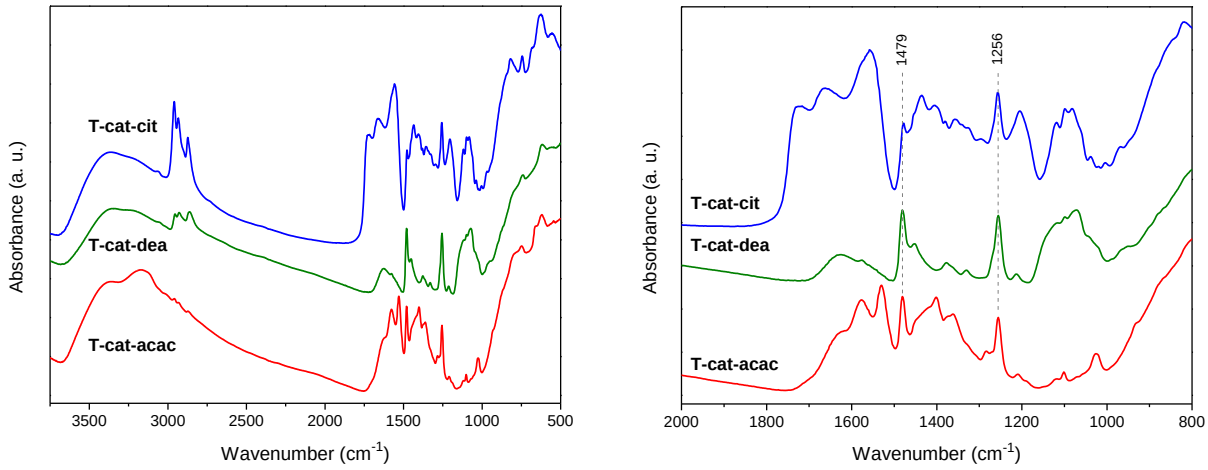

Figure 4.17. *FT-IR absorbance spectra of mixed TiO_2–catechol xerogels, containing also acetylacetone, diethanolamine or citrate, with magnification of the most relevant range.*

In the spectrum of T-cat-dea typical features of diethanolamine can be seen, partly overlapped with catechol bands: a contribution of the N-H deformations around 1600 cm^{-1}, C-H bending at 1450 and 1375 cm^{-1}, and the sum of C-O, C-N vibrations and C-H bending around 1100 cm^{-1} [97]. The only significant variation can be observed in T-cat-acac, where a band centred at 1400 cm^{-1} appears, absent in both the hybrid samples with acac or catechol, and possibly indicating some interaction between the two molecules.

TiO_2 – dopamine.

Dopamine is expected to behave in a similar way as catechol in the complexation of metal ions. However, from the examination of the spectrum of a T-dop gel with dop/Ti molar ratio = 0.05 (Figure 4.18), analogies and differences with that of T-cat (Figure 4.16) can be detected.

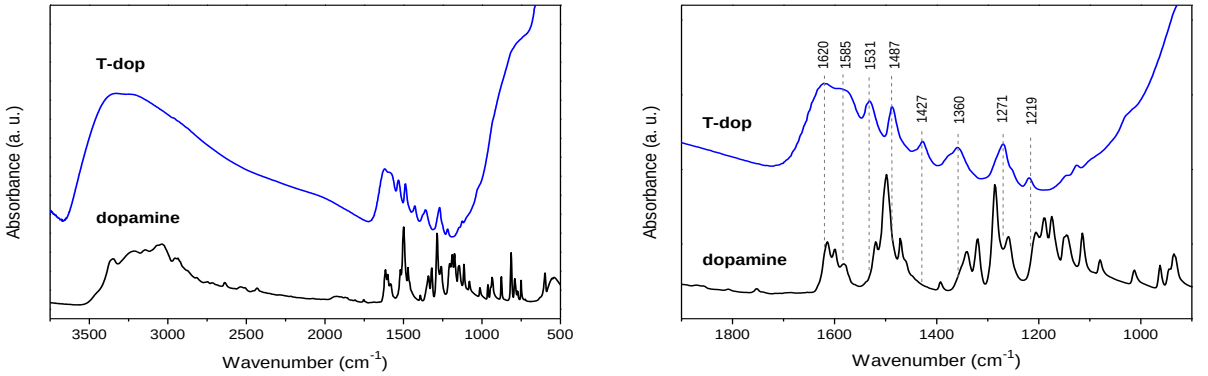

Figure 4.18. *FT-IR absorbance spectra of TiO_2–dop xerogel and pure dopamine hydrochloride, with magnification of the most relevant range.*

In the spectrum of T-dop all the bands have similar intensity. The two strongest bands in T-cat here are found at slightly higher frequencies, 1487 and 1271 cm^{-1}, again related to aromatic C=C-C stretching and C-O stretching respectively [126,163]. These values result shifted to lower wavenumbers of about 10 cm^{-1} with respect to both free dopamine and dopamine adsorbed on some TiO_2 materials, possibly attesting a strong complexation which perturbs also the benzene ring. The overlapped bands between 1620 and 1585 cm^{-1} can receive contributions from aromatic ring stretching, asymmetric bending of N-H, besides of O-H bending of adsorbed water. The band at 1530 cm^{-1} is not reported in other works; it could be assimilated to the aromatic ν (C=C-C) coupled with δ (C-H), found at 1515-1530 cm^{-1} for catechol, free or adsorbed on TiO_2 at acidic pH [107,108]. Curiously, a similar band appears also in the spectra of T-cat hybrid samples with 0.1 cat/Ti ratio (but not on Ti-cat04). The new band at 1427 cm^{-1} was revealed also by Dugandzic et al., who assigned it to a symmetric N-H umbrella mode characteristic for the protonated NH_3^+ group of dopamine [126]. Indeed, from recent calculations by Ronchi et al. emerges that the dopamine amino group has a relevant role in the coordination on TiO_2 surface, being able to bind a Ti atom, and that its protonation is favoured at high surface coverage [122]. Finally, the band at 1360 cm^{-1} is usually attributed to O-H bending in catechol but is supposed to be absent of weak in the coordinated molecule; a hypothesis could be a shift to higher frequency of the methylene bending vibrations, reported at 1340 cm^{-1} in dopamine [126], caused by coordination of the adjacent amino group to Ti. Valverde-Aguilar et al. assigned a band at 1350 cm^{-1} in TiO_2-dopamine films to a C-C stretching of dopaminechrome, an oxidation products of dopamine, pointing out that it is easily oxidized [117], anyway here other bands possibly due to oxidized derivatives are not observed, so this eventuality can be discarded.

TiO_2 – ascorbic acid.

The complexation of ascorbate to Ti was evaluated by FT-IR. The IR spectrum of ascorbic acid (Figure 4.19) displays characteristic bands, such as the four O-H vibrations of its four hydroxyls between 3220 and 3520 cm^{-1}, the stretching of the lactone C=O at 1755 cm^{-1}. the stretching of the C=C around 1665 cm^{-1}. and a semicircle stretch mode, where the top half of the ring stretches with the bottom half contracting (coupled ν (C=C) and δ (C-C), with likely contribution of O-H bending) at 1320 cm^{-1} [131]. The T-asc xerogel exhibits remarkable shifts of the bands, indicative of the bidentate complexation, which is supposed to occur through the two hydroxyls of the enediol group, favoured by resonance of the deprotonated structure. The charge delocalization involves the ν (C=O), shifted to 1722 cm^{-1} and the ν (C=C), shifted to 1616 cm^{-1}, indicating a decrease in their electron density, and the vibration of the ring, shifted to 1363 cm^{-1}, meaning a slight increase in the vibration energy [131]. The stretching of C-O groups coordinated to Ti is associated to the bands at 1172 cm^{-1} and lower frequencies [133]. The first two variations seem larger than those recorded by Rajh et al., suggesting that the Ti-ascorbate complex obtained can have a stronger electronic coupling than that realized by chemisorption.

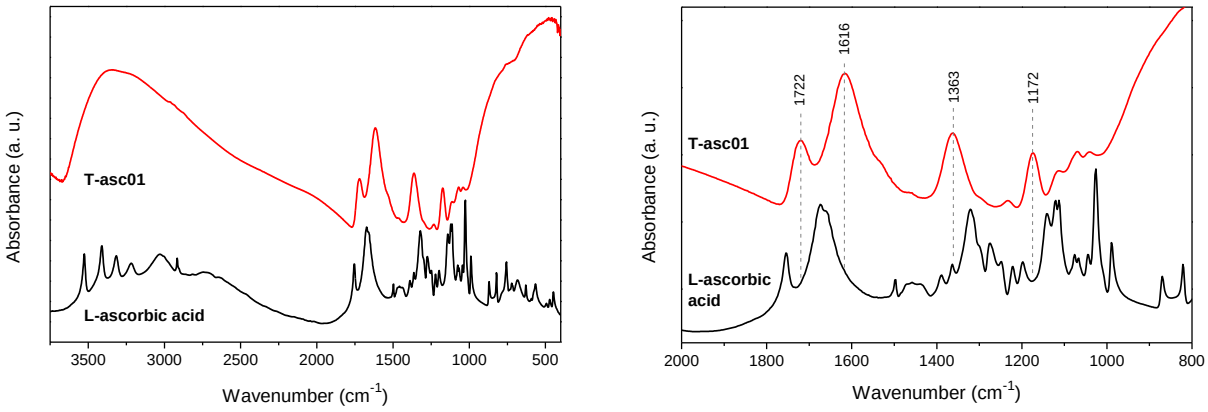

Figure 4.19. FT-IR absorbance spectra of pure ascorbic acid and a TiO_2–ascorbate xerogel, with magnification of the most relevant range.

The results are consistent with chelating binding, with the formation of a five-membered ring around the surface Ti atoms having a favourable conformation of bond angles and distances for octahedrally coordinated Ti [131].

To summarize, FT-IR spectroscopy gives a detailed view on the structure of the organic components and of their binding to the inorganic matrix, attesting for all the hybrid materials the existence of strong bidentate coordination of the ligands to Ti atoms.

Less information is gathered about the materials after calcination at 400 °C. The FT-IR spectra of the reference SGT treated in air for 1 h and the T-acac sample treated in air or N_2 for the same time (Figure 4.19) do not show any defined signal of organic compounds, indicating that the ceramic oxides are obtained. The main difference between the samples is the higher amount of adsorbed water and surface hydroxyls on SGT-400, related to a higher surface area and porosity of the particulate material.

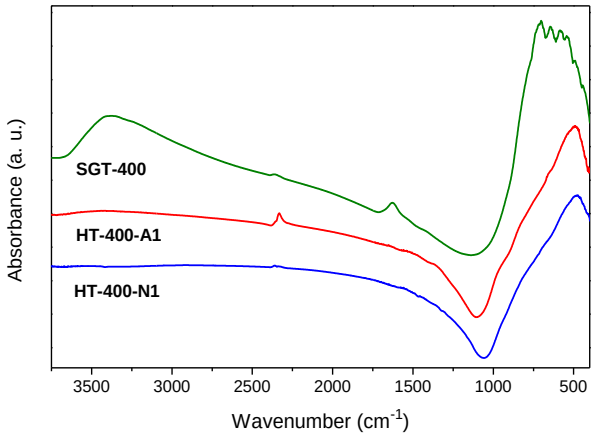

Figure 4.20. *FT-IR absorbance spectra of reference TiO_2 and hybrid T-acac after calcination at 400 °C in air (SGT-400, HT-400-A1) or nitrogen (HT-400-N1).*

4.1.4. XPS characterization

A deeper insight into the chemical and electronic structure of some of the materials was achieved by means of X-ray photoelectron spectroscopy, performed at the University of Cagliari. The technique allows to find out a series of information about the surface composition, purity, chemical speciation, oxidation state of the elements and valence band structure.

This characterization included four samples:

- T-acac04 (HSGT, hybrid sol-gel TiO_2) xerogel;
- SGT, reference TiO_2 powder;
- HSGT sample calcined in air at 400 °C for 1 h (HSGT-400);
- SGT sample calcined in air at 400 °C for 1 h (SGT-400).

The survey spectra are shown in Figure 4.21. For all the samples only the signals of titanium, oxygen and carbon were detected. Ti and O are confirmed to be the only components, with a ratio close to the stoichiometric one. Carbon is present in very small amounts, except in the HSGT sample, containing acetylacetonate [10]. Some C contamination is normally found on samples which have been in contact with atmosphere. In the materials prepared by sol-gel and dried at low temperature a contribution of organic impurities is expected, mainly alkoxide deriving from the metal precursor and solvent molecules, as shown by some FT-IR spectra. In the calcined samples, the carbon is believed to be principally due to atmospheric contamination, even if the possibility of a small amount of carbon residual after the decomposition of the organic components of the materials cannot be excluded.

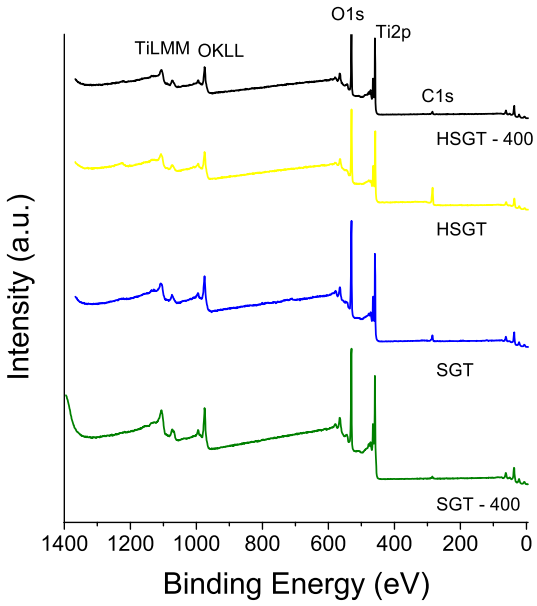

Figure 4.21. *XPS survey spectra of the investigated samples. X-ray source: Al Kα (1486.6 eV) [10].*

The C1s XPS spectra for all samples are shown in Figure 4.22, with the components of the spectrum of HSGT resolved using the curve fitting parameters of the C1s signal of titanyl acetylacetonate, $TiO(acac)_2$, taken as a reference compound. The peaks are individuated as sp^2, sp^3 and C-O components, corresponding to those of the acac ligand in the reference compound, providing further confirmation of the formation of a stable Ti-acac complex in the material [10].

The quantitative composition of the surface samples, calculated considering the Ti2p and the O1s signals, is reported in Table 4.7. It is always close to the stoichiometric one (Ti = 33.3 at%, O = 66.7 at%), and among the samples the composition closest to the expected one is achieved by SGT-400, while the lowest oxygen content is found for HSGT-400.

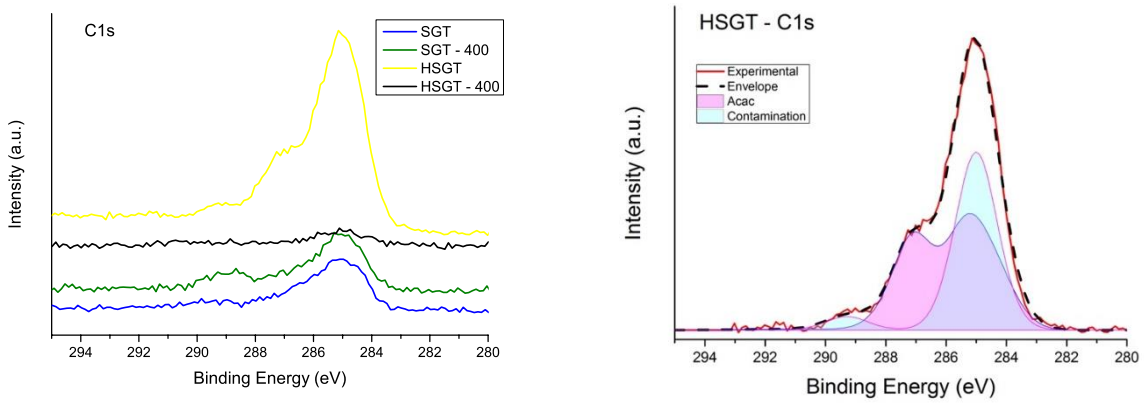

Figure 4.22. *High-resolution C1s spectra of the investigated samples (left); deconvolution of C1s spectrum of HSGT (right). X-ray source: Al Kα [10].*

The inspection of the Ti2p spectra (Figure 4.23) shows that the signals are multi-component except for SGT-400. The binding energy of the $Ti2p_{3/2}$ peak is found to be 459.1 eV in this sample and is assigned to Ti(IV) in TiO_2 according to literature [10,164]. Together with Ti(IV) also Ti(III), at BE about 457.3 eV, is present at the surface the samples SGT, HSGT and HSGT-400. In the last sample also a third component was observed, at even lower BE values (455.8 eV). This component might be assigned to Ti oxides with stoichiometry between Ti_2O_3 and TiO (sub-oxides), being the literature BE value for TiO at 455.1 eV [10,165].

The annealing in air at 400 °C for one hour gives, as a matter of fact, two opposite results for SGT and HSGT. For the former the complete oxidation of Ti^{3+} to Ti^{4+} occurs giving a stoichiometric white anatase sample. On the contrary for the hybrid gel a strong reduction of Ti to lower oxidation states occurs giving the HSGT-400 dark grey sample, whose composition can be expressed as $TiO_{1.85}$ and where the overall surface fraction of reduced Ti sites (Ti^{3+} and Ti with oxidation state lower than +3) results about 26 % (see Table 4.7).

Table 4.7. *Calculated O/Ti ratios, binding energy (BE) of the most intense photoelectron peaks and valence band edge potential for the analyzed samples. Mean values and standard deviations over three measurements given in parentheses [10].*

Sample	**Composition** (at. %)	**Ti2p$_{3/2}$ BE** (eV)	**Peak area** (%)	**Valence band edge** (eV)
HSGT	Ti = 30.2 (0.4) O = 69.8 (0.4)	Ti (IV): 459.0 (0.1) Ti (III): 457.1 (0.1)	94 (1) 6 (1)	3.9
SGT	Ti = 30.0 (0.7) O = 70.2 (0.2)	Ti (IV): 459.3 (0.1) Ti (III): 457.5 (0.1)	91 (3) 9 (3)	4.2
HSGT-400	Ti = 35 (1) O = 65 (1)	Ti (IV): 459.3 (0.1) Ti (III): 457.3 (0.1) Ti (?): 455.8 (0.1)	74 (1) 16 (1) 10 (1)	4.3
SGT-400	Ti = 32(1) O = 68 (1)	Ti (IV): 459.1 (0.1)	100	3.7

The removal of acetylacetone from the structure must be held in some way responsible for this phenomenon. Although the annealing was performed in air, the large amount of organic molecules escaping from the solid, also due to the relatively fast heating ramp (10 °C/min) might have locally induced the formation of a reducing atmosphere in the tubular furnace, since it was in a static atmosphere, without a forced gas flow.

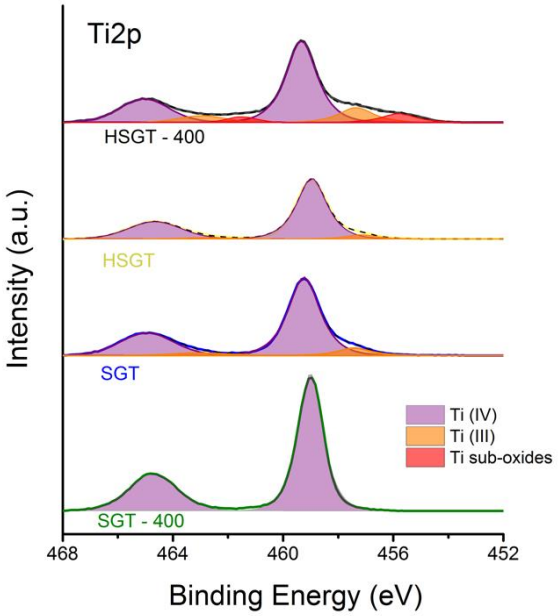

Figure 4.23. *High-resolution spectra of the investigated samples; the shaded areas are the Gaussian-Lorentzian model functions used in the curve-fitting procedure X-ray source: Al Kα [10].*

It is worth considering that, in gels prepared by the present procedure, part of surface and bulk Ti atoms are complexed by chelating acac, providing O atoms that fulfil Ti coordination. When heating causes the breakage of the Ti-O coordination bonds and the removal of the organic, oxygen deficiency (vacancies) remain. Oxygen vacancies can host a different number of electrons (a neutral vacancy is associated to 2 electrons), which can also localize on neighbouring Ti^{4+} ions reducing them to Ti^{3+} [49]. Another hypothesis, suitable in particular for easily oxidizable ligands, is their actual oxidation during the annealing, for instance by a mechanism of Mars-Van Krevelen type, in which an oxygen of the lattice is incorporated in the oxidized product, leaving behind a vacancy. Some data supporting the presence of oxygen vacancies in the HSGT-400 sample are offered by EPR spectroscopy (see Section 4.3).

The reduction of TiO_2, and more generally the production of TiO_2 materials containing structural defects, like vacancies, has recently attracted wide interest as an alternative strategy to extend the radiation absorption and enhance the photocatalytic efficiency of this oxide, as discussed in Section 1.5. Usually harsh conditions are needed for the purpose, for instance vacuum annealing, hydrogenation or the use of reducing agents [50,51]. The possibility to prepare defective TiO_2 by a simple annealing in air at moderate temperatures would certainly represent a practical advantage. Therefore, the process of Ti^{4+} reduction is worth a deeper investigation, to understand its mechanism, reproducibility, the effect of process variables and so on. Preliminary characterization data on the annealing of HSGT at 400 °C for a longer time or in a different atmosphere (N_2 or H_2/N_2) seem not to produce the same outcome, suggesting that the conditions needed are specific and require a careful control. However, the topic is the object of ongoing research.

To conclude the XPS data examination, the estimated valence band edge values can be considered (Table 4.7). The shifts in the valence band edge follow an opposite direction as a consequence of thermal treatment: for HSGT the potential turns more positive (from 3.9 to 4.3 eV), while for SGT it shifts to a more negative value (from 4.2 to 3.7 eV). These data might be put in correlation with the band gap energy evaluated by DRUV-vis spectra and with electrochemical data, with the aim to depict the electronic structure of the materials, since the band potentials, as well as the intra-gap electronic states, are important in determining which photoinduced reactions and processes can occur on a semiconductor.

4.2. Optical properties: Diffuse Reflectance UV-visible characterization

The absorption of electromagnetic radiation in the ultraviolet – visible range is a fundamental property for semiconductors in view of photocatalytic, photoelectrochemical, photovoltaic, optoelectronic or related applications. Titanium dioxide is a suitable material in such fields owing to its excellent photoinduced activity in the UV range. However, to improve the conversion of solar energy it is necessary to activate harvesting and utilization of visible light, constituting about 45 % of the solar spectrum. Photosensitization of TiO_2 is a viable strategy to achieve this goal, as described in Section 1.5 and later on, and represents one of the objectives of this work.

Hybrid gels.

The optical absorption of the synthesized materials was studied by diffuse reflectance UV-visible spectroscopy (DRUV-vis). The spectra show the absorption as the Kubelka-Munk function of reflectance, F(R), and the corresponding Tauc plot (or alpha plot) elaboration for allowed indirect transitions, which offers an estimation of the band gap energy, is also reported. The data for selected hybrid materials (T-acac04, T-cat01p and T-asc01) are displayed in Figure 4.24.

All the analysed hybrid samples reveal a marked red shift in the absorption edge compared to bare TiO_2, represented by SGT: the absorption tails reach 550 nm with acac, 700 nm with ascorbate and over 800 nm with catechol, while the onset for SGT is about 390 nm. The data are consistent with the observed coloration of the samples: yellow-orange for T-acac, dark red for T-cat and T-asc, typically white for SGT (Figure 4.25).

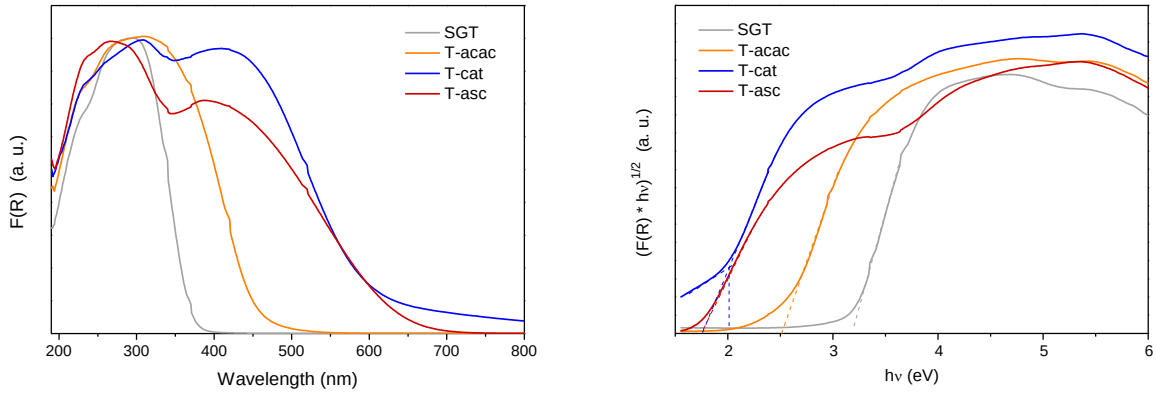

Figure 4.24. *DRUV-vis spectra of hybrid TiO_2 with acac, catechol and ascorbate, and SGT, reported as the normalized Kubelka-Munk function, F(R) (left); Tauc plot with band gap evaluation (right).*

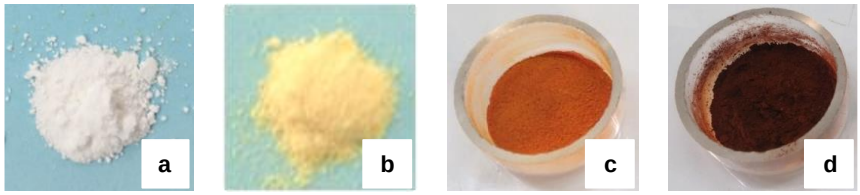

Figure 4.25. *Photographs of ground dried gels: SGT (a), T-acac04 (b), T-cat005 (c), T-asc01 (d).*

These three organic molecules taken singularly are colourless; free acac, catechol and ascorbic acid present a π – π* transition between 265 and 275 nm, and no absorption above 300 nm [131,166,167]. This implies that the absorption bands in the visible range must arise from electronic transitions involving both the inorganic and organic components of the hybrid materials. The mechanism proposed is a direct charge injection from the ligand into the conduction band of the oxide, more precisely through a direct excitation from the HOMO of the ligand to the 3d-Ti orbitals composing the conduction band. The process is referred to as ligand-to-metal charge transfer (LMCT), although ligand-to-band charge transfer would be the more appropriate definition when the injected electron is delocalized in the conduction band instead of being trapped on a Ti^{4+} centre, turning it into Ti^{3+} [46]. The holes generated by such charge transfer are localized on the organic ligand. This kind of process requires a staggered alignment of the bands at the hybrid interface, as shown by the energy diagram, reported in Scheme 1.2 (Section 1.5.1).

The broadness of the absorption band indicates that there is a broad distribution of electronic states. Interestingly, the charge transfer bands are not merely a shoulder of the main TiO_2 absorption band, conversely the intensities of the charge transfer bands are comparable to those of the valence to conduction band transition, indicating the presence of a large concentration of complexes throughout the surface and likely the bulk of the materials. A fitting of the peaks composing the absorption curve was performed with two peaks (Table 4.8). Although it is a rough simplification, since at least the TiO_2 absorption band has more contributions, it is useful to individuate the position of the two main bands. The band gap energies evaluated from Tauc plot linearization are referred in the hybrid samples to the energy difference between the conduction band edge and the HOMO of the ligand (not the valence-conduction band distance), so they can be considered as apparent or effective band gaps, resulting from the charge transfer complex [131]. For T-acac, in whose spectrum the two components are merged into a single large band, the charge transfer band is found centred at about 368 nm, with a resulting band gap of 2.5 eV. T-cat and T-asc have charge transfer band centred around 440 and 420 nm and an absorption edge corresponding to 2.0 and 1.8 eV respectively.

***Table 4.8**. Wavelength maximum of peaks calculated by 2-peaks fitting of the F(R) curves, and band gap energy values estimated by Tauc plot linearization.*

Sample	Fitted peak 1 (nm)	Fitted peak 2 (nm)	E_g (eV)
SGT	285	-	3.2
T-acac	267	368	2.5
T-cat	270	440	2.0
T-asc	248	417	1.8

The observed red shifts, between 0.7 and 1.4 eV with respect to bare TiO_2, are consistent with literature reports. Few data are available on the effect of acetylacetone, showing a similar absorption up to about 500 nm [72]. Previous optical measurements revealed the existence of a charge-transfer band near 420 nm, appearing as a shoulder in UV-visible spectra on a TiO_2-catechol nanopowder and a TiO_2 nanoparticle suspension in aqueous catechol solution [102,161,167]. It is interesting to note that the peak of the TiO_2 gap transition seems to be shifted to slightly higher energies in the presence of the complexes (peak 1 in Table 4.8). This could be explained with a large reorganization of the surface electronic structure, compatible with a strong electronic coupling between the ligand and the semiconductor, following the model of Creutz-Brunschwig-Sutin [46,168].

All the works found in literature on such charge transfer complexes deal with surface modified nanoparticles, and in some cases thin films. A variation of the nanoparticles size was observed to induce a change of absorption intensity at the same ligand/TiO_2 ratio, leaving the onset unchanged: smaller particles show an enhancement of absorption correlated to the higher fraction of surface Ti atoms. The present data show that gels or larger particles, modified in the bulk and surface with the same compounds, do not display remarkably different optical properties.

In Figure 4.26 some TiO_2-catechol materials are compared. In the particulate gel with the highest nominal catechol content (0.4 molar ratio), the absorption intensity of the charge transfer band grows relatively to the conduction-valence band transition, especially in the extended tail ending up in the near IR range. Such band tails are usually associated with highly disordered electronic states near the band edges. An increasing amount of catechol introduces a larger distribution of states, possibly both around the conduction band edge and the ligand ground state. It should also be noticed that the hybrid materials are amorphous, which causes the valence and conduction bands boundaries to be diffuse rather than neatly defined.

The mixed hybrid gels with acac or citrate in addition to catechol exhibit spectra in which the features of both ligands can be individuated, which is more obvious in T-cat01-A. The absorption threshold is more defined in these samples, with lower band tails and a slightly lower effective band gap (1.8 – 1.9 eV).

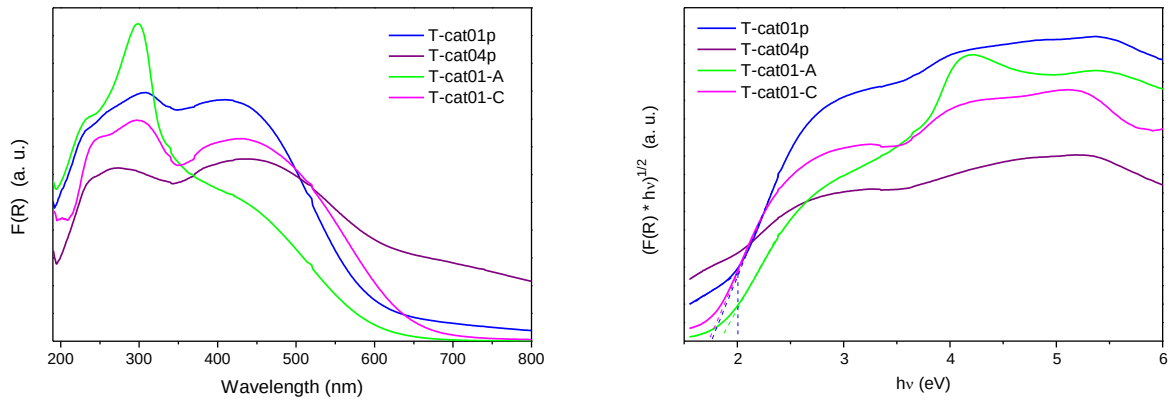

Figure 4.26. *DRUV-vis spectra of different hybrid TiO_2-catechol samples, reported as the Kubelka-Munk function, F(R) (left); Tauc plot with band gap evaluation (right).*

In summary, all the analysed hybrid TiO_2 samples exhibit visible light absorption, ascribed to direct charge transfer from the ground state of the ligand to the oxide conduction band. The shift is larger with catechol and ascorbate than with acetylacetone, owing to the redox potentials relative to the conduction band potential. For TiO_2-dibenzoylmethane the optical properties were analysed on thin films (see Chapter 5), finding an extended absorption band similar to that of TiO_2-acac. For TiO_2-dopamine comparable results to TiO_2-catechol are expected [68,72]. The intense visible light absorption of these materials was correlated to their photoresponsivity by photoelectrochemical measurements, as described in Section 4.4.

Annealed gels.

The materials produced by thermal treatment of T-acac samples show a dark coloration. The DRUV-vis spectrum of a T-acac04 xerogel calcined in air at 400 °C for 1 h (HT-400-A1, Figure 4.27) reflects this observation, showing a wide diffuse visible light absorption, prolonged above 800 nm, in the infrared range. The SGT powder treated in the same conditions keeps both the white colour and the usual absorption profile of TiO_2, with a small shift of the threshold, from 3.20 eV in SGT to 3.15 eV, maybe due to the crystal growth. In the calcined hybrid sample the band gap transition seems shifted to lower energy. However, taking in the Tauc plot the intersection between the two sections of the curve with different slope, instead of the intersection with the abscissa axis, a band gap of 3.15 eV is

estimated. In such cases, when an intense and wide band is overlapped, this method should provide a more accurate estimation of the real band gap energy.

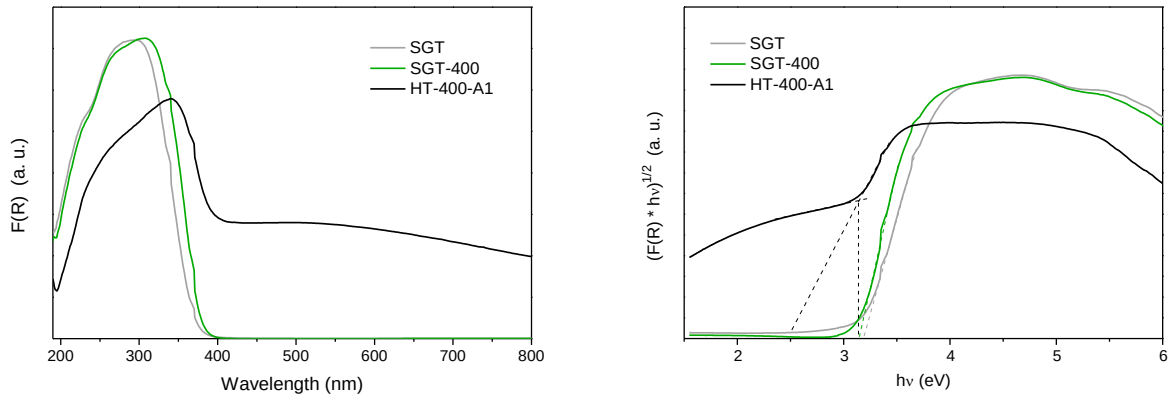

Figure 4.27. *DRUV-vis spectra of SGT, as dried and after calcination at 400 °C for 1 h in air, and T-acac04 calcined in the same conditions, reported as the Kubelka-Munk function, F(R) (left); Tauc plot with band gap evaluation (right).*

The diffuse absorption in the visible range, associated to a dark grey coloration, makes the HT-400 materials resemble the so-called "black titania" materials, intensely investigated in the recent years. This definition encompasses a variety of TiO_2 materials in which structural defects, such as Ti^{3+} and/or oxygen vacancies, are introduced during the synthesis or post-treatments, resulting in blue, grey, brown or black coloration, with highly enhanced solar light harvesting [50,51]. This is caused by mid-gap electronic states, often located around 1 eV below the conduction band, and can be accompanied by shifts in the band potentials. An outlook on this kind of photoresponsive titanium oxides is provided in Section 1.5.

In the present work, "black titania" samples were obtained by heat treatment in mild conditions of the xerogels, differently than in most of literature reports. Their features are likely associated to the content of reduced Ti revealed by XPS measurements (see Section 4.1.4), although other types of defects could also give a contribution to the outstanding optical absorption, as suggested by EPR spectroscopy, discussed in the next section.

4.3. Electronic properties: EPR characterization

The functional properties of semiconducting oxides are related to their ability to separate, conduct and transfer charge carriers, either electrons or holes. The catalytic and photocatalytic activity of titanium oxide is based on redox processes, so the possibility to exchange electrons at the interface and store them at trapping lattice sites. They are also correlated with the ability of the material to store oxygen on its surface, activate it and finally release it. Hence a technique allowing to detect unpaired electrons on solid samples or in solution, is really useful in the investigation of electron-related features, regarding both the materials' surface and the mechanisms of radical reactions. Electron paramagnetic resonance (EPR) spectroscopy, also called electron spin resonance (ESR), is a technique which reveals species with unpaired electrons in solid or liquid samples, based on the excitation of electron spin transitions by absorption of microwave radiation under an applied magnetic field. Inorganic and organic free radicals, many transition metals in oxidation states that make them paramagnetic, molecules in electronic triplet state, impurities and defects in semiconductors can be studied by means of EPR spectroscopy. In the present work it represented a key technique, providing extremely interesting results.

4.3.1. Superoxide radical generation and stabilization

Recently, the activity of a ZrO_2-acetylacetonate hybrid material in the oxidation of organic compounds was explained by the unusual generation and stabilization on its surface of superoxide radical anions, $O_2^{\bullet -}$, detected by EPR measurements [6,7]. On the basis of those results, the hybrid TiO_2-based materials studied here were analysed by EPR spectroscopy to check the presence of adsorbed radicals or other paramagnetic species.

The spectra of a series of T-acac samples, recorded at room temperature without any pretreatment, are displayed in Figure 4.27. While the reference SGT is practically silent, all the materials containing acac show an anisotropic lineshape, with three components, corresponding to the characteristic signal of superoxide radical anion on the surface of TiO_2. The g tensor values for the three peaks (g_{xx}, g_{yy}, g_{zz}), reported in Figure 4.28, are in good agreement with those reported in literature [30,32,169]. The anisotropic shape of the curve is due to the geometry of the $2\pi^*$ antibonding orbital of $O_2^{\bullet -}$ where the unpaired electron is located, which causes the three axes to be not magnetically equivalent. In other words, the orientation of a radical with respect to the magnetic field can yield different components to the microwave absorption signal in the three directions, depending on the symmetry of the site. The signal detected in EPR spectroscopy is the first derivative of the absorption intensity.

Superoxide anion is one of the most important reactive oxygen species (ROS), as discussed in Section 1.3. It can be generated in different ways to employ it in oxidative processes, most commonly by the one-electron reduction of molecular oxygen:

$$O_2 + e^- \rightarrow O_2^{\bullet -}$$

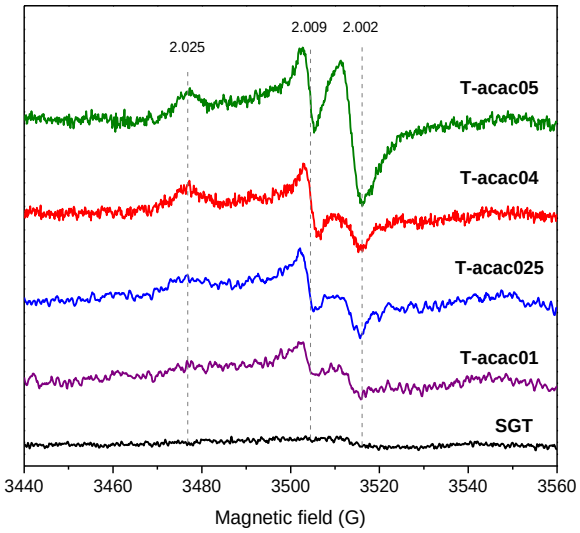

Figure 4.28. *EPR spectra of TiO_2-acac xerogels and SGT powder, recorded at room temperature; g values are reported.*

The half-life of superoxide is very short; in solution it depends on the type of solvent and pH because it is easily protonated to form the hydroperoxide ($HO_2^{\bullet}$) radical first, and then hydrogen peroxide, H_2O_2, therefore a protic solvent and an acidic pH decrease its lifetime. The half-time in physiological conditions was estimated to be in the order of seconds [29]. When superoxide anion is strongly adsorbed on a metal oxide surface, it can acquire a relatively increased stability in ambient conditions, however it is generally produced *in situ* before its utilization and, although there is some report about a lifetime of days of superoxide on the surface of pre-treated TiO_2 or ZrO_2 [32,36], it not considered suitable for a long-term storage. Mechanisms tested for the activation of O_2 as superoxide on oxides include:

- irradiation to excite the band gap transition, and O_2 reduction by photogenerated electrons (photocatalytic mechanism);
- thermal reduction of the metal oxide surface by annealing, often in vacuum, providing excess electrons stabilized on metal cations (e.g. Ti^{3+}) or in vacancy sites or delocalized in the conduction band [32,36,169];

- visible light irradiation in the presence of sensitizing compounds, like porphyrins or carotenoids [33–35] or other adsorbed organics inducing surface intermolecular electron transfer [30,36].

On some hybrid materials studied in the present work, superoxide radical anions are generated on the surface of the dried gels by simple contact with air at room temperature and remain stably adsorbed for months, up to at least one year. This is an outstanding feature, apparently not reported previously, besides on the analogous gel-derived ZrO_2-acac hybrids studied by the same research group [6,7]. It should be noted that in some studies ROS are generated and detected at low temperature, even if they are reported to remain temporarily stable at room temperature. EPR spectra are frequently recorded at liquid N_2 (77 K) or He (4 K) temperature to retard charge recombination and relaxations processes, with few exceptions [34]. In this work all the EPR measurements were performed at room temperature. It seems clear that the presence of a ligand, such as acetylacetone, forming a charge transfer complex with the metal, is necessary for the oxygen reduction and stabilization, as confirmed by DFT calculations performed on the ZrO_2-based system. The *ab-initio* modelling of the ZrO_2-acac interface showed that the bound ligand significantly lowers the formation energy of oxygen vacancies and concurrently the O_2 adsorption energy, driving its reduction [7].

The formation of superoxide anions on the surface seems to occur during (and maybe after) the gel drying, independently on the conditions (at room temperature, at 50 or 80 °C, or by lyophilisation at -50 °C), given that there is contact with air. When the solvent is evacuated from the wet gel and the material acquires its final morphology, it develops a large surface area, with several ligand molecules coordinating Ti atoms exposed at the interface with the atmosphere. Indeed, an EPR measurement on a partially wet gel did not detect the presence of radicals, but they started to appear while the analysed sample continued to dry. Some questions, connected with each other, arise. How does the mechanism of O_2 reduction work? Which is the exact role of acetylacetonate? Do other organic ligands have the same effect?

Recalling the charge transfer character of the Ti-acac complex in the materials, discussed in Section 4.2, it may be hypothesised that the electrons needed for the reduction of O_2 are those injected from acac ground state to the conduction band, possibly localized on Ti^{3+} ions (a small amount of Ti^{3+} is in fact found in a dried T-acac sample by XPS, see Section 4.1.4). Since the complex partially absorbs visible light, ambient illumination should be sufficient to activate the electron transfer. The possibility that oxygen vacancies are involved, suggested by the theoretical modelling on ZrO_2-acac and on other studies on TiO_2 interaction with O_2 [32,170], cannot be discarded nor confirmed with the available data. The formation of defects like vacancies might be favoured on amorphous hybrid gels, in which the chelating molecules can contribute to the structural disorder and induce a surface reconstruction

of undercoordinated Ti sites, and a consequent change in the electronic properties, possibly influencing proximal O sites.

The spin density, namely the concentration of paramagnetic centres (here $O_2^{\bullet-}$ radicals) is calculated by double integration of the EPR spectrum of the sample recorded together with an internal standard, as described in Section 2.3. For the T-acac materials, represented in Figure 4.27, the spin density values are in the order of $1{\cdot}10^{15}$ spin/g. A limited trend of increasing density with the nominal acac content can be seen, going from 0.1 to 0.5 acac/Ti molar ratio. The spectrum of T-acac05 presents an additional feature, a single peak superimposed to the orthorhombic signal of superoxide. The subtraction of the curve relative to $O_2^{\bullet-}$ alone from that spectrum shows that it is a singlet centred roughly at g = 2.004, with broadness (ΔB, distance between the abscissa values of the maximum and the minimum of the peak) of about 6 G. This kind of signal could be related to a carbon radical located on the acac ligand, as argued in the case of other hybrid systems (*vide infra*), but the reason for its appearance only in the T-acac05 sample is not clear.

With the purpose to understand the effect of the ligand molecular structure, different complexing molecules were chosen to synthesise TiO_2-based hybrids. Dibenzoylmethane is another β-diketone, with two phenyl rings in place of methyls, giving a fully conjugated structure in the enol form. The high charge delocalization and the electron-rich substituents are supposed to increase the efficiency of ligand-to-metal charge transfer. The EPR spectra of T-dbm xerogels and precipitated samples are shown in Figure 4.29.

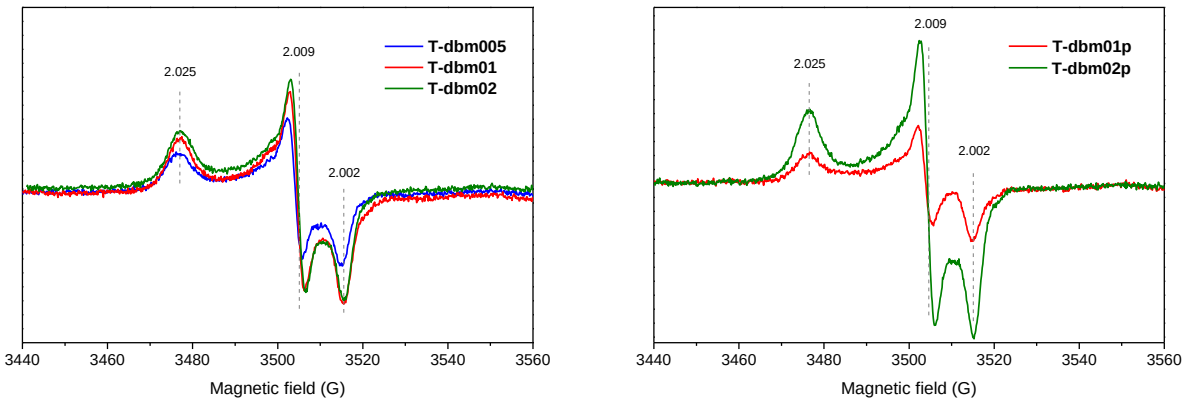

Figure 4.29. *EPR spectra of TiO_2-dbm xerogels (left) and particulate gels (right), recorded at room temperature; g values are reported; signal intensity (in arbitrary units) is in the same scale.*

All the spectra have the typical lineshape of the adsorbed superoxide anion, with the same g values as the T-acac samples, but substantially higher intensity: the estimated spin densities are in the order of 10^{16} spin/g, reaching $1{\cdot}10^{17}$ spin/g for T-dbm02p particulate sample, meaning that the density of radicals is about 10 to 100 times that found on T-acac. This drastic increase strongly points at a relevant

role played by the charge transfer in the generation of the radicals, supporting the hypothesis that the direct injection of electrons from the ligand is the primary source involved into the reduction of adsorbed O_2. Considering the content of dbm in the hybrid samples comparable, if not lower, with respect to that of acac, it can be envisaged that the extended electron density delocalization on the complexing dbm molecule renders the direct injection more favoured and slows down the back electron transfer, because it stabilizes the oxidized dbm radical. The result is a higher availability of electrons in the TiO_2 conduction band. Other factors that can be considered include the redox potential of the HOMO of the ligand, which is not expected to be largely different between acac and dbm from their similar optical absorption, the size of the ligand, the specific surface area of the material and other characteristics of the surface. Sojka and co-workers showed that superoxide anions, adsorbed on the surface of amorphous ZrO_2 after reaction with H_2O_2, interact with vicinal hydroxyls and proposed that surface protonation enhances the stability of $O_2^{\bullet-}$ balancing its charge. Thus they explained the very small amount of superoxide produced on a crystalline ZrO_2 with the loss of hydroxyls and the decrease of surface area [37]. On the T-dbm amorphous xerogels the concentration of the radicals does not vary largely with the initial amount of dbm added, while the T-dbm02p produced by precipitation, characterized by a high dbm content (deduced from TG data, not reported) and by small crystalline domains, is the sample with the highest radical density ($1{\cdot}10^{17}$ spin/g). The possibility to prepare either xerogels or small particles bearing superoxide radicals on the surface opens to applications which require materials with different size and structure. A preliminary test in oxidative degradation in analogous conditions to those led on T-acac showed very promising results for a T-dbm sample. These hybrids are expected to have a higher activity due to the largest density of surface ROS.

In order to assess the effectiveness of a different class of organic compounds in the generation and stabilization of superoxide radicals, two carboxylic acids were chosen: acetic acid, a small monocarboxylic one, and citric acid, a more complex tricarboxylic acid. The EPR spectra for two representative samples of these systems, displayed in Figure 4.30 in comparison with those of the diketonate systems, demonstrate that carboxylic acids are able to stabilize superoxide as well.

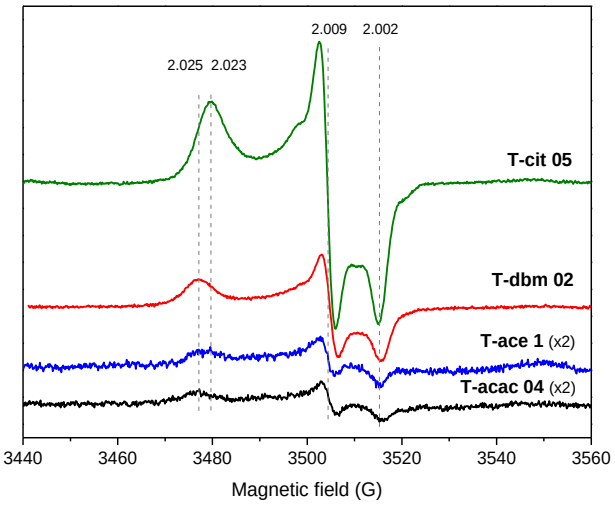

Figure 4.30. *Comparison of EPR spectra of the xerogel samples with the highest signal intensity for each system: TiO_2-acac, TiO_2-acetate, TiO_2-dbm and TiO_2-citrate. Spectra recorded at room temperature; g values reported.*

The spectrum of TiO_2-acetate xerogel is similar to a T-acac one, both in the intensity and g values (g_{zz} results slightly shifted, to 2.024). On the contrary the TiO_2-citrate xerogel with the highest citric acid nominal content (T-cit05) exhibits the largest spin density recorded for samples containing superoxide radicals. Among three T-cit xerogels a definite trend of spin density with the concentration of citric acid used in the synthesis is not found (Figure 4.31).

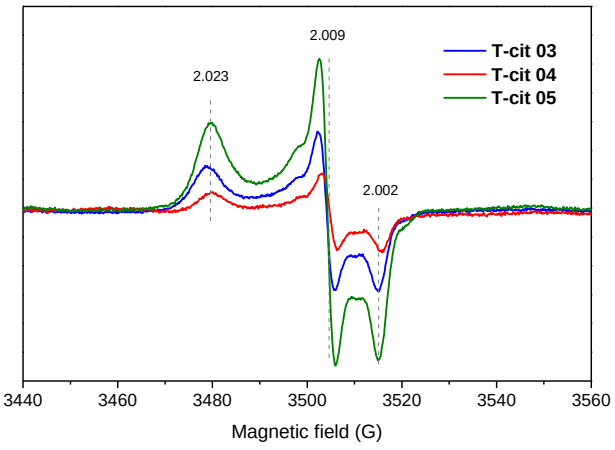

Figure 4.31. *EPR spectra of TiO_2-citrate xerogels, recorded at room temperature; g values are reported.*

A difference with the signals of the diketonate systems is observed for the g_{zz} value: in T-cit it is slightly more shifted than in T-acetate, to 2.023, while the other two components of the g tensor remain unchanged. The g_{zz} component is the most sensitive to the chemical environment on the surface around the superoxide radical site. It depends on the electric field experienced by the anion: a lower

g_{zz} value will be given by either a higher charge/radius ratio of the metal cation or its lower coordination, exerting a stronger electric field, and vice versa [30,32]. For example, the superoxide signal on the ZrO_2-acac hybrids have g_{zz} = 2.034, as a consequence of the larger size of the Zr^{4+} ion [6]. In some works, two or three overlapped signals of superoxide anion adsorbed on different sites of the same material are reported, with g_{zz} values ranging between 2.019 to 2.029, assigned to radicals adsorbed on a vacancy site or on undercoordinated Ti^{4+} ions [32,169,171]. The vacancy sites should correspond to g_{zz} = 2.019-2.020, lower than the values found here for the hybrid materials.

The dependence of g_{zz} on the type of organic ligand suggests that the adsorption site of superoxide is in close proximity to the coordinated Ti atom, and that the coordination mode itself could affect it: citrate is bound as a bidentate ligand, as shown by FT-IR spectroscopy, but with respect to the β-diketonates, which form a chelating 6-membered ring, with a O-Ti-O bonding angle around 120°, citrate is more probably bridging and, in case of a chelating mode, should form 4- or 5-membered cycles, providing a single coordination bond to each Ti atom or a more strained chelation. Therefore β-diketonates are supposed to fill more efficiently the coordination of Ti atoms, in agreement with a slightly weaker electric field exerted on the close adsorbed superoxide anion. On the other hand, the non-coordinating carboxylate groups of citrate molecules could find themselves in proximity to the radical, so some possible interaction cannot be excluded. These additional groups can contribute also to the coordination and charge transfer, since citrate does not show the same charge delocalization as dbm, but produces a higher amount of radicals than acetate.

EPR analysis of the other hybrid TiO_2 materials, containing catechol, dopamine or ascorbic acid, gave different signals which are not ascribed to superoxide radicals (*vide infra*), but are probably due to carbon radicals on the oxidized form of the ligand resulting from charge transfer. These enediol ligands attest that not every kind of organic complexing molecule is able to stabilize superoxide on the surface of hybrid TiO_2.

An interesting question concerns the reason for the different behaviour of enediols in regard to diketones and carboxylic acids. The different coordination geometry, which in this case is bidentate chelating with formation of a 5-membered ring, should not be the only determining factor. A difference between the two groups of compounds is in the redox potential of the HOMO upon complexation: for enediols it is more negative than for the other ligands, as visible by the further red shift of the optical absorption edge. Approximate potential values were obtained for the enediols by cyclic voltammetry (Section 4.4). Related to the chemical and electronic structure of the complex, the electronic coupling between the ligand and the semiconductor is considered an important indicator of the efficiency of the charge transfer process [46,72,102].

Varaganti and Ramakrishna studied the nature of the charge transfer of a series of organics adsorbed on TiO_2, among them acetylacetone, catechol and dopamine, by femtosecond fluorescence and absorption [72]. They found evidence for a prevalently localized charge transfer with the catecholic compounds, whereas for acetylacetone and salicylic acid they observed slower emission components and lower fluorescence anisotropy, suggesting a partial delocalization of the exciton, compatible with a weaker electronic coupling of the conduction band states and trap states with the oxidized molecule. A more delocalized charge separation increases its lifetime, delaying the back electron transfer [72]. This should facilitate the capture of an excited electron by adsorbed O_2. Similar conclusions are reported for salicylate, whose behaviour could be correlated with that of citrate, since it is also believed to complex through adjacent carbonyl and hydroxyl groups, or through the carboxylate group.

A proof that the bottom-up synthesis method adopted in this work is needed to form charge transfer complexes with sufficiently strong coupling or in a suitable concentration to stabilize superoxide anions was provided by the EPR analysis of a sample prepared by adsorption of acetylacetone from water solution on the surface of SGT, an amorphous TiO_2 powder. The sample was EPR silent. Moreover, on a T-acac sample heated at 250 °C, a temperature at which acac is still present but has started to undergo modifications, the signal of superoxide was replaced by a sharp singlet, confirming again that a stable complexation is necessary to keep the radicals on the surface.

4.3.2. Reactivity and recovery of superoxide radicals

The stability of the superoxide radical anions adsorbed on the surface of TiO_2-based hybrid materials is remarkable. As concerns T-acac04 xerogel, after one year of storage in the laboratory the signal was still present, though with a reduced intensity, and only after almost two years it was found to disappear. Control tests on the stability on other systems are in progress; from the first data a decrease of signal intensity seems to occur after 4 months in T-dbm and T-cit samples. Such long-term stabilization of superoxide or other short-lived ROS does not result to have been reported to date.

In the long run $O_2^{\bullet-}$ could be desorbed, could react with moisture or other components of air, be reoxidized to O_2, or even accept an electron and remain bound to the oxide as peroxo ion, O_2^{2-}. Nevertheless, it was revealed that the superoxide radicals can be easily recovered on the material's surface after their disappearance. A sample stored for a long time and washed in water for 24 h to check its stability in aqueous environment showed again the EPR signal of the superoxide anion. The experiment was repeated washing the sample for different times (Figure 4.31). Time did not seem to be relevant, as after 1 h or even only 10 min of contact with water, the xerogel, dried at 50 °C, showed a signal with intensity at least equal to the original value of the freshly prepared sample.

As a matter of fact, the superoxide recovery was found to be even easier, requiring only an exposure to air and ambient light: an aged sample was spread on a Petri dish and kept on the laboratory bench for 1 h, mixing it a few times. The result was again a fully restored EPR signal in the "aerated" sample (Figure 4.32).

It was proven that the process of O_2 reduction and $O_2^{\bullet-}$ stabilization is reproducible, it can occur repeatedly on the material surface. The ability of the material to restore the surface superoxide radicals by a simple washing and drying, once it is depleted of radicals because they have been consumed in a reaction or during a long storage, is important for practical applications.

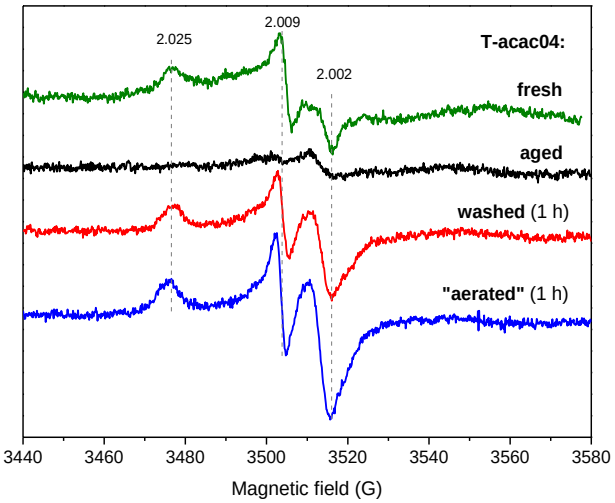

Figure 4.32. *EPR spectra of TiO_2-acac xerogels: as prepared (fresh), stored for 20 months (aged), then washed in water for 1 h or exposed to air for 1 h. Spectra recorded at room temperature, g values reported.*

Since many possible applications, such as the removal of polluting substances, are in aqueous medium, it is interesting to study what happens in water. Most reactive oxygen species, including superoxide, hydroxyl and alkyl radicals, cannot be evaluated by direct measurement in water at room temperature, due to their short lifespan. Spin trapping is a technique in which a nitrone or nitroso compound reacts with a target free radical to form a radical adduct, a stable and identifiable free radical that is detected by EPR spectroscopy. 5,5-dimethyl-1-pyrroline *N*-oxide (DMPO), is the most popular spin trap, owing to its ability to form specifically stable adducts with different oxygen, sulphur or carbon-centred radicals, by their reaction with the C adjacent to the nitroxide group (Figure 4.33) [33,172–174].

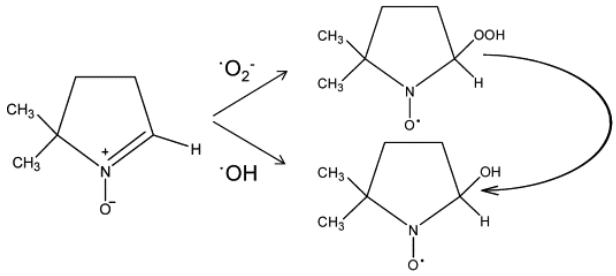

Figure 4.33. *Scheme of DMPO reaction with superoxide and hydroxyl radicals producing the respective radical adducts. The curved arrow indicates the tendency of the superoxide adduct to transform into the hydroxyl adduct.*

The spin trapping tests were performed on solutions kept in the dark, in order to exclude the contribution of photoinduced phenomena, first in water, then in a 4-chlorophenoxyacetic acid (4-CPA) solution, to simulate the conditions of a catalytic activity test (see Section 5.1). DMPO in water or in 4-CPA solution does not produce interfering signals (Figure 4.34 A).

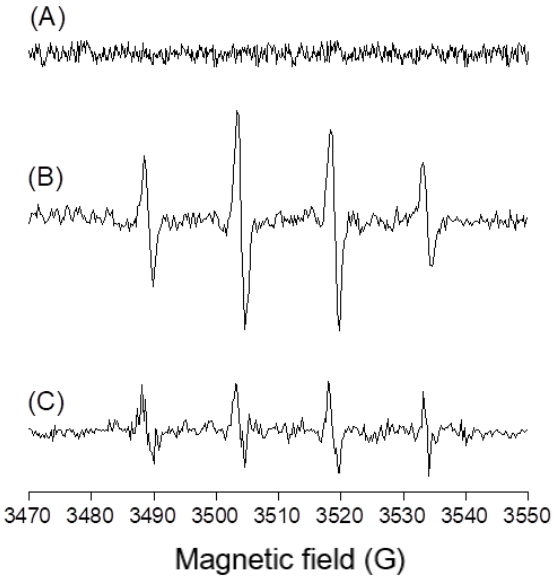

Figure 4.34. *EPR spectra recorded at room temperature in solution: DMPO in a 4-CPA herbicide solution (A); DMPO in a T-acac suspension in water (B); DMPO in a T-acac suspension in 4-CPA solution (C).*

When DMPO is introduced in a water suspension of T-acac04 xerogel, a signal in the EPR spectrum is observed (Figure 4.34 B), showing a characteristic quartet with a 1:2:2:1 intensity ratio, which corresponds to the DMPO-OH adduct formed from the trapping of ˙OH radical on DMPO [173,174]. A quantitative analysis of this spectrum was realized determining the hyperfine coupling constants for the nitroxide nitrogen and the β-proton, $a_N = a_H = 14.8 \pm 0.1$ G. These values are consistent with those reported in the literature for the DMPO-OH adducts, confirming the formation of significant amounts of ˙OH radicals. The signal of DMPO-OH adduct was also present when analysing a mixture of T-acac

with 4-CPA, although with a lower intensity (Figure 4.34 C), probably due to an involvement of ˙OH radicals in the oxidative degradation of the herbicide.

EPR spin-trapping demonstrates that hydroxyl radicals are produced by the material in contact with water in the dark. The typical mechanism of ˙OH generation in photocatalytic processes is the oxidation of adsorbed water molecules or OH^- ions by holes generated in the valence band by light absorption, although alternative mechanisms were also proposed [16]. In the absence of light there is no separation of electron/hole pairs, so a different route must be considered, likely starting from the superoxide radicals adsorbed on the surface. In water, adsorbed superoxide readily reacts with protons, forming hydroperoxide radicals, $HO_2^{\bullet}$:

$$O_2^{\bullet -} + H^+ \rightarrow HO_2^{\bullet}$$

Hydroperoxide radical can further react to produce hydrogen peroxide:

$$HO_2^{\bullet} + H^+ + e^- \rightarrow H_2O_2$$

The latter is able to decompose, giving ˙OH, directly under short wavelength UV irradiation:

$$H_2O_2 \rightarrow 2\,{}^{\bullet}OH$$

or by a peroxidase-like reaction, involving another superoxide radical or a conduction band electron [15]:

$$H_2O_2 + O_2^{\bullet -} \rightarrow {}^{\bullet}OH + OH^- + O_2$$

Superoxide and hydroperoxide radicals can be detected by DMPO spin trapping, but in water their lifetimes and the half-life of the corresponding DMPO adducts are very short, therefore different environment (aprotic solvents, e.g. DMSO) and spin traps are preferred for their individuation. In this case ˙OH was the only species clearly identified in solution by spin trapping, but it cannot be excluded that other ROS are concomitantly present and could participate in the reactivity of the material with organic compounds.

The tests of oxidative degradation of model pollutants, demonstrating the functional activity of the hybrid TiO_2 related to the radicals, are presented in Section 5.1.

4.3.3. Charge transfer complexes and defectivity

As previously mentioned, the other hybrid systems studied do not show the EPR signal of superoxide radicals. Anyway they are EPR active, and their signals offer more information about the materials. The EPR spectra of TiO_2-catechol hybrids are displayed in Figure 4.35. TiO_2-cat particulate samples with different catechol/Ti molar ratio (on the left) present all the same features: a singlet centred at g

about 2.003, with a shoulder at lower field, indicative of another overlapped peak with somewhat higher g value. It should be noted that the T-cat04p spectrum is not in scale with the others, because it was collected with a lower instrumental gain, owing to its extremely high intensity which caused the signal to go out of range. A trend of signal intensity with the initial concentration of catechol is followed, suggesting that the signal is in fact related to the catechol ligand.

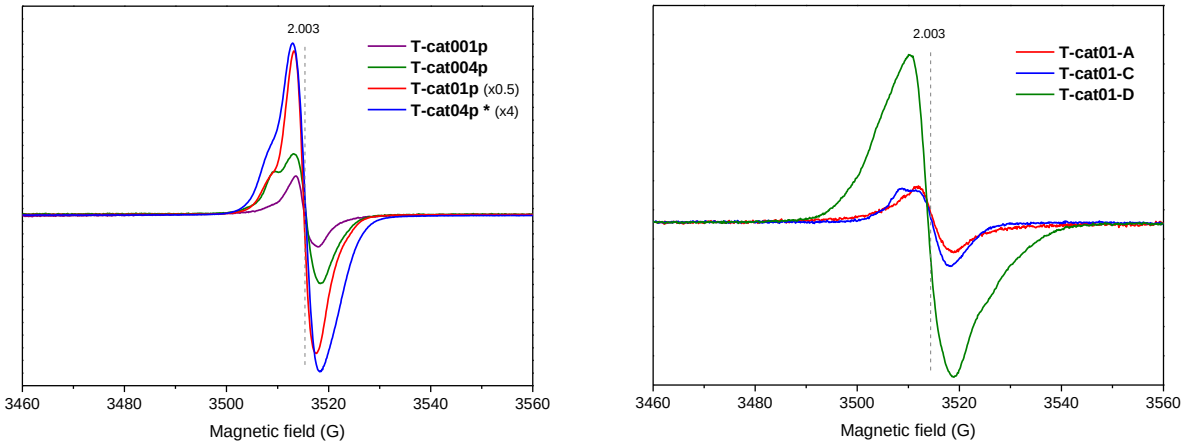

Figure 4.35. *EPR spectra: TiO_2-catechol precipitates with different catechol content (left); TiO_2-catechol xerogels with a second ligand (acetylacetone, citric acid or diethanolamine) (right). Spectra recorded at room temperature, g values reported. * T-cat04p spectrum recorded with gain = 40 dB, instead of 60 dB.*

Among the few works in which similar materials have been investigated by means of EPR spectroscopy there are some interesting studies by Rajh and co-workers on TiO_2 nanoparticles modified by surface adsorption of various molecules, including catechol, dopamine and ascorbic acid [68,123,131]. Recording EPR spectra on aqueous colloids at cryogenic temperature, under visible light illumination, they identified the radical species formed by charge separation: the electron trapped at Ti^{3+} sites, with a larger component at g = 1.988, and the hole localized on the organic ligand, associated with a broad singlet centred at g between 2.003 and 2.006, depending on the number of π electrons in the molecule. The latter signal strongly resembles those collected for most of the TiO_2-catechol, TiO_2-dopamine and TiO_2-ascorbate hybrid materials studied here (Figures 4.35 and 4.36). In the above cited papers, in particular, g values of 2.0036, 2.0038 and 2.004-2.0049 were found respectively for dopamine, catechol and ascorbate, with line width ΔB about 11 G. While the g values are in excellent agreement, some differences are observed in the line width: ΔB for particulate T-cat are 4-5 G, increasing in the mixed T-cat samples up to ΔB = 9 G in the mixed hybrid with diethanolamine, whereas ΔB = 10.5 G results for T-dop gel and ΔB = 9 G for T-asc gel.

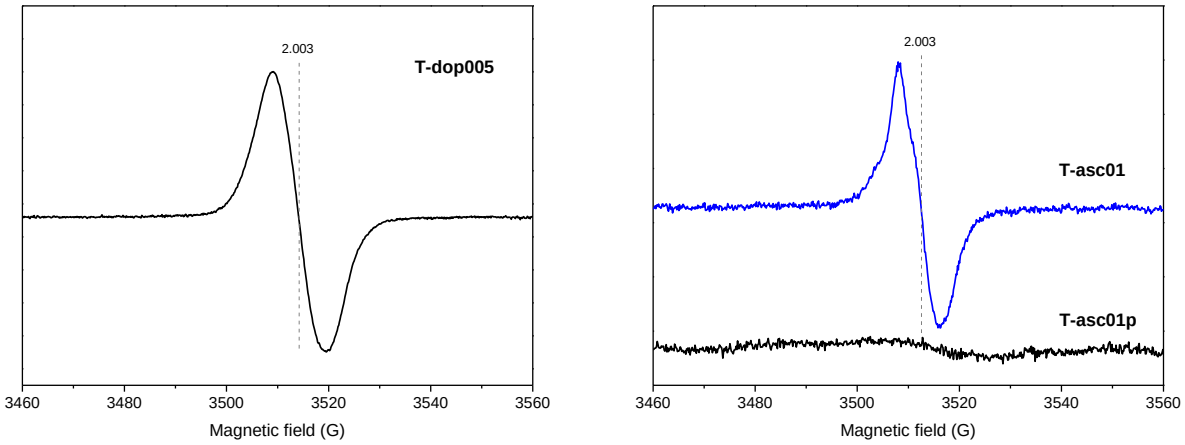

Figure 4.36. *EPR spectra: TiO_2-dopamine xerogel (left); TiO_2-ascorbate xerogel and precipitate (right). Spectra recorded at room temperature, g values reported.*

The peak width is reported to broaden with the size of the ligand, due to the increasing number of H and other atoms which give coupling with the unpaired electron [68]. In the mixed-ligand samples the broadening of the signal could therefore be explained by some interactions between adjacent catechol and added ligand, especially marked in T-cat01-D. A similar spectrum, with g = 2.0033 and ΔB = 6 G, was reported for a TiO_2 thin film modified on the surface with catechol, but only after an activation through a cyclic voltammetry scan, oxidizing catechol to the semiquinone radical anion, which remained stably bound to TiO_2 during successive electrochemical tests [175].

The attribution of the EPR signals of these hybrid samples to organic radicals produced by electron transfer to the oxide seems reasonable and consistent with literature reports. Only the TiO_2-ascorbate sample obtained by precipitation does not show a visible signal; maybe the hybrid complex in the structure of the precipitate is less stable than in the gel, so more ascorbate is removed washing the particles and a lower or more weakly bound fraction is retained in the structure.

It should be emphasised that in the present work the EPR spectra were collected at room temperature, without continuous irradiation or any kind of activation of the as prepared materials, besides the natural exposure to ambient light. It can be deduced that the strong chemical bonding and subsequent electronic coupling obtained in these systems generate a stable charge separation, with a hole stabilized on the enediol ligand.

Concerning the pathway of the injected electron, there seems not to be any clear evidence from the EPR spectra, although the overlapped signal observed in all the T-cat spectra has not been assigned. It could be present also in the T-asc spectrum, which shows an asymmetric line, and perhaps in T-dop, hidden behind the broad singlet. A possible attribution of such signal is to oxygen vacancies (*vide*

infra), in which excess electrons could be hosted, anyway another source, for instance a different organic radical, cannot be ruled out. Ti^{3+} is a typical trap sites for electrons, and can be well characterized by EPR, but unfortunately only at low temperatures, therefore its occurrence in these samples cannot be verified by the available data. Another possible fate for free electrons is the reduction of O_2 to superoxide anions, as discussed above. Nonetheless, the anisotropic signal of $O_2^{\bullet-}$ is not spotted in any of these spectra, curiously neither on the mixed-ligand hybrids containing acac or citrate. This is an unexpected result, since acac and citrate have proven the ability to generate and stabilize superoxide on the hybrid surface. A relatively low catechol amount (cat/acac and cat/citrate 1 : 3 molar ratios) inhibits the process. The likely complex interplay of the various components of these mixed systems make it difficult to formulate hypotheses on the interpretation of the observed phenomenon.

Dimitrijevic et al. identified superoxide as the major ROS produced by a TiO_2-dopamine illuminated suspension [123], suggesting that exploring the behaviour of these materials in solution, by means of spin traps or scavengers, could be interesting also to evaluate their potential activity.

Annealed samples.

With the aim to gain more information about the electronic characteristics of the annealed TiO_2 materials, EPR spectra were collected on six samples prepared by thermal treatment at 400 °C in different atmospheres and for different times (see Section 3.8). The results are shown in Figure 4.37.

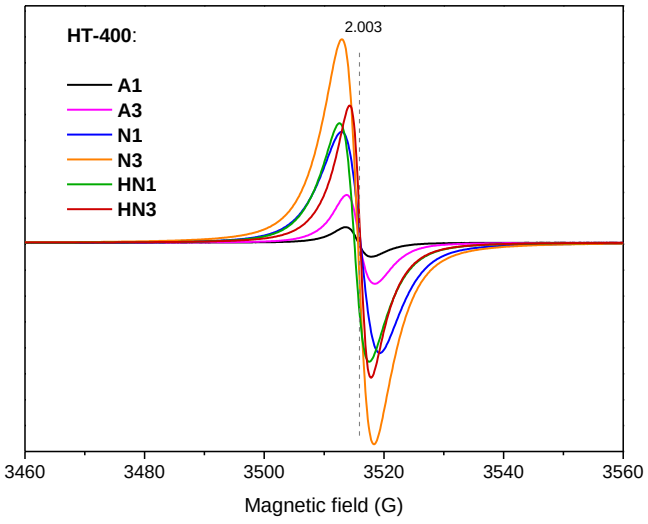

Figure 4.37. *EPR spectra of TiO_2-acac xerogel (T-acac04) after thermal treatment at 400 °C in different conditions: A = air, N = N_2, HN = H_2/N_2; the number is the duration of the treatment, in hours. Spectra recorded at room temperature with gain = 40 dB; g value reported.*

All the samples exhibit the same isotropic lineshape: a singlet centred at g about 2.003. The line width, ΔB, varies in the range 4-6 G. The intensity of the signal is visibly lower in the air-treated samples than in the others; a smaller difference can be observed between the ones treated nitrogen ("N") and hydrogen/nitrogen ("HN"). The intensity follows also a quite defined trend with the annealing time: it increases going from 1 to 3 h, and between HN1 and HN3 a narrowing of the peak is obvious. The observed signals have some features in common with those recorded on the hybrid samples containing enediol ligands. Some residual carbon species after the pyrolysis/combustion of acetylacetonate ligand could carry unpaired electrons and show up in EPR spectra. C-centred radicals originated in this way were reported to have a single but broader peak, with ΔB about 10 G, owing to the presence and interaction of different radical sites [176]. However these values are variable according to the distribution and delocalization of the electrons. On the other hand, similar singlets with g value close to that of the free electron (2.0023) have been frequently assigned to electrons trapped in oxygen vacancy sites [49,51,177,178]. Oxygen vacancies (V_O), as already mentioned, are among the most important defects in titanium and other metal oxides. They are relevant adsorption and active sites, strongly influencing the reactivity of metal oxides in heterogeneous catalysis, especially in redox processes. The electronic structure, charge transport and various surface and photochemical properties, including visible light absorption, have been shown to be closely related to the presence and type of vacancies [49]. The methods tested to reduce the surface of TiO_2 or introduce vacancies include thermal treatment in oxygen depleted conditions, so the generation of these defects by annealing in N_2 and H_2/N_2 is a plausible outcome, while would seems more unusual in air. Anyway, the evacuation of the organic component from the structure could be directly or indirectly responsible for the formation of vacancies in the bulk and on the surface of the materials, as proposed in Section 4.1.4. Further analyses might elucidate the attribution of the EPR signals.

In conclusion, the EPR spectra can be interpreted in combination with the results of XPS and DRUV-vis measurements, to draw a picture of the defectivity of the annealed samples, possibly represented by the sum of more contributions. Another fundamental point concerns the stability of defective samples. While a common limitation of reduced TiO_2 is the poor stability due to the easy reoxidation in ambient conditions, the gel-derived samples presented here do not show noticeable changes in the coloration and in the EPR signal after a long storage, suggesting that their structural features are not modified.

The variety of interesting properties discovered on these materials, as well as on the different hybrid gels, motivated to progress their investigation with an assessment of photoelectrochemical and photocatalytic properties.

4.4. Photoelectrochemical characterization

The photocatalytic, photoelectrochemical, photovoltaic or related application of a semiconductor requires not only the absorption of electromagnetic radiation in a defined or extended range, but also the ability to employ the absorbed photons to separate electrons and holes, and then conduct them to the surface. If this process occurs efficiently and the charge carriers reach the surface, they become able to reduce or oxidize adsorbed substrates, or to conduct electrical current at the interface with an electrode. Electrochemical analytical techniques are extremely useful to evaluate and understand the behaviour of a semiconductor under irradiation. Photocurrent measurement is a suitable way to gain a deep outlook on its photoresponse, generally linked to its photocatalytic performance. It is carried out in an electrochemical cell, detecting the current generated by a sample deposited on the working electrode under illumination. The capability of the material to induce reduction or oxidation reactions of substrates in the electrolytic solutions is usually aided by varying the applied potential from a negative to a positive value. Two types of photocurrents can be detected:

- *anodic* (positive) photocurrent, when holes photogenerated in the valence band oxidize a hole acceptor (e.g. water or an alcohol) and electrons are transferred from the sample to the electrode;
- *cathodic* (negative) photocurrent, when electrons photogenerated in the conduction band reduce an electron acceptor (e.g. molecular O_2) and holes migrate from the sample to the electrode [18].

If the radiation source allows to explore a wavelength range, a photocurrent spectroscopy can be realised, offering even more information about the photoactivity of a material. In addition, coupling classical electrochemistry with a spectrophotometric technique originates an advantageous method to inspect the electronic structure of a material.

4.4.1. Photocurrent generation

The activities carried out at the Jagiellonian University in Krakow (Poland), in the research group of prof. Macyk (Team of Photocatalysis), included photocurrent spectroscopy measurements on a series of samples investigated in the present work.

Hybrid xerogels.

The photocurrent data gathered for different hybrid xerogels and the reference SGT are reported in Figure 4.38. In the three-dimensional maps the blue areas represent the cathodic photocurrent, the

red areas the anodic one. In Figure 4.38 the same current scale is used in all graphs to facilitate the comparison. The reference TiO_2 shows both anodic and cathodic photocurrents prevalently in the UV range, with a low intensity halo reaching 450 nm, probably due to some defects in the amorphous disordered structure of the sample, inducing some electronic states near the bands edge. On the contrary, all the hybrid gels produce significant currents in the visible range: in T-acac and T-dbm the photocurrent onset is moderately shifted, consistently with their limited visible light absorption (the data can be compared with the optical absorption spectra, Sections 4.2 and 6.2), while in the hybrids with enediol ligands, which have wider visible light absorption, the photocurrents are extended above 500 nm. The samples present different distributions of anodic and cathodic photocurrents. T-dbm and T-dop show almost exclusively anodic currents, while T-asc shows cathodic currents up to 200 mV, with intensities higher than the anodic ones. A stronger oxidizing or reducing power depends on the electronic structure of the semiconductor, so the band potential and Fermi energy levels, but also on its surface properties and modifications.

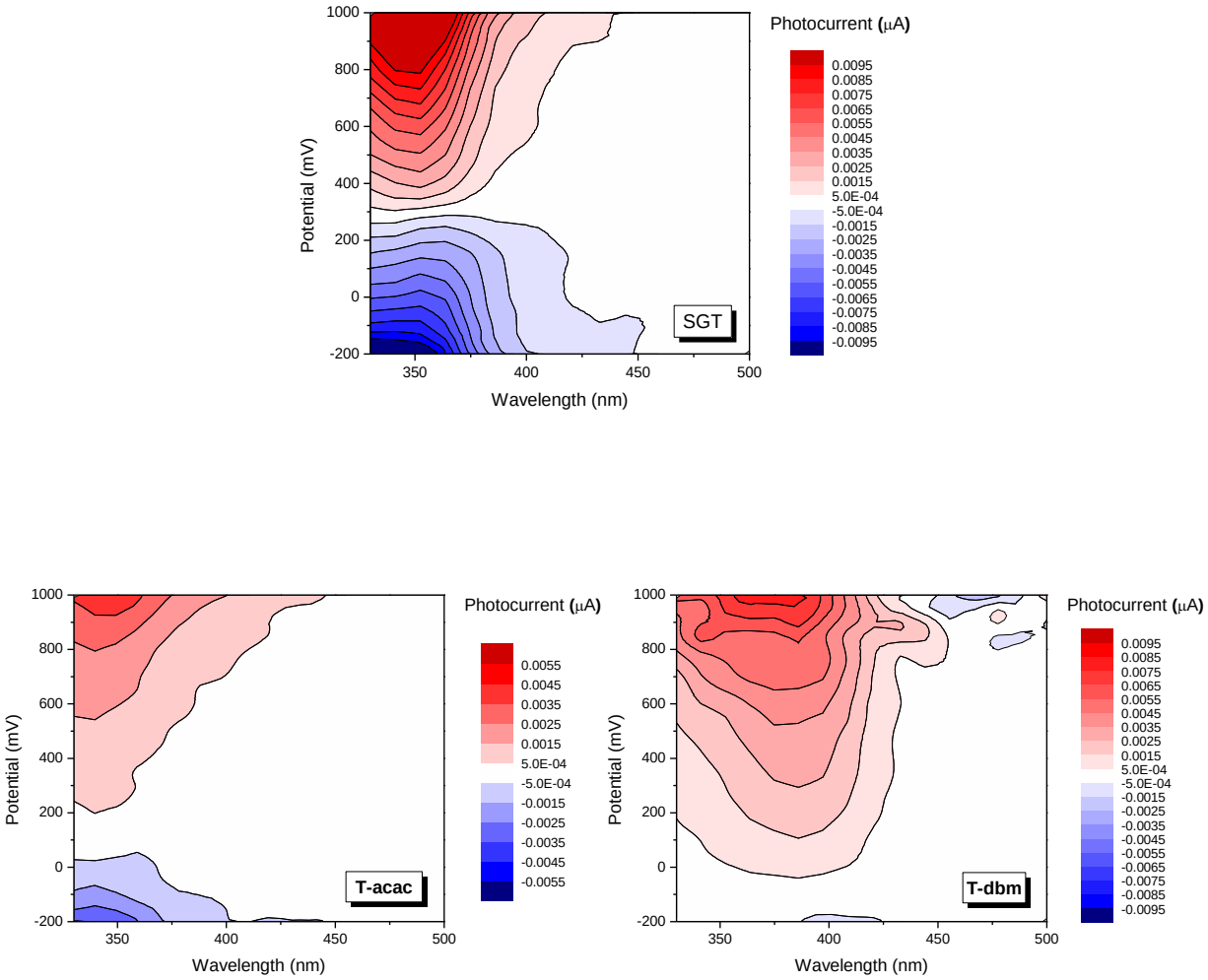

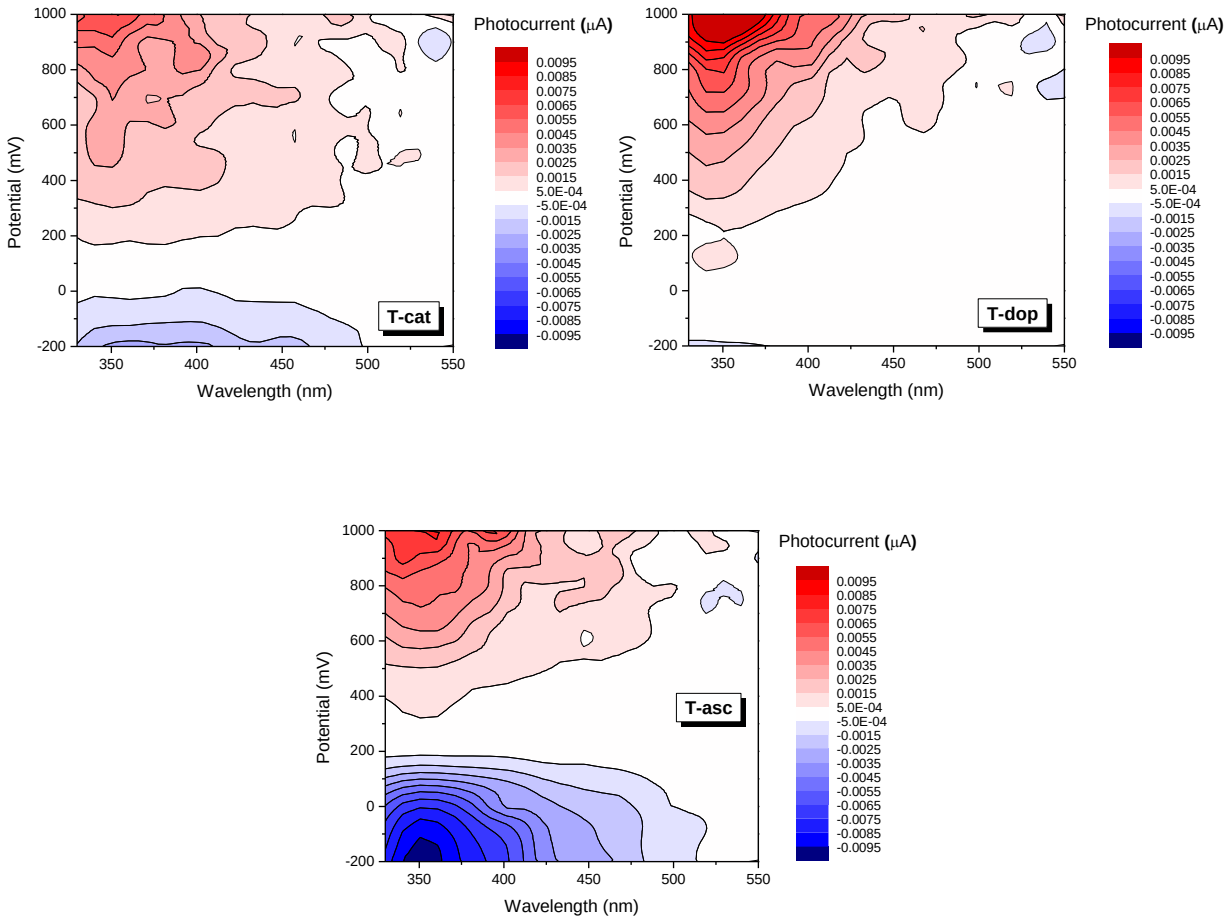

Figure 4.38. *Photocurrent as a function of potential (vs Ag/AgCl) and incident light wavelength, recorded on PET/ITO electrode covered with samples: SGT, T-acac04, T-dbm02, T-cat005, T-dop005, T-asc005. Measurement taken in aqueous 0.1 M KNO_3 solution saturated with Ar.*

Studies on crystalline TiO_2 indicate that anatase produces exclusively or principally anodic signal in the potential range from -0.2 to 1.0 V, while rutile, especially in the presence of O_2, produces intense cathodic currents. Its higher reducing efficiency has been related to a better oxygen adsorption and an apparently lower CB edge potential [18,19]. In the present experiments argon is insufflated in the solution, evacuating O_2, the major electron acceptor, so the cathodic photocurrent is supposed to be decreased. Despite this, if the surface of a sample has a high affinity for O_2, it can remain adsorbed and then get reduced.

To check the influence of the electron acceptor on the photoactivity of two samples (SGT and T-acac) two subsequent measurements were done: the first with a longer Ar purging (60 min instead of 15 min), the second insufflating pure O_2. The results for SGT (which showed significant cathodic current), reported in Figure 4.39 as an extract of the photocurrent intensity in function of time at negative potential, show that cathodic (negative) currents are approximately doubled in the presence of O_2.

This suggests an effective O_2 adsorption on the amorphous TiO_2 particulate gel. On the contrary, the same experiment on a T-acac xerogel did not evidence relevant changes, although this material is supposed to have a strong interaction with oxygen, considering its ability to stably reduce it to superoxide.

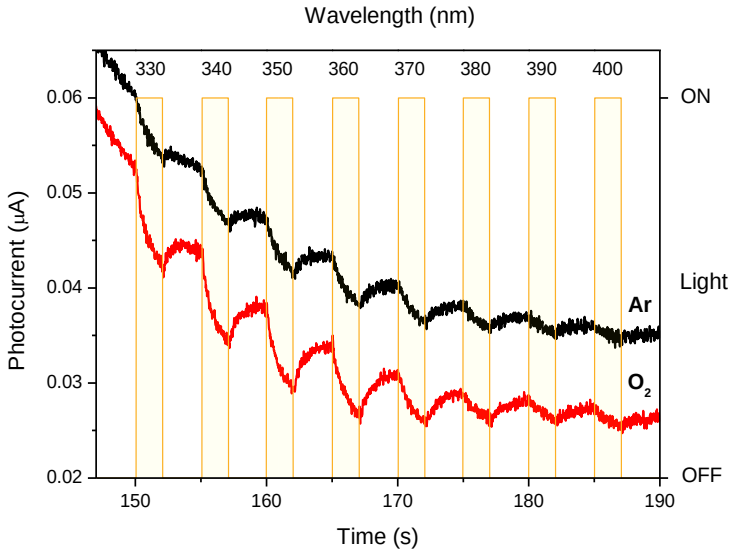

Figure 4.39. *Photocurrent recorded as a function of time on PET/ITO electrode covered with SGT sample, at applied potential E = -0.1 V vs Ag/AgCl, in aqueous 0.1 M KNO_3 solution saturated with Ar or with O_2. Light switching intervals are marked by the bars and the corresponding wavelengths are indicated.*

The photocurrent intensities recorded, in the order of 10 nA, are quite low compared to the available literature data [110,111,132,135,179,180]. However, this is not surprising if the structural features of the materials studied here are taken into account:

- they are amorphous, while the literature data mainly concern highly crystalline samples, which are expected to possess higher conductivity and more efficient charge separation;
- they are xerogels of micrometric granulometry (except SGT), while the literature data concern nanometric particles, whose small size and high surface/volume ratio considerably improve charge transport and separation by interparticle electron transfer [181], as well as the contact with the electrode in the photocurrent measurements.

Moreover, different experimental conditions can significantly affect the results. The outcome depends on the intensity of incident radiation, which is variable with wavelength. Anyhow, the photocurrent results attest the photosensitization of TiO_2 realised through the charge transfer complexes formed in the first step of the sol-gel synthesis of the hybrid gels.

The occurrence of oxidation and reduction phenomena in a molecule or a material can be analysed by cyclic voltammetry (CV), which also provides thermodynamic and kinetic information. A continuous voltage scan is applied toward positive and then negative values, recording the current intensity at the working electrode. CV scans were performed on the samples in the same system and configuration used for photocurrent measurements, normally before and after their acquisition. The results are displayed in Figure 4.40.

All the samples have basically the same behaviour as the SGT reference, with a consistent hysteresis related to the capacitance of the materials and a rise of detected current toward the upper limit of the potential window (1 V), close to the water oxidation potential. Some of the hybrid samples exhibit an oxidation peak: this is clearly visible in T-cat and T-asc, centred around 650 and 600 mV respectively, and can be individuated in T-dop as a slope change, around 600 mV, while it is not evident in T-acac and T-dbm. The oxidations observed are electrochemically irreversible processes, and their width and low intensity can be due to slow kinetics and also to the low scan rate. They are in agreement with data reported in literature on TiO_2 modified with pyrocatechol and ascorbic acid [132,135,175], and are attributed to their oxidation to semiquinone and ascorbate radical. These species, as well as dopamine semiquinone, can undergo also a second oxidation step to o-benzoquinone and dehydroascorbic acid. T-cat and T-dop hybrids exhibit a reduction peak, at about -100 and 50 mV respectively, indicating that ligand oxidation equilibrium can be at least partially inverted, although the large peak separation (ΔE) suggests that there is a high resistance to the reduction. Acetylacetone is expected to have a higher oxidation potential, because of its chemical structure, which would be in agreement with the higher effective band gap of T-acac with respect to the enediol hybrids. Assuming that the conduction band edges have a similar potential in all the hybrids, the acac HOMO in the complex should be found at about 0.7 V more positive potential than the HOMO of enediols, so beyond the scanned window, and a comparable situation can be figured for T-dbm.

During a photocurrent measurement the material is subjected to an increasing oxidative potential under irradiation for a prolonged time. The voltammograms recorded after the photocurrent scan are shown in Figure 4.40. In the hybrid samples a decrease of the currents at positive potentials and of the oxidation peak intensity is observed, while SGT is practically unaffected. This can be explained with the partial irreversible oxidation of the organic ligands during the photoinduced reactions.

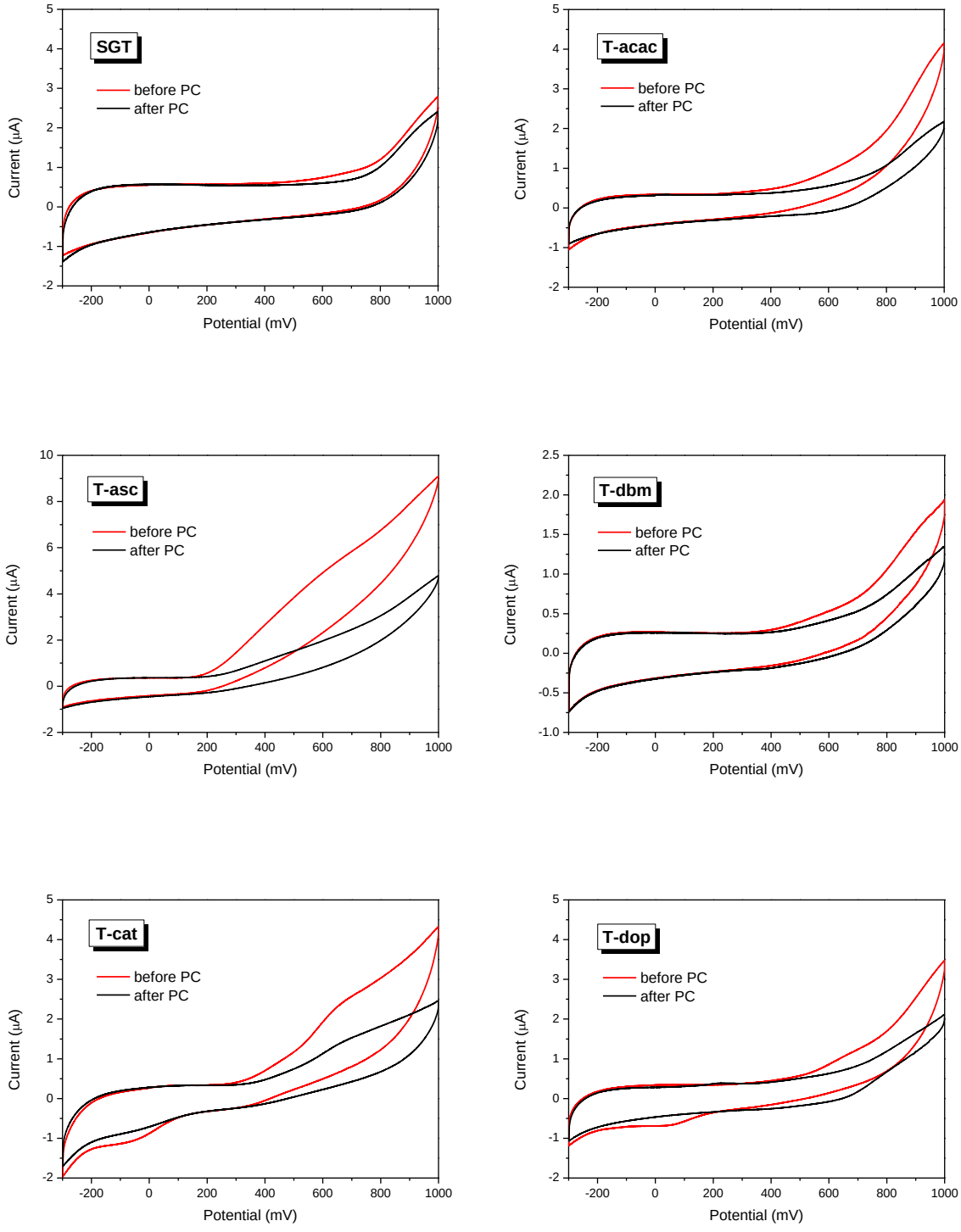

Figure 4.40. *Cyclic voltammograms recorded on PET/ITO electrode covered with samples: SGT, T-asc005, T-acac04, T-dbm02, T-cat005, T-dop005. Measurements taken in aqueous 0.1 M KNO_3 solution saturated with Ar, at scan rate 10 mV/s (the second CV sweep before and after photocurrent measurement is shown). Reference electrode: Ag/AgCl.*

When a photosensitizer injects electrons into the conduction band of the coupled semiconductor, an electron donor should be available to reduce it back to its initial state, and allow the catalytic cycle to

be repeated, as happens in dye sensitized solar cells, containing a I^-/I_3^- or equivalent redox couple in the electrolyte. Ligand-to-metal charge transfer has been demonstrated to be the first step of oxidative photodegradation under visible light of some small organic pollutants with hydroxyl and carboxylate binding groups [47,94,111,182]. The self-sensitization of such complexes on TiO_2 can be followed by attack of ROS on the organic radical, leading to its autoxidation. A molecule with a strong coupling between its HOMO and the Ti-3d orbitals of the conduction band (like catechol), should give an enhanced electron transfer, but also show a higher susceptibility to self-degradation with respect to molecules with a lower coupling, which can prefer an indirect electron transfer through their LUMO (like salicylic acid) but result to be more stable. Therefore, upon testing the photocatalytic efficiency of hybrid semiconductors with organic sensitizers attention must be paid to the stability and reuse possibility of the material.

Annealed samples.

The photoresponsivity of the dark coloured TiO_2 materials produced by calcination of a T-acac hybrid xerogel in different conditions was also studied by photocurrent spectroscopy. The results are displayed in Figure 4.41.

The photocurrent maps reveal that the activity recorded in the visible range is rather limited for all the samples, despite their light absorption extended throughout the whole visible spectrum. The photocurrents are concentrated in the UV range, with tails reaching about 450 nm. This result testifies that the absorption of radiation in a given range does not necessarily imply photoactivity in the same range, as verified also by preliminary photocatalytic tests (Chapter 5). Many literature reports find an enhancement of activity in the visible light as consequence of the wide light absorption by "black titania" prepared by different methods, correlating it with the structural defects (Ti^{3+} and/or oxygen vacancies) or, in the case of hydrogenation, also to higher surface hydroxylation, or to the insertion of hydrogen in the lattice with a doping effect [50,51,177]. Nonetheless, other authors do not record visible light activity in this kind of materials. Liu et al. measured photocurrents on a series of coloured hydrogenated anatase nanoparticles, registering signals only in the UV range. They proposed that either the formed electronic states can electronically couple with the CB of anatase, or that recombination from these states is strongly favoured over a thermal excitation to the conduction band [177]. This interpretation could apply to the samples studied here as well. Considering that the band gap does not appear consistently changed (see Section 4.2), if the states linked to the defects lie mainly close in energy to the CB, the excitation of other electrons from the VB to replenish those states, once they have given away their electrons, can be hampered, needing energy close to the UV range. Moreover, if many defects are located in the bulk of the material, as could be the case of these gel-

derived samples, the diffusion length that charge carriers have to overcome to reach the surface is longer and recombination might be favoured.

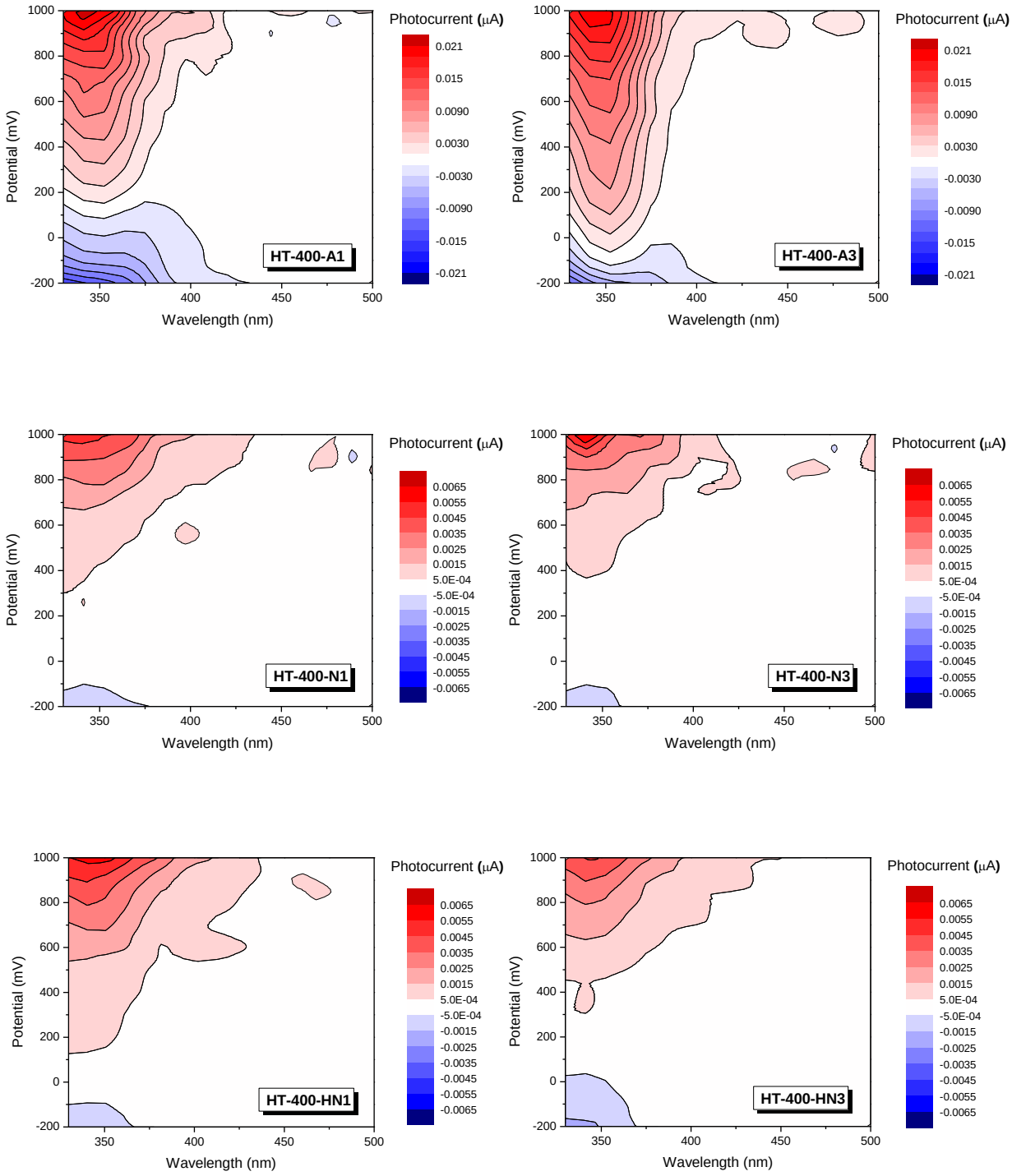

Figure 4.41. *Photocurrent as a function of potential (vs Ag/AgCl) and incident light wavelength, recorded on PET/ITO electrode covered with T-acac (HT) samples treated at 400 °C with different atmosphere and time: A1, A3, N1, N3, HN1, HN3. Measurement taken in aqueous 0.1 M KNO_3 solution saturated with Ar. The photocurrent scales are different.*

The photocurrent spectra of the calcined materials show that the air-treated ones have the most intense currents (over 20 nA) and that currents are also distributed in the whole potential range. In fact, at potentials around 0 V these samples showed the coexistence of cathodic and anodic photocurrents, meaning that they are able to catalyse simultaneously reduction and oxidation reactions. The samples annealed in N_2 or H_2/N_2, on the contrary, show limited photocurrents (lower than 10 nA) and very similar behaviours between each other.

The observed differences could be interpreted in relationship to structural or electronic differences. BET surface analysis found a stronger decrease in surface area in the N and HN samples compared to air-treated ones. Annealing in a more reducing atmosphere possibly leads to a less complete removal of the products of organic species, so carbon impurities could accumulate on the surface. Other hints about the electronic features of these materials are provided by the spectroelectrochemical measurements (*vide infra*) and photocatalytic activity tests. The tests in photoreforming for hydrogen production from a glycerol solution, discussed in Section 5.3, revealed a striking activity of some samples under UV irradiation.

To get insight into the properties-activity relationships, two materials were chosen for further photoelectrochemical characterization: HT-400-A1 and HT-400-N3. The former has the simplest preparation procedure, has been widely characterized and shows the highest photocurrents, the latter provided the best results in photoreforming and do not need H_2 in its preparation.

Photocurrent multiplication is a phenomenon occurring when a photogenerated charge carrier initiates a series of reactions which involve multiple electron transfers. An example is represented by the oxidation of an alcohol on TiO_2. Simple alcohols adsorbed on TiO_2 surface, prevalently by a dissociative pathway, are very effective hole scavengers. The first step includes the cleavage of a C-H bond, resulting in the formation of the respective α-hydroxyalkyl radical. Taking methanol as a model compound:

$$CH_3OH \rightarrow {}^{\bullet}CH_2OH + H^+ + e^-$$

The second step brings to the formation of the aldehyde under injection of another electron into the CB of the oxide [15]:

$${}^{\bullet}CH_2OH \rightarrow CH_2O + H^+ + e^-$$

Therefore, when an alcohol is added to the electrolyte solution in a photocurrent experiment every photogenerated hole can cause the injection of at least two electrons into the CB (hence the alternative term “photocurrent doubling”). Actually, the oxidation can also proceed, with the transfer of additional electrons.

To evaluate the oxidative behaviour of two heat treated materials a photocurrent measurement was performed adding 5 wt% of glycerol to the electrolyte, simulating the conditions employed in the photoreforming tests. The results are illustrated in Figures 4.42 and 4.43. The response of the two samples was different: HT-400-N3 approximately doubled its photocurrent, while HT-400-A1 exhibited at least a 4-fold increase, reaching values over 120 nA; the remarkable effect, together with the extended anodic currents up to negative potentials, is evident comparing the photocurrent maps (Figure 4.43). Glycerol, as a triol, can effectively undergo multiple oxidations and donate more than two electrons; the air-treated gel shows a more efficient interaction with glycerol allowing for further oxidation steps. It can be noted by the time profiles of photocurrent in Figure 4.42 that in the short time of the shutter opening (2 s) a plateau is not reached, so a longer measuring time may give more accurate (and higher) results. Further characterization will aid the interpretation of the performances of these materials.

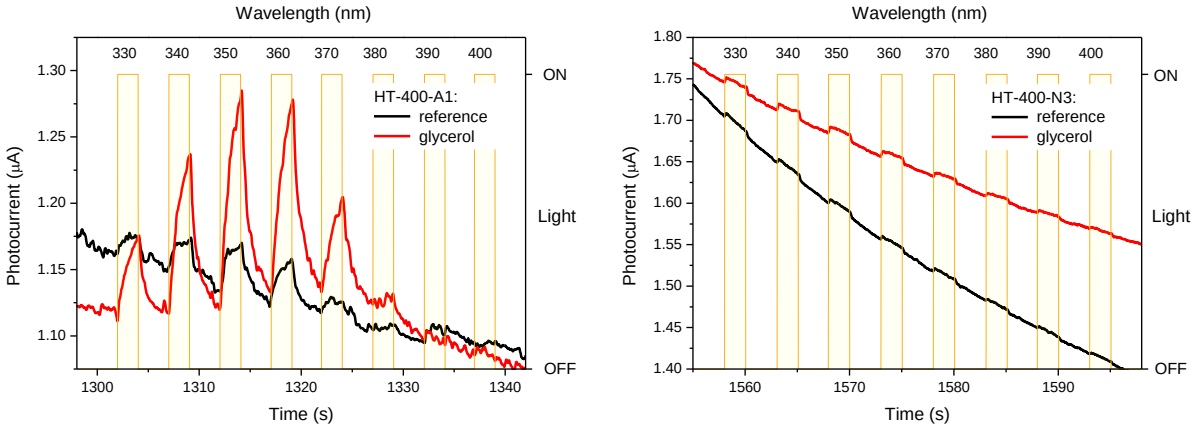

Figure 4.42. *Photocurrent recorded as a function of time on PET/ITO electrode covered with HT-400-A1 (left) or HT-400-N3 (right) sample, at applied potential E = 0.8 V vs Ag/AgCl, in aqueous 0.1 M KNO_3 solution saturated with Ar (black curves). The red curves refer to the same measurement with the addition of 5 wt% glycerol to the electrolyte solution. Light switching intervals are marked by the bars and the corresponding wavelengths are indicated.*

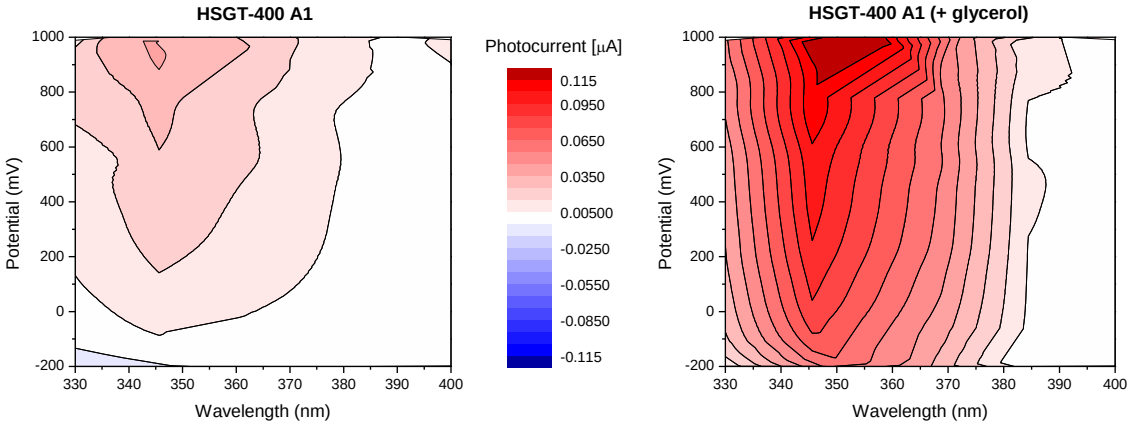

Figure 4.43. *Photocurrent as a function of potential (vs Ag/AgCl) and incident light wavelength, recorded on PET/ITO electrode covered with HT-400-A1 sample, in regular conditions and with the addition of 5 wt% glycerol to the electrolyte (aqueous 0.1 M KNO_3 solution, saturated with Ar).*

4.4.2. Electronic structure investigation

The interfacial charge transfer processes that can take place at the surface of a semiconductor are determined by the potentials of conduction and valence band edges, which indicate whether the electrons and holes have the suitable energy to participate in a specific redox reaction. The redox potentials of a material are influenced by several factors, for example crystal structure, particle size, doping type and level, surface modifications, environment (solvent, pH) and so on, therefore they are largely variable. The photochemical properties of semiconductors are also affected by the presence of electronic levels within the band gap, arising from defects, dopants or other additives. These states can act as charge carrier trapping sites or electron donors, contributing to the separation or recombination of electron/hole pairs. The available methods to analyse the electronic structure of semiconductors generally measure the quasi-Fermi energy for electrons in the excited state, and present some limitations [64,65,183].

A spectroelectrochemical method was recently developed by Prof. Wojciech Macyk, Dr. Marcin Kobielusz and their co-workers at the Jagiellonian University in Krakow on the basis of a method previously proposed by Fitzmaurice et al. [184]. It correlates the variation of reflectance of a solid material as a function of the applied voltage with the potential and density of electronic states. The measurements take advantage of a potentiostat and a UV-vis spectrophotometer in diffuse reflectance mode. The sample is casted on a Pt foil, inserted in an electrochemical cell, as described in the experimental Section 2.3.8. As the potential sweeps to more negative values, electronic states in

proximity or in correspondence to the conduction band edge are met. Electrons are trapped in those states, causing an increase of light absorbance. In titanium oxide the reduction consists in the formation of Ti^{3+} centres, characterized by a broad absorption centred around 780 nm [64,65].

A selection of materials was analysed by this spectroelectrochemical method to gain insight in their electronic structure. The wavelength of the spectrometer detector was fixed at 600 nm, since preliminary scans at different wavelengths had shown that at this value the reflectance variations are higher than at 780 nm, allowing a better sensitivity to be achieved. Figure 4.44 shows the reflectance measured at 600 nm as a function of the applied voltage (swept from 0 to -2.7 V vs. Ag/Ag^+) for the reference SGT sample, a T-acac04 xerogel, and the latter annealed at 400 °C for 1 h in air or for 3 h in nitrogen (HT-400-A1 and HT-400-N3).

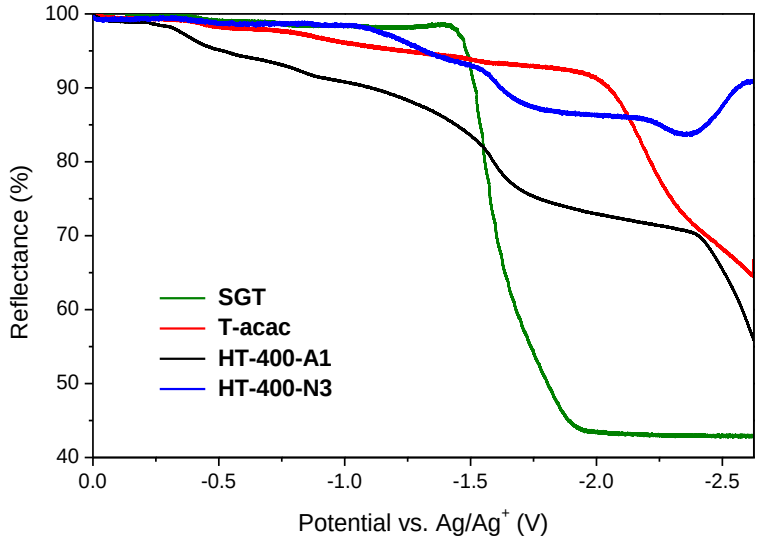

Figure 4.44. *Reflectance at λ = 600 nm as a function of time recorded on a Pt electrode covered with SGT, T-acac04, and the latter annealed in different conditions. Electrolyte: 0.1 M $LiClO_4$ acetonitrile solution saturated with Ar. Potential sweep from 0 to -2.7 V, steps ΔE = 0.025 V. Reference electrode: Ag/Ag^+.*

A slope variation in the reflectance profile indicates the onset of an electronic state which is filled with electrons as the measurement proceeds, causing an increase of visible light absorption. A marked and steep drop in reflectance, like the ones observed in the profiles of SGT and T-acac, at about -1.5 and -2.0 V respectively, can usually be attributed to the onset of the conduction band states, and the corresponding voltage be regarded as the flat band potential, at the conditions of the measurement. It is worth noting that the difference in the total reflectance change is theoretically related to the density of states, however it may depend also on the coloration of the samples: T-acac is yellow, HT-400-A1 grey and HT-400-N3 black, so their initial reflectance is lower than that of the white SGT and the sensitivity in their analysis is expected to be lower. The anomalous profile of HT-400-N3, whose

reflectance rises toward the end of the measurement, should be verified. Such variations could be attributed to some powder detaching from the Pt foil during the scan, particularly if the thickness of the casted layer is larger than needed.

The relative density of states, in arbitrary units, are calculated from the difference in the Kubelka-Munk function between subsequent potential steps, by means of a code run in R software. The results for the above mentioned samples and for the two gels annealed in air for 1 h and in N_2 for 3 h, are illustrated in Figure 4.45.

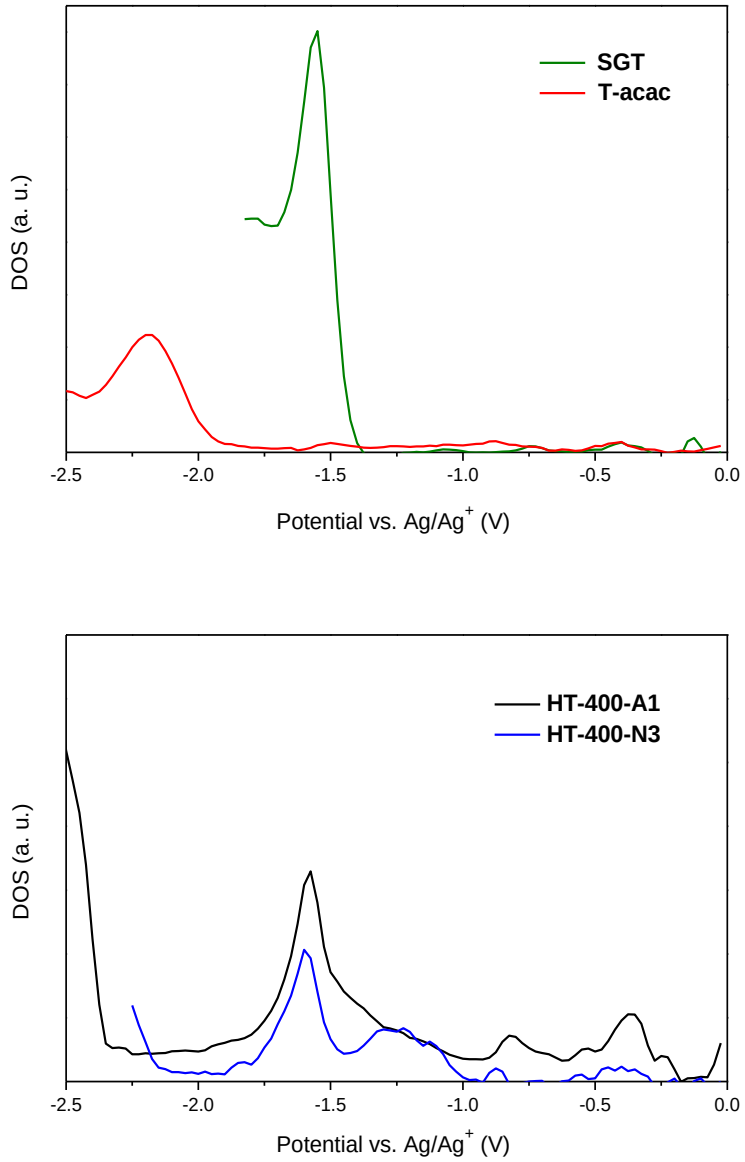

Figure 4.45. *Representative density of vacant states (DOS) profiles for TiO_2 samples: SGT, T-acac04; HT-400-A1 and HT-400-N3. Data calculated from the reflectance recorded in a 0.1 M $LiClO_4$ acetonitrile solution saturated with Ar. Reference electrode: Ag/Ag^+. DOS values not in scale between the two graphs.*

The amorphous TiO_2 prepared by sol-gel shows a CB onset at -1.4 V, corresponding to -0.6 V vs. NHE (the reference electrode redox potential is $E°(Ag/Ag^+)$ = +0.80 V vs. NHE). This value is very close to that found with the same method for rutile or P25 titania, about 0.2 V lower that the potential measured for some anatase samples [18,65]. The constant reflectance value after the large drop related to the onset does not mean that there are no more available electronic states, but that the signal is saturated, so that a further reduction does not cause any absorbance change. As a matter of fact, the sample layer on the electrode became black after the measurement, turning gradually to its original white colour in contact with air due to reoxidation.

The TiO_2-acac hybrid xerogel presents a strikingly lower CB edge potential, with an onset at -1.9 V (corresponding to -1.1 V vs. NHE). This proves that the electronic structure of the oxide is strongly modified by the presence of a charge transfer complex. Even if acetylacetonate is considered to have a weaker electronic coupling with TiO_2 than other ligands [72], the interaction of its molecular orbitals with the Ti-3d orbitals at the base of the CB induces an electronic level rearrangement with a shift of about 0.5 V with respect to unmodified TiO_2.

The signals in the mid-gap zone, although low in intensity, seem to be ascribable to electronic states, possibly related to the acac complex, as they can be individuated also as small changes of slope in the reflectance profile (Figure 4.44). A more negative value of the flat band potential means a higher energy of electrons in the CB, i.e. a higher reductive potential of the material. A reaction like the reduction of O_2 to superoxide anion should be therefore favoured; even if the Ti-acac complex shows relatively low visible light absorption and photocurrent, the electrons transferred to the oxide have a higher reduction ability than those generated in the CB of other TiO_2 materials.

A material with such features could be more suitable for applications in which the key steps are reductions, anyway T-acac shows also oxidative activity, both in the dark, owing to the stabilized superoxide, and under visible light, through a photocatalytic mechanism *via* hydroxyl radicals, as discussed in Sections 5.1 and 5.2.

The two anatase samples derived by the annealing of T-acac show a comparable DOS profile. Despite the significant absorbance of both samples at 600 nm, the resolution of the resulting profile is satisfying, showing that the spectroelectrochemical method can manage to complete the measurement even on intensely absorbing materials, in a more limited reflectance variation range. The interpretation of the results is less straightforward in this case. Observing the DOS profile, one could argue that the CB onset is at -2.2 V and below, and the peak at -1.6 V is a localized state. Indeed, this interpretation does not seem reliable. The remaining part of the profile, below -1.6 V, may correspond to a range in which the reflectance change is not proportional to the density of states anymore, taking into account the characteristics of the samples, and therefore should be neglected.

The CB edge potential could be rather assigned to the onset between -1.4 and -1.5 V, although both samples show a wide electronic state with onset at -1.0 V, which is continuous rising in density up to the presumable CB signal in HT-400-A1. A CB edge corresponding to -0.6 or -0.7 V vs. NHE would be slightly lower than the typical values for anatase. The noticeable distribution of states below the conduction band (at higher potentials) is compatible with the defectivity predicted on the basis of XPS, DRUV-vis and EPR data.

- CHAPTER 5 -

CATALYTIC AND PHOTOCATALYTIC ACTIVITY OF TiO_2 GELS

Catalysis and photocatalysis are among the most important application fields for titanium dioxide-based materials. TiO_2 is the reference material in the research on photocatalytic processes, while in catalysis it is often employed coupled with metals, as an active support, or other semiconductors, due to its relatively low intrinsic activity. The uncommon properties of some of the hybrid materials studied in the present work, in particular the surface stabilization of ROS, suggested the possibility to explore their intrinsic redox activity, independently on the activation by light irradiation. The degradation of organic contaminants in water, a typical application of advanced oxidation processes, has been tested with this purpose.

Preliminary results about the photocatalytic activity are also presented. Although amorphous TiO_2 is generally considered scarcely useful as photocatalyst, some of the xerogels were evaluated in preliminary tests of photodegradation, together with the crystalline annealed samples, which show promising results in photoreforming for hydrogen production.

5.1. Dark degradation of organic pollutants

The recently studied ZrO_2-acetylacetonate hybrid material showed an unusual efficiency in the removal of organic compounds from water solution by oxidative pathways, not encountered in bare ZrO_2. Experimental evidences based on EPR spectroscopy and theoretical calculations pointed to the superoxide radical anions adsorbed on the material's surface as the origin of the oxidative activity [6,7,185]. The investigation of TiO_2-based hybrids exhibiting the same unique property, representing the core of this PhD research activity, has allowed to improve the understanding of the phenomenon, extending it to other organic ligands which provide materials with enhanced superoxide radicals production and diverse properties [9,10]. The evaluation of the activity of the hybrid gels, focused to date on the TiO_2-acac system, has concerned the degradation of organic contaminants in aqueous phase.

A variety of toxic, harmful or undesired organic compounds reach ground and surface water as a consequence of human activities, including dyes, surfactants, pharmaceuticals, herbicides, pesticides, etc. Advanced oxidation processes are aimed at the decomposition of such contaminants, as described in Section 1.3. In heterogeneous photocatalytic processes, semiconducting oxides are normally used with UV irradiation or supported by the addition of oxidants. The development of materials able to decompose pollutants on their own would therefore be advantageous for practical water purification processes.

The experimental work dedicated to the removal of contaminants from water was performed at the Department of Agricultural Sciences of the University of Naples Federico II, in the group of prof. Filomena Sannino. Different classes of organic compounds were selected, with the double aim of checking the performance of the materials towards different substrates and trying to gather information about the reactions mechanisms by this comparison. The following molecules, whose structure is reported in Figure 5.1, all listed as priority pollutants by the U.S. Environmental Protection Agency (EPA), were used in the degradation tests:

- phenanthrene (PHE), a representative polycyclic aromatic hydrocarbon (PAH), characterized by high stability, due to the delocalized electrons, low solubility in water, facilitating bioaccumulation, and recalcitrance to common chemical removal methods;
- 2,4-dichlorophenol (2,4-DCP), representing chlorophenols, compounds commonly found in waters and considered hazardous and potentially mutagenic and carcinogenic to humans and other mammals;

- four different chlorinated phenoxyalkanoic acid herbicides, widespread in the environment because of their use for weed control in agricultural crops, chemically stabile, resistant to biodegradation, sufficiently water soluble, and held harmful to human health for their potential toxicity and mutagenicity: 4-chlorophenoxyacetic acid (4-CPA), 2,4-dichlorophenoxyacetic acid (2,4-D), 4-chloro-2-methylphenoxyacetic acid (MCPA) and 4-(4-chloro-2-methylphenoxy)butanoic acid (MCPB).

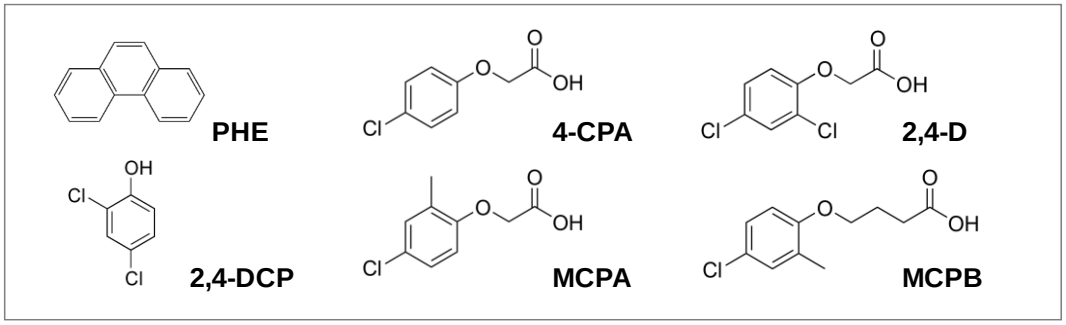

Figure 5.1*. Molecular structures of the six model organic pollutant compounds used in the tests of oxidative degradation in the dark on T-acac04 hybrid material.*

All these experiments were performed in batch systems avoiding the exposure to light, in order to examine the intrinsic reactivity of the material, excluding photoexcitation and consequent photocatalytic effects. The sample mostly used is the T-acac04 hybrid xerogel, as powder with granulometry < 90 μm.

Phenanthrene.

The first results on a phenanthrene aqueous solution (1 mg/L, close to the solubility limit) showed its complete removal after 1 h of reaction, for solid loads (R) as low as 0.1 g/L. Gas chromatography (GC) was used to identify reaction products. After 1 h of reaction at R = 5 g/L no organic intermediates were found, indicating that phenanthrene had been either completely adsorbed on the surface of the material or completely mineralized. GC analysis after 4 h of reaction at R = 0.05 g/L, with 90 % phenanthrene removal, displayed the presence of a series of compounds, namely diisobutyl phthalate and some long-chain alkanoic acids, which were reported in literature as intermediate products of the photodegradation of phenanthrene by TiO_2 under UV irradiation [6,186,187]. These data demonstrated that oxidation reactions are catalysed, or at least initiated by the hybrid material, in the absence of photoexcitation, since it is assumed that the short time when the reaction system is exposed to the laboratory light, before and after the run, is not sufficient to trigger photocatalysed reactions and reach a total conversion of the substrate. The results are comparable to those achieved on ZrO_2-acac in analogous experiments, from a qualitative viewpoint. In that case GC/MS analysis after a longer

reaction time (24 h) revealed the presence of a mixture of alkanes as principal products, showing that advanced degradation of phenanthrene can be achieved by this radical-mediated mechanism. Anyway a higher load of ZrO_2-acac (5 g/L) was needed to reach a total disappearance of the substrate [6]. The TiO_2-based hybrid is therefore clearly more active than the ZrO_2 counterpart. Considering that the concentration of superoxide radicals on the surface, evaluated from EPR data, appears to be in the same order of magnitude for both materials (~ 10^{15} spin/g), some other characteristic must be responsible for this difference.

The results are remarkable, considering that phenanthrene is not one of the common model pollutants, since the highly stable structure of PAHs, lacking substituted carbons on the aromatic rings, which often represent a suitable site for the attack of oxidizing species, makes it hard to accomplish their chemical degradation on metal oxides. As a consequence, few papers can be found about the heterogeneous photodegradation of phenanthrene, and other methods, such as biodegradation, are preferred for its removal [186,187]. Proposed mechanisms for the decomposition of PAHs usually start with the attack of some ROS on two adjacent carbons, forming hydroxyl groups, followed by oxidation of the same C leading to ring opening. The efficient mechanism occurring on the acac-containing hybrid oxides is worth deeper insight.

2,4-dichlorophenol.

Another series of tests was performed on 2,4-dichlorophenol. It is a toxic compound, intermediate for both the production and the degradation of various phenoxy herbicides. The concentration profile as a function of reaction time for a typical experiment is shown in Figure 5.2. In this case the initial concentration was higher (0.3 mmol/L), as 2,4-DCP has good water solubility. An initial fast decrease is observed, then the removal rate decreases, achieving completion in about 1 h [10].

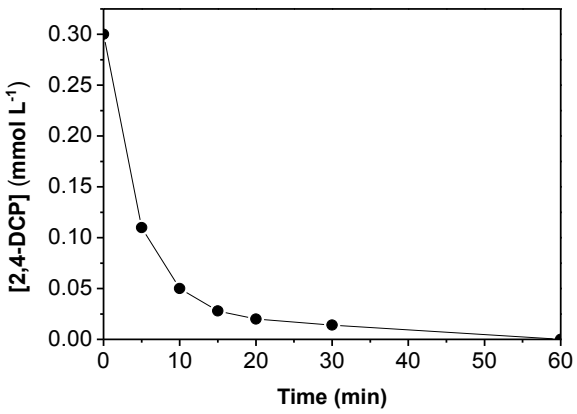

Figure 5.2*. Removal of 2,4-DCP (0.3 mmol/L aqueous solution) in the presence of T-acac xerogel (10 g/L), at room temperature, in the dark.*

Interestingly, a higher solid/substrate ratio was necessary to achieve this result than with phenanthrene (10 g/L, corresponding to about 300 mol TiO_2/mol 2,4-DCP vs. 100 mol TiO_2/mol PHE). The actual degradation of the substrate is confirmed by the appearance of new peaks in the HPLC chromatogram, associated with typical oxidation products of 2,4-DCP, such as chlorophenol, phenol and cyclohexanone. From the concentration profile it can be supposed that the process is composed of two steps, a fast adsorption of 2,4-DCP on the surface, followed by the oxidation reaction (*vide infra*).

Some information about the surface properties of the material was deduced from the comparison of the degradation kinetics between two different granulometric distributions of the solid: one with diameter less than 90 μm, the other with uncontrolled granulometry, including larger particles. With the latter, the 2,4-DCP concentration decay was sensibly slower. A first possible explanation is that the kinetic of at least one step of the process is limited by mass transfer resistance. However, this hypothesis was contradicted by the evaluation of the Thiele modulus, carried out as described in the experimental Section 2.5.1: the calculated value ($\varphi^2 \approx 1 \cdot 10^{-4}$) shows that the diffusion rate is much larger than the reaction rate, so the intraparticle diffusion effect is not significant on the overall kinetics. A more convincing explanation of the influence of the surface/volume ratio is that the active sites are not uniformly distributed within the particles, but prevalently formed on the external surface, possibly because the adsorption and reduction of O_2 to superoxide occurs more effectively on the surface than in the small pores of the xerogel [10].

Chlorinated phenoxyalkanoic herbicides.

This family of herbicides was chosen because it is widespread in the environment, so there is an interest in the remediation of waters and soils contaminated by this kind of chemicals. Moreover, it allows to study the material's activity on different molecular structures, and to learn more about the mechanism and kinetics of the process by the comparison of the degradation trends.

Sets of experimental tests were carried out adopting different initial herbicide concentration (C_0, 0.2 mmol/L or higher values, close to the solubility of each compound) and solid loads (R, 5.0 or 1.0 g/L). Two representative sets of data are shown in Figure 5.3.

In all the explored conditions, the concentration-time profiles obtained with the four herbicides tend asymptotically to zero, showing that a complete removal of the herbicides can be accomplished in about two hours. The behaviour is partially comparable to that reported for the treatment of the same herbicides on ZrO_2-acac, but in that case the kinetics was much slower and the degradation of MCPA and 2,4-D at the highest concentration was incomplete [185]. This confirms the higher activity of TiO_2-acac in the process, independently on the type of substrate.

The profiles recorded support the hypothesis of a process with two distinguished stages (particularly evident in the profiles with higher solid dosage, not shown):

1. reversible first-order adsorption of the contaminant (C) on T-acac surface;
2. oxidation of the adsorbed molecule to yield the products (P).

The model is expressed by the following scheme:

$$C_{sol} \underset{k_1}{\overset{k_1}{\rightleftharpoons}} C_{ads} \xrightarrow{k_2} P$$

where k_1 and k_{-1} are the direct and inverse first-order kinetic constants of the sorption, and k_2 is the first-order kinetic constants of the herbicide degradation.

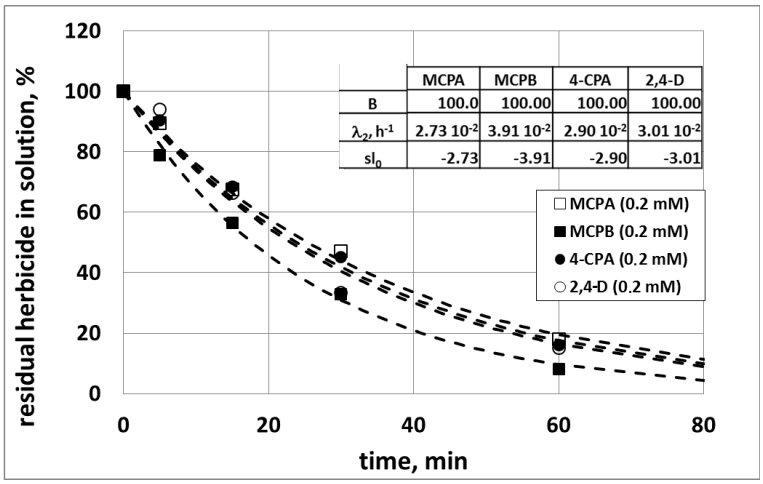

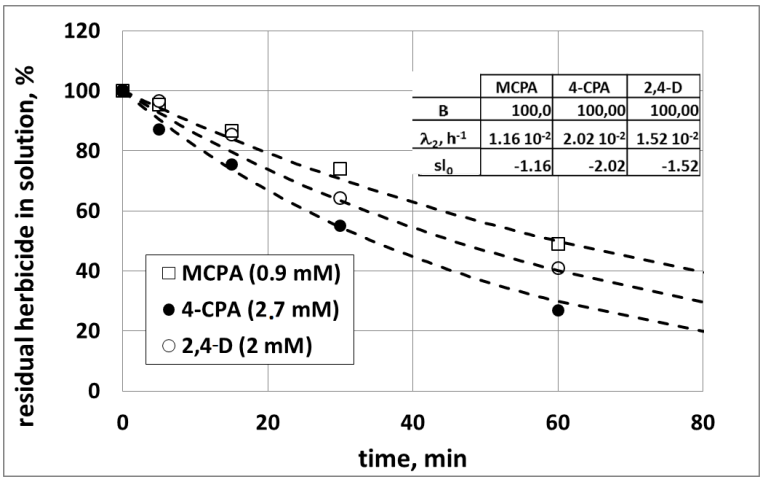

***Figure 5.3**. Kinetics of herbicides removal at 30 °C, in the dark, in the presence of T-acac xerogel (1 g/L), with different initial herbicide concentrations (reported in the box). Interpolation curves obtained using the exponential mathematical model (see text). The estimated parameters are reported in the box.*

The experimental curves for higher solid dosage (5 g/L) could be properly fitted adopting a physico-mathematical model previously developed for herbicide removal by zirconia, described by a double-exponential function accounting for the two separate steps [185]. When a lower amount of T-acac is used (1 g/L), the shape of the curves becomes more linear (Figure 5.3). Adsorption reaches rapidly surface saturation and the degradation becomes the rate-determining step, so that the curves can be fitted by a simple exponential function:

$$C_{sol}(t) = Be^{-\lambda_2 t}$$

where C_{sol} is the concentration of the substrate in solution, t is the time, B and λ_2 are fitting parameters (reported in the insets of Figure 5.3 together with sl_0, the initial removal rate), proportional to the herbicide remaining in solution once the pseudostationary adsorption equilibrium is reached, and to the kinetic constant for the reaction, k_2, respectively [185]. The degradation rates of the four herbicides are comparable. However, at higher initial concentration some difference can be observed (Figure 5.3): 4-CPA and 2,4-D, having one or to Cl atoms as substituents on the aromatic ring, are removed faster than MCPA, which carries also a methyl on the ring, likely because the Cl-substituted carbons are more labile to the attack of oxygen radicals.

Degradation products were individuated during the analysis of the samples carried out by HPLC. Figure 5.4 displays typical chromatograms of two herbicides at 0.2 mM concentration and the chromatograms of the samples taken after 1 h of reaction of the same compounds with T-acac at solid concentration of 5 g/L.

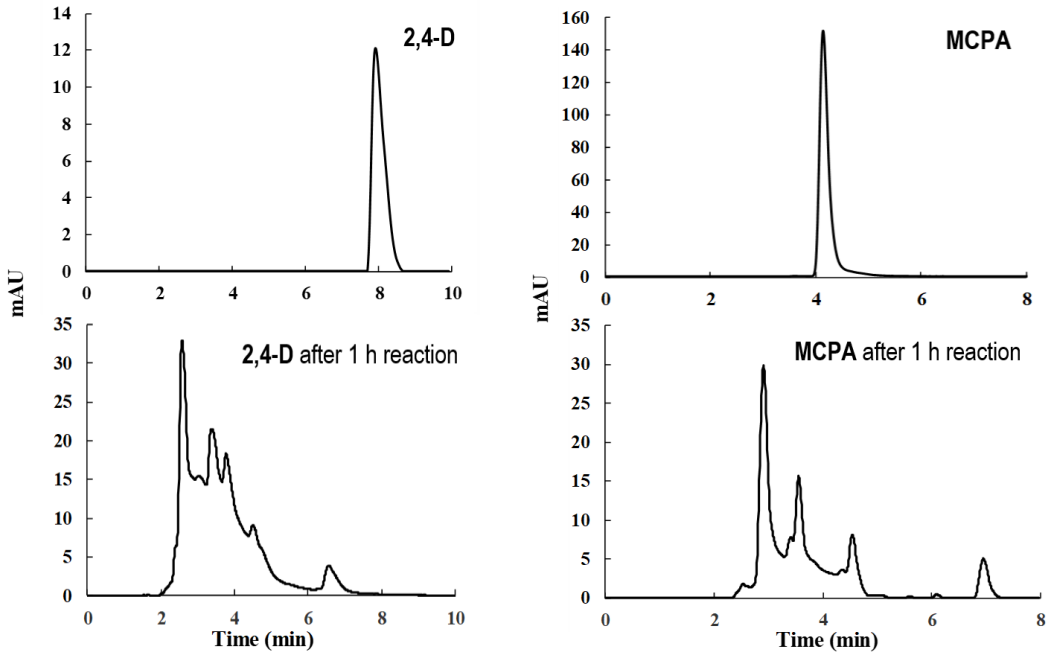

***Figure 5.4**. HPLC chromatograms of 2,4-D and MCPA at 0.2 mmol/L concentration before and after 1 h of reaction with T-acac (5 g/L).*

A complete removal of 2,4-D and MCPA and the appearance of a mixture of reaction intermediates is observed. Oxidative degradation products deriving from 2,4-D and likely attributable to 2,4-DCP, 2-chloro-1,4-benzoquinone and chlorohydroquinone have been detected. These aromatic derivatives, well-known in literature, are obtained through advanced oxidation processes, e.g. the photodegradation of 2,4-D with modified TiO_2 [188,189]. With regard to MCPA, reaction intermediates probably ascribable to 4-chlorophenol, 5-chloro-2-hydroxy-3-methylphenylacetic acid and 4-chloro-2-methylphenylformate have been found, already identified in a previous study on ZrO_2-acac [75].

Since the reaction products detected are compatible with those observed through other AOP, like photocatalysis, it can be inferred that the mechanisms are similar and activated by the same ROS. In the photocatalytic studies, different reactive species are found to be the dominant oxidants according to the reaction examined. For example, it was shown that in the photoxidation of different substituted phenols on Ag^+-modified TiO_2 the superoxide ion is the major oxidant; it can attack phenol rings acting both as a nucleophile or electrophile, depending on the electron-donating or withdrawing nature of the substituents [188]. In the degradation of 2,4-DCP and chlorinated phenoxy herbicides on T-acac a similar direct involvement of superoxide anions may take place. Anyway, superoxide in aqueous solution can rapidly generate other ROS, as described in Section 4.3.3. In fact, EPR spin-trapping experiments demonstrated that hydroxyl radicals are produced by the material in water in the dark (Figure 4.33). A lower concentration of $^{\bullet}OH$ is detected when an herbicide is dissolved in the solution, suggesting that they also play a role in the degradation, as can be expected by such a strong, non-selective oxidant. On the other hand, another method to check the formation of $^{\bullet}OH$, the reaction with terephthalic acid (see Section 5.2), did not recognize these radicals in the presence of T-acac. This suggests that, even if $^{\bullet}OH$ radicals are generated by the material, as proven by EPR, they are probably not the primary or not the sole ROS responsible for the activity of the materials.

Further experiments, like spin trapping or the addition of specific scavenger during the degradation run, could give more indications about the role of oxygen radicals in the activity of this material.

Role of the hybrid material.

Once ascertained that a hybrid material like TiO_2-acac causes the oxidation of a variety of organic compounds through non-photoinduced radical mechanisms, it is important to prove its actual function: does it act as a real catalyst or rather as an initiator, carrying superoxide radicals as a reservoir? A first approach to answer this question is a simple calculation of the concentrations of species in the reaction system compared with the stoichiometry. Even considering the large uncertainty associated with EPR quantitative data, in typical reaction conditions the initial molar amount of organic substrate results to be at least 1000 times higher than the initial amount of

superoxide radicals on the material surface. Holding the hypothesis that the degradation of each substrate molecule requires at least one radical to start and propagate, the amount of superoxide stored on T-acac is by far substoichiometric. Therefore, for the reaction to advance in the dark (without photoexcitation) more radicals must be produced. Molecular oxygen is always dissolved in solution (the air volume in the reactor is in large excess) and its direct role in the oxidation pathways should not be neglected [16]. It could be inferred that the same process occurring in air on the hybrid surface (adsorption of O_2 and reduction to $O_2^{\bullet-}$) can take place in water with dissolved O_2, causing the cyclic regeneration of the active superoxide once it is consumed.

To definitely confirm that the material is an efficient and durable catalyst, the possibility to reuse it several times should be verified, without any intermediate treatment, or with a simple drying in air to regenerate the surface radicals (like it was proven to occur when the material had lost most adsorbed superoxide after long storage, see Section 4.3.2). A preliminary experiment of repeated batch runs, adding new herbicide solution to the separated T-acac powder, showed a decrease of activity from the third run, however the stability of the material is still to be fully addressed. Considering the EPR data, indicating that other hybrid systems, such as TiO_2-dbm and TiO_2-citrate, are able to stabilize on the surface a much higher concentration of superoxide radicals, and that this peculiar property could be possibly found in the analogous hybrid films, the perspectives for the application of these materials in advanced oxidation processes seem really promising.

5.2. Photoxidation of model organic compounds

A typical test of heterogeneous photocatalytic activity is the degradation of a model compound in water. The development of photocatalytic water and air treatment processes attracts large interest and research efforts. As such reactions in water phase are relatively simple to perform and extensively studied, it is easier to compare photocatalytic performances with literature data. They occur with the intervention of various photogenerated ROS and allow to evaluate their production. The most commonly used model contaminants are dyes (e.g. methylene blue, Rhodamine B, methyl orange) and phenol with its derivatives, although the photodegradation of a wide range of organic compounds are found in literature. Dyes represent a practical model substrate, since their concentration in solution can be monitored by a quick spectrophotometric analysis. On the other side, results obtained from the decolouration of dyes should be interpreted with care, because they can give sensitization of the photocatalyst, and activate parallel self-degradation pathways [190].

Notwithstanding, a first indication on the activity of a T-acac hybrid xerogel was provided by preliminary tests on a methylene blue solution under visible light irradiation. The data, not reported, showed a partial disappearance of the dye, divided in a faster and a slower concentration decrease, possibly ascribable to an adsorption followed by a slow degradation. The same rate of disappearance was not observed in the dark, or on methylene blue alone, suggesting that some photocatalytic process must be involved.

During the research activity at the Jagiellonian University in Krakow, a screening of the photocatalytic performances of some samples was carried out by means of the conversion of terephthalic acid (TA). The oxidation of TA occurs specifically by the attack of a hydroxyl radical to one of the carbons adjacent to the carboxylic groups (Figure 5.5). The product, 2-hydroxyterephthalic acid (TAOH), is strongly fluorescent, so its formation can be followed recording the emission spectra of the supernatant. Due to the selectivity of the reaction, it permits to compare the efficiency in the generation of ˙OH, recognised as the dominant ROS in many photocatalytic oxidations [18,191].

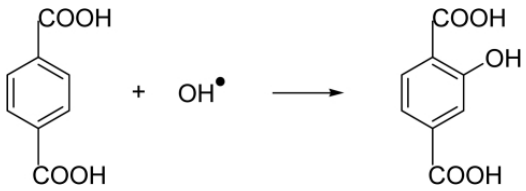

Figure 5.5*. Scheme of the oxidation of terephthalic acid to 2-hydroxyterephthalic acid by hydroxyl radical.*

The results relative to T-acac under visible light (with a 420 nm cutoff) are shown in Figure 5.6. During 2 h of irradiation TAOH was produced at a low but constant rate. In the reference test conducted in the dark in analogous conditions, there was no evidence of TAOH formation. Considering that the basic pH of the TA solution (given by the addition of NaOH to enhance its solubility) can inhibit the reactions that convert superoxide to hydroxyl radicals involving protonation steps, a test at neutral pH was performed, still without the detection of TAOH. This seems in contrast with the DMPO spin trapping measurements, indicating the production of ˙OH by the material in water in the dark (see Section 4.3.2). The discrepancy may be explained with the higher sensitivity of the EPR analysis, able to detect even small concentrations of hydroxyl radicals, which do not produce significant amounts of TAOH. Anyway, the negative results of the dark tests ensure that a purely photocatalytic mechanism accounts for the activity shown T-acac under visible light.

A preliminary test in the same conditions on hybrid gels with other organic ligands showed results apparently similar to T-acac, but the fluorescence spectra contained also additional features causing a rise of the background and consequent uncertainties in the quantification of the concentration of TAOH produced. This behaviour could be related to the self-oxidation of a small fraction of the

ligands, with the release of fluorescent products. However, further experiments are needed to draw conclusions.

Interestingly, not only the amorphous SGT, but also two annealed T-acac samples (HT-400-A1 and HT-400-N3) do not show appreciable activity with TA under visible light (Figure 5.6). The result is in agreement with the limited photocurrent recorded in the visible range for these materials, despite their wide absorption in the entire spectrum. The possible reasons are discussed in Section 4.4.

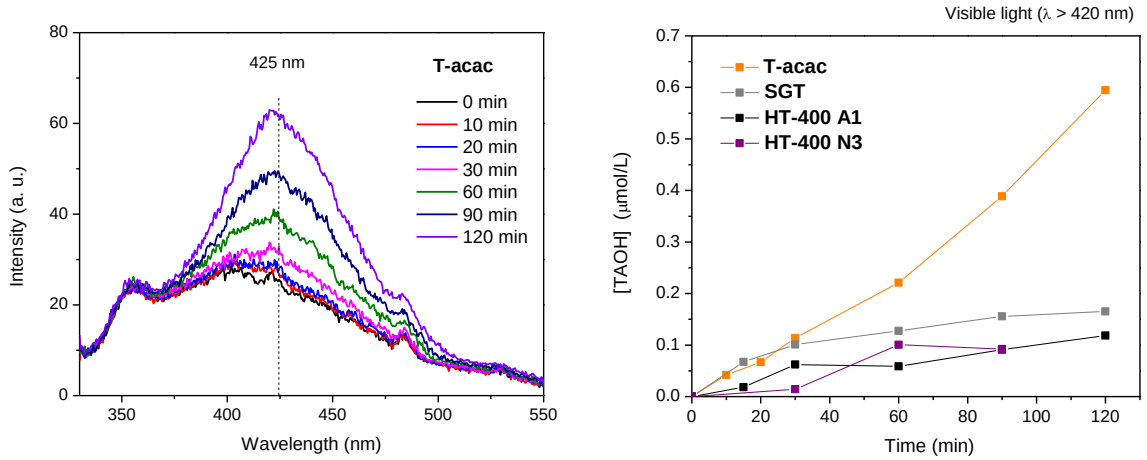

***Figure 5.6**. Fluorescence spectra recorded during the reaction of T-acac (1 g/L) in a 0.3 mmol/L TA solution with visible light irradiation (cutoff > 420 nm) at different times (excitation λ = 315 nm) (left); concentration profiles of TAOH produced in the same conditions on T-acac and three other TiO_2 samples (right).*

The xerogels annealed in different conditions were therefore tested under a wide irradiation spectrum, simulating solar light, produced by the Xe lamp with cut-off at 320 nm. The results in the conversion of terephthalic acid are shown in Figure 5.7. All the calcined samples show photocatalytic activity in these conditions, although with different kinetics: the two air-treated samples (A1 and A3) are by far the most active, together with the one treated in N_2/H_2 for 3 h (HN3). These results can be compared with the photocurrent spectra, evidencing a higher anodic current production in the UV range for the air-treated materials. The differences in activity recorded between A1 and A3 and between HN3 and the other samples has to be verified and supported by further experiments.

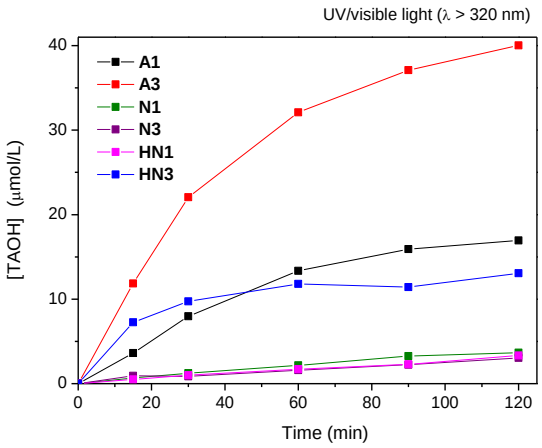

***Figure 5.7**. Concentration profiles of TAOH produced from a 0.3 mmol/L TA solution with UV/visible light irradiation (cutoff > 320 nm) on six annealed TiO_2 samples of the HT-400 series.*

5.3. Photoreforming for hydrogen production

Hydrogen is an important bulk chemical and is considered a key green fuel for the future. Nowadays it derives mainly from the reforming or gasification of fossil fuels, so the research of alternative ways for its production, based on renewable sources, is of paramount relevance. Water splitting is an attractive process exploiting solar energy to reduce H_2O to H_2, however it is thermodynamically limited. The use of oxygenated organic compounds as electron donors (or hole acceptors) allows to improve the yields of this energetically uphill process, which is referred to as photocatalytic reforming [44,66,192]. If these sacrificial reagents come from biomass, for example glucose, cellulose or ethanol, and the energy source is solar light, the overall result is a green and sustainable process.

At the University of Salerno, prof. Vincenzo Vaiano and co-workers have tested the annealed defective TiO_2 materials studied in the present work in the photoreforming reaction of glycerol. Glycerol (propane-1,2,3-triol) is a widely used compound in food, cosmetic and pharmaceutical industry. It is an abundant by-product of biomass valorisation, like the transesterification of vegetable oils for the production of biodiesel and biolubricants. Glycerol was recently shown to be also an effective sacrificial substrate for H_2 generation [66,192].

The photocatalytic tests were performed under UV irradiation on a 5 wt% glycerol solution, without the addition of a metal co-catalyst. In most literature reports, nanoparticles of a noble metal (usually Pt) or a metal oxide (often NiO and RuO_2) are deposited on TiO_2 in order to collect photogenerated

electrons and catalyse the reduction, which is considered the rate limiting stage of the process. The present tests gave excellent results, shown in Figure 5.8, despite the absence of a co-catalyst. After 4 h of reaction the highest H_2 production was yielded by the xerogels treated in N_2 or N_2/H_2 for 3 h (N3 and HN3), followed by the air-treated for 1 h (A1).

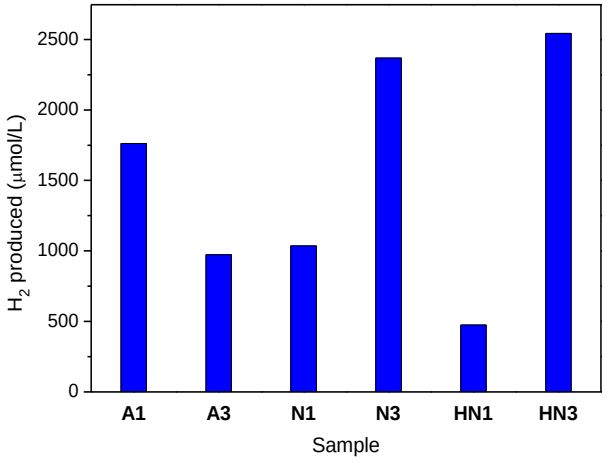

***Figure 5.8**. Amount of generated hydrogen after 4 h of reaction on a 5 wt% glycerol aqueous solution, under UV light, with six TiO_2 samples of the HT-400 series, annealed in different conditions, and catalyst dosage 1.5 g/L.*

The observed trend is different than that seen above for the oxidation of terephthalic acid. This is not necessarily a contradiction, since the two processes are completely different: the production of TAOH is an oxidation specifically mediated by hydroxyl radicals, while photoreforming is a more complex network, including oxidation and reduction stages, with the latter determining the kinetics. In contrast to the photoxidation tests, showing activity only in the UV range, a preliminary photoreforming test on the N3 sample under visible light irradiation revealed an interesting activity.

The results can be correlated with the photocurrent measured on A1 and N3 samples in the presence of glycerol, which exhibited a marked growth, especially for A1, proving the ability of the materials to directly oxidize glycerol, increasing the available electrons in the CB. The noteworthy reduction ability of the materials without a co-catalyst is probably related to their structural defects, as argued in some recent works [177]. The slightly lower CB edge potential with respect to common anatase TiO_2, indicated by the spectroelectrochemical measurements, can also contribute. At the present stage it is complex to account for the diverse photocatalytic performances shown by the samples. In any case, these first results are really promising, and open wide perspectives for the study of these materials in energy uphill photocatalytic processes.

- CHAPTER 6 -

CHARACTERIZATION OF TiO_2-BASED THIN FILMS

This PhD research activity has included the investigation of TiO_2-based thin films, in the framework of a collaboration between the Department of Chemical, Materials and Production Engineering of the University of Naples Federico II and the ENEA Research Centre in Portici (Naples), specifically with the group of Dr. Maria Luisa Addonizio. The project belongs to the research program "Ricerca di sistema elettrico" (research of electrical system), promoted by the Italian Ministry of Economic Development, and its topic is the production of TiO_2 thin films suitable as electron transport layers for perovskite solar cells.

Perovskite photovoltaics is an emerging technology, deriving from dye-sensitized solar cells and evolving extremely fast, with a current conversion efficiency record of 22.7 % achieved in 2017, as reported by the US National Renewable Energy Laboratory (NREL). A hybrid material with perovskite structure, originally methylammonium lead halide, constitutes the light absorbing layer, inserted between two layers which transfer electrons and holes to the electrodes (Figure 6.1). The most employed electron transport material is TiO_2, deposited through solution or vapor techniques and annealed at temperatures higher than 400 °C to obtain dense crystalline structures and better performances. Another mesoporous TiO_2 layer is frequently added as a scaffold for the perovskite,

increasing the interfacial area and the electron collection efficiency, in the mesoscopic architecture devices. Cells with planar architecture, lacking the mesoporous scaffold, are attracting increasing interest. One of the fundamental aspects to improve, besides the stability of the devices in the working conditions, is the electron transport layer, which should possess suitable morphological and electrical properties, including high electron mobility, hole blocking ability, proper energy level alignment and contact at the interfaces with the perovskite and electrode [193].

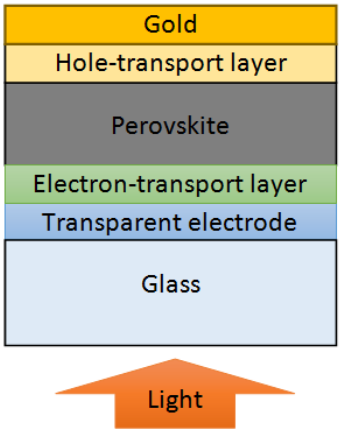

Figure 6.1. *Scheme of a perovskite solar cell with regular planar architecture.*

The first aim of the project is the development of a simple and inexpensive solution procedure for the preparation of films, possibly avoiding high temperature heat treatments. The last requirement is due to the fact that the usual annealing step at 400 °C or higher temperature to obtain compact crystallized TiO_2 makes the manufacturing of the film slower, more costly and energy consuming, and incompatible with some applications, e.g. flexible coatings and solar cells on polymeric substrates or tandem cell architectures. A crystalline structure is commonly considered necessary for achieving efficient electron transport in solar cells, nevertheless in some recent studies amorphous TiO_2 showed good performances in perovskite cell [146,194].

The approach adopted for the realisation of the films is the adaptation of the sol-gel procedure successfully applied to the synthesis of the hybrid gels, in order to achieve the prolonged stabilization of sols, to be deposited by spin coating (as discussed in Section 3.7). Sets or organic thin films with different organic ligands have been prepared and characterized in terms of structural, morphological, optical and electric properties. Particular attention has been devoted to the effect of the UV irradiation on the hybrid films. Such treatment is often performed on TiO_2 surface before the deposition of another material in multilayer devices to improve the wettability of the surface, because high energy irradiation increases its defectivity and hydroxylation. Recently, high energy UV irradiation was proposed as an effective photochemical activation method of sol-gel amorphous oxide semiconductors, in alternative to thermal annealing, allowing to achieve similar conductive

performances and stability. Hence this method was found useful to obtain efficient compact and crystallized TiO_2 layers for solar cells [195].

The functionalization of TiO_2 films with organic molecules attracts interest in various fields, including interface engineering in solar cells. For instance, it was demonstrated that a self-assembled layer of an aminoacid or pyridine between TiO_2 and the perovskite absorber can improve its adhesion, act as a passivation layer and suppress charge recombination, increasing the solar conversion efficiency [196].

6.1. Structural and morphological analysis

A number of films were produced on glass substrates, exploring widely the conditions of sol preparation and deposition, as discussed in Section 3.8. The samples are labelled by a short name with information on their composition and preparation:

- the organic ligand used: A = acetylacetonate (acac), B = dibenzoylmethane (dbm), C = citrate (cit), D = diethanolamine (dea); SGT = sol-gel TiO_2 with no ligand;
- the ligand/Ti molar ratio, indicated by a number, as for the gels;
- the number of layers deposited, if larger than one, indicated by a number in parentheses;
- the temperature of heating/annealing (after drying at 80 °C): -h = 150 °C, -a = 400 °C;
- the UV irradiation treatment, when performed: -uv.

A first inspection on the films' surface was taken through optical microscopy (Figure 6.2). When a single deposited layer was too thick (for example, with [Ti] > 0.5 mol/L in the sol), cracks were observed on the surface, increasing after a treatment at higher temperature. The mechanism of crack formation for sol–gel-derived films is attributed to the generation of tensile stresses, induced by capillary force during the drying and densification process. This mechanism can be also responsible for some inhomogeneities and signs of stress, which were occasionally spotted, together with some fine particulate which can form in the stock sol by aggregation. The synthetic conditions were optimized in order to improve the quality of the obtained films. In most cases the surface appeared sufficiently uniform and clean.

Atomic force microscopy gave a view on the surface morphology at nanometric scale (Figure 6.3). Most of the analysed films, both amorphous and semicrystalline, show a flat and quite uniform surface, like the sample A1(3). An advantage in sol-gel processing of thin films is the uniformity of the coating,

formed by the gelation of the sol during the spinning or dipping. Satisfying results in this direction were obtained with all the ligands tested. An interesting exception to the smoothness and regularity of the coatings was observed with dbm. As suggested by optical microscopy (Figure 6.2) and confirmed by AFM images (Figure 6.3) the B02 sample exhibits a deeply uneven and rough surface. The TiO_2-dbm sol is the only one in a mixed cyclohexane/n-propanol solvent, due to high hydrophobicity of the dbm ligands chelated to Ti. It is plausible that their assembly on the surface of molecular clusters favoured the formation of relatively large primary particles prior to the spin coating.

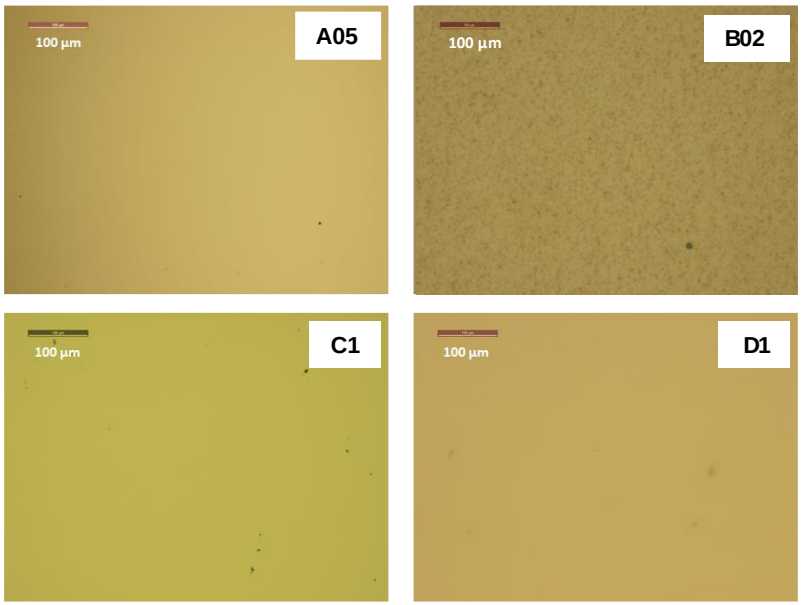

***Figure 6.2**. Optical micrographs of four representative TiO_2 films containing acac (A05), dbm (B02), citrate (C1), dea (D1) (100x magnification)*

The higher volatility of cyclohexane than n-propanol could also contribute to the disordered coating structure formation during the evaporation of the solvent, as it occurs with an increase in polarity of the mixture, leading the particles to further aggregate. The root mean square (RMS) roughness of the B02 film was estimated to be as high as 52 nm (with a thickness of 142 nm). After annealing at 400 °C most of the organic is removed and crystal nucleation has started, but the film retained its morphology, as visible in Figure 6.3 (B02-a) with a RMS roughness about 28 nm, decreased proportionally to the thickness (73 nm). Although many applications request a flat and even surface, others can benefit from such a rough morphology, for example where a larger surface area or an enhanced light scattering is needed.

The structure of the hybrid films dried at 80 °C and treated up to 150 °C is amorphous, as shown by grazing incidence X-ray diffraction (GIXRD, Figure 6.4). In the diffractograms the wide band between 15 and 30° is principally due to the amorphous halo of the glass substrate, although the amorphous

phase of TiO_2 can give a contribution. Annealing in air at 400 °C for 1 h films of the A05 or SGT series induces at least partial crystallization, with the formation of anatase nanocrystals. The grain size is about 8-10 nm, evaluated by Scherrer's formula, depending on the preparation conditions of the film. In particular, a dependence of the crystallization degree with the thickness was observed: annealed films thinner than 20 nm tend to show a poor crystalline fraction compared to thicker ones, in the same conditions (data not shown).

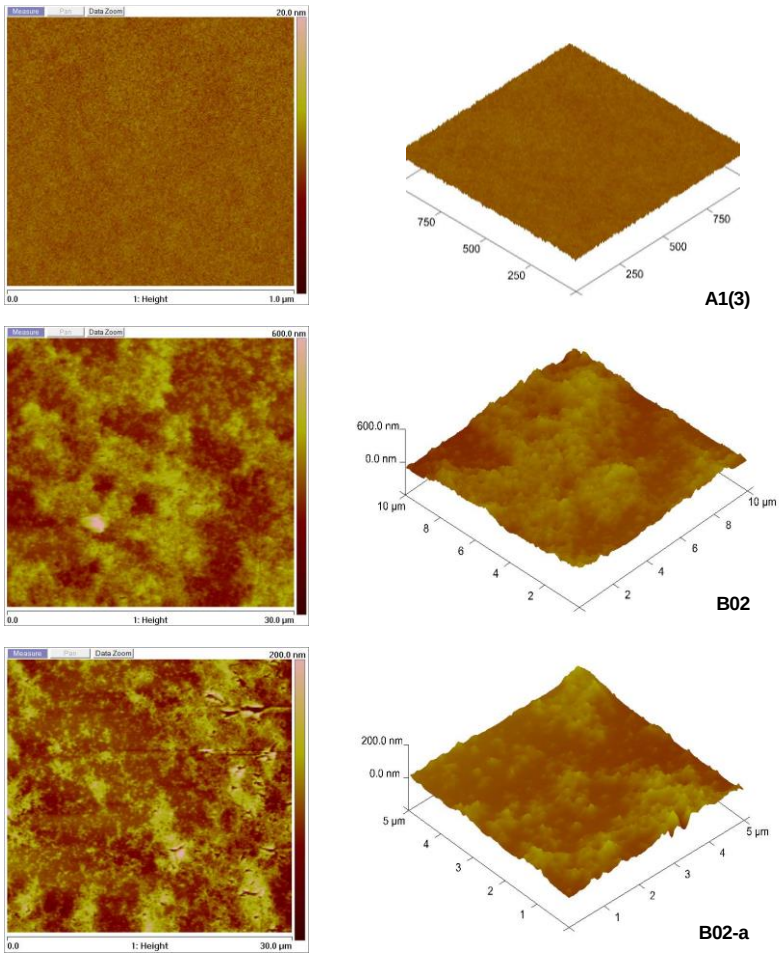

***Figure 6.3**. Atomic force microscopy (AFM) images of the surface of three representative TiO_2 films: one prepared with acac (A1(3)), two with dbm (dried, B02, and annealed at 400 °C for 1 h, B02-a). The maps are in different scales.*

The crystallization behaviour is comparable to that of the T-acac xerogels (see Section 4.1.1). The above mentioned B02-a annealed film was still mainly amorphous, in agreement with the higher crystallization temperature deduced for T-dbm gels from TG-DTA data (Section 4.1.2). It was also noticed that UV treatment does not induce crystallization of the films, as was found by some authors after a longer irradiation time of 90 min [195].

Thickness is a fundamental feature of a thin film, especially on the nanometric scale, since even intensive (bulk) properties, such as electrical conductivity, can vary as a function of thickness in a defined range. The thickness of the studied films was measured either by profilometry or by ellipsometry. When both techniques were compared on the same sample, they provided practically coincident results, ensuring their accuracy. Thickness values of selected films are reported in Table 6.1. The expected trend of a thickness increase with the increase of $Ti(OBu)_4$ concentration and with a reduction of the spinning rate was confirmed.

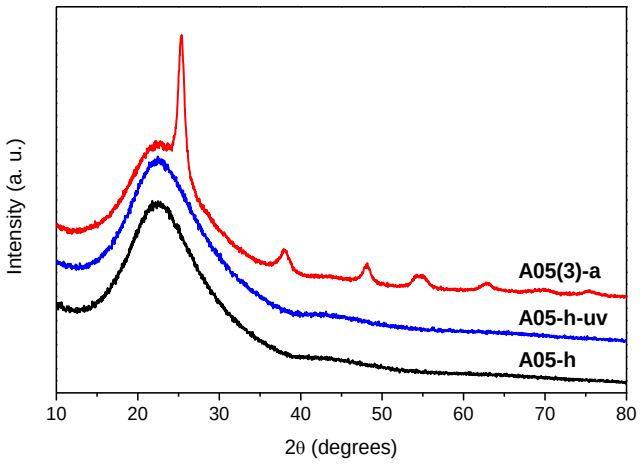

***Figure 6.4**. GIXRD profiles of three TiO_2-acac films: A05 heated at 150 °C for 1 h (A05-h), the same after 30 min UV treatment (A05-h-uv), A05 (3 layers) annealed at 400 °C for 1 h (A05(3)-a).*

A strong dependence on the type and concentration of ligand was also observed. In similar deposition conditions, at equimolar ligand/Ti ratio the thickness followed the trend: acac < dea < cit. This is due not only on the size of the molecule, but also on its ability to stabilize smaller or larger molecular aggregates. Citrate proved less efficient as a stabilizing agent, also in the synthesis of bulk gels (see Section 3.3), therefore the TiO_2-citrate sol has probably a higher degree of polymerization and viscosity, producing thicker layers. Heating at 150 °C induces a limited thickness decrease (about 10 %), while the annealing at 400 °C causes a large decrease, proportional to the amount of organics contained in the structure that are evacuated. Also the SGT films experience a thickness reduction of at least 30 % upon annealing, indicating that a significant amount of alkoxide was not hydrolysed by moisture and remained in the structure of the films dried at 80 °C. The high temperature treatment is anyway expected to induce a densification and sintering of the xerogel films.

It is interesting to note the effect of UV irradiation on the films thickness, which varies with the composition. SGT and A films are practically unmodified, while the others undergo a marked thinning, with the trend: cit > dea > dbm. These data indicate a density increase of the films and the modification and probably removal of the organic component under intense UV irradiation. The most obvious

variation occurs on citrate and diethanolamine samples, in which the strong thickness reduction is consistent with the loss of large part of the organic phase. This observation agrees with FT-IR and UV-vis-NIR data (*vide infra*).

Table 6.1. *Thickness of representative TiO_2 films, before and after a UV irradiation treatment (15 or 30 min). The values are the average of more measurements on the same sample and often on more analogous samples. The Ti precursor concentration is reported; spin rate = 2000 rpm.*

Sample	**[Ti]** (mol/L)	**Thickness** (nm ± 5 %)	**Thickness after UV** (nm ± 5 %)
SGT	0.15	21	20
SGT(2)	0.15	42	42
A05-H	0.15	40	40
A05-A	0.15	23	-
A05'-H	0.3	65	64
A05'-A	0.3	44	43
B02	0.15	142	110
C1	0.3	320	57
C1-H	0.3	290	56
D1	0.3	120	47
D1-H	0.3	108	46

The hybrid structure of the films was ascertained by FT-IR spectra, recorded in transmittance mode on films deposited on Si substrates. In Figures 6.5 the transmittance spectra of three samples with acac, dea and citrate heated at 150 °C are reported. They show that at 150 °C the organic compounds are maintained in the structure without significant changes. These spectra can be compared with those collected on powdered gels (Section 4.1.3). The A05'-h film displays the same bands seen in T-acac gels, and D1-h shows compatible features with those seen in T-cat-dea gel: the N-H deformations above 1600 cm^{-1}, the C-H bending at 1450 cm^{-1}, and the sum of C-O, C-N vibrations and C-H bending around 1100 cm^{-1} [97]. The spectrum of the C1-h film has common features with the spectra of both T-cit gels and free citric acid (e.g. the intense band at 1750 cm^{-1} related to carboxylic C=O). This can be explained with the higher citrate content in the film, leaving more carboxylic groups not coordinated to Ti. The splitting between the bands indicating coordination is 130 – 160 cm^{-1}, close to that observed

in the gels and coherent with a bidentate binding mode. The FT-IR spectrum of a dried TiO_2-dbm film is shown in Figure 6.6 (right): also in this case the analogous complexation of the ligands with Ti atoms is confirmed.

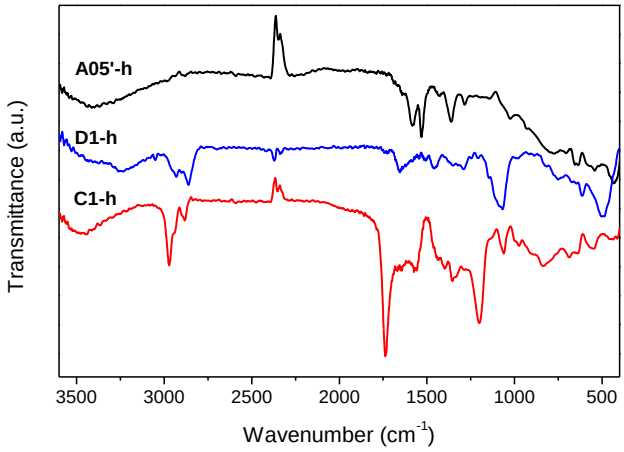

***Figure 6.5**. Transmittance FT-IR spectra of three hybrid TiO_2 films heated at 150 °C for 1 h: T-acac (A05'-h), T-dea (D1-h), T-cit (C1-h).*

The effect of UV treatment on the hybrid coatings was studied with FT-IR spectroscopy, recording the spectra after 15 min of UV irradiation. The results for films containing acac and dbm are reported in Figure 6.6, together with the as-prepared samples. Both show a decreased intensity, but while in A05' the band positions are almost unmodified, in B02 a change is evident: the band at 1360 cm^{-1}, which was ascribed to the stretching of a chelating carbonyl, as discussed in Section 4.1.3, disappeared after UV exposure, together with the band at 1480 cm^{-1}, and a new one appeared at 1414 cm^{-1}. The same transformation is reported by Segawa et al., who studied the photoreactivity of TiO_2 films containing dbm and methacrylic acid and observed the disappearance of the mentioned band during UV irradiation up to 60 min [82]. They deduced the breaking of the coordination bonds and argued that released dbm can undergo a C-C cleavage, forming radicals that initiate methacrylic acid polymerization. The loss of Ti-dbm complexation under UV light is supported by optical measurements (see Section 6.2).

The FT-IR spectra of hybrid films with citrate and dea recorded after UV treatment did not clearly show the features related to these ligands anymore. In agreement with the large thinning, it has to be concluded that these compounds undergo photodecomposition, probably supported by the photocatalytic activity of TiO_2 in the UV range. Diketones result to be less susceptible to degradation, although their concentration in the sample seems to decrease and the Ti-dbm complex is dissociated.

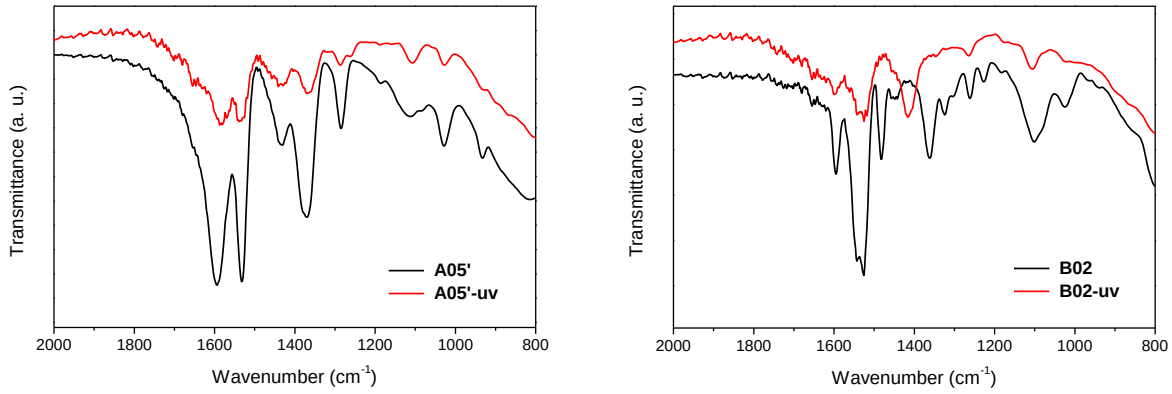

***Figure 6.6**. Transmittance FT-IR spectra of two hybrid TiO_2 films before and after UV irradiation for 15 min: T-acac (A05', left), T-dbm (B02, right).*

6.2. Optical properties

The optical properties are fundamental for photovoltaic and correlated applications. In regular architecture solar cells, the anode is the transparent front electrode, so the TiO_2 layer, intercalated between the transparent conductive oxide (typically FTO or ITO) and the absorbing layer, is required to show high transmission, allowing the largest possible fraction of solar radiation to reach the absorber (see the scheme in Figure 6.1).

The transmittance and reflectance spectra in the UV/visible/NIR range were collected for most of the studied films. The data for samples with different composition, thickness, treatment temperature and after UV irradiation are shown in Figures 6.7 – 6.11, with the calculated absorption spectra. All the samples present comparable characteristics: an absorption edge around 350 nm, corresponding to the typical values for amorphous TiO_2 films, which have generally slightly larger band gaps than bulk materials [142,197], and a high transmittance, between 80 and 90 %, almost constant in the whole visible and NIR range.

More specifically, several parameters result to affect the profiles of the optical properties. On films prepared in identical conditions the results were highly reproducible. Interestingly, the absorbance band relative to the charge transfer complex formation is evident only in the T-dbm film, centred at 390 nm and extending up to 480 nm (Figure 6.9). The T-acac and T-citrate films (Figures 6.8 and 6.10) do not show a yellow coloration like the corresponding gels, and their absorption band is only marginally shifted to higher wavelengths with respect to bare TiO_2 films (SGT, Figure 6.7). At the

nanoscale different properties can arise than those encountered in bulk materials, as in the case of the absorption edge, indicating a larger band gap, and probably a larger energy gap between the HOMO of the ligands and the conduction band edge potential.

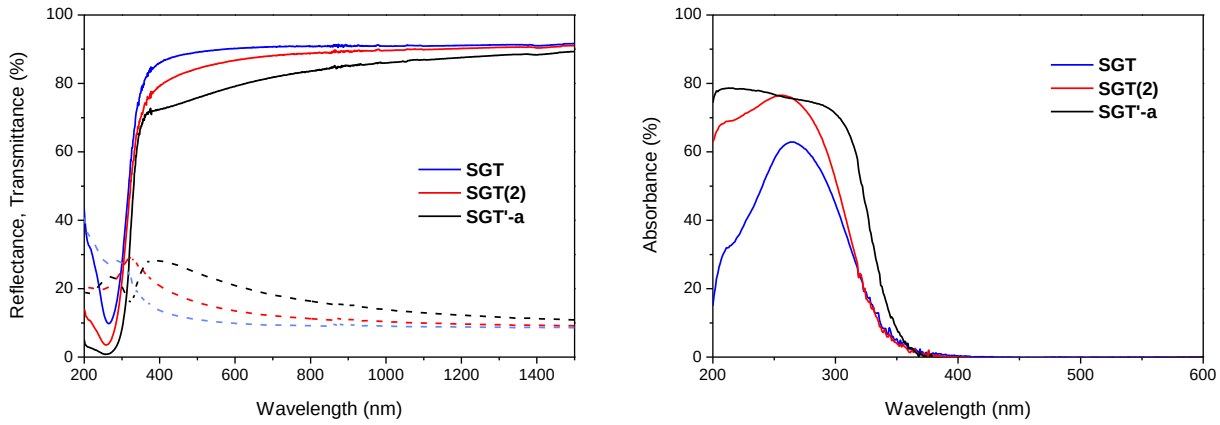

***Figure 6.7**. Transmittance (solid line), reflectance (dashed line) and absorbance UV/vis/NIR spectra of two dried TiO_2 films with different thickness, one layer (SGT) and 2 layers (SGT(2)), and a thicker film annealed at 400 °C for 1 h (SGT'-a).*

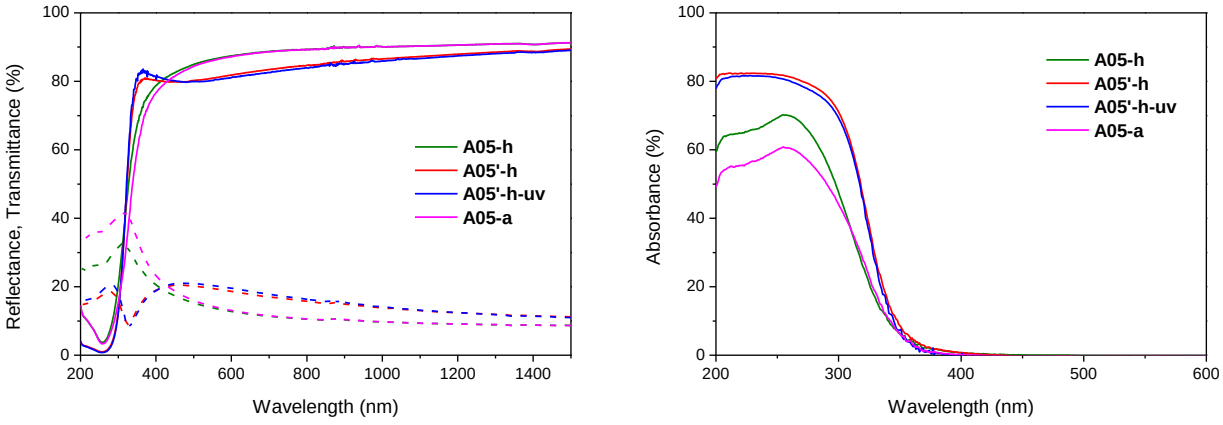

***Figure 6.8**. Transmittance (solid line), reflectance (dashed line) and absorbance UV/vis/NIR spectra of four TiO_2–acac hybrid films: two with different thickness, heated at 150 °C for 1 h (A05-h and A05'-h), the latter after UV irradiation for 15 min (A05'-h-uv), and a film annealed at 400 °C for 1 h (A05-a).*

At parity of composition and other factors, a larger thickness, obtained by deposition of a double layer or a more concentrated stock solution, as in the case of SGT and A05, respectively, caused a decrease in transmittance. The heating at 150 °C induces limited variation, as seen for C1 and D1 films. The annealing and subsequent densification and partial crystallization are accompanied by an enlargement of the absorption band in SGT, compatible with anatase formation, while almost no changes are seen in A05. Different consequences of UV irradiation on the films can be observed. The spectra of A05 are

practically unaffected, confirming the T-acac coatings as the most stable under irradiation, as suggested also by thickness and FT-IR data.

The disappearance of the charge transfer band of the Ti-dbm complex after UV treatment (Figure 6.9) is in agreement with the interpretation of FT-IR spectra and with literature reports [82]. An extended absorption shoulder remains, due to the residual dbm and derived organic products, which disappears after annealing at 400 °C. In the films containing citrate and diethanolamine, a marked reduction of transmittance and an increase in reflectance occur in the visible range. The results are practically identical in both cases (Figures 6.10 and 6.11). This modification can be due to decomposition products of citrate and dbm ligands, or to the altered structure of the films.

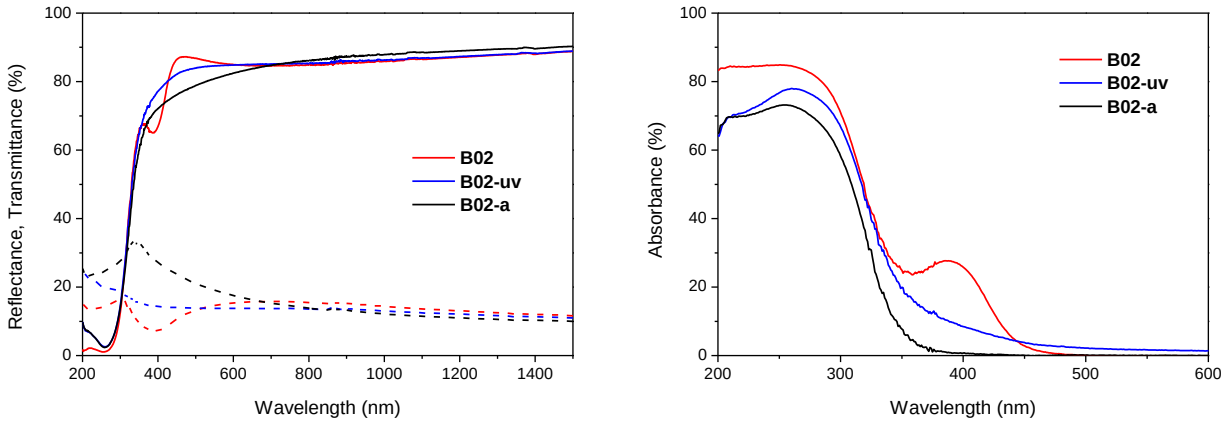

***Figure 6.9**. Transmittance (solid line), reflectance (dashed line) and absorbance UV/vis/NIR spectra of three TiO_2–dbm hybrid films: B02, the same after UV irradiation for 15 min (B02-uv) and the first one annealed at 400 °C for 1 h (B02-a).*

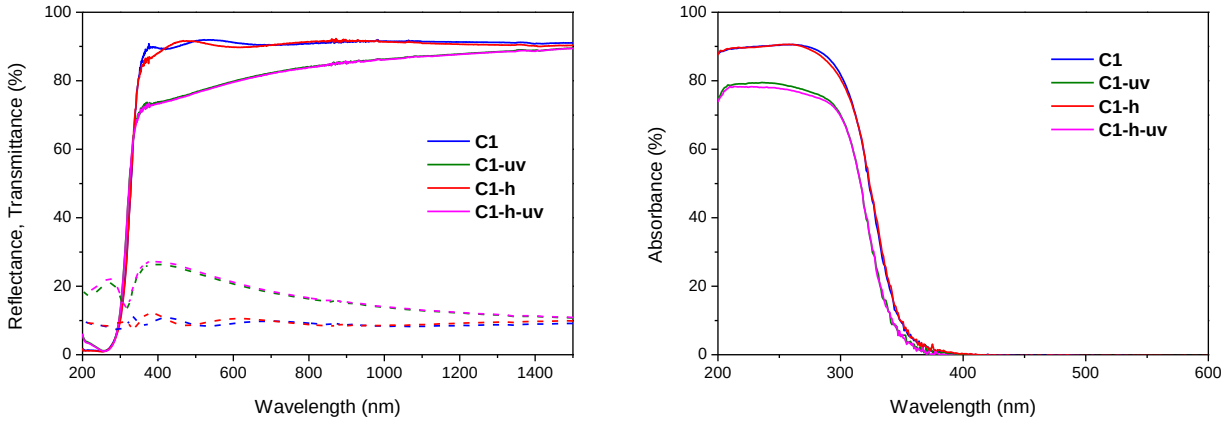

***Figure 6.10**. Transmittance (solid line), reflectance (dashed line) and absorbance UV/vis/NIR spectra of four TiO_2-cit hybrid films, dried at 80 °C (C1), heated at 150 °C for 1 h (C1-h), and the same samples after UV irradiation for 30 min (C1-uv and C1-h-uv).*

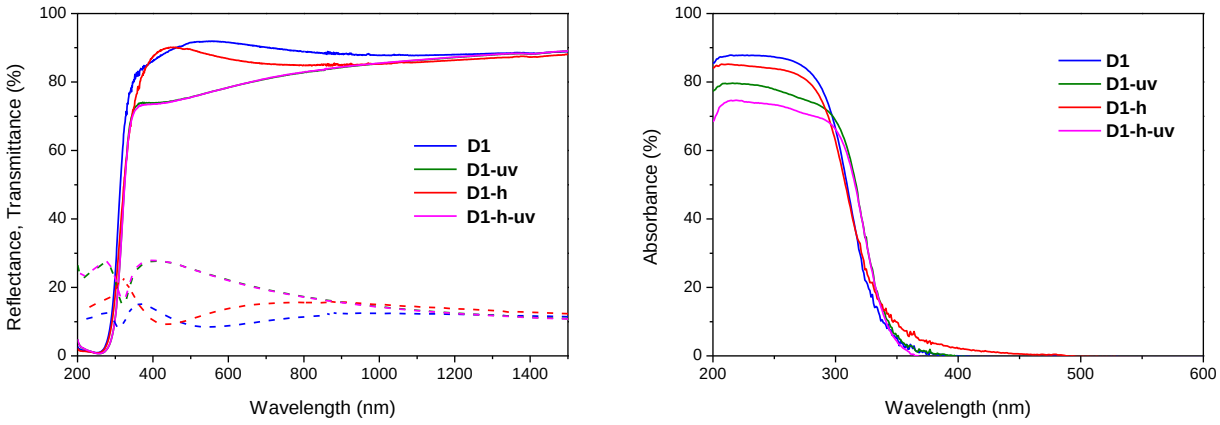

Figure 6.11*. Transmittance (solid line), reflectance (dashed line) and absorbance UV/vis/NIR spectra of four TiO_2-dea hybrid films, dried at 80 °C (D1), heated at 150 °C for 1 h (D1-h), and the same samples after UV irradiation for 30 min (D1-uv and D1-h-uv).*

In general, the amorphous hybrid gels investigated present a high transparency in the visible and NIR range, independently on the organic ligand, and show limited variations in the optical behaviour with their structural properties, treatment temperature and UV irradiation.

6.3. Electrical properties

A suitable electrical conduction is one of the pivotal properties of a semiconductor, especially in photovoltaic devices. The electrical resistivity was measured in longitudinal geometry, by means of two silver contacts drawn on the film's surface. The samples normally showed ohmic behaviour, with direct proportionality between the applied voltage and the measured current. A selection of electrical resistivity data on different kinds of films are listed in Table 6.2, along with the thickness values, because of the strong correlation observed between the two parameters. The electrical resistivities measured vary widely and result comparable with those reported in literature for amorphous and in some cases crystalline TiO_2 films (10^6 – 10^8 Ω cm) [194,197,198].

With respect to the reference TiO_2 (SGT), most amorphous films present a relatively higher resistivity, although some T-acac samples show values in the same range. When films with similar composition but different thickness were compared, an inverse proportionality between the resistivity and thickness was always recorded. This is a common characteristic of very thin films, where the surface electrical conduction is more relevant than in thicker layers with regard to the bulk conduction.

Table 6.2. *Thickness and electrical resistivity measured for representative amorphous TiO_2 films, before and after a UV irradiation treatment (15 or 30 min). The values are the average of more measurements on the same sample and often on more analogous samples.*

Sample	**Thickness** (nm)	**ρ** (Ω cm)	**Thickness** (nm) **after UV**	**ρ** (Ω cm) **after UV**
SGT(2)	42	$3\ 10^6$	42	$4\ 10^5$
A05-H	40	$7\ 10^7$	40	$5\ 10^5$
A05'-H	65	$4\ 10^6$	64	$2\ 10^5$
SGT+A05	71	$8\ 10^5$	70	$1\ 10^5$
B02	142	-	110	$5\ 10^6$
D1	120	-	47	$1\ 10^5$
D1-H	108	$2\ 10^8$	46	$1\ 10^5$
C1	320	$1\ 10^7$	57	$1\ 10^6$
C1-H	290	$5\ 10^7$	56	$2\ 10^6$

Beyond a defined thickness threshold, the resistivity should return to behave as an intensive property. In this work the dependence was found to be kept at least up to 150 – 200 nm. It affected also crystalline films, which are supposed to exhibit better conductivity than amorphous counterparts. The thinnest films (below 20 – 30 nm) annealed at 400 °C, despite being partially crystallized did not show ohmic behaviour, so a reliable resistivity value was impossible to obtain. On the other hand, some films prepared with acac and thicker than 100 nm gave excellent resistivity in the order of 10^4 Ω cm, with some further increase after annealing.

An interesting observation came from the comparison of films dried at 80 °C and those subsequently heated at 150 °C for 1 h. According to the common conception, even a mild thermal treatment at that temperature should increase the density and compactness of the oxide framework, and, in the case of solution processed coatings, remove residual solvent, with a positive influence on electrical conductivity. Nevertheless, in most studied samples the inverse trend was detected. This is in agreement with the report of Deng et al., who measured resistivities in the range of 10^6 – 10^7 Ω cm, growing with the heating temperature, in amorphous TiO_2 films prepared by a simple sol-gel procedure, similar to the SGT films studied here [194]. They affirmed that the substoichiometric composition, i.e. oxygen defectivity, favours the electrical conduction in the low-temperature processed films, and that the relatively high resistivity did not hamper the efficiency of the perovskite cells.

The UV irradiation treatment revealed a dramatic influence also on the electrical properties, causing in all cases an outstanding decrease of resistivity, from one to three orders of magnitude. A similar effect was observed in sol-gel TiO_2 films by some authors and correlated again an increase of n-type conductivity to the formation of lattice or electronic defects, like oxygen vacancies or interstitial Ti^{4+} ions [195]. In the hybrid films the removal of excess organics, achieving a denser and more ordered structure, probably contributes to reduce the resistance to electron conduction, together with the induced defects.

Another option was tested with the purpose to enhance the performances: a double-layer film, with bare TiO_2 on the bottom and hybrid layer on the top. In this way, only the side closer to the surface is functionalized, while the foundations could gain better stability and conductivity. The first preliminary results on bilayer samples "SGT+A05" showed reduced resistivity compared to the single components. As usual, the thickness of both layers can be tuned varying the precursor concentration and the spinning rate. This may prove as a simple but effective way to improve the applicability of the hybrid sol-gel route to the functionalization of surfaces with organic complexes.

The project that encompasses this activity is expected to advance towards the realization and testing of perovskite cell prototypes based on different kinds of TiO_2 films examined. However, the remarks and findings presented may turn useful for various possible applications of hybrid thin films.

CONCLUSIONS

This dissertation presents the research activity carried out during a three years PhD program in Industrial Product and Process Engineering at the University of Naples Federico II. The subject was the design, synthesis and characterization of a series of hybrid inorganic-organic TiO_2-based materials, with the aim to introduce enhanced optical, electronic, photoresponsive and catalytic properties with respect to pure TiO_2.

A hydrolytic sol-gel route has been proposed for the synthesis of TiO_2 with small organic compounds linked to the oxide matrix through coordination bonds with titanium. The procedure, performed at room temperature, is simple, generally fast and avoids the use of hazardous or expensive reagents and solvents, therefore it can be considered as a green synthetic route. A variety of organic complexing ligands was employed: diketones (acetylacetone and dibenzoylmethane), carboxylic acids (citric and acetic acid), enediols (catechol, dopamine, ascorbic acid). Each ligand induces a different behaviour of the system in the sol-gel processing. A careful exploration and optimization of the process variables, such as the concentration of the reagents, the nature of the solvent and the solution pH, has allowed to yield for each composition homogeneous chemical gels, physical or particulate gels or stable sols. The latter are useful for the deposition of thin gel films. The products were characterized by strong complexation binding between Ti atoms and the organic components, distributed throughout the bulk.

The amorphous samples prepared were characterized by several complementary techniques, to obtain a complete view of their chemical and electronic structure, optical and photoelectrochemical behaviour and catalytic activity. The organic molecules employed form ligand-to-metal charge transfer complexes, with a varying degree of electronic coupling with TiO_2, as observed by the coloration of the xerogels (from yellow to dark red) and confirmed by UV-visible and EPR spectroscopy. The consequent properties depend on the type of ligand. All the materials exhibit optical absorption and the generation of photocurrents in the visible light range, more widely shifted in the case of catechol, dopamine and ascorbate ligands. Preliminary data on the photoxidation of model compounds indicate a detectable photocatalytic activity under visible light. A comparable behaviour was reported in

literature for crystalline TiO_2 nanomaterials with surface adsorbed catechol, ascorbate and derivatives, but no reports have dealt with amorphous bulk gels. An effective photosensitization was demonstrated also in this kind of materials, offering some advantages over the surface modified nanoparticles, such as a high control on the composition, a homogeneous mixing of the organic and inorganic components, a good stability and the macroscopic particle size, more compatible with practical catalytic applications.

Some samples, in particular TiO_2-acetylacetonate xerogels, were subjected to thermal treatments at 400 °C to obtain nanocrystalline anatase TiO_2, removing the organic component. The materials resulted grey to black in colour, for the presence of structural defects such as oxygen vacancies or reduced Ti^{3+} sites, as shown by XPS and EPR spectra, with a possible contribution by residual carbon. They show a surprising activity in the photoreforming of glycerol, with remarkable hydrogen production without the use of a metal co-catalyst. The wide visible light absorption of these samples seem to bring about a moderate visible light activation for the same reaction. An innovative spectroelectrochemical method was employed to investigate the electronic structure of some of the annealed samples and of the parent TiO_2-acetylacetonate, observing an apparent shift of the conduction band edge to lower potentials than in common anatase and the presence of electronic states within the band gap.

The most important and innovative result of this work regards the generation and stabilization for long times (several months) of superoxide radical anions on the surface of the hybrid materials containing β-diketonate and carboxylate ligands. This is observed after mere contact with air of the dried gels, without any pretreatment. The hypothesis on the mechanisms of this very peculiar phenomenon is the partially delocalized charge transfer from the HOMO of the ligand to the oxide conduction band, providing electrons available for the reduction of adsorbed molecular oxygen. Switching from acetylacetone or acetic acid to dibenzoylmethane or citric acid, ligands with a higher charge delocalization, allows to increase the density of adsorbed radicals of one or two orders of magnitude. EPR spectroscopy also reveals that these materials produce hydroxyl radicals in water, without the need for photoexcitation.

A consequence of the generation of reactive oxygen species (ROS) by the materials is a remarkable activity in the oxidative degradation of different recalcitrant organic pollutants, like phenanthrene, 2,4-dichlorophenol and its derivatives, in the dark. The reactions occur by ROS-mediated mechanisms which can eventually lead to the mineralization of the aqueous contaminants. A relevant finding is that the adsorbed superoxide layer can be restored on the surface of the materials after a long storage, by simple contact with air, possibly favoured by washing in water.

Some of the hybrid materials were prepared also as thin films, by spin coating of stabilized sols. Amorphous and crystalline films with different composition and thickness were studied. In general light transmission and absorption appeared less affected by the presence of organic complexes than in bulk gels. The electrical conductivity of the hybrid films was variable, depending on the organic ligand. A negative trend of conductivity was recorded annealing the films at 150 °C with respect to the low temperature dried ones. A UV irradiation of about 15 min induces the decomposition of most organic ligands, with marked changes of the film properties. Acetylacetone results to give the more resistant complex under irradiation. In all cases, a noticeable increase of conductivity followed the UV treatment. This experimental activity will support the evaluation of the performances of suitable amorphous films, prepared by a simple solution method at low temperature, as electron transport layers for perovskite solar cells, in the continuance of the project in collaboration with the ENEA Research Centre.

The principal outcomes of the present research activity can be summarized as follows.

- A simple and versatile hydrolytic sol-gel route has been designed and optimized to prepare hybrid TiO_2 materials with complexing organic compounds in the form of xerogels, particulates or sols.
- The structural, physicochemical and photoresponsive properties of bulk and thin films hybrids were shown to vary widely depending on the different organic components.
- The photosensitization by direct ligand-to-metal charge transfer, a relatively less studied mechanism of visible light activation of TiO_2, has been verified in the hybrid amorphous gels.
- The appearance of structural defects, mainly oxygen vacancies and/or Ti^{3+} sites, was induced by the removal of acetylacetonate ligand from the relative hybrid gel during a simple annealing, and caused interesting performances in hydrogen production under UV light.
- A long term stabilization of adsorbed superoxide radicals on the surface of some classes of hybrid TiO_2 samples was discovered for the first time and investigated in detail, along with the consequent oxidative catalytic activity of the materials in the dark.

It can be expected that these promising innovative results will stimulate vast future research, since there are several aspects which deserve deeper insight and understanding, from both a fundamental and especially an applicative viewpoint.

The flexible bottom-up approach proposed can be certainly extended to the synthesis of other TiO_2-based hybrid materials, in the form of xerogels, nanoparticles or films, and possibly also monoliths and aerogels.

The possible developments of the presented materials should take into account some aspects. The stability of the hybrid materials in the reaction environment, i.e. in water, with or without irradiation,

has been only partially assessed. Since this is often a limitation in such systems, due to the possible leaching of the organic molecules, in view of multiple recycling or long operative time the stability should be carefully checked. Under UV irradiation in some of the samples self-degradation of the organic ligand seems to be activated, therefore their applications should be rather oriented to visible light processes. The data on the photocatalytic activity of the hybrid materials are only preliminary. There is much space for a better definition of their photoactivity and for the optimization of their structural and functional properties, adjusting for instance the synthesis conditions and the amount of complexing ligand. Moreover, obtaining crystallized hybrid materials by the adopted sol-gel procedure is challenging, but it may have a positive impact on their photoinduced features.

Some of the studied amorphous hybrids, in particular TiO_2-acetylacetonate, are multifunctional materials: they are able to generate stable ROS and catalytically oxidize organics in the dark, they show an independent visible light photoactivity, and can also be used as precursors for the preparation of highly defective anatase samples. The optimization of TiO_2-acetylacetonate and other hybrid materials with similar potential are therefore recommended.

The spontaneous stabilization of ROS like superoxide radicals on the surface of amorphous hybrid oxides owns a great potential. Their high efficiency, stability and recyclability in the oxidative degradation should be definitely verified and eventually improved, taking into account the promising data about the TiO_2-dibenzoylmethane and TiO_2-citrate hybrids. As a matter of fact, this "ROS-mediated dark degradation" may be regarded as a novel advantageous alternative to common advanced oxidation processes. Along with water purification, new applications of such systems can be envisaged where ROS are involved, for example in the abatement of organic compounds from air, where molecular oxygen, needed to form superoxide, is freely available, or in antimicrobial materials.

The gel-derived crystalline TiO_2 is also worth deeper investigation. Its UV photoactivity is really promising, especially for processes requiring strong reductive potential, and its visible light efficiency should be inspected. Moreover, the possibility of tuning the type and concentration of defects, varying the organic compound in the precursor gel or the heat treatment conditions, could affect the final catalytic performances.

Although most of the present work has focused on bulk samples, thin films offer a variety of uses related to the possibility to realise active TiO_2 coatings on different substrates. For instance, if the surface stabilization of superoxide radicals was confirmed also on analogous hybrid films, the production of self-cleaning and perhaps self-sterilizing coatings active even without illumination would be possible. The testing of the studied films as electron transport layers in solar cells is already in progress and will likely require efforts to improve their charge separation and transfer properties.

Hopefully, some of the mentioned considerations might inspire even wider research developments, for instance through the application of similar approaches to other metal oxides.

REFERENCES

[1] M. Cheng, G. Zeng, D. Huang, C. Lai, P. Xu, C. Zhang, Y. Liu, Hydroxyl radicals based advanced oxidation processes (AOPs) for remediation of soils contaminated with organic compounds: A review, *Chemical Engineering Journal* 284 (**2016**) 582–598.

[2] C. Comninellis, A. Kapalka, S. Malato, S.A. Parsons, J. Poulios, D. Mantzavinos, Advanced oxidation processes for water treatment: advances and trends for R&D, *Journal of Chemical Technology and Biotechnology* 83 (**2008**) 769–776.

[3] Z. Zhang, P.A. Maggard, Investigation of photocatalytically-active hydrated forms of amorphous titania, $TiO_2 \cdot nH_2O$, *Journal of Photochemistry and Photobiology A: Chemistry* 186 (**2007**) 8–13.

[4] D. Zywitzki, H. Jing, H. Tüysüz, C.K. Chan, High surface area, amorphous titania with reactive Ti^{3+} through a photo-assisted synthesis method for photocatalytic H_2 generation, *Journal of Materials Chemistry A* 5 (**2017**) 10957–10967.

[5] J. Seo, H. Lee, H.J. Lee, M.S. Kim, S.W. Hong, J. Lee, K. Cho, W. Choi, C. Lee, Visible light-photosensitized oxidation of organic pollutants using amorphous peroxo-titania, *Applied Catalysis B: Environmental* 225 (**2018**) 487–495.

[6] F. Sannino, D. Pirozzi, G. Vitiello, G. D'Errico, A. Aronne, E. Fanelli, P. Pernice, Oxidative degradation of phenanthrene in the absence of light irradiation by hybrid ZrO_2-acetylacetonate gel-derived catalyst, *Applied Catalysis B: Environmental* 156–157 (**2014**) 101–107.

[7] A.B. Muñoz-García, F. Sannino, G. Vitiello, D. Pirozzi, L. Minieri, A. Aronne, P. Pernice, M. Pavone, G. D'Errico, Origin and Electronic Features of Reactive Oxygen Species at Hybrid Zirconia-Acetylacetonate Interfaces, *ACS Applied Materials & Interfaces* 7 (**2015**) 21662–21667.

[8] F. Sannino, P. Pernice, L. Minieri, G.A. Camandona, A. Aronne, D. Pirozzi, Oxidative Degradation of Different Chlorinated Phenoxyalkanoic Acid Herbicides by a Hybrid ZrO_2 Gel-Derived Catalyst without Light Irradiation, *ACS Applied Materials & Interfaces* 7 (**2015**) 256–263.

[9] F. Sannino, P. Pernice, C. Imparato, A. Aronne, G. D'Errico, L. Minieri, M. Perfetti, D. Pirozzi, Hybrid TiO_2-acetylacetonate amorphous gel-derived material with stably adsorbed superoxide radical active in oxidative degradation of organic pollutants, *RSC Advances* 5 (**2015**) 93831–93839.

[10] A. Aronne, M. Fantauzzi, C. Imparato, D. Atzei, L. De Stefano, G. D'Errico, F. Sannino, I. Rea, D. Pirozzi, B. Elsener, P. Pernice, A. Rossi, Electronic properties of TiO_2 -based materials characterized by high Ti^{3+} self-doping and low recombination rate of electron–hole pairs, *RSC Advances* 7 (**2017**) 2373–2381.

[11] O. Carp, C.L. Huisman, A. Reller, Photoinduced reactivity of titanium dioxide, *Progress in Solid State Chemistry* 32 (**2004**) 33–177.

[12] X. Chen, S.S. Mao, Titanium dioxide nanomaterials: Synthesis, properties, modifications and applications, *Chemical Reviews* 107 (**2007**) 2891–2959.

[13] S.G. Kumar, K.S.R.K. Rao, Polymorphic phase transition among the titania crystal structures using a solution-based approach: From precursor chemistry to nucleation process, *Nanoscale* 6 (**2014**) 11574–11632.

[14] K. Nakajima, R. Noma, M. Kitano, M. Hara, Titania as an Early Transition Metal Oxide with a High Density of Lewis Acid Sites Workable in Water, *The Journal of Physical Chemistry C* 117 (**2013**) 16028–16033.

[15] J. Schneider, M. Matsuoka, M. Takeuchi, J. Zhang, Y. Horiuchi, M. Anpo, D.W. Bahnemann, Understanding TiO_2 Photocatalysis: Mechanisms and Materials, *Chemical Reviews* 114 (**2014**) 9919–9986.

[16] A. Fujishima, X. Zhang, D.A. Tryk, TiO_2 photocatalysis and related surface phenomena, *Surface Science Reports* 63 (**2008**) 515–582.

[17] A. Fujishima, K. Honda, Electrochemical Photolysis of Water at a Semiconductor Electrode, *Nature* 238 (**1972**) 37–38.

[18] M. Buchalska, M. Kobielusz, A. Matuszek, M. Pacia, S. Wojtyła, W. Macyk, On Oxygen Activation at Rutile- and Anatase-TiO_2, *ACS Catalysis* 5 (**2015**) 7424–7431.

[19] D.O. Scanlon, C.W. Dunnill, J. Buckeridge, S.A. Shevlin, A.J. Logsdale, S.M. Woodley, C.R.A. Catlow, M.J. Powell, R.G. Palgrave, I.P. Parkin, G.W. Watson, T.W. Keal, P. Sherwood, A. Walsh, A.A. Sokol, Energy band alignment between anatase and rutile TiO_2, *Nature Materials* 12 (**2012**) 798-801.

[20] B. Ohtani, Y. Ogawa, S. Nishimoto, Photocatalytic Activity of Amorphous–Anatase Mixture of Titanium(IV) Oxide Particles Suspended in Aqueous Solutions, *Journal of Physical Chemistry B* 101 (**1997**) 3746–3752.

[21] M. Carrus, M. Fantauzzi, F. Riboni, M. Makosch, A. Rossi, E. Selli, J. van Bokhoven, Increased conversion and selectivity of 4-nitrostyrene hydrogenation to 4-aminostyrene on Pt nanoparticles supported on titanium-tungsten mixed oxides, *Applied Catalysis A: General* 519 (**2016**) 130–138.

[22] C. Fan, C. Chen, J. Wang, X. Fu, Z. Ren, G. Qian, Z. Wang, Black Hydroxylated Titanium Dioxide Prepared via Ultrasonication with Enhanced Photocatalytic Activity, *Scientific Reports* 5 (**2015**) 11712.

[23] C. Sanchez, B. Julián, P. Belleville, M. Popall, Applications of hybrid organic-inorganic nanocomposites, *Journal of Materials Chemistry* 15 (**2005**) 3559–3592.

[24] C. Sanchez, F. Ribot, B. Lebeau, Molecular design of hybrid organic–inorganic nanocomposites synthesized, *Journal of Materials Chemistry* 9 (**1999**) 35–44.

[25] D. Pirozzi, E. Fanelli, A. Aronne, P. Pernice, A. Mingione, Lipase entrapment in a zirconia matrix: Sol-gel synthesis and catalytic properties, *Journal of Molecular Catalysis B: Enzymatic* 59 (**2009**) 116–120.

[26] J. Sedõ, J. Saiz-Poseu, F. Busqué, D. Ruiz-Molina, Catechol-based biomimetic functional materials, *Advanced Materials* 25 (**2013**) 653–701.

[27] R. Andreozzi, V. Caprio, A. Insola, R. Marotta, Advanced oxidation processes (AOP) for water purification and recovery, *Catalysis Today* 53 (**1999**) 51–59.

[28] K. Krumova, G. Cosa, Overview of Reactive Oxygen Species, in: Singlet Oxyg. Appl. Biosci. Nanosci., Royal Society of Chemistry, 2016: pp. 3–21.

[29] M. Hayyan, M.A. Hashim, I.M. Alnashef, Superoxide Ion: Generation and Chemical Implications, *Chemical Reviews* 116 (**2016**) 3029–3085.

[30] M. Anpo, M. Che, B. Fubini, E. Garrone, Generation of Superoxide Ions at Oxide Surfaces, *Topics in Catalysis* 8 (**1999**) 189–198.

[31] A.L. Attwood, D.M. Murphy, J.L. Edwards, T.A. Egerton, R.W. Harrison, An EPR study of thermally and photochemically generated oxygen radicals on hydrated and dehydrated titania surfaces, *Research on Chemical Intermediates* 29 (**2003**) 449–465.

[32] E. Carter, A.F. Carley, D.M. Murphy, Evidence for O_2^- radical stabilization at surface oxygen vacancies on polycrystalline TiO_2, *The Journal of Physical Chemistry C* 111 (**2007**) 10630–10638.

[33] C.E. Diaz-Uribe, M.C. Daza, F. Martínez, E.A. Páez-Mozo, C.L.B. Guedes, E. Di Mauro, Visible light superoxide radical anion generation by tetra(4-carboxyphenyl) porphyrin/TiO_2: EPR characterization, *Journal of Photochemistry and Photobiology A: Chemistry* 215 (**2010**) 172–178.

[34] J. Yu, J. Chen, C. Li, X. Wang, B. Zhang, H. Ding, ESR Signal of Superoxide Radical Anion Adsorbed on TiO_2 Generated at Room Temperature, *The Journal of Physical Chemistry B* 108 (**2004**) 2781–2783.

[35] T.A. Konovalova, J. Lawrence, L.D. Kispert, Generation of superoxide anion and most likely singlet oxygen in irradiated TiO_2 nanoparticles modified by carotenoids, *Journal of Photochemistry and Photobiology A: Chemistry* 162 (**2004**) 1–8.

[36] A.F. Bedilo, M. a Plotnikov, N. V Mezentseva, A.M. Volodin, G.M. Zhidomirov, I.M. Rybkin, K.J. Klabunde, Superoxide radical anions on the surface of zirconia and sulfated zirconia: formation mechanisms, properties and structure, *Physical Chemistry Chemical Physics: PCCP* 7 (**2005**) 3059–3069.

[37] K. Sobańska, P. Pietrzyk, Z. Sojka, Generation of Reactive Oxygen Species via Electroprotic Interaction of H_2O_2 with ZrO_2 Gel: Ionic Sponge Effect and pH-Switchable Peroxidase- and Catalase-Like Activity, *ACS Catalysis* 7 (**2017**) 2935–2947.

[38] M. Pelaez, N.T. Nolan, S.C. Pillai, M.K. Seery, P. Falaras, A.G. Kontos, P.S.M. Dunlop, J.W.J. Hamilton, J.A. Byrne, K. O'Shea, M.H. Entezari, D.D. Dionysiou, A review on the visible light active titanium dioxide photocatalysts for environmental applications, *Applied Catalysis B: Environmental* 125 (**2012**) 331–349.

[39] V. Etacheri, C. Di Valentin, J. Schneider, D. Bahnemann, S.C. Pillai, Visible-light activation of TiO_2 photocatalysts: Advances in theory and experiments, *Journal of Photochemistry and Photobiology C: Photochemistry Reviews* 25 (**2015**) 1–29.

[40] B. Ohtani, Titania Photocatalysis beyond Recombination: A Critical Review, *Catalysts* 3 (**2013**) 942–953.

[41] M.D. Hernández-Alonso, F. Fresno, S. Suárez, J.M. Coronado, Development of alternative photocatalysts to TiO_2: Challenges and opportunities, *Energy and Environmental Science* 2 (**2009**) 1231–1257.

[42] U.I. Gaya, A.H. Abdullah, Heterogeneous photocatalytic degradation of organic contaminants over titanium dioxide: A review of fundamentals, progress and problems, *Journal of Photochemistry and Photobiology C: Photochemistry Reviews* 9 (**2008**) 1–12.

[43] U.G. Akpan, B.H. Hameed, Parameters affecting the photocatalytic degradation of dyes using TiO_2-based photocatalysts: A review, *Journal of Hazardous Materials* 170 (**2009**) 520–529.

[44] X. Zhang, T. Peng, S. Song, Recent advances in dye-sensitized semiconductor systems for photocatalytic hydrogen production, *Journal of Materials Chemistry A* 4 (**2016**) 2365–2402.

[45] S.G. Kumar, L.G. Devi, Review on modified TiO_2 photocatalysis under UV/visible light: Selected results and related mechanisms on interfacial charge carrier transfer dynamics, *Journal of Physical Chemistry A* 115 (**2011**) 13211–13241.

[46] W. Macyk, K. Szaciłowski, G. Stochel, M. Buchalska, J. Kuncewicz, P. Łabuz, Titanium(IV) complexes as direct TiO_2 photosensitizers, *Coordination Chemistry Reviews* 254 (**2010**) 2687–2701.

[47] G. Zhang, G. Kim, W. Choi, Visible light driven photocatalysis mediated via ligand-to-metal charge transfer (LMCT): an alternative approach to solar activation of titania, *Energy & Environmental Science* 7 (**2014**) 954–966.

[48] H. Dong, G. Zeng, L. Tang, C. Fan, C. Zhang, X. He, Y. He, An overview on limitations of TiO_2-based particles for photocatalytic degradation of organic pollutants and the corresponding countermeasures, *Water Research* 79 (**2015**) 128–146. .

[49] X. Pan, M.-Q. Yang, X. Fu, N. Zhang, Y.-J. Xu, Defective TiO_2 with oxygen vacancies: synthesis, properties and photocatalytic applications, *Nanoscale* 5 (**2013**) 3601.

[50] X. Chen, L. Liu, F. Huang, Black titanium dioxide (TiO_2) nanomaterials., *Chemical Society Reviews* 44 (**2015**) 1861–1885.

[51] X. Liu, G. Zhu, X. Wang, X. Yuan, T. Lin, F. Huang, Progress in Black Titania: A New Material for Advanced Photocatalysis, *Advanced Energy Materials* 6 (**2016**) 1–29.

[52] X. Chen, L. Liu, P.Y. Yu, S.S. Mao, Increasing solar absorption for photocatalysis with black hydrogenated titanium dioxide nanocrystals, *Science* 331 (**2011**) 746–750.

[53] S.G. Ullattil, S.B. Narendranath, S.C. Pillai, P. Periyat, Black TiO_2 Nanomaterials: A Review of Recent Advances, *Chemical Engineering Journal* 343 (**2018**) 708–736.

[54] C.J. Brinker, G.W. Scherer, Sol-Gel Science: The Physics and Chemistry of Sol-Gel Processing, Academic Press, Boston, 1990.

[55] A.E. Danks, S.R. Hall, Z. Schnepp, The evolution of 'sol–gel' chemistry as a technique for materials synthesis, *Materials Horizons* 3 (**2016**) 91–112.

[56] S.G. Ulattil, P. Periyat, Sol-Gel Synthesis of Titanium Dioxide, in: S.C. Pillai, S. Hehir (Eds.), Adv. Sol-Gel Deriv. Mater. Technol., Springer, 2017: pp. 271–283.

[57] J. Livage, M. Henry, C. Sanchez, Sol-gel chemistry of transition metal oxides, *Progress in Solid State Chemistry* 18 (**1988**) 259–341.

[58] A. Leaustic, F. Babonneau, J. Livage, Structural investigation of the hydrolysis-condensation process of titanium alkoxides $Ti(OR)_4$ (OR = OPr-iso, OEt) modified by acetylacetone. 1. Study of the alkoxide modification, *Chemistry of Materials* 1 (**1989**) 240–247.

[59] S. Doeuff, M. Henry, C. Sanchez, J. Livage, Hydrolysis of titanium alkoxides: Modification of the molecular precursor by acetic acid, *Journal of Non-Crystalline Solids* 89 (**1987**) 206–216.

[60] U. Schubert, Chemical modification of titanium alkoxides for sol–gel processing, *Journal of Materials Chemistry* 15 (**2005**) 3701.

[61] V.G. Kessler, G.I. Spijksma, G.A. Seisenbaeva, S. Håkansson, D.H.A. Blank, H.J.M. Bouwmeester, New

insight in the role of modifying ligands in the sol-gel processing of metal alkoxide precursors: A possibility to approach new classes of materials, *Journal of Sol-Gel Science and Technology* 40 (**2006**) 163–179.

[62] V.G. Kessler, The chemistry behind the sol-gel synthesis of complex oxide nanoparticles for bio-imaging applications, *Journal of Sol-Gel Science and Technology* 51 (**2009**) 264–271.

[63] N.D. Yordanov, V. Gancheva, V.A. Pelova, Studies on some materials suitable for use as internal standards in high energy EPR dosimetry, *Journal of Radioanalytical and Nuclear Chemistry* 240 (**1999**) 619–622.

[64] E. Świętek, K. Pilarczyk, J. Derdzińska, K. Szaciłowski, W. Macyk, Redox characterization of semiconductors based on electrochemical measurements combined with UV-Vis diffuse reflectance spectroscopy, *Physical Chemistry Chemical Physics* 15 (**2013**) 14256.

[65] M. Kobielusz, K. Pilarczyk, E. Świętek, K. Szaciłowski, W. Macyk, Spectroelectrochemical analysis of TiO_2 electronic states – Implications for the photocatalytic activity of anatase and rutile, *Catalysis Today* 309 (**2018**) 35–42.

[66] V. Vaiano, M.A. Lara, G. Iervolino, M. Matarangolo, J.A. Navio, M.C. Hidalgo, Photocatalytic H_2 production from glycerol aqueous solutions over fluorinated Pt-TiO_2 with high {001} facet exposure, *Journal of Photochemistry and Photobiology A: Chemistry* 365 (**2018**) 52–59.

[67] Q. Ye, F. Zhou, W. Liu, Bioinspired catecholic chemistry for surface modification, *Chemical Society Reviews* 40 (**2011**) 4244–4258.

[68] T. Rajh, L.X. Chen, K. Lukas, T. Liu, M.C. Thurnauer, D.M. Tiede, Surface Restructuring of Nanoparticles: An Efficient Route for Ligand - Metal Oxide Crosstalk, *Journal of Physical Chemistry B* 106 (**2002**) 10543–10552.

[69] I.A. Janković, Z. V. Šaponjić, E.S. Džunuzović, J.M. Nedeljković, New Hybrid Properties of TiO_2 Nanoparticles Surface Modified With Catecholate Type Ligands, *Nanoscale Research Letters* 5 (**2010**) 81–88.

[70] A. Ponton, S. Barboux-Doeuff, C. Sanchez, Physico-chemical control of sol-gel transition of titanium alkoxide-based materials studied by rheology, *Journal of Non-Crystalline Solids* 351 (**2005**) 45–53.

[71] M.M. Haridas, S. Datta, J.R. Bellare, Time and temperature based gellability zones in modified titanium alkoxide sols, *Ceramics International* 25 (**1999**) 601–606.

[72] S. Varaganti, G. Ramakrishna, Dynamics of Interfacial Charge Transfer Emission in Small-molecule Sensitized TiO_2 Nanoparticles: Is it Localized or Delocalized?, *Journal of Physical Chemistry C* 114 (**2010**) 13917–13925.

[73] A. Sadeghzadeh Attar, M. Sasani Ghamsari, F. Hajiesmaeilbaigi, S. Mirdamadi, K. Katagiri, K. Koumoto, Study on the effects of complex ligands in the synthesis of TiO_2 nanorod arrays using the sol-gel template method, *Journal of Physics D: Applied Physics* 41 (**2008**).

[74] L.F. Cueto, E. Sánchez, L.M. Torres-Martínez, G.A. Hirata, On the optical, structural, and morphological properties of ZrO_2 and TiO_2 dip-coated thin films supported on glass substrates, *Materials Characterization* 55 (**2005**) 263–271.

[75] A. Aronne, F. Sannino, S.R. Bonavolontà, E. Fanelli, A. Mingione, P. Pernice, R. Spaccini, D. Pirozzi, Use of a new hybrid sol-gel zirconia matrix in the removal of the herbicide MCPA: A sorption/degradation process, *Environmental Science and Technology* 46 (**2012**) 1755–1763.

[76] C. Imparato, A. Aronne, L. Minieri, G. D'Errico, D. Pirozzi, F. Sannino, P. Pernice, Sol–Gel Synthesis and Characterization of Hybrid TiO_2-Acetylacetonate Materials, *Advanced Science Letters* 23 (**2017**) 5912–5915.

[77] A. Ponton, S. Barboux-Doeuff, C. Sanchez, Rheology of titanium oxide based gels: Determination of gelation time versus temperature, *Colloids and Surfaces A: Physicochemical and Engineering Aspects* 162 (**2000**) 177–192.

[78] F. Tayyari, J.S. Emampour, M. Vakili, A.R. Nekoei, H. Eshghi, S. Salemi, M. Hassanpour, Vibrational assignment and structure of benzoylacetone, *Journal of Molecular Structure* 794 (**2006**) 202–214.

[79] A.R. Nekoei, M. Vakili, M. Hakimi-Tabar, S.F. Tayyari, R. Afzali, H.G. Kjaergaard, Theoretical study, and infrared and Raman spectra of copper(II) chelated complex with dibenzoylmethane, *Spectrochimica Acta - Part A: Molecular and Biomolecular Spectroscopy* 128 (**2014**) 272–279.

[80] N. Tohge, R. Ueno, F. Chiba, K. Kintaka, J. Nishii, Characteristics of diffraction gratings fabricated by the two-beam interference method using photosensitive hybrid gel films, *Journal of Sol-Gel Science and Technology* 19 (**2000**) 119–123.

[81] H. Segawa, S. Adachi, Y. Arai, K. Yoshida, Fine patterning of hybrid titania films by ultraviolet irradiation, *Journal of the American Ceramic Society* 86 (**2003**) 761–764.

[82] H. Segawa, S. Inque, K. Watanabe, R. Ohashi, H. Nitani, M. Nomura, A study of photoreactions in photosensitive TiO_2 hybrid gel films induced by UV irradiation, *Journal of the Ceramic Society of Japan* 123 (**2015**) 793–799.

[83] Y.S. K. Tanitsu, M. Nakayama, Process for formation of metal oxide film, Patent 4960618A, 1987.

[84] O.P. H. Kim, R. D. Miller, Methods of forming metal oxide nanostructures, and nanostructures thereof, Patent 8771632B2, 2009.

[85] D. Kundu, D. Ganguli, Monolithic zirconia gels from metal-organic solutions, *Journal of Materials Science Letters* 5 (**1986**) 293–295.

[86] I.A. Mudunkotuwa, V.H. Grassian, Citric Acid Adsorption on TiO_2 Nanoparticles in Aqueous Suspensions at Acidic and Circumneutral pH: Surface Coverage, Surface Speciation, and its Impact on Nanoparticle - Nanoparticle Interactions, *Journal of American Chemical Society* 132 (**2010**) 14986–14994.

[87] S.R. Dhage, R. Pasricha, V. Ravi, Synthesis of ultrafine TiO_2 by citrate gel method, *Materials Research Bulletin* 38 (**2003**) 1623–1628.

[88] G. Liu, Y. Liu, G. Yang, S. Li, Y. Zu, W. Zhang, M. Jia, Preparation of Titania - Silica Mixed Oxides by a Sol-Gel Route in the Presence of Citric Acid, *The Journal of Physical Chemistry C* 113 (**2009**) 9345–9351.

[89] Z. Guo, C. Li, S. Lu, Y. Pan, H. Gu, Citrate/F^- assisted phase control synthesis of TiO_2 nanostructures and their photocatalytic properties, *RSC Advances* 5 (**2015**) 74230–74237.

[90] T. Kemmitt, N.I. Al-Salim, G.J. Gainsford, A. Bubendorfer, M. Waterland, Unprecedented oxo-titanium citrate complex precipitated from aqueous citrate solutions, exhibiting a novel bilayered Ti_8O_{10} structural core, *Inorganic Chemistry* 43 (**2004**) 6300–6306.

[91] M. Marszewski, J. Marszewska, S. Pylypenko, M. Jaroniec, Synthesis of Porous Crystalline Doped Titania Photocatalysts Using Modified Precursor Strategy, *Chemistry of Materials* 28 (**2016**) 7878–7888.

[92] M.P. Pechini, Method of preparing lead and alkaline earth titanates and niobates and coating method

using the same to form a capacitor, Patent 3330697A, 1967.

[93] J.M. Collins, R. Uppal, C.D. Incarvito, A.M. Valentine, Titanium(IV) citrate speciation and structure under environmentally and biologically relevant conditions, *Inorganic Chemistry* 44 (**2005**) 3431–3440.

[94] N. Wang, L. Zhu, K. Deng, Y. She, Y. Yu, H. Tang, Visible light photocatalytic reduction of Cr(VI) on TiO_2 in situ modified with small molecular weight organic acids, *Applied Catalysis B: Environmental* 95 (**2010**) 400–407.

[95] C. Legrand-Buscema, C. Malibert, S. Bach, Elaboration and characterization of thin films of TiO_2 prepared by sol-gel process, *Thin Solid Films* 418 (**2002**) 79–84.

[96] Y. Djaoued, S. Badilescu, P.. Ashrit, D. Bersani, P.P. Lottici, J. Robichaud, Study of Anatase to Rutile Phase Transition in Nanocrystalline Titania Films, *Journal of Sol-Gel Science and Technology* 24 (**2002**) 255–264.

[97] A. Verma, S.B. Samanta, A.K. Bakhshi, S.A. Agnihotry, Effect of stabilizer on structural, optical and electrochemical properties of sol-gel derived spin coated TiO_2 films, *Solar Energy Materials and Solar Cells* 88 (**2005**) 47–64.

[98] H. Choi, E. Stathatos, D.D. Dionysiou, Sol-gel preparation of mesoporous photocatalytic TiO_2 films and TiO_2/Al_2O_3 composite membranes for environmental applications, *Applied Catalysis B: Environmental* 63 (**2006**) 60–67.

[99] A.L. Anderson, R. Binions, The effect of Brij surfactants in sol-gel processing for the production of TiO_2 thin films, *Polyhedron* 85 (**2015**) 83–92.

[100] C. Suresh, V. Biju, P. Mukundan, K.G.K. Warrier, Anatase to rutile transformation in sol-gel titania by modification of precursor, *Polyhedron* 17 (**1998**) 3131–3135.

[101] C.G. Pierpont, C.W. Lange, The Chemistry of Transition Metal Complexes Containing Catechol and Semiquinone Ligands, *Progress in Inorganic Chemistry* 41 (**2007**) 331-442.

[102] J. Moser, S. Punchihewa, P.P. Infelta, M. Gratzel, Surface Complexation of Colloidal Semiconductors Strongly Enhances Interfacial Electron-Transfer Rates, *Langmuir: The ACS Journal of Surfaces and Colloids* 7 (**1991**) 3012–3018.

[103] Y.H. Wang, K. Hang, N.A. Anderson, T.Q. Lian, Comparison of electron transfer dynamics in molecule-to-nanoparticle and intramolecular charge transfer complexes, *Journal of Physical Chemistry B* 107 (**2003**) 9434–9440.

[104] C. Creutz, M.H. Chou, Binding of catechols to mononuclear titanium(IV) and to 1- and 5-nm TiO_2 nanoparticles, *Inorganic Chemistry* 47 (**2008**) 3509–3514.

[105] P.Z. Araujo, P.J. Morando, M.A. Blesa, Interaction of catechol and gallic acid Langmuir, with titanium dioxide in aqueous suspensions. 1. Equilibrium studies, *Langmuir* 21 (**2005**) 3470–3474.

[106] T. Lana-Villarreal, A. Rodes, J.M. Perez, R. Gomez, A spectroscopic and electrochemical approach to the study of the interactions and photoinduced electron transfer between catechol and anatase nanoparticles in aqueous solution, *Journal of the American Chemical Society* 127 (**2005**) 12601–12611.

[107] H. Gulley-Stahl, P.A. Hogan, W.L. Schmidt, S.J. Wall, A. Buhrlage, H.A. Bullen, Surface complexation of catechol to metal oxides: An ATR-FTIR, adsorption, and dissolution study, *Environmental Science and Technology*.44 (**2010**) 4116–4121.

[108] T.D. Savić, M.I. Čomor, J.M. Nedeljković, D.Ž. Veljković, S.D. Zarić, V.M. Rakić, I. a Janković, The effect of substituents on the surface modification of anatase nanoparticles with catecholate-type ligands: a combined DFT and experimental study, *Physical Chemistry Chemical Physics: PCCP* 16 (**2014**) 20796–805.

[109] Sreejith Kaniyankandy, S. Rawalekar, A. Sen, B. Ganguly, H.N. Ghosh, Does Bridging Geometry Influence Interfacial Electron Transfer Dynamics? Case of the Enediol-TiO_2 System, *Journal of Physical Chemistry C* 116 (**2012**) 98–103.

[110] R. Sadowski, M. Strus, M. Buchalska, P.B. Heczko, W. Macyk, Visible light induced photocatalytic inactivation of bacteria by modified titanium dioxide films on organic polymers, *Photochemical & Photobiological Sciences* 14 (**2015**) 514–519.

[111] K. Qi, F. Zasada, W. Piskorz, P. Indyka, J. Gryboś, M. Trochowski, M. Buchalska, M. Kobielusz, W. Macyk, Z. Sojka, Self-Sensitized Photocatalytic Degradation of Colorless Organic Pollutants Attached to Rutile Nanorods: Experimental and Theoretical DFT+D Studies, *Journal of Physical Chemistry C* 120 (**2016**) 5442–5456.

[112] P. Karthik, R. Vinoth, P. Selvam, E. Balaraman, M. Navaneethan, Y. Hayakawa, B. Neppolian, A visible-light active catechol–metal oxide carbonaceous polymeric material for enhanced photocatalytic activity, *Journal of Materials Chemistry A* 5 (**2017**) 384–396.

[113] D. Finkelstein-Shapiro, S.K. Davidowski, P.B. Lee, C. Guo, G.P. Holland, T. Rajh, K.A. Gray, J.L. Yarger, M. Calatayud, Direct Evidence of Chelated Geometry of Catechol on TiO_2 by a Combined Solid-State NMR and DFT Study, *Journal of Physical Chemistry C* 120 (**2016**) 23625–23630.

[114] H. Honda, K. Suzaki, Y. Sugahara, Control of hydrolysis and condensation reactions of titanium tert-butoxide by chemical modification with catechol, *Journal of Sol-Gel Science and Technology* 22 (**2001**) 133–138.

[115] K. Egawa, K. Suzaki, Y. Sugahara, Hydrolysis and condensation processes of titanium iso-propoxide modified with catechol: An NMR study, *Journal of Sol-Gel Science and Technology* 30 (**2004**) 83–88.

[116] A. Verma, M. Kar, D.P. Singh, Aging effect of diethanolamine derived precursor sol on TiO_2 films deposited at different annealing temperatures, *Journal of Sol-Gel Science and Technology* 54 (**2010**) 129–138.

[117] G. Valverde-Aguilar, G. Prado-Prone, P. Vergara-Aragón, J. Garcia-Macedo, P. Santiago, L. Rendón, Photoconductivity studies on nanoporous TiO_2/dopamine films prepared by sol-gel method, *Applied Physics A: Materials Science and Processing* 116 (**2014**) 1075–1084.

[118] M. Alzamani, A. Shokuhfar, E. Eghdam, S. Mastali, Influence of catalyst on structural and morphological properties of TiO_2 nanostructured films prepared by sol-gel on glass, *Progress in Natural Science: Materials International* 23 (**2013**) 77–84.

[119] R.A. Zangmeister, T.A. Morris, M.J. Tarlov, Characterization of polydopamine thin films deposited at short times by autoxidation of dopamine, *Langmuir* 29 (**2013**) 8619–8628.

[120] M. Vega-Arroyo, P.R. Lebreton, T. Rajh, P. Zapol, L.A. Curtiss, Density functional study of the TiO_2-dopamine complex, *Chemical Physics Letters* 406 (**2005**) 306–311.

[121] A.G. Thomas, K.L. Syres, Adsorption of organic molecules on rutile TiO_2 and anatase TiO_2 single crystal surfaces, *Chemical Society Reviews* 41 (**2012**) 4207–4217.

[122] C. Ronchi, D. Selli, W. Pipornpong, C. Di Valentin, Proton Transfers at a Dopamine-Functionalized TiO_2 Interface, *Journal of Physical Chemistry C* (**2018**) acs.jpcc.8b04921.

[123] N.M. Dimitrijevic, E. Rozhkova, T. Rajh, Dynamics of localized charges in dopamine-modified TiO_2 and their effect on the formation of reactive oxygen species., *Journal of the American Chemical Society* 131 (**2009**) 2893–2899.

[124] G.L. Wang, J.J. Xu, H.Y. Chen, Dopamine sensitized nanoporous TiO_2 film on electrodes: Photoelectrochemical sensing of NADH under visible irradiation, *Biosensors and Bioelectronics* 24 (**2009**) 2494–2498.

[125] S. Kim, G. hee Moon, G. Kim, U. Kang, H. Park, W. Choi, TiO_2 complexed with dopamine-derived polymers and the visible light photocatalytic activities for water pollutants, *Journal of Catalysis* 346 (**2017**) 92–100.

[126] I.M. Dugandžić, D.J. Jovanović, L.T. Mančić, O.B. Milošević, S.P. Ahrenkiel, Z. V. Šaponjić, J.M. Nedeljković, Ultrasonic spray pyrolysis of surface modified TiO_2 nanoparticles with dopamine, *Materials Chemistry and Physics* 143 (**2013**) 233–239.

[127] W.X. Mao, X.J. Lin, W. Zhang, Z.X. Chi, R.W. Lyu, A.M. Cao, L.J. Wan, Core-shell structured TiO_2@polydopamine for highly active visible-light photocatalysis, *Chemical Communications* 52 (**2016**) 7122–7125.

[128] G. Vitiello, A. Pezzella, V. Calcagno, B. Silvestri, L. Raiola, G. D'Errico, A. Costantini, F. Branda, G. Luciani, 5,6-Dihydroxyindole-2-carboxylic Acid-TiO_2 Charge Transfer Complexes in the Radical Polymerization of Melanogenic Precursor(s), *Journal of Physical Chemistry C* 120 (**2016**) 6262–6268.

[129] K.M. Buettner, J.M. Collins, A.M. Valentine, Titanium(IV) and vitamin C: Aqueous complexes of a bioactive form of Ti(IV), *Inorganic Chemistry* 51 (**2012**) 11030–11039.

[130] C. Kuiper, M.C.M. Vissers, Ascorbate as a Co-Factor for Fe- and 2-Oxoglutarate Dependent Dioxygenases: Physiological Activity in Tumor Growth and Progression, *Frontiers in Oncology* 4 (**2014**) 359.

[131] T. Rajh, J.M. Nedeljkovic, L.X. Chen, O. Poluektov, M.C. Thurnauer, Improving Optical and Charge Separation Properties of Nanocrystalline TiO_2 by Surface Modification with Vitamin C, *The Journal of Physical Chemistry B* 103 (**1999**) 3515–3519.

[132] A. Xagas, M.. Bernard, A. Hugot-Le Goff, N. Spyrellis, Z. Loizos, P. Falaras, Surface modification and photosensitisation of TiO_2 nanocrystalline films with ascorbic acid, *Journal of Photochemistry and Photobiology A: Chemistry* 132 (**2000**) 115–120.

[133] Y. Ou, J.D. Lin, H.M. Zou, D.W. Liao, Effects of surface modification of TiO_2 with ascorbic acid on photocatalytic decolorization of an azo dye reactions and mechanisms, *Journal of Molecular Catalysis A: Chemical* 241 (**2005**) 59–64.

[134] C. Yang, C. Gong, T. Peng, K. Deng, L. Zan, High photocatalytic degradation activity of the polyvinyl chloride (PVC)-vitamin C (VC)-TiO_2 nano-composite film, *Journal of Hazardous Materials* 178 (**2010**) 152–156.

[135] P. Labuz, R. Sadowski, G. Stochel, W. Macyk, Visible light photoactive titanium dioxide aqueous colloids and coatings, *Chemical Engineering Journal* 230 (**2013**) 188–194.

[136] M. Wajid Shah, Y. Zhu, X. Fan, J. Zhao, Y. Li, S. Asim, C. Wang, Facile Synthesis of Defective TiO_{2-x}

Nanocrystals with High Surface Area and Tailoring Bandgap for Visible-light Photocatalysis, *Scientific Reports* 5 (**2015**) 1–8.

[137] A.C. Ribeiro Neto, R.F. Pires, R.A. Malagoni, M.R. Franco, Solubility of vitamin C in water, ethanol, propan-1-ol, water + ethanol, and water + propan-1-ol at (298.15 and 308.15) K, *Journal of Chemical and Engineering Data* 55 (**2010**) 1718–1721.

[138] A. V. Vinogradov, V. V. Vinogradov, Low-temperature sol-gel synthesis of crystalline materials, *RSC Advances* 4 (**2014**) 45903–45919.

[139] S.-H. Nam, S.-J. Cho, C.-K. Jung, J.-H. Boo, J. Šícha, D. Heřman, J. Musil, J. Vlček, Comparison of hydrophilic properties of TiO_2 thin films prepared by sol–gel method and reactive magnetron sputtering system, *Thin Solid Films* 519 (**2011**) 6944–6950.

[140] X. Deng, G.C. Wilkes, A.Z. Chen, N.S. Prasad, M.C. Gupta, J.J. Choi, Room-Temperature Processing of TiO_x Electron Transporting Layer for Perovskite Solar Cells, *The Journal of Physical Chemistry Letters* 8 (**2017**) 3206–3210.

[141] B. Babiarczuk, A. Szczurek, A. Donesz-Sikorska, I. Rutkowska, J. Krzak, The influence of an acid catalyst on the morphology, wettabillity, adhesion and chemical structure properties of TiO_2 and ZrO_2 sol-gel thin films, *Surface and Coatings Technology* 285 (**2016**) 134–145.

[142] E. Blanco, J.M. González-Leal, M. Ramírez-del Solar, Photocatalytic TiO_2 sol-gel thin films: Optical and morphological characterization, *Solar Energy* 122 (**2015**) 11–23.

[143] G.I. Spijksma, D.H.A. Blank, H.J.M. Bouwmeester, V.G. Kessler, Modification of different zirconium propoxide precursors by diethanolamine. Is there a shelf stability issue for sol-gel applications?, *International Journal of Molecular Sciences* 10 (**2009**) 4977–4989.

[144] G. Yang, H. Tao, P. Qin, W. Ke, G. Fang, Recent Progress on Electron Transport Layer for Efficient Perovskite Solar Cells, *Journal of Materials Chemistry A* 4 (**2016**) 1–21.

[145] A. Huang, J. Zhu, J. Zheng, Y. Yu, Y. Liu, S. Yang, S. Bao, L. Lei, P. Jin, Room-temperature processible TiO2electron selective layers with controllable crystallinity for high efficiency perovskite photovoltaics, *Solar Energy Materials and Solar Cells* 163 (**2017**) 15–22.

[146] D. Yang, R. Yang, J. Zhang, Z. Yang, S. Liu, C. Li, High efficiency flexible perovskite solar cells using superior low temperature TiO_2, *Energy & Environmental Science* 8 (**2015**) 3208–3214.

[147] S. Girish Kumar, K.S.R.K. Rao, Polymorphic phase transition among the titania crystal structures using a solution-based approach: from precursor chemistry to nucleation process, *Nanoscale* 6 (**2014**) 11574–11632.

[148] N.T. Nolan, M.K. Seery, S.C. Pillai, Spectroscopic Investigation of the Anatase-to- Rutile Transformation of Sol-Gel Synthesised TiO_2 Photocatalysts, *Journal of Physical Chemistry C* 113 (**2009**) 16151–16157.

[149] J. Guilment, O. Poncelet, J. Rigola, S. Truchet, Spectroscopic Study of Halogenoalkoxides as Molecular Precursors of Metal Oxides, *Journal of Sol-Gel Science and Technology* 8 (**1997**) 299–304.

[150] S.F. Tayyari, H. Reissi, F. Milani-Nejad, I.S. Butler, Vibrational assignment of α-cyanoacetylacetone, *Vibrational Spectroscopy* 26 (**2001**) 187–199.

[151] A.K. Singh, B.P. Baranwal, Spectroscopic investigations of nano-sized titanium(IV) complexes containing electron-rich oxygen-based ligands, *Spectrochimica Acta - Part A: Molecular and Biomolecular*

Spectroscopy 98 (**2012**) 302–306.

[152] L. David, O. Cozar, V. Chis, C. Cra, C. Agut, D. Rusu, M. Rusu, Spectroscopic studies of some oxygen-bonded copper(II) b-diketonate complexes, *Journal of Molecular Structure* 564 (**2001**) 1–6.

[153] I. Diaz-Acosta, J. Baker, J.F. Hinton, P. Pulay, Calculated and experimental geometries and infrared spectra of metal tris-acetylacetonates: Vibrational spectroscopy as a probe of molecular structure for ionic complexes. Part II, *Spectrochimica Acta - Part A: Molecular and Biomolecular Spectroscopy* 59 (**2003**) 363–377.

[154] A. Dualeh, T. Moehl, N. Tétreault, J. Teuscher, P. Gao, M.K. Nazeeruddin, M. Grätzel, Impedance spectroscopic analysis of lead iodide perovskite-sensitized solid-state solar cells, *ACS Nano* 8 (**2014**) 362–373.

[155] M. Buchalska, P. Labuz, Ł. Bujak, G. Szewczyk, T. Sarna, S. Maćkowski, W. Macyk, New insight into singlet oxygen generation at surface modified nanocrystalline TiO_2 - the effect of near-infrared irradiation, *Dalton Transactions* 42 (**2013**) 9468–75.

[156] J. Méndez-Vivar, R. Mendoza-Serna, L. Valdez-Castro, Control of the polymerization process of multicomponent (Si, Ti, Zr) sols using chelating agents, *Journal of Non-Crystalline Solids* 288 (**2001**) 200–209.

[157] T.A. Egerton, N.J. Everall, J.A. Mattinson, L.M. Kessell, T.I. R, Interaction of TiO_2 nano-particles with organic UV absorbers, *Journal of Photochemistry and Photobiology A: Chemistry* 193 (**2008**) 10–17.

[158] F.X. Perrin, V. Nguyen, J.L. Vernet, FT-IR Spectroscopy of Acid-Modified Titanium Alkoxides: Investigations on the Nature of Carboxylate Coordination and Degree of Complexation, *Journal of Sol-Gel Science and Technology* 28 (**2003**) 205–215.

[159] K.B. Klepper, O. Nilsen, P. Hansen, H. Fjellvag, Atomic layer deposition of organic–inorganic hybrid materials based on saturated linear carboxylic acids, *Dalton Transactions* 40 (**2011**) 4636.

[160] S. Li, J. Wang, P. Jacobson, A. Selloni, U. Diebold, M.A.T. Article, X. Gong, Correlation between Bonding Geometry and Band Gap States at Organic - Inorganic Interfaces: Catechol on Rutile TiO (110), *Journal of the American Chemical Society* 2 (**2009**) 980–984.

[161] R. Rodriguez, M.A. Blesa, A.E. Regazzoni, Surface Complexation at the TiO_2 (anatase)/ Aqueous Solution Interface: Chemisorption of Catechol, *Journal of Colloid and Interface Science* 177 (**1996**) 122–131.

[162] S.-C. Li, Y. Losovyj, U. Diebold, Adsorption-Site-Dependent Electronic Structure of Catechol on the Anatase TiO_2 (101) Surface, *Langmuir* 27 (**2011**) 8600–8604.

[163] D. Gutiérrez-Tauste, X. Domènech, C. Domingo, J.A. Ayllón, Dopamine/TiO_2 hybrid thin films prepared by the liquid phase deposition method, *Thin Solid Films* 516 (**2008**) 3831–3835.

[164] W. Fang, M. Xing, J. Zhang, A new approach to prepare Ti^{3+} self-doped TiO_2 via $NaBH_4$ reduction and hydrochloric acid treatment, *Applied Catalysis B: Environmental* 160–161 (**2014**) 240–246.

[165] M. Berrettoni, M. Ciabocco, M. Fantauzzi, M. Giorgetti, A. Rossi, E. Caponetti, Physicochemical characterization of metal hexacyanometallate–TiO_2 composite materials, *RSC Advances* 5 (**2015**) 35435–35447.

[166] I. Georgieva, N. Danchova, S. Gutzov, N. Trendafilova, DFT modeling, UV-Vis and IR spectroscopic study of acetylacetone-modified zirconia sol-gel materials, *Journal of Molecular Modeling* 18 (**2012**) 2409–2422.

[167] Y. Liu, J.I. Dadap, D. Zimdars, K.B. Eisenthal, Study of Interfacial Charge-Transfer Complex on TiO_2 Particles in Aqueous Suspension by Second-Harmonic Generation, *The Journal of Physical Chemistry B* 103 (**1999**) 2480–2486.

[168] C. Creutz, B.S. Brunschwig, N. Sutin, Interfacial charge transfer absorption: Application to metal-molecule assemblies, *Chemical Physics* 324 (**2006**) 244–258.

[169] T. Berger, M. Sterrer, O. Diwald, E. Knozinger, D. Panayotov, T.L. Thompson, J.T. Yates, Light-induced charge separation in anatase TiO_2 particles, *Journal of Physical Chemistry B* 109 (**2005**) 6061–6068.

[170] Y. Li, U. Aschauer, J. Chen, A. Selloni, Adsorption and dissociation of O_2 on Anatase TiO_2, *Accounts of Chemical Research* 47 (**2014**) 3361–3368.

[171] K. Komaguchi, T. Maruoka, H. Nakano, I. Imae, Y. Ooyama, Y. Harima, ESR study on the reversible electron transfer from O_2^{2-} to Ti^{4+} on TiO_2 Nanoparticles Induced by Visible-Light illumination, *Journal of Physical Chemistry C* 113 (**2009**) 1160–1163.

[172] P. Pieta, A. Petr, W. Kutner, L. Dunsch, In situ ESR spectroscopic evidence of the spin-trapped superoxide radical, $O_2^{\cdot-}$, electrochemically generated in DMSO at room temperature, *Electrochimica Acta* 53 (**2008**) 3412–3415.

[173] J.M. Fontmorin, R.C. Burgos Castillo, W.Z. Tang, M. Sillanpää, Stability of 5,5-dimethyl-1-pyrroline-N-oxide as a spin-trap for quantification of hydroxyl radicals in processes based on Fenton reaction, *Water Research* 99 (**2016**) 24–32.

[174] Z. Wang, W. Ma, C. Chen, H. Ji, J. Zhao, Probing paramagnetic species in titania-based heterogeneous photocatalysis by electron spin resonance (ESR) spectroscopy - A mini review, *Chemical Engineering Journal* 170 (**2011**) 353–362.

[175] Z. Tachan, I. Hod, A. Zaban, The TiO_2-catechol complex: Coupling type II sensitization with efficient catalysis of water oxidation, *Advanced Energy Materials* 4 (**2014**) 1–7.

[176] A. Valavanidis, K. Fiotakis, E. Bakeas, T. Vlahogianni, Electron paramagnetic resonance study of the generation of reactive oxygen species catalysed by transition metals and quinoid redox cycling by inhalable ambient particulate matter, *Redox Report* 10 (**2005**) 37–51.

[177] N. Liu, X. Zhou, N.T. Nguyen, K. Peters, F. Zoller, I. Hwang, C. Schneider, M.E. Miehlich, D. Freitag, K. Meyer, D. Fattakhova-Rohlfing, P. Schmuki, Black Magic in Gray Titania: Noble-Metal-Free Photocatalytic H_2 Evolution from Hydrogenated Anatase, *ChemSusChem* 10 (**2017**) 62–67.

[178] X. Zou, J. Liu, J. Su, F. Zuo, J. Chen, P. Feng, Facile synthesis of thermal- and photostable titania with paramagnetic oxygen vacancies for visible-light photocatalysis, *Chemistry - A European Journal* 19 (**2013**) 2866–2873.

[179] I. Kondratyeva, Ł. Orzeł, I. Kobasa, A. Doroshenko, W. Macyk, Photosensitization of titanium dioxide with 4′-dimethylaminoflavonol, *Materials Science in Semiconductor Processing* 42 (**2016**) 62–65.

[180] G. Kim, S.H. Lee, W. Choi, Glucose-TiO_2 charge transfer complex-mediated photocatalysis under visible light, *Applied Catalysis B: Environmental* 162 (**2015**) 463–469.

[181] H. Park, H. Kim, G. Moon, W. Choi, Photoinduced charge transfer processes in solar photocatalysis based on modified TiO_2, *Energy & Environmental Science* 9 (**2016**) 411–433.

[182] A.G. Agrios, K.A. Gray, E. Weitz, Narrow-band irradiation of a homologous series of chlorophenols on

TiO_2: Charge-transfer complex formation and reactivity, *Langmuir* 20 (**2004**) 5911–5917.

[183] R. Beranek, (Photo)electrochemical methods for the determination of the band edge positions of TiO_2-based nanomaterials, *Advances in Physical Chemistry* 2011 (**2011**) 80–83.

[184] G. Rothenberger, D. Fitzmaurice, M. Grätzel, Spectroscopy of conduction band electrons in transparent metal oxide semiconductor films: Optical determination of the flatband potential of colloidal titanium dioxide films, *Journal of Physical Chemistry* 96 (**1992**) 5983–5986.

[185] F. Sannino, P. Pernice, L. Minieri, G.A. Camandona, A. Aronne, D. Pirozzi, Oxidative Degradation of Different Chlorinated Phenoxyalkanoic Acid Herbicides by a Hybrid ZrO_2 Gel-Derived Catalyst without Light Irradiation, *ACS Applied Materials & Interfaces* 7 (**2015**) 256–263.

[186] Y. Zhang, J.W.C. Wong, P. Liu, M. Yuan, Heterogeneous photocatalytic degradation of phenanthrene in surfactant solution containing TiO_2 particles, *Journal of Hazardous Materials* 191 (**2011**) 136–143.

[187] X. Zhao, Z. Cai, T. Wang, S.E. O'Reilly, W. Liu, D. Zhao, A new type of cobalt-deposited titanate nanotubes for enhanced photocatalytic degradation of phenanthrene, *Applied Catalysis B: Environmental* 187 (**2016**) 134–143.

[188] J. Xiao, Y. Xie, Q. Han, H. Cao, Y. Wang, F. Nawaz, F. Duan, Superoxide radical-mediated photocatalytic oxidation of phenolic compounds over Ag^+/TiO_2: Influence of electron donating and withdrawing substituents, *Journal of Hazardous Materials* 304 (**2016**) 126–133.

[189] S. Li, X. Ma, L. Liu, X. Cao, Degradation of 2,4-dichlorophenol in wastewater by low temperature plasma coupled with TiO_2 photocatalysis, *RSC Advances* 5 (**2015**) 1902–1909.

[190] M. Rochkind, S. Pasternak, Y. Paz, Using dyes for evaluating photocatalytic properties: A critical review, *Molecules* 20 (**2015**) 88–110.

[191] K. Ishibashi, A. Fujishima, T. Watanabe, K. Hashimoto, Quantum yields of active oxidative species formed on TiO_2 photocatalyst, *Journal of Photochemistry and Photobiology A: Chemistry* 134 (**2000**) 139–142.

[192] L. Clarizia, D. Spasiano, I. Di Somma, R. Marotta, R. Andreozzi, D.D. Dionysiou, Copper modified-TiO_2 catalysts for hydrogen generation through photoreforming of organics. A short review, *International Journal of Hydrogen Energy* 39 (**2014**) 16812–16831.

[193] G. Yang, H. Tao, P. Qin, W. Ke, G. Fang, Recent progress in electron transport layers for efficient perovskite solar cells, *Journal of Materials Chemistry A* 4 (**2016**) 3970–3990.

[194] X. Deng, G.C. Wilkes, A.Z. Chen, N.S. Prasad, M.C. Gupta, J.J. Choi, Room-Temperature Processing of TiOx Electron Transporting Layer for Perovskite Solar Cells, *Journal of Physical Chemistry Letters* 8 (**2017**) 3206–3210.

[195] L. Huang, J. Xu, X. Sun, C. Li, R. Xu, Y. Du, J. Ni, H. Cai, J. Li, Z. Hu, J. Zhang, Low-temperature photochemical activation of sol-gel titanium dioxide films for efficient planar heterojunction perovskite solar cells, *Journal of Alloys and Compounds* 735 (**2018**) 224–233.

[196] Y.C. Shih, L.Y. Wang, H.C. Hsieh, K.F. Lin, Enhancing the photocurrent of perovskite solar cells via modification of the TiO_2 /CH_3 NH_3 PbI_3 heterojunction interface with amino acid, *Journal of Materials Chemistry A* 3 (**2015**) 9133–9136.

[197] N.R. Mathews, E.R. Morales, M.A. Cortés-Jacome, J.A. Toledo Antonio, TiO_2 thin films - Influence of

annealing temperature on structural, optical and photocatalytic properties, *Solar Energy* 83 (**2009**) 1499–1508.

[198] W. Chen, Y. Wu, Y. Yue, J. Liu, W. Zhang, X. Yang, H. Chen, E. Bi, I. Ashraful, M. Grätzel and L. Han, Efficient and stable large-area perovskite solar cells with inorganic charge extraction layers, *Science* 350 (**2015**) 1–6.

SCIENTIFIC CONTRIBUTIONS

The research activity carried out in the framework of this PhD course contributed to date to six publications on peer-reviewed journals. Four of these deal with the topic of the PhD dissertation:

- F. Sannino, P. Pernice, **C. Imparato**, A. Aronne, G. D'Errico, L. Minieri, M. Perfetti, D. Pirozzi, Hybrid TiO_2–acetylacetonate amorphous gel-derived material with stably adsorbed superoxide radical active in oxidative degradation of organic pollutants, *RSC Advances* 5 (**2015**) 93831-93839.
- A. Aronne, M. Fantauzzi, **C. Imparato**, D. Atzei, L. De Stefano, G. D'Errico, F. Sannino, I. Rea, D. Pirozzi, B. Elsener, P. Pernice, A. Rossi, Electronic properties of TiO_2-based materials characterized by high Ti^{3+} self-doping and low recombination rate of electron–hole pairs, *RSC Advances* 7 (**2017**) 2373-2381.
- **C. Imparato**, A. Aronne, L. Minieri, G. D'Errico, D. Pirozzi, F. Sannino, P. Pernice, Sol–Gel Synthesis and Characterization of Hybrid TiO_2-Acetylacetonate Materials, *Advanced Science Letters* 23 (**2017**) 5912-5915.
- D. Pirozzi, F. Sannino, B. Pietrangeli, M. Abagnale, **C. Imparato**, G. Zuccaro, L. Minieri, A. Aronne, Oxidative degradation of organic pollutants by a new hybrid titania based gel-derived material with stable radical species, *Chemical Engineering Transactions* 57 (**2017**) 769-774.

Two publications pertain other topics in materials chemistry, chemical engineering and catalysis:

- A. Aronne, M. Di Serio, R. Vitiello, N.J. Clayden, L. Minieri, **C. Imparato**, A. Piccolo, P. Pernice, P. Carniti, A. Gervasini, An Environmentally Friendly Nb-P-Si Solid Catalyst for Acid-Demanding Reactions, *Journal of Physical Chemistry C* 121 (**2017**) 17378-17389.
- A. Gervasini, P. Carniti, F. Bossola, **C. Imparato**, P. Pernice, N. J. Clayden, A. Aronne, New Nb-P-Si ternary oxide materials and their use in heterogeneous acid catalysis, *Molecular Catalysis* 458 (**2018**) 280-286.

Other papers are currently in preparation.

The personal contributions of the author to the following national and international conferences can be mentioned:

- **C. Imparato**, A. Aronne, P. Pernice, D. Pirozzi, L. Minieri, G. D'Errico, F. Sannino, L. De Stefano, I. Rea, "Hybrid TiO_2-acetylacetonate catalyst: characterization and activity in organic pollutants degradation", *FEMS Junior Euromat 2016*, Lausanne (Switzerland) 10-14 July 2016 (oral presentation).
- **C. Imparato**, C. Florio, F. Sannino, A. Aronne, P. Pernice, G. D'Errico, L. Minieri, D. Pirozzi, "A novel hybrid catalyst based on TiO_2 for the oxidation of aromatic organic compounds", *Convegno Nazionale GRICU 2016*, Anacapri (NA) 12-14 September 2016 (oral presentation).
- **C. Imparato**, A. Aronne, L. Minieri, G. D'Errico, D. Pirozzi, F. Sannino, P. Pernice, "Sol-Gel Synthesis and Characterization of Hybrid TiO_2-acetylacetonate Materials", *VI International Workshop on Oxide-based Materials*, Naples 21-24 September 2016 (oral presentation).
- **C. Imparato**, A. Aronne, P. Pernice, D. Pirozzi, L. Minieri, G. D'Errico, F. Sannino, "Hybrid TiO_2 and ZrO_2-based materials: properties and catalytic activity in organic pollutants degradation", *5th International Conference on Multifunctional, Hybrid and Nanomaterials (HYMA 2017)*, Lisbon (Portugal) 6-10 March 2017 (poster presentation).
- **C. Imparato**, G. D'Errico, A. Aronne, "Sol-gel synthesis of hybrid TiO_2 photosensitized through charge transfer complexes", *Merck Young Chemists Symposium (MYCS 2017)*, Milano Marittima (RA) 13-15 November 2017 (oral presentation).
- **C. Imparato**, A. Aronne, G. D'Errico, F. Sannino, D. Pirozzi, A. Rossi, M. Fantauzzi, I. Rea L. De Stefano, "TiO_2 hybrid gels: from reactive oxygen species stabilization to Ti^{3+} self-doping" *3rd International Symposium on Energy and Environmental Photocatalytic Materials (EEPM3)*, Krakow (Poland) 15-19 May, 2018 (poster presentation).
- **C. Imparato**, A. Aronne, G. D'Errico, M. Fantauzzi, C. Passiu, C. Ricca, U. Aschauer, L. De Stefano, I. Rea, A. Rossi, "Inducing defects in gel-derived ZrO_2 for visible light absorption", *XX Congresso Nazionale di Catalisi – XX Congresso Nazionale della Divisione di Chimica Industriale (GIC-DiChIn2018)*, Milano 2-5 September 2018 (oral presentation).
- **C. Imparato**, A. Aronne, M. Fantauzzi, A. Rossi, D. Pirozzi, M. Kobielusz, W. Macyk, "Sintesi di ossidi semiconduttori attivi al buio e fotosensibili alla luce visibile ed UV", *XI Congresso Nazionale AICIng*, Bologna 9-12 September 2018 (oral presentation).